

**Gas/Aerosol Partitioning:  
A simplified Method  
for  
Global Modeling**

Swen Metzger

# **Gas/Aerosol Partitioning:**

## **A simplified Method for Global Modeling**

Gas/Aërosol Verdeling:

Een vereenvoudigde Methode voor Mondiale Modellerings

(met een samenvatting in het Nederlands)

### **Proefschrift**

ter verkrijging van de graad van doctor  
aan de Universiteit van Utrecht  
op gezag van de Rector Magnificus, Prof. Dr. H.O. Voorma,  
ingevolge het besluit van het College voor Promoties  
in het openbaar te verdedigen  
op woensdag 20 september 2000 des middags te 12.45 uur

door

**Swen Marcus Metzger**

geboren op 25 april 1967 te Heidelberg, Duitsland

**Promotoren: Prof. Dr. J. Lelieveld**

Instituut voor Marien en Atmosferisch Onderzoek  
Faculteit Natuur- en Sterrenkunde  
Universiteit Utrecht

**Prof. Dr. H. Grassl**

Max-Planck-Institut für Meteorologie Hamburg en  
Faculteit Meteorologie  
Universiteit Hamburg, Duitsland

**Co-Promotor: Dr. ir. F.J. Dentener**

Instituut voor Marien en Atmosferisch Onderzoek  
Faculteit Natuur- en Sterrenkunde  
Universiteit Utrecht

**Paranimfen: Dr. Axel Timmermann**

**Drs. Alexander Los**

This thesis was initiated through a stipendium from the European Community, N° ENV4-CT96-5036 (DG 12-ASAL), and performed at the Instituut voor Marien en Atmosferisch Onderzoek (IMAU), at the Universiteit Utrecht, The Netherlands.

ISBN: 90-393-2510-3

Drukkerij Zuidam & Uithof B.V

This Ph.D. thesis is also available (in full color) in the portable document format (pdf). We refer to the Homepage of the Universiteitsbibliotheek Utrecht, Faculteit Natuur- & Sterrenkunde, (<http://www.library.uu.nl/>).

## CONTENT

Summary .....	v
Samenvatting .....	vii
<b>Chapter I: Introduction .....</b>	<b>1</b>
1.1 Aerosol Climate Forcing .....	1
1.2 Aerosol Production Rates .....	3
1.3 Changing Aerosol Composition .....	5
1.4 Modeling Aerosol Composition .....	7
1.5 Modeling Demands .....	8
1.6 Thesis Outline .....	9
<b>Chapter II: Equilibrium Models and Modeling Theory .....</b>	<b>11</b>
2.1 General Overview .....	11
2.2 General Assumptions .....	13
2.3 Equilibrium Constants .....	14
2.4 Concentration Domains .....	17
2.5 Relative Humidity of Deliquescence .....	18
2.6 Aqueous Phase .....	21
2.6.1 Water Activity .....	21
2.6.2 ZSR-Relation .....	22
2.6.3 Aerosol Associated Water .....	22
2.6.4 Activity Coefficients .....	23
2.7 Gas/Aqueous Phase Equilibria .....	25
2.8 Solid Phase and Gas/Solid Phase Equilibria .....	27
2.9 Solution Algorithm .....	30
<b>Chapter III: A new Method and Equilibrium Model .....</b>	<b>33</b>
3.1 Implications of the General Assumptions .....	34
3.2 Vapor Pressure Reduction and the Generalization of Raoult's Law .....	35
3.3 Relation between Aerosol Molality and Relative Humidity .....	37
3.4 Relation between Aerosol Water and Relative Humidity .....	39
3.5 Parameterizations .....	40
3.5.1 Parameterization of Aerosol Water .....	42
3.5.2 Parameterization of Aerosol Molality .....	42
3.5.3 Parameterization of Aerosol Activity Coefficients .....	43
3.6 Sensitivities of the Activity Coefficient Calculation (ACC) .....	47
3.6.1 ACC vs. Aerosol Concentrations and Temperature .....	47
3.6.2 ACC vs. Aerosol Compositions .....	48
3.6.3 ACC vs. Aerosol Concentration Domains .....	50
3.7 Non-iterative vs. iterative ACC Method .....	52
3.8 A new and simplified Gas/Aerosol Model (EQSAM) .....	54
3.8.1 Schematic Description .....	54

<b>Chapter IV: Equilibrium Model Comparison .....</b>	<b>57</b>
4.1 Box-model Calculations .....	57
4.2 Global offline Calculations.....	63
4.2.1 CPU-time .....	68
4.3 Global online Calculations .....	70
<b>Chapter V: Global Gas/Aerosol Partitioning Modeling .....</b>	<b>73</b>
5.1 Atmosphere/Chemistry Model Transport (TM3) .....	73
5.1.1 Tracer Transport Processes .....	75
5.1.2 Meteorological Data .....	75
5.1.3 Emissions .....	76
5.1.4 Chemistry .....	77
5.1.5 Aerosol Module.....	78
5.1.6 Dry Deposition .....	78
5.1.7 Wet Deposition .....	79
5.2 Aerosol Distributions .....	80
5.2.1 Gas/Aerosol Partitioning .....	80
5.2.2 Global Aerosol Patterns.....	86
5.2.3 Space-Time Variability .....	90
5.2.4 Zonal Distributions.....	94
5.2.5 Feedback on Chemistry .....	99
5.3 Aerosol Budgets .....	103
5.3.1 Annual Cycle .....	103
5.3.2 Feedback on Chemistry .....	104
<b>Chapter VI: Gas/Aerosol Partitioning Sensitivities.....</b>	<b>105</b>
6.1 Dependence on Modeling Assumptions.....	105
6.1.1 Aerosol Run (metastable) vs. non-Aerosol Run (Sulfate only) .....	105
6.1.2 Aerosol Run: metastable vs. solids .....	106
6.1.3 Aerosol Run: metastable vs. hysteresis .....	107
6.2 Dependence on the Model Version (TM3).....	109
6.2.1 Resolution and Boundary Layer .....	109
<b>Chapter VII: Comparison with Ground-based Measurements .....</b>	<b>111</b>
7.1 Sulfate/Nitrate at Petten (The Netherlands) .....	111
7.2 Ammonium/Sulfate/Nitrate at various EMEP stations .....	113
7.3 Closing Remarks .....	116
<b>Chapter VIII: Discussion and Conclusions.....</b>	<b>117</b>
Appendix.....	APP
List of Acronyms.....	LOA
List of Symbols .....	LOS
List of Figures .....	LOF
List of Tables .....	LOT
Bibliography.....	BIB
Epilogue .....	EPI
Curriculum Vitae.....	CV

## Summary

The main focus of this thesis is the development of a simplified method to routinely calculate gas/aerosol partitioning of multicomponent aerosols and aerosol associated water within global atmospheric chemistry and climate models.

Atmospheric aerosols are usually multicomponent mixtures, partly composed of acids (e.g.  $\text{H}_2\text{SO}_4$ ,  $\text{HNO}_3$ ), their salts (e.g.  $(\text{NH}_4)_2\text{SO}_4$ ,  $\text{NH}_4\text{NO}_3$ , respectively), and water. Because these acids and salts are highly hygroscopic, water, that is associated with aerosols in humid environments, often exceeds the total dry aerosol mass. Both the total dry aerosol mass and the aerosol associated water are important for the role of atmospheric aerosols in climate change simulations. Still, multicomponent aerosols are not yet routinely calculated within global atmospheric chemistry or climate models. The reason is that these particles, especially volatile aerosol compounds, require a complex and computationally expensive thermodynamical treatment. For instance, the aerosol associated water depends on the composition of the aerosol, which is determined by the gas/liquid/solid partitioning, in turn strongly dependent on temperature, relative humidity, and the presence of pre-existing aerosol particles.

Based on thermodynamical relations such a simplified method has been derived. This method is based on the assumptions generally made by the modeling of multicomponent aerosols, but uses an alternative approach for the calculation of the aerosol activity and activity coefficients. This alternative approach relates activity coefficients to the ambient relative humidity, according to the vapor pressure reduction and the generalization of Raoult's law. This relationship, or simplification, is a consequence of the assumption that the aerosol composition and the aerosol associated water are in thermodynamic equilibrium with the ambient relative humidity, which determines the solute activity and, hence, activity coefficients of a multicomponent aerosol mixture. Thus, the necessary equilibrium equations can be solved analytically, so that numerical and therefore expensive iterative calculations are avoided.

Subsequently, a new thermodynamic gas/aerosol partitioning model has been developed, called EQSAM (Equilibrium Simplified Aerosol Model). EQSAM has been compared with various other thermodynamical models presently in use, which shows that the results of EQSAM are well within the range produced by these more complex models. The application to global modeling further shows that EQSAM is indeed sufficiently fast and accurate. Especially the results of the global gas/aerosol partitioning calculations show that differences resulting from the thermodynamical treatment affect much less the aerosol composition compared to other, non-thermodynamical parameters, such as the model resolution or the boundary layer mixing scheme used. This indicates that the gas/aerosol partitioning calculations in atmospheric chemistry models are largely governed by transport processes, including meteorology, emission sources, as well as wet and dry deposition processes.

Modeling results further indicate that gas/aerosol partitioning, especially at lower temperatures (during winter and nights), is of great importance for both the gas phase concentrations and the aerosol composition, including aerosol associated water. For instance, the mean surface gaseous nitric acid concentration is predicted to partition almost completely into the aerosol phase during winter and summer nights. This considerably increases the predicted aerosol load, compared to model calculations excluding gas/aerosol partitioning. This consequently affects the aerosol associated water (because the aerosol water is proportional to the amount of dissolved matter). Additionally, aerosol mass from gas/aerosol partitioning, such as ammonium nitrate, has a longer residence time than the precursor gases ( $\text{NH}_3$  and  $\text{HNO}_3$ ) and might, therefore, be subject to long-range transport from the sources. This is, for example, the case for ammonium nitrate originating from gas-to-particle conversion over northern India. Our model results indicate that these particles, through convective redistribution, can be transported at altitudes of 200-300 hPa as far as Europe during the Indian summer monsoon. Verification of these results, however, would require aircraft measurements, which are presently not available.

Comparison with ground-based measurements indicates that the simplified aerosol module coupled to a global atmospheric chemistry model (TM3), for the considered ammonium/sulfate/nitrate/water system, yields realistic results at locations where ammonium nitrate is important. For remote locations, the comparison also indicates that it is important to account for other aerosol species such as sea salt and mineral dust. Although these compounds have not (yet) been included in the global gas/aerosol partitioning calculations with TM3, it seems to be possible to consider them with our simplified approach, as indicated by the results of box-model calculations.

## Samenvatting

De belangrijkste doelstelling van dit proefschrift is de ontwikkeling van een vereenvoudigde methode waarmee de verdeling van aerosolbestanddelen tussen gas- en aerosolfase kan worden gesimuleerd in mondiale chemie- en klimaatmodellen.

Atmosferisch aerosol bestaat doorgaans uit een mengsel van meerdere componenten zoals de zuren  $\text{H}_2\text{SO}_4$  en  $\text{HNO}_3$ , de zouten  $(\text{NH}_4)_2\text{SO}_4$  en  $\text{NH}_4\text{NO}_3$  en water. Omdat deze componenten zeer hygroscopisch zijn zal onder vochtige condities water het leeuwendeel uitmaken van de totale aerosolmassa. Desalniettemin wordt dit "multi-component" aerosol bijna nooit meegenomen in mondiale modellen, omdat het moeilijk te modelleren is. Vooral vluchtige aerosolbestanddelen vereisen vaak een complexe thermodynamische berekening. De hoeveelheid water die door het aerosol kan worden opgenomen hangt bijvoorbeeld af van de samenstelling van het aerosol en de verdeling van de aerosolbestanddelen tussen gas en aerosolfase, van de relatieve vochtigheid en de temperatuur, en van de aanwezigheid van reeds bestaande aerosoldeeltjes.

In dit proefschrift hebben we een vereenvoudigde methode afgeleid, die gebaseerd op thermodynamische grootheden, die het mogelijk maakt om op routinematige basis mondiale modelberekeningen uit te voeren met voldoende nauwkeurigheid en tegen bescheiden computerkosten. De methode is gebaseerd op aannames die meestal worden gemaakt bij de modellering van "multi-component" aerosol, en maakt daarnaast gebruik van een alternatieve benadering voor de berekening van de aerosolactiviteit en de activiteitscoëfficiënten.

Deze alternatieve methode legt een relatie tussen de activiteitscoëfficiënten en de relatieve vochtigheid van de omgeving volgens de afname van de dampspanning en de toepassing van de algemene wet van Raoult. Deze relatie is een gevolg van de aanname dat de aerosolsamenstelling en het aerosol geassocieerde water in evenwicht is met de luchtvochtigheid die de activiteit van het oplosmiddel (water) en dus ook de overige activiteitscoëfficiënten van het aerosolmengsel bepalen. Het blijkt hierdoor mogelijk om met deze relatie analytische oplossingen te berekenen voor het evenwicht tussen gas- en aerosolfase voor de belangrijkste aerosolbestanddelen. Dure iteratieve berekeningsmethoden worden hiermee overbodig. Vergelijking van dit vereenvoudigde analytische "aerosol-equilibrium-model" (EQSAM) met verscheidene andere veelgebruikte "state-of-the art" modellen laat zien dat de resultaten goed met elkaar in overeenkomst zijn terwijl de rekenkosten slechts een fractie bedragen. Berekeningen met een mondiale chemie-transportmodel (TM3) laten bovendien zien dat de factoren zoals de modelresolutie en de grenslaagbeschrijving de aerosolsamenstelling sterker bepalen dan de specifieke beschrijving van de aerosol thermodynamische processen. Dit betekent dat grootschalig transport van aerosol en aerosolprecursors een dominante rol speelt. Modelresultaten laten tevens zien dat een goede berekening van het thermodynamische gas-aerosol evenwicht op regionale schaal van groot belang kan zijn voor de bepaling van de aerosolsamenstelling en de gasfase concentraties, vooral bij lage



temperaturen ('swinters en 'snachts). Zo berekent het model bijvoorbeeld dat salpeterzuur in de winter en 'snachts, nabij het oppervlak, wordt opgenomen. Hierdoor neemt de totale berekende aerosolmassa flink toe in vergelijking met modelberekeningen waarbij de aerosol thermodynamische evenwichtsberekening achterwege is gelaten. Als gevolg hiervan neemt ook de berekende aerosolwatermassa toe, hetgeen leidt tot een verandering van de optische eigenschappen die belangrijk zijn voor de berekening van de stralingsforcering van het klimaat.

Omdat het aerosol een langere levensduur heeft dan de voorlopergassen kan het over grote afstanden getransporteerd worden, ver weg van de emissiebronnen. Zo blijkt uit onze modelberekeningen dat ammonium-nitraat aerosol, gevormd boven noord-India, over grote afstanden (tot Europa aan toe) getransporteerd wordt op een hoogte van 200 à 300 hPa tijdens de Indiase zomermoeson. Echter, vliegtuigmetingen waarmee deze modelresultaten kunnen worden geverifieerd ontbreken nog.

De vergelijking van modelresultaten met grondmetingen laat zien dat TM3, in combinatie met EQSAM, goede resultaten oplevert voor het gesimuleerde ammonium/sulfaat/nitraat/water-systeem op plaatsen waar ammonium nitraat een belangrijke rol speelt. Voor afgelegen locaties blijkt dat het gemodelleerde systeem nog te eenvoudig is, en dat ook ander aerosolbestanddelen zoals zeezout en mineraal stof (woestijnzand) meegenomen moeten worden. Met enige aanpassing is het goed mogelijk om ook deze componenten mee te nemen in EQSAM, hetgeen ook blijkt uit boxmodelberekeningen. Deze aanpassing zal in de nabije toekomst plaatsvinden.

## Chapter I: Introduction

In the past 2-3 decades, the atmospheric chemistry of energy-related air-pollutants has been of public and scientific interest. Principal substances of attention have been, besides greenhouse gases ( $\text{CO}_2$ ,  $\text{CH}_4$ ,  $\text{N}_2\text{O}$ , CFCs) and ozone ( $\text{O}_3$ ), sulfur and nitrogen oxides ( $\text{SO}_2$  and  $\text{NO}_x$ ), and their oxidation products, e.g. sulfuric acid ( $\text{H}_2\text{SO}_4$ ) and nitric acid ( $\text{HNO}_3$ ). The latter two are aerosol<sup>1</sup> precursor gases. For instance, they form aerosols if they react with the trace gas ammonia ( $\text{NH}_3$ ), a major agricultural pollutant. The corresponding neutralization products are inorganic salts, e.g. ammonium sulfate ( $(\text{NH}_4)_2\text{SO}_4$ ) and ammonium nitrate ( $\text{NH}_4\text{NO}_3$ ), respectively. Both trace gases and aerosols affect air quality and human health. They lead to detrimental effects on buildings, soils, vegetation, and aquatic systems due to acidic dry and wet deposition, or to eutrophication. In addition, they disturb the earth's radiation balance and climate. In the 1970s, these substances were first of concern from the perspective of human health, acid deposition, visibility reduction, and in the 1990s, also from the perspective of radiative forcing of the earth's climate, the so-called climate change issue (IPCC, 1996).

### 1.1 Aerosol Climate Forcing

Although the anthropogenic emissions of long-lived greenhouse gases have increased during the past century, it seems that the global temperature has not risen as much as initially predicted with climate models by only accounting for greenhouse gases (IPCC, 1996). A possible explanation might be, the combination of several effects: natural variability and the simultaneous increase of anthropogenic aerosols. The latter is expected to mask an anticipated "Global Warming" due to greenhouse gas increase (Charlson et al., 1994; Charlson and Heintzenberg, 1995).

Anthropogenic aerosols can alter the earth's radiation balance both through direct and indirect mechanisms (Charlson and Heintzenberg, 1995). The direct forcing is induced by scattering and absorption of solar radiation by the aerosol particles themselves. Indirect forcing is the effect of aerosols on cloud optical depth and albedo, caused by alteration of the available cloud condensation nuclei (CCN). Changes of CCN concentration affect the droplet size distribution, size and coverage of clouds on both temporal and spatial scales. Specifically, it is assumed that an increase of CCN leads to smaller droplet sizes, yielding brighter and more reflective clouds (Twomey et al., 1977a,b). Especially the indirect effect is of great importance, because of its potentially large significance in the planetary radiation budget. For example, marine boundary layer clouds contribute to about one third of the Earth's albedo (Charlson et al., 1987).

Therefore, much of recent atmospheric research focuses on the radiative influence of aerosols on climate. Although most modeling results indicate that anthropogenic aerosols are exerting an influence on climate change that is comparable (but of opposite sign) to the anthropogenic

---

<sup>1</sup> The expression *aerosol* refers to a population of particles (liquid or dry) suspended in air.

greenhouse effect by long-lived gases, the magnitude of these aerosol influences is quite uncertain in comparison to that of the long-wave (thermal infrared) radiative forcing by greenhouse gases. The estimates from the IPCC (Intergovernmental Panel on Climate Change) of the several contributions to radiative forcing over the industrial period are shown in the Figure 1.1, including the uncertainties associated with each of these quantities.

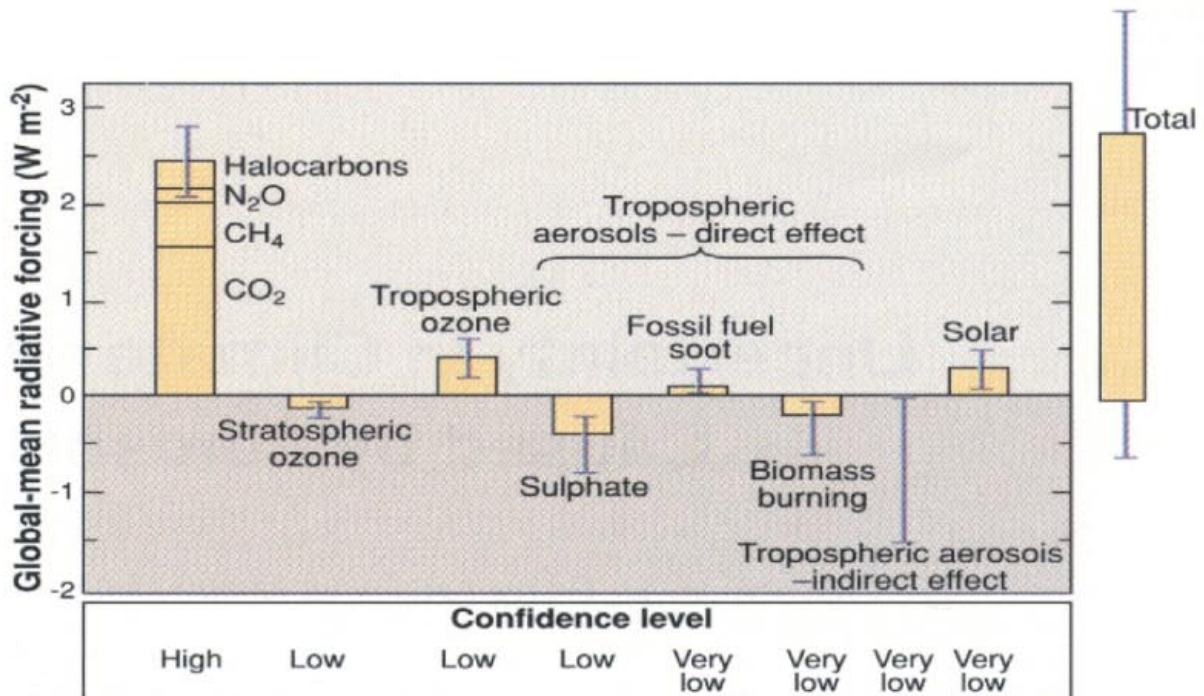


**Figure 1.1.** Uncertainty in climate change caused by aerosols (Schwartz and Andreae, 1996).

While the uncertainties of the several aerosol forcings substantially exceed those associated with the greenhouse gases and other forcings, no estimate could be given for the indirect forcing; only the range of possible values is indicated (the labels under the several bars denote the confidence of IPCC that the actual forcing lies within the range indicated by the uncertainties). In addition to the uncertainty range given by IPCC, Schwartz and Andreae (1996) inferred the total forcing and the associated uncertainty to make the following point (<http://www.ecd.bnl.gov/steve/stephen.html>):

*That if one takes the IPCC estimates of uncertainty in the several forcings at face value, then the present state of understanding is that even the sign of forcing of climate change over the industrial period is not known. If the negative (cooling) forcing is at the high end of the uncertainty range, then aerosol forcing could be offsetting much if not all of the greenhouse forcing over the industrial period. However, It should be emphasized that one should not take any comfort in this situation - in fact just the opposite. Because the atmospheric residence time of tropospheric aerosols is short (about a week) compared to the decades-to-centuries lifetimes of the greenhouse gases, then to whatever extent greenhouse gas forcing is being offset by aerosol forcing, it is last week's aerosols that are offsetting forcing by decades worth of greenhouse gases. Because the greenhouse gases are long-lived in the atmosphere, their atmospheric loadings tend to approximate the integral of emissions. Because the aerosols are short-lived, their loading tend to be*

*proportional to the emissions themselves. There is only one function that is proportional to its own integral, the exponential function. So only if society is to make a commitment to continued exponential growth of emissions can such an offset be maintained indefinitely. And of course exponential growth cannot be maintained forever. So if the cooling influence of aerosols is in fact offsetting much of the warming influence of anthropogenic greenhouse gases, then when society is unable to maintain this exponential growth, the climate could be in for a real and long-lasting shock.*

Because of the uncertainties associated with aerosol forcing, which explain at least part of the uncertainties in climate forcing, it is crucial to focus on the aerosol forcing if any progress is to be made in understanding anthropogenically induced climate change. Consequently, much of the research is directed recently to developing such improved understanding.

A number of studies have tried to provide estimates of the uncertainties associated with the aerosol forcing. Much of the uncertainty arises from the fact that (in contrast to the long-lived greenhouse gases, which are rather uniformly distributed in the atmosphere) the loadings of aerosols are highly variable in space and time, as a consequence of highly localized sources and of sporadic removal, mainly by precipitation. Additionally, aerosol microphysical properties are not a universal constant, but depend on sources and composition and evolve as a consequence of chemical and physical processes occurring in the atmosphere. The mass loading, composition, and the microphysical properties of aerosols such as number concentration and size distribution directly affect their direct and indirect radiative forcing of climate.

## 1.2 Aerosol Production Rates

Atmospheric aerosols consist of multicomponent particles, which can include water, inorganic compounds (e.g. ammonium, sulfate, nitrate) and the corresponding salts (e.g. ammonium sulfates and nitrate), sea salt, mineral dust, volatile organic compounds (VOC), elemental carbon (soot), and a variety of trace metals. Most prevalent are the inorganic species, sulfate, nitrate, and ammonium, which in urban regions typically comprise up to 50% of anhydrous atmospheric aerosol mass (Heintzenberg, 1989). If water is considered, the fraction might be considerably higher (especially in high relative humidity environments). The sizes of these particles cover a broad range, and the composition and mechanisms that generate them differ for each size section. The three mechanisms are:

- **Emission** of material from the earth's surface and anthropogenic activities, such as mineral dust, sea salt from sea spray, and pollen.
- Homogeneous condensation of supersaturated vapors, often referred to as **nucleation**. Such vapors are likely the result of (photo-) chemical reactions of precursor gases in the atmosphere, e.g. sulfuric acid vapor which is an oxidation product of  $\text{SO}_2$ .
- Heterogeneous **condensation** of supersaturated vapors on pre-existing particles, often referred to as condensation only.

Emissions and nucleation lead to formation of new aerosol particles (primary aerosols), while condensation only increases the total aerosol surface and mass (secondary aerosols). Nucleation and condensation involve the gas-to-particle conversion (GPC).

To give an estimate of the production rates, we summarize the total aerosol sources (based on a compilation of various sources by Roedel, 1992) in Table 1.1. For the anthropogenic aerosol sources, it appears that approximately twice as much aerosol mass originates from GPC compared to the amount that is directly emitted. Although highly uncertain, the estimates of the natural aerosol sources illustrate that GPC accounts for approximately half the total mass of wind blown particles, and almost of about a factor four compared to the anthropogenic GPC sources. Thus, it is desirable to adequately account for GPC processes in model studies.

**Table 1.1. Natural and anthropogenic aerosol production rates (estimates)**

Sources [Tg/a]	GPC	wind blown particles
Natural	515-800	1293 - 1570
Anthropogenic	160-240	90 - 135

*Note: the GPC includes both nucleation and condensation. These values should give an indication only. Values are based on a compilation of various sources (Roedel 1992).*

There are various possible pathways leading to condensable vapors (e.g. Warneck, 1988). The (photo-)chemical oxidation of sulfur dioxide,  $\text{SO}_2$ , to sulfuric acid ( $\text{H}_2\text{SO}_4$ ), or sulfate ( $\text{SO}_4^{2-}$ ), is probably one of the most important reactions in the atmosphere leading to GPC. Although in many industrialized regions the production rate of nitric acid can be of the same order as that of sulfuric acid, the GPC processes involving volatile vapors such as  $\text{HNO}_3$  and  $\text{NH}_3$  are difficult to measure and, hence, poorly quantified. The importance of  $\text{H}_2\text{SO}_4$  is due to its extremely low vapor pressure, which can lead to instantaneous nucleation, i.e. in the coexistence of water vapor and/or ammonia (e.g. Kulmala et al., 1995; 1998).

While nucleation is more likely to occur in less polluted regions (e.g. the free troposphere), because of the much smaller surface area of pre-existing aerosol particles,  $\text{H}_2\text{SO}_4$  and  $\text{HNO}_3$ , which are strong acids, preferably condense on pre-existing particles (such as pollution aerosol, sea salt, or mineral dust) in environments with a high aerosol load. Although the secondary aerosols do not increase the total aerosol number, they are important because they often alter pre-existing aerosols to hygroscopic mixed aerosols, which might be composed of acids (e.g.  $\text{H}_2\text{SO}_4$  and  $\text{HNO}_3$ ), or of their salts (e.g.  $(\text{NH}_4)_2\text{SO}_4$ , and  $\text{NH}_4\text{NO}_3$ ). In the presence of sea salt or mineral dust, condensation can lead to the formation of sodium or calcium sulfates and nitrates. Especially the condensation on sea salt and dust particles leads to aerosols in the size-range beyond a few microns, i.e. the coarse mode (size range  $> 0.5 \mu\text{m}$ ), while the nucleation only leads to new-born particles, i.e. the nucleation mode ( $< 0.01 \mu\text{m}$ ), which are with a few nano-meters in diameter small compared to the condensation aerosols.

However, most of the mass of the secondary aerosols resides in the so-called accumulation mode (size range 0.1 - 0.5  $\mu\text{m}$ ), since nucleation particles rapidly grow into the accumulation mode due to coagulation and uptake of water vapor, while coarse mode particles are more effectively removed by dry deposition (sedimentation), or wet deposition, i.e. by in and below cloud scavenging. While accumulation mode particles have the longest residence time in the atmosphere compared to aerosol particles in the other size ranges, they are also most critical with respect to health and visibility; this size range covers the size range of bacteria, and of the electromagnetic wave length of visible light. Because of their interaction with electromagnetic radiation, aerosols also reduce visibility.

### 1.3 Changing Aerosol Composition

A problem involved with the calculation of aerosol radiative forcing is that, up to now, mainly the influence of sulfate aerosols, black or elemental carbon (soot), and desert or mineral dust have been investigated separately with climate models. Although sulfate may contribute a major fraction to the total anthropogenic aerosol mass and therefore to the direct aerosol radiative forcing, which has been accounted for in the IPCC climate reports, there are large uncertainties involved with the calculation of aerosol radiative forcing. One of the problems is that most aerosols are hygroscopic and take up water under humid conditions (Tang and Munkelwitz, 1994; ten Brink et al., 1996). Model studies have shown (Pilinis et al., 1995) that the most important parameter affecting the direct forcing of aerosols was the relative humidity, i.e. water uptake, which however, depends non-linearly on the aerosol composition.

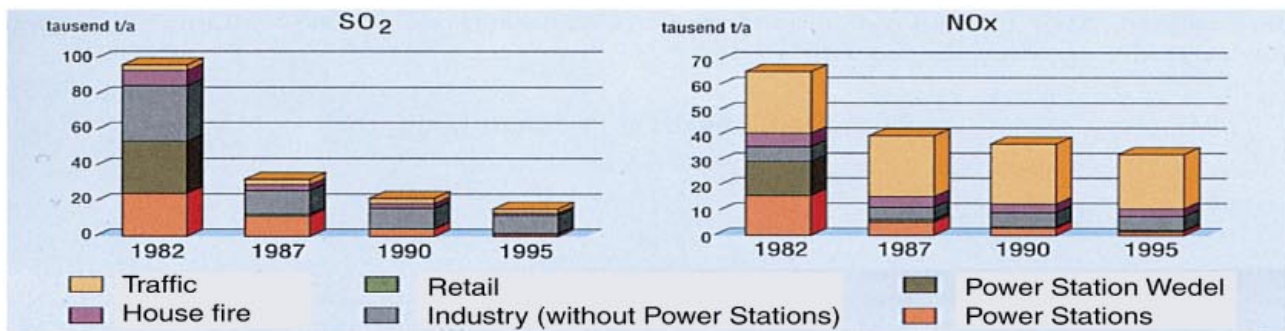


**Figure 1.2.** Emissions of SO<sub>2</sub> and NO<sub>x</sub> in Hamburg, Germany (*Umweltatlas, 1994*).

To correctly account for the aerosol composition, aerosol compounds other than sulfate must be considered. For instance, nitrate may regionally exert a similar radiative forcing as sulfate. Recent measurements indicate that the mass fraction of nitrate can exceed that of sulfate for urban aerosols (Diederer et al., 1985; ten Brink et al., 1996). Furthermore, nitrate may gain importance in the near future. Due to air pollution abatement in the USA and Western Europe, the emissions of sulfur gases from fossil fuel use have been reduced by a factor of 2 to 4 since the 1970s, but despite control measures, such as the introduction of catalytic converters, emissions of nitrogen oxides has decreased less during this period, which is mainly due to the compensating effect of the growing transport sector. Indeed, the relative importance of NO<sub>x</sub> versus SO<sub>2</sub> and, hence, the relative

importance of nitrate versus sulfate aerosols is increasing in most industrialized regions of Europe and North America. For instance, the emission change of  $\text{NO}_x$  and  $\text{SO}_2$  over the last decade, as published by the environmental office in Hamburg (Germany), is shown in [Figure 1.2](#).

Consequently, changes in emissions will lead to changes in aerosol loadings and composition, e.g. a shift in the concentrations of sulfate and nitrate in aerosols. The latter is in turn important for the aerosol associated water, and subsequently for the aerosol optical properties. Differences between sulfate and nitrate aerosols are:

- sulfate is non-volatile  $\Rightarrow$  therefore remains in particle phase
- nitrate is volatile  $\Rightarrow$  maintains gas/aerosol equilibria.

Inorganic sulfate, due to its low volatility, usually occurs in the particulate phase. Nitrate and ammonia, on the other hand, are significantly more volatile. Therefore, ammonium salt condensates, such as ammonium nitrate ( $\text{NH}_4\text{NO}_3$ ), are distributed relative to existing and size-segregated aerosol particles (Wexler and Seinfeld, 1990). Such compounds can therefore evaporate from accumulation mode particles and condense at larger particles, as for instance sea salt or mineral dust. Therefore, the size distribution of nitrate aerosols frequently shows an additional peak in the coarse mode size-range, in addition to the main peak in the accumulation mode; the latter in conjunction with the peak of sulfate aerosols.

An other important difference between sulfate and nitrate salts is their deliquescence behavior (see also Chapter 2.5). Atmospheric aerosols containing sulfate, nitrate and ammonia are hygroscopic; they can be dry and solid below their deliquescence RH, while at higher RH, they absorb water to form an aqueous solution. For instance, ammonium nitrate deliquesces at a lower relative humidity than ammonium sulfate. The so-called relative humidities of deliquescence (RHD) at  $25^\circ\text{C}$  are approximately 60% and 80%, respectively. Subsequently, differences in the deliquescence points occur for mixtures of ammonium nitrate ( $\text{NH}_4\text{NO}_3$ ) and ammonium chloride ( $\text{NH}_4\text{Cl}$ ) containing salt, compared to a mixture of ammonium sulfate ( $(\text{NH}_4)_2\text{SO}_4$ ) and ammonium chloride ( $\text{NH}_4\text{Cl}$ ). It has been shown theoretically (e.g. Potukuchi and Wexler, 1995a,b), and experimentally (e.g. Tang and Munkelwitz, 1993) that the mutual deliquescence relative humidity of a salt mixture (MDRH) is lower than the minimum RHD of each component.

Consequently, multicomponent mixtures will lead to more water uptake and to aqueous droplets at lower relative humidities, affecting the aerosol size, which can be thus particularly important for the aerosol optical properties. This can potentially affect the predicted role of aerosols; the presence of aerosol water also affects the partitioning of volatile species because of changes in the particle size. This is potentially important for accumulation mode particles, which are optically the most active, since they are mostly multicomponent mixtures.

Furthermore, some aerosols might exhibit hysteresis (Charlson et al., 1978; Tang, 1980): An aqueous salt solution can exist in a supersaturated state below the deliquescence RH if the salt formed under wet conditions, or if it has been wet and the RH drops below the RHD. On the other hand, the same salt may be a pure solid if it has been formed under dry conditions, i.e. an RH lower than the corresponding RHD; the salt deliquesces if the RH exceeds the RHD. However, some salt solutions do not crystallize at all. For instance, an aerosol composed of an ammonium nitrate and sulfate salt mixture, containing more  $\text{NH}_4\text{NO}_3$  than  $(\text{NH}_4)_2\text{SO}_4$ , does not show deliquescence behavior. Instead, it only exists in a supersaturated state (ten Brink et al., 1996). The same is true for sufficiently acidic solutions, i.e. a non-neutralized sulfuric acid droplets. Thus, particulate matter can contain a considerable mass of water. For instance, at 90% RH and a temperature of 298K, a particle composed of pure ammonium sulfate contains over 70% water mass by weight (Saxena et al., 1986; Pilinis et al., 1989; Meng et al., 1995). Hence, knowledge about the aerosol associated water, which depends non-linearly on the aerosol composition, is critical in estimating particle mass, size, and optical properties, which in turn are important for both the direct and indirect climate effect of aerosols. Therefore, the formation of secondary aerosol particles from the gaseous air pollutants  $\text{H}_2\text{SO}_4$ ,  $\text{HNO}_3$ , and  $\text{NH}_3$  has been subject of many theoretical and experimental investigations.

#### 1.4 Modeling Aerosol Composition

In the past two decades much effort was devoted to calculate aerosol properties that are difficult to measure, such as the aerosol composition and the aerosol associated water mass. Most attention focused on the often predominant inorganic aerosol compounds sulfate, ammonium, nitrate and aerosol water, and the partitioning between the liquid-solid aerosol phases and the gas phase, e.g. the aerosol precursor gases such as  $\text{HNO}_3$  and  $\text{NH}_3$ .

Especially the ammonium-sulfate-nitrate-water aerosol system has been subject of much air pollution modeling. This has led to the development of a wide range of thermodynamical gas/aerosol box-models, including numerous gas/aerosol equilibrium models (Basset and Seinfeld, 1983; Basset and Seinfeld, 1984; Saxena et al., 1986; Binkowski, 1991; Pilinis and Seinfeld, 1987; Wexler and Seinfeld, 1991; Kim et al., 1993a,b; Kim and Seinfeld, 1995; Nenes et al., 1998; Clegg, et al., 1998a,b; Jacobson et al. 1996, Jacobson, 1999), and several gas/aerosol dynamic models (Meng and Seinfeld 1996; Meng et al. 1998; Jacobson et al. 1996; Sun and Wexler 1998; Pilinis, et al., 2000). While the first generation models simply assumed thermodynamic equilibrium between the gas-liquid-solid aerosol phases, the second generation models calculate mass transfer between the liquid/solid aerosol phases and the gas/phase explicitly.

Although most of these models were developed for incorporation into larger air quality models, they are by far too comprehensive for global modeling (see Chapter II). Even the equilibrium box-models (EQMs), which are relatively fast compared to the aerosol dynamic models, are not directly



suited for global modeling (the latter often incorporate EQMs, e.g. Pilinis et al., 2000). The reason is that all EQM schemes numerically solve the gas/aerosol equilibria, i.e. iteratively, by which the number of iterations needed to solve the equilibria strongly depend on the aerosol composition and the meteorological condition. For instance, if some aerosol compounds are predicted to be solid, additional iterations are needed to calculate both the liquid-solid phase transitions, and the partitioning between liquid / solid aerosol phases and the gas phase. Even in the relatively simple case of pure aqueous phase particles, the composition is solved iteratively because common calculation methods of the aerosol composition require information about the solute activity, which includes the aerosol associated water, and which determines the vapor pressure above the aerosol droplet (the iterative model structure is illustrated in Figure 2.1, Chapter II).

### **1.5 Modeling Demands**

The point of departure of this thesis is the insight that existing models (that can calculate the aerosol composition and the associated water uptake) are too comprehensive and computationally expensive for global modeling. Consequently, aerosol composition and water uptake have been only recently investigated on a global scale (Metzger et al., 1999; Adams et al., 1999). A second premise in this work is that the computational costs of the aerosol calculations should be in reasonable balance with other calculations in both CTMs and GCMs. This would finally allow to routinely calculate aerosol composition, including aerosol associated water, on timescales of decades to centuries, by which the accuracy of the aerosol calculations need not necessarily exceed that of other processes in the model.

To reduce the computational costs of the gas/aerosol partitioning calculations, different approaches have been proposed as an alternative to the iterative calculations. These range from neural networks (Potukuchi et al., 1997) to obtain the gas partial pressure of the equilibrium composition, the use of pre-calculated sets of activity coefficients which are the crucial part of the iteration procedure (Nenes et al., 1998), to polynomial fits to pre-calculated activity coefficients (Metzger et al., 1999).

However, none of the above methods provides a real alternative for global modeling. Therefore, a new thermodynamic gas/aerosol partitioning model, called EQSAM (Equilibrium Simplified Aerosol Model), will be introduced in this thesis, which determines the gas/aerosol partitioning sufficiently fast and accurate for global modeling. The simplified gas/aerosol module is based on a new method, which allows to analytically calculate activity coefficients and aerosol equilibria, according to the activity coefficient - RH relationship (Metzger et al., 1999, see Chapter III). Because this new method utilizes fundamental physical relations, such as the vapor pressure reduction and the generalization of Raoult's law, computing time demanding numerical solutions are avoided, allowing to solve gas/aerosol partitioning non-iteratively.

## 1.6 Thesis Outline

The central questions are:

1. Is it possible to simplify the gas/aerosol partitioning calculations so that multicomponent aerosols can be routinely calculated within global atmospheric chemistry and climate models?
2. What is the global aerosol budget?
3. Is gas/aerosol partitioning relevant for global atmospheric chemistry modeling?

Therefore, this work focuses on: a) the development of a simplified method to calculate gas/aerosol partitioning and multicomponent aerosols, including aerosol associated water, within global atmospheric chemistry and climate models; b) the subsequent development of a simplified aerosol model; c) the comparison of this simplified model with more complex thermodynamic models; d) the estimation of the uncertainties inherent in the simplified method relative to various other uncertainties which are associated with the assumptions on the aerosol state, i.e. gas/liquid/solid partitioning, gas/liquid partitioning, combination of both (hysteresis), or non-thermodynamical uncertainties, such as associated with different model resolutions or the use of different boundary layer mixing schemes; e) global gas/aerosol partitioning calculations; and f) the comparison of the model calculations with measurements.

In Chapter II, the present concept of equilibrium models will be reviewed. Based on the assumptions generally made, a new approach for the activity coefficient calculation will be introduced in Chapter III. This approach will be applied to various EQMs in use, and the sensitivity of activity coefficients will be evaluated. The results of the sensitivity study will then lead to further assumptions, and subsequently to new thermodynamic gas/aerosol partitioning model, called EQSAM (Equilibrium Simplified Aerosol Model), for global modeling.

In Chapter IV, EQSAM will be applied to various modeling tasks. First, EQSAM will be compared with various EQMs presently in use in box-model, and secondly, in so-called global offline calculations. Third, in so-called online calculations, EQSAM will be applied to global atmospheric chemistry modeling and compared with a state-of-the-art equilibrium routine, by coupling both routines into an atmospheric/chemistry transport model.

In Chapter V, results of global gas/aerosol calculations will be investigated, focusing on the space-time variability, the gas/aerosol partitioning, the vertical distribution, the feedback of the gas/aerosol calculations on chemistry, the global aerosol budgets. In Chapter VI, the assumptions made on the aerosol state will be evaluated with various sensitivity runs and compared with uncertainties of non-thermodynamic origin. In Chapter VII, results of the online gas/aerosol calculations will be compared with ground-based measurements of various European sites.

The thesis closes with a discussion of the main results; conclusions will be drawn with respect to future investigations. A summary in English, and Dutch is presented before this introduction.



## Chapter II: Equilibrium Models and Modeling Theory

Generally, two different types of models can calculate the aerosol composition and the aerosol associated water mass: thermodynamic gas/aerosol equilibrium models and aerosol dynamic models. From these models we focus, for reasons given below, on the equilibrium models (EQMs), and in particular on the following EQMs which will be used later: MARS (Saxena et al., 1986; Binkowski, 1991), SEQUILIB (Pilinis and Seinfeld, 1987), SCAPE (Kim et al., 1993ab, Kim and Seinfeld, 1995), SCAPE2 (Meng et al. 1998), and ISORROPIA (Nenes et al., 1998). Both SCAPE versions are based on Kim et al. (1993a,b), but differ in the representation of carbonates.

To derive a parameterization for global modeling, we first focus on the EQMs since aerosol dynamic models often include EQMs to calculate the aerosol composition which is then used to explicitly calculate the mass fluxes. For instance the new multicomponent aerosol dynamic model MADM (Pilinis et al., 2000) incorporates the EQM ISORROPIA. However, as we will see in the following (in particular in Chapter 4.2.1), even this EQM is by far too comprehensive and expensive for global atmosphere/chemistry and climate modeling, so that alternative aerosol thermodynamic models are needed. Before we introduce an alternative model in chapter III, we will discuss here the important aspects of the modeling theory, and the assumptions on which EQMs are generally based. From the same assumptions, we will then develop a new method, and subsequently a new and simplified EQM (Chapter III).

This chapter only presents a review of the present understanding of the aerosol thermodynamics with respect to the formulation of the thermodynamic gas/aerosol equilibrium models, according to the literature of Denbigh (1981), Seinfeld (1986), Seinfeld and Pandis (1998), and Wexler and Potukuchi (1998), and the references therein. Crucial aspects of the modeling theory/assumptions, which are important for the new method (developed in the next chapter), are highlighted.

### 2.1 General Overview

The thermodynamical gas/aerosol equilibrium models presented (Chapter 1.4) can calculate the equilibrium partitioning of the gas-liquid-solid aerosol phases of various aerosol compounds most relevant to air pollution modeling. The models differ in their degree of complexity, as well as in computational and thermodynamic approaches. Generally, they treat sulfate, ammonium, and nitrate species. Some, for instance SEQUILIB and ISORROPIA, include sodium and chloride, whereas in SCAPEa,b potassium, calcium and magnesium as important crustal constituents have been added. The species considered in various EQMs are listed in [Table 2.1](#) (list not complete, see introduction).

**Table 2.1. Comparison of Chemical Components in Equilibrium Models.**

	EQUIL / KEQUIL <sup>b</sup>	MARS	SEQUILIB	AIM	SCAPE <sup>c</sup>	ISORROPIA <sup>f</sup>
Species	SO <sub>4</sub> <sup>2-</sup> , NO <sub>3</sub> <sup>-</sup> , NH <sub>4</sub> <sup>+</sup>	SO <sub>4</sub> <sup>2-</sup> , NO <sub>3</sub> <sup>-</sup> , NH <sub>4</sub> <sup>+</sup>	SO <sub>4</sub> <sup>2-</sup> , NO <sub>3</sub> <sup>-</sup> , NH <sub>4</sub> <sup>+</sup> , Na <sup>+</sup> , Cl <sup>-</sup>	SO <sub>4</sub> <sup>2-</sup> , NO <sub>3</sub> <sup>-</sup> , NH <sub>4</sub> <sup>+</sup> , Na <sup>+</sup> , Cl <sup>-</sup>	SO <sub>4</sub> <sup>2-</sup> , NO <sub>3</sub> <sup>-</sup> , NH <sub>4</sub> <sup>+</sup> , Na <sup>+</sup> , Cl <sup>-</sup> , K <sup>+</sup> , Ca <sup>2+</sup> , Mg <sup>2+</sup>	SO <sub>4</sub> <sup>2-</sup> , NO <sub>3</sub> <sup>-</sup> , NH <sub>4</sub> <sup>+</sup> , Na <sup>+</sup> , Cl <sup>-</sup>
Number of reactions <sup>d</sup>	13[7]	7[6]	13[5]	.. <sup>e</sup>	25[6]	13[5]
Number of components	16	16	22	20	37	22
Liquid components	H <sup>+</sup> , NH <sub>4</sub> <sup>+</sup> , NO <sub>3</sub> <sup>-</sup> , HSO <sub>4</sub> <sup>-</sup> , SO <sub>4</sub> <sup>2-</sup> , H <sub>2</sub> O	H <sup>+</sup> , NH <sub>4</sub> <sup>+</sup> , NO <sub>3</sub> <sup>-</sup> , HSO <sub>4</sub> <sup>-</sup> , SO <sub>4</sub> <sup>2-</sup> , H <sub>2</sub> O, NH <sub>3</sub>	H <sup>+</sup> , NH <sub>4</sub> <sup>+</sup> , Na <sup>+</sup> , NO <sub>3</sub> <sup>-</sup> , Cl <sup>-</sup> , HSO <sub>4</sub> <sup>-</sup> , SO <sub>4</sub> <sup>2-</sup> , H <sub>2</sub> SO <sub>4</sub> , H <sub>2</sub> O	H <sup>+</sup> , NH <sub>4</sub> <sup>+</sup> , Na <sup>+</sup> , NO <sub>3</sub> <sup>-</sup> , Cl <sup>-</sup> , HSO <sub>4</sub> <sup>-</sup> , SO <sub>4</sub> <sup>2-</sup> , H <sub>2</sub> O	H <sup>+</sup> , NH <sub>4</sub> <sup>+</sup> , Na <sup>+</sup> , K <sup>+</sup> , Ca <sup>2+</sup> , Mg <sup>2+</sup> , NO <sub>3</sub> <sup>-</sup> , Cl <sup>-</sup> , OH <sup>-</sup> , HSO <sub>4</sub> <sup>-</sup> , SO <sub>4</sub> <sup>2-</sup> , H <sub>2</sub> SO <sub>4</sub> , H <sub>2</sub> O	Same as SEQUILIB
Solid components	NH <sub>4</sub> NO <sub>3</sub> , NH <sub>4</sub> HSO <sub>4</sub> , (NH <sub>4</sub> ) <sub>2</sub> SO <sub>4</sub> , (NH <sub>4</sub> ) <sub>3</sub> H(SO <sub>4</sub> ) <sub>2</sub> , (NH <sub>4</sub> ) <sub>2</sub> SO <sub>4</sub> · 2NH <sub>4</sub> NO <sub>3</sub> , (NH <sub>4</sub> ) <sub>2</sub> SO <sub>4</sub> · 3NH <sub>4</sub> NO <sub>3</sub>	NH <sub>4</sub> NO <sub>3</sub> , NH <sub>4</sub> HSO <sub>4</sub> , (NH <sub>4</sub> ) <sub>2</sub> SO <sub>4</sub> , (NH <sub>4</sub> ) <sub>3</sub> H(SO <sub>4</sub> ) <sub>2</sub>	NH <sub>4</sub> NO <sub>3</sub> , NH <sub>4</sub> Cl, NH <sub>4</sub> HSO <sub>4</sub> , (NH <sub>4</sub> ) <sub>2</sub> SO <sub>4</sub> , (NH <sub>4</sub> ) <sub>3</sub> H(SO <sub>4</sub> ) <sub>2</sub> , NaNO <sub>3</sub> , NaCl, NaHSO <sub>4</sub> , Na <sub>2</sub> SO <sub>4</sub>	Same as SEQUILIB	Same as SEQUILIB + KNO <sub>3</sub> , KCl, KHSO <sub>4</sub> , K <sub>2</sub> SO <sub>4</sub> , Ca(NO <sub>3</sub> ) <sub>2</sub> , CaCl <sub>2</sub> , CaSO <sub>4</sub> , Mg(NO <sub>3</sub> ) <sub>2</sub> , MgCl <sub>2</sub> , MgSO <sub>4</sub>	Same as SEQUILIB
Gas components	NH <sub>3</sub> , HNO <sub>3</sub> , H <sub>2</sub> SO <sub>4</sub> , H <sub>2</sub> O	NH <sub>3</sub> , HNO <sub>3</sub> , H <sub>2</sub> O	NH <sub>3</sub> , HNO <sub>3</sub> , HCl, H <sub>2</sub> O	NH <sub>3</sub> , HNO <sub>3</sub> , HCl, H <sub>2</sub> O	NH <sub>3</sub> , HNO <sub>3</sub> , HCl, H <sub>2</sub> O	NH <sub>3</sub> , HNO <sub>3</sub> , HCl, H <sub>2</sub> O

<sup>a</sup> EQUIL: Basset and Seinfeld (1983); KEQUIL: Basset and Seinfeld (1984); MARS: Saxena et al. (1986) (revised by Binkowski (1991)); SEQUILIB: Pilinis and Seinfeld (1987); AIM: Wexler and Seinfeld (1991); SCAPE: Kim et al. (1993a,b); Kim and Seinfeld (1995); Nenes et al. (1998).

<sup>b</sup> KEQUIL same as EQUIL except that the 'Kelvin' effect is considered.

<sup>c</sup> a recent update of SCAPE, which has been used for this work, includes carbonates and size-segregation.

<sup>d</sup> Number in brackets is the number of equilibria not involving solids.

<sup>e</sup> Reactions are not considered in AIM.

<sup>f</sup> same reactions considered as in SEQUILIB but code numerically optimized in terms of speed and accuracy.

While the more comprehensive EQMs (e.g. EQUIL and KEQUIL) do not apply approximations on the equilibrium concentrations - they solve a set of nonlinear equations for the chemical potentials to calculate equilibrium concentrations - they require, as a consequence, relatively large amounts of computing time. MARS and SEQUILIB are much simpler and therefore computationally more efficient, but include approximations on the equilibrium concentrations. These latter models were developed for incorporation into larger air quality models, as was SCAPE. SCAPE, however, has less limiting assumptions, although it is the most comprehensive of all EQMs in terms of species considered. SCAPE also uses consistent thermodynamic data and includes the temperature dependence of thermodynamical parameters such as equilibrium constants and deliquescence relative humidities, which is, for instance, not considered in MARS. Its results have been comprehensively compared with other EQMs (Kim et al., 1993a,b; Zhang et al., 1999a,b), and with measurements (Meng et al., 1995; 1998; Hayami et al. 1997; Hayami and Carmichael, 1997; 1998).

The most sophisticated EQM in terms of accuracy and computational efficiency is ISORROPIA. For instance, it uses mutual deliquescence relative humidities (MDRH) of various species. Special

attention was devoted to make ISORROPIA as fast and computationally efficient as possible. For instance, the system of nonlinear equations were ordered and written in a way so that analytical solutions could be obtained for as many equations as possible. Expensive numerical solutions were minimized, since the number of iterations performed during the numerical solution determines to a large degree the computational burden - considerably speeding up ISORROPIA compared to the previous EQMs. In addition, ISORROPIA uses an internal database of pre-calculated aerosol properties (binary activity coefficients), which therefore need not be calculated during runtime.

## 2.2 General Assumptions

To model the gas/aerosol partitioning, assumptions are made with respect to the computational efficiency. For instance, it is mostly assumed that aerosols are internally mixed, and that they obey thermodynamic gas/aerosol equilibria. Both assumptions are safely made under moderate atmospheric conditions, since most inorganic compounds form highly hygroscopic salts or are acids, and hence, take up so much water vapor so that they are deliquescent and internally mixed. In addition, the thermodynamic gas/aerosol equilibrium models presented here are developed for air pollution modeling. In polluted regions the condensation of the aerosol precursor gases on pre-existing particles is pre-dominant and new particle formation (nucleation) can be ignored. The nucleation is therefore not considered in any EQM, nor the condensation on very small particles, because very fine particles do not add much to the total aerosol mass (note that these dynamic processes are usually included in the overall aerosol module of which the EQM is a component). Therefore, the Kelvin effect, which accounts for an increase in equilibrium vapor pressure with decreasing particle diameter due to an enhanced surface curvature, is not considered in any of the EQMs presented, except by Basset and Seinfeld (1984); they have included the Kelvin-effect into the same model as used in Basset and Seinfeld (1983) and concluded that it is only important for very small particles ( $\varnothing < 0.05 \mu\text{m}$ ).

Thus, for the calculation of the mass and composition of aerosols, the common assumption is made that volatile species in the gas and aerosol phases are in chemical equilibrium (Stelson and Seinfeld, 1982; Basset and Seinfeld, 1983, 1984; Saxena et al. 1986; Pilinis and Seinfeld, 1987). Although in many cases this has proven to be a valid assumption, there are situations in which the time needed to achieve chemical equilibrium is long compared to the time during which local air and particles remain in contact. When this happens, the equilibrium approach is not valid and a model incorporating transfer processes should be applied (Wexler and Seinfeld, 1990; 1991). Although experimental evidence for the non-equilibrium state has been found (Allen et al., 1989), for marine aerosols and/or warmer environments the equilibrium assumption is valid and has been experimentally confirmed (Hildemann et al., 1984; Quinn et al., 1992). In addition, box model calculations (Meng and Seinfeld, 1996) have shown that the time required for gas/aerosol equilibration depends primarily on the aerosol size and less on the temperature; small particles have a larger surface to volume ratio than larger particles and therefore equilibrate faster. The

equilibration times of the relevant aerosol components have been shown to be in the order of minutes (Khlystov 1998; Dassios and Pandis, 1999).

- Note that these time scales usually encompass the time steps of global atmosphere/chemistry models, calculating chemistry and transport processes, so that the equilibrium approach can be assumed to be sufficient for global modeling, especially if only accumulation mode particles are considered (such as ammonium-sulfate-nitrate compounds).

### 2.3 Equilibrium Constants

To calculate the equilibrium composition of atmospheric aerosols, a set of non-linear equations for the chemical potentials is usually solved to obtain the equilibrium concentrations.

Generally, a closed multiphase system is in chemical equilibrium, if changes in the total Gibbs free energy,  $G$ , of the system are at a minimum. With the definition of  $G$ ,  $G \equiv U + p \cdot V - T \cdot S$ , a differential change can be expressed as

$$dG = dU + p \cdot dV + V \cdot dp - T \cdot dS - S \cdot dT. \quad (2.1)$$

$U$  denotes the internal energy,  $T$  the temperature,  $S$  the entropy,  $p$  the pressure and  $V$  the volume. Eliminating  $dU$  with the Gibbs-relation gives

$$dG = \sum_i \mu_i \cdot dn_i + V \cdot dp - S \cdot dT, \quad (2.2)$$

where  $\mu_i$  and  $n_i$  are the chemical potential and number of moles of compound  $i$ , respectively.

For a given temperature and pressure,  $dT = 0$  and  $dp = 0$ , Eq. (2.2) reduces to

$$dG|_{T,p} = \sum_i \mu_i \cdot dn_i = 0. \quad (2.3)$$

If the system is restricted to only one chemical reaction, the amount of each component in the system can be expressed as  $n_i = n_i^o + \nu_i \cdot \varepsilon$  where  $n_i^o$  is the initial amount of each compound;  $\nu_i$  is their stoichiometric coefficients and  $\varepsilon$  the reaction coordinate. Taking the derivative,  $dn_i = \nu_i \cdot d\varepsilon$ , which when substituted into Eq. (2.3) gives (Denbigh, 1981)

$$\sum_i \nu_i \cdot \mu_i = 0. \quad (2.4)$$

The chemical potentials,  $\mu_i$ , of each compound can be expressed in terms of their activities,  $a_i$  (defined later in this section), by which  $\mu_i = \mu_i^o + R \cdot T \cdot \ln a_i$ , with  $\mu_i^o$  the chemical potential at a standard state, and  $R$  the universal gas constant. Substitution into equation (2.4) yields  $\sum_i \nu_i \mu_i^o + RT \sum_i \nu_i \ln a_i = 0$ , and the sum of logarithms, which is equal to the logarithm of the product, yields, upon exponentiation of both sides, the required expression for the equilibrium constant,  $K$  (of a given equilibrium reaction):

$$\exp [- 1 / ( R \cdot T) \cdot \sum_i ( v_i \cdot \mu_i^o ) ] = \prod_i a_i^{v_i} = K. \quad (2.5)$$

The temperature dependence of the equilibrium constant is calculated using the van't Hoff equation

$$d \ln K ( T) / d T = \Delta H ( T) / ( R \cdot T^2 ), \quad (2.6)$$

where  $\Delta H ( T)$  is the standard molar enthalpy change of the reaction at temperature  $T$ . For a small temperature range, a change in  $H$  can be approximated by

$$\Delta H ( T) = \Delta H^o ( T_o) + \Delta C_p^o \cdot ( T - T_o). \quad (2.7)$$

$\Delta H^o ( T)$  denotes the standard molar enthalpy change of the reaction at a reference temperature  $T_o$ , (usually the standard-state temperature 298.15 K), and  $\Delta C_p^o ( T)$  the change of the standard molar heat capacity at constant pressure compared to  $T_o$ ; it is implicitly assumed here that  $\Delta H_f^o$  and  $\Delta C_p^o$  are constant over the temperature range  $T - T_o$ .

Substituting Eq. (2.7) into Eq. (2.6) and integrating over  $T$  to  $T_o$ , the temperature dependency of the equilibrium constant is obtained:

$$K ( T) = K ( T_o) \cdot \exp [ - \Delta H^o / ( R \cdot T_o) \cdot ( T_o / T - 1) - \Delta C_p^o / R \cdot ( 1 + \ln ( T_o / T) - T_o / T ) ]. \quad (2.8)$$

The data on  $\Delta G_f^o$ ,  $\Delta H_f^o$ , and  $\Delta C_p^o$  (which are needed to calculate equilibrium constants and their temperature dependence) can be obtained, for instance, from the NBS Thermodynamic Tables of Wagman et al. (1982).

Finally, the activity of a single-salt solution containing an  $i$ - $j$  ion pair (used in Eq. 2.5), is usually expressed as (Robinson and Stokes, 1965)

$$a_{ij} = a_i^{v_i} \cdot a_j^{v_j} = (m_i \cdot \gamma_i)^{v_i} \cdot (m_j \cdot \gamma_j)^{v_j} = m_i^{v_i} \cdot m_j^{v_j} \cdot \gamma_{ij}^v, \quad (2.9)$$

with  $v = v_i + v_j$  and  $v_i$  the number of moles of ions  $i$  per 1 mol of  $i$ - $j$  ion pair dissociating completely.  $m_i$  denotes the molality, i.e. the concentration of the solution, and is defined as mole solute per kg solvent (water).  $\gamma_{ij}$  is the mean binary activity coefficient of the  $i$ - $j$  ion pair.

Eq. (2.5), in terms of activity coefficients and molality, becomes

$$K = \prod_i (m_i \cdot \gamma_i)^{v_i}, \quad (2.10)$$

where subscript  $i$  denotes an ion pair. The equilibrium constants and the thermodynamic data, as used in the SCAPE EQM and partly in other EQMs, are listed in [Table 2.2](#).



**Table 2.2. Equilibrium relation constants used in SCAPE**

$\text{NH}_3(\text{g}) = \text{NH}_3(\text{aq})$	$\frac{[\text{NH}_3(\text{aq})] \gamma_{\text{NH}_3}}{P_{\text{NH}_3}}$	57.639	13.79	-5.39	mol / kg atm
$\text{HNO}_3(\text{g}) = \text{H}^+(\text{aq}) + \text{NO}_3^-(\text{aq})$	$\frac{[\text{H}^+][\text{NO}_3^-] \gamma_{\text{H}^+} \gamma_{\text{NO}_3^-}}{P_{\text{HNO}_3}}$	$2.511 \times 10^6$	29.17	16.83	mol <sup>2</sup> / kg <sup>2</sup> atm
$\text{HCl}(\text{g}) = \text{H}^+(\text{aq}) + \text{Cl}^-(\text{aq})$	$\frac{[\text{H}^+][\text{Cl}^-] \gamma_{\text{H}^+} \gamma_{\text{Cl}^-}}{P_{\text{HCl}}}$	$1.971 \times 10^6$	30.20	19.91	mol <sup>2</sup> / kg <sup>2</sup> atm
$\text{H}_2\text{O}(\text{aq}) = \text{H}^+(\text{aq}) + \text{OH}^-(\text{aq})$	$\frac{[\text{H}^+][\text{OH}^-] \gamma_{\text{H}^+} \gamma_{\text{OH}^-}}{a_w}$	$1.010 \times 10^{-14}$	-22.52	26.92	mol <sup>2</sup> / kg <sup>2</sup>
$\text{NH}_3(\text{aq}) + \text{H}_2\text{O}(\text{aq}) = \text{NH}_4^+(\text{aq}) + \text{OH}^-(\text{aq})$	$\frac{[\text{NH}_4^+][\text{OH}^-] \gamma_{\text{NH}_4^+} \gamma_{\text{OH}^-}}{[\text{NH}_3(\text{aq})] \gamma_{\text{NH}_3} a_w}$	$1.805 \times 10^{-5}$	-1.50	26.92	mol / kg
$\text{HSO}_4^-(\text{aq}) = \text{H}^+(\text{aq}) + \text{SO}_4^{2-}(\text{aq})$	$\frac{[\text{H}^+][\text{SO}_4^{2-}] \gamma_{\text{H}^+} \gamma_{\text{SO}_4^{2-}}}{[\text{HSO}_4^-] \gamma_{\text{HSO}_4^-}}$	$1.015 \times 10^{-2}$	8.85	25.14	mol / kg
$\text{NH}_4\text{Cl}(\text{s}) = \text{NH}_3(\text{g}) + \text{HCl}(\text{g})$	$P_{\text{NH}_3} P_{\text{HCl}}$	$1.086 \times 10^{-16}$	-71.00	2.40	atm <sup>2</sup>
$\text{NH}_4\text{NO}_3(\text{s}) = \text{NH}_3(\text{g}) + \text{HNO}_3(\text{g})$	$P_{\text{NH}_3} P_{\text{HNO}_3}$	$5.746 \times 10^{-17}$	-74.38	6.12	atm <sup>2</sup>
$(\text{NH}_4)_2\text{SO}_4(\text{s}) = 2 \text{NH}_4^+(\text{aq}) + \text{SO}_4^{2-}(\text{aq})$	$[\text{NH}_4^+]^2 [\text{SO}_4^{2-}] \gamma_{\text{NH}_4^+}^2 \gamma_{\text{SO}_4^{2-}}$	1.817	-2.65	38.57	mol <sup>3</sup> / kg <sup>3</sup>
$\text{NH}_4\text{HSO}_4(\text{s}) = \text{NH}_4^+(\text{aq}) + \text{HSO}_4^-(\text{aq})$	$[\text{NH}_4^+][\text{HSO}_4^-] \gamma_{\text{NH}_4^+} \gamma_{\text{HSO}_4^-}$	$1.383 \times 10^4$	-2.87	15.83	mol <sup>2</sup> / kg <sup>2</sup>
$(\text{NH}_4)_3\text{H}(\text{SO}_4)_2(\text{s}) = 3 \text{NH}_4^+(\text{aq}) + \text{HSO}_4^-(\text{aq}) + \text{SO}_4^{2-}(\text{aq})$	$[\text{NH}_4^+]^3 [\text{HSO}_4^-] [\text{SO}_4^{2-}] \gamma_{\text{NH}_4^+}^3 \gamma_{\text{HSO}_4^-} \gamma_{\text{SO}_4^{2-}}$	29.72	-5.19	54.40	mol <sup>5</sup> / kg <sup>5</sup>
$\text{NaCl}(\text{s}) = \text{Na}^+(\text{aq}) + \text{Cl}^-(\text{aq})$	$[\text{Na}^+][\text{Cl}^-] \gamma_{\text{Na}^+} \gamma_{\text{Cl}^-}$	37.661	-1.56	16.90	mol <sup>2</sup> / kg <sup>2</sup>
$\text{NaNO}_3(\text{s}) = \text{Na}^+(\text{aq}) + \text{NO}_3^-(\text{aq})$	$[\text{Na}^+][\text{NO}_3^-] \gamma_{\text{Na}^+} \gamma_{\text{NO}_3^-}$	11.971	-8.22	16.01	mol <sup>2</sup> / kg <sup>2</sup>
$\text{Na}_2\text{SO}_4(\text{s}) = \text{Na}^+(\text{aq}) + \text{SO}_4^{2-}(\text{aq})$	$[\text{Na}^+]^2 [\text{SO}_4^{2-}] \gamma_{\text{Na}^+}^2 \gamma_{\text{SO}_4^{2-}}$	$4.799 \times 10^{-1}$	0.98	39.75	mol <sup>3</sup> / kg <sup>3</sup>
$\text{NaHSO}_4(\text{s}) = \text{Na}^+(\text{aq}) + \text{HSO}_4^-(\text{aq})$	$[\text{Na}^+][\text{HSO}_4^-] \gamma_{\text{Na}^+} \gamma_{\text{HSO}_4^-}$	$2.413 \times 10^4$	0.79	14.746	mol <sup>2</sup> / kg <sup>2</sup>
$\text{KCl}(\text{s}) = \text{K}^+(\text{aq}) + \text{Cl}^-(\text{aq})$	$[\text{K}^+][\text{Cl}^-] \gamma_{\text{K}^+} \gamma_{\text{Cl}^-}$	8.680	-6.902	19.95	mol <sup>2</sup> / kg <sup>2</sup>
$\text{KNO}_3(\text{s}) = \text{K}^+(\text{aq}) + \text{NO}_3^-(\text{aq})$	$[\text{K}^+][\text{NO}_3^-] \gamma_{\text{K}^+} \gamma_{\text{NO}_3^-}$	0.872	-14.08	19.39	mol <sup>2</sup> / kg <sup>2</sup>
$\text{K}_2\text{SO}_4(\text{s}) = 2\text{K}^+(\text{aq}) + \text{SO}_4^{2-}(\text{aq})$	$[\text{K}^+]^2 [\text{SO}_4^{2-}] \gamma_{\text{K}^+}^2 \gamma_{\text{SO}_4^{2-}}$	$1.569 \times 10^{-2}$	-9.585	45.81	mol <sup>3</sup> / kg <sup>3</sup>
$\text{KHSO}_4(\text{s}) = \text{K}^+(\text{aq}) + \text{HSO}_4^-(\text{aq})$	$[\text{K}^+][\text{HSO}_4^-] \gamma_{\text{K}^+} \gamma_{\text{HSO}_4^-}$	24.016	-8.423	17.96	mol <sup>2</sup> / kg <sup>2</sup>
$\text{CaCl}_2(\text{s}) = \text{Ca}^{2+}(\text{aq}) + 2\text{Cl}^-(\text{aq})$	$[\text{Ca}^{2+}][\text{Cl}^-]^2 \gamma_{\text{Ca}^{2+}} \gamma_{\text{Cl}^-}^2$	$7.974 \times 10^{11}$	--	--	mol <sup>3</sup> / kg <sup>3</sup>
$\text{Ca}(\text{NO}_3)_2(\text{s}) = \text{Ca}^{2+}(\text{aq}) + 2\text{NO}_3^-(\text{aq})$	$[\text{Ca}^{2+}][\text{NO}_3^-]^2 \gamma_{\text{Ca}^{2+}} \gamma_{\text{NO}_3^-}^2$	$6.067 \times 10^5$	--	--	mol <sup>3</sup> / kg <sup>3</sup>
$\text{CaSO}_4 \cdot 2\text{H}_2\text{O}(\text{s}) = \text{Ca}^{2+}(\text{aq}) + \text{SO}_4^{2-}(\text{aq}) + 2 \text{H}_2\text{O}$	$[\text{Ca}^{2+}][\text{SO}_4^{2-}] \gamma_{\text{Ca}^{2+}} \gamma_{\text{SO}_4^{2-}} a_w^2$	$4.319 \times 10^{-5}$	--	--	mol <sup>2</sup> / kg <sup>2</sup>
$\text{MgCl}_2(\text{s}) = \text{Mg}^{2+}(\text{aq}) + 2\text{Cl}^-(\text{aq})$	$[\text{Mg}^{2+}][\text{Cl}^-]^2 \gamma_{\text{Mg}^{2+}} \gamma_{\text{Cl}^-}^2$	$9.577 \times 10^{21}$	--	--	mol <sup>3</sup> / kg <sup>3</sup>
$\text{Mg}(\text{NO}_3)_2(\text{s}) = \text{Mg}^{2+}(\text{aq}) + 2\text{NO}_3^-(\text{aq})$	$[\text{Mg}^{2+}][\text{NO}_3^-]^2 \gamma_{\text{Mg}^{2+}} \gamma_{\text{NO}_3^-}^2$	$2.507 \times 10^{15}$	--	--	mol <sup>3</sup> / kg <sup>3</sup>
$\text{MgSO}_4(\text{s}) = \text{Mg}^{2+}(\text{aq}) + \text{SO}_4^{2-}(\text{aq})$	$[\text{Mg}^{2+}][\text{SO}_4^{2-}] \gamma_{\text{Mg}^{2+}} \gamma_{\text{SO}_4^{2-}}$	$1.079 \times 10^5$	--	--	mol <sup>2</sup> / kg <sup>2</sup>

<sup>a</sup> Constants  $a$  and  $b$  are in  $K = K(T_0) \cdot \exp\left[a\left(\frac{T_0}{T} - 1\right) - b\left(1 + \ln\left(\frac{T_0}{T}\right) - \frac{T_0}{T}\right)\right]$ , where  $T_0 = 298 \text{ K}$ .

Aerosol equilibrium is calculated from Eq. (2.10). The equilibrium composition therefore depends on the solute activity (Eq. 2.5), by which the activity  $a_i$  is expressed in terms of molality,  $m_i$ , and activity coefficient,  $\gamma_i$ , in order to account for the effect of non-ideal behavior at high ionic strength on equilibria.

For the *gas phase*, the activity is defined as  $a_i = p_i/p$ , with  $p_i$  the partial pressure of the compound  $i$  and the atmospheric pressure  $p$ , since all vapors considered (e.g. water vapor, ammonia and nitric acid), are at sufficiently low partial pressures, so that they are assumed to behave as an ideal solution of ideal gases. In the *crystalline phase*, the compound is assumed to be pure and the activity is unity,  $a_i = 1$ . In solid solutions (supersaturated solutions, where individual compounds can crystallize) the activities of the compound may be less than unity, but these cases are not considered. However, *aqueous solutions* of atmospheric aerosols are often highly concentrated, so that activity coefficients must be known to obtain the solute activity, i.e.  $a_i = m_i \gamma_i$ . Thus, activity coefficients are needed only for the for the aqueous phase.

## 2.4 Concentration Domains

Most EQMs have been developed for incorporation into larger air quality models. To increase the efficiency of the calculations, the total number of equilibrium reactions are minimized by making use of certain concentration domains, so that each of which contains fewer species than the entire set of possible aerosol compositions.

These domains are based on the following assumptions. Because sulfuric acid has a very low vapor pressure, it is assumed that it resides completely in the aerosol phase. The same assumption is made for sodium. Depending on the amount of sodium and ammonia, sulfate can be either completely or partially neutralized. In some EQMs, there is also the possibility of complete neutralization of sulfuric acid by sodium alone. In each of these cases, the possible species are different. To determine which case is considered, two parameters can be defined (following Nenes et al. 1998).

$$(i) \quad R_{SO_4} = ([Na^+] + [NH_4^+]) / [SO_4^{2-}]$$

$$(ii) \quad R_{Na} = [Na^+] / [SO_4^{2-}]$$

$R_{SO_4}$  is known as the sulfate ratio, while  $R_{Na}$  is the sodium ratio. The concentrations are expressed in molar units. Based on the value of these two ratios, four domains (types of aerosols) are usually defined:

- **Sulfate very rich (free acid):** This applies to  $R_{SO_4} < 1$ . Sulfate occurs in excess and part of it is in the form of free sulfuric acid. In this case, there is always a liquid phase, because sulfuric acid is extremely hygroscopic (i.e., no RHD is assumed).
- **Sulfate rich (non free acid):** This applies to  $1 < R_{SO_4} < 2$ . There is enough ammonia and sodium to partially (but not fully) neutralize the sulfates. The sulfates are a mixture of bisulfates and sulfates, the ratio of which is determined by thermodynamic equilibrium.
- **Sulfate neutral (both sulfate and sodium poor):**  $R_{SO_4} > 2$ ;  $R_{Na} < 2$ . There is enough ammonia and sodium to fully neutralize the sulfates, but sodium does not neutralize the sulfates by itself.

In this case, excess ammonia can react with the other species ( $\text{HNO}_3$ ,  $\text{HCl}$ ) to form volatile salts.

- **Sulfate poor, sodium rich:**  $R_{\text{SO}_4} > 2$ ;  $R_{\text{Na}} > 2$ . There is enough sodium to fully neutralize the sulfates. In this case, ammonia and excess sodium can react with the other gaseous species ( $\text{HNO}_3$ ,  $\text{HCl}$ ) to form salts, while no ammonium sulfate is formed (since all sulfates have been neutralized with sodium).

For each domain approximations are made for certain concentrations:

- the concentrations of  $\text{H}^+$  and  $\text{HSO}_4^-$  are assumed to be negligible for the sulfate-poor case;
- for some sulfate rich, very rich cases, the  $\text{SO}_4^{2-}$  concentration is assumed to be zero;
- ammonia gas,  $\text{NH}_3(\text{g})$ , is assumed to be zero for the sulfate-rich and very rich case;
- for the cases in which the  $\text{RH}$  is lower than the lowest deliquescence point, it is assumed that the particle is a pure solid.

Subsequently, each concentration domain is divided into several subdomains, according to the regime of deliquescence relative humidity to which the considered ions in the solution corresponds.

## 2.5 Relative Humidity of Deliquescence

Whether gas-aerosol equilibria are calculated between the gas phase and a pure solid or ions in an aqueous solution, or an aerosol with both aqueous and solid phases, depends on the deliquescence behavior of the considered aerosol compound. Certain salts, such as ammonium sulfate or ammonium nitrate deliquesce if the relative humidity reaches a certain value; below that these salts may be crystalline. However, certain aerosol mixtures (e.g. solutions containing sulfuric acid) do not deliquesce; they rather remain aqueous regardless the actual relative humidity. In EQMs, the deliquescence of various salt compounds is determined in corresponding subdomains. Generally, the deliquescence of salt aerosols depends on the ambient relative humidity ( $\text{RH}$ ) and temperature. The deliquescence behavior has been investigated for single salt solutions by, for instance, Wexler and Seinfeld (1991), and for multiple-salt solutions by e.g. Tang and Munkelwitz (1993).

The so-called relative humidity of deliquescence ( $\text{RHD}$ ) is approximated as follows (Wexler and Seinfeld, 1991). The relative humidity is defined as the ratio of  $p_w$ , the ambient partial pressure of water, to  $p_s$ , its saturation vapor pressure,  $\text{RH} = p_w/p_s$ . Taking the natural logarithm of both sides and differentiating with respect to temperature gives

$$d \ln \text{RH} / dT = d \ln p_w / dT - d \ln p_s / dT, \quad (2.11)$$

The  $\text{RH}$  on the left-hand side of equation (2.11) is the deliquescence point if the aerosol particles contain a solid phase in equilibrium with an aqueous phase. The terms on the right-hand side of

equation (2.11) can be evaluated using the Clausius-Clapeyron equation:

$$d \ln p / d T = \Delta H / (R \cdot T^2), \quad (2.12)$$

where the latent heat of vaporization,  $\Delta H$ , is dependent on the composition of the solution.

For pure water, the heat of vaporization is equal to the latent heat of water,  $\Delta H = L_{\text{pure}}$ . For the aqueous solution phase of the aerosol particle, a small amount of water evaporation coincides with a small amount of solute precipitation to maintain the solution molality constant so that the appropriate heat of vaporization is

$$\Delta H = L_{\text{solvent}} + M_w / 1000 \cdot \sum_i m_{\text{solute},i} \cdot L_{\text{solute},i}, \quad (2.13)$$

$M_w$  is the molar mass of water,  $m_{\text{solute},i}$  is the molality of electrolyte  $i$  that deliquesces,  $L_{\text{solvent}}$  and  $L_{\text{solute},i}$  are the latent heat of vaporization of water in the saturated solution and the latent heat of fusion of salt  $i$ , respectively (Denbigh, 1981; Tang and Munkelwitz, 1993).

Combining these expressions with equations (2.11) and (2.12) gives

$$d \ln RHD / d T = (L_{\text{solvent}} + M_w / 1000 \cdot \sum_i m_{\text{solute},i} \cdot L_{\text{solute},i} - L_{\text{pure}}) / (R \cdot T^2), \quad (2.14)$$

It is now assumed that the heat of vaporization of water is not altered substantially if it is pure or in solution, i.e.

$$M_w / 1000 \cdot \sum_i m_{\text{solute},i} \cdot L_{\text{solute},i} \gg L_{\text{solvent}} - L_{\text{pure}}, \quad (2.15)$$

so that equation (2.14) can be simplified to

$$d \ln RHD / d T = M_w / 1000 \cdot \sum_i (m_{\text{solute},i} \cdot L_{\text{solute},i}) / (R \cdot T^2), \quad (2.16)$$

It is further assumed that, for modest atmospheric temperature variations, the molality and latent heats are constant, so that equation (2.16) can be integrated to obtain the relative humidity of deliquescence (RHD) for a single salt particle

$$\ln [RHD(T) / RHD(T_o)] = - (M_w \cdot m_{\text{solute}} \cdot L_{\text{solute}}) / (R \cdot 1000) \cdot (1/T - 1/T_o). \quad (2.16a)$$

Accordingly, for multicomponent salt particles the mutual deliquescence relative humidity (MDRH) can be obtained

$$\ln [MDRH(T) / MDRH(T_o)] = - M_w / 100 \cdot \sum_i (m_{\text{solute},i} \cdot L_{\text{solute},i}) / R \cdot (1/T - 1/T_o), \quad (2.16b)$$

where  $RHD(T_o)$  and  $MDRH(T_o)$  are known (usually at  $T_o=298.15\text{K}$ ).

Equations (2.16a,b) agree well with experimental data over typical ambient temperature excursions (Wexler and Seinfeld, 1991). Tang and Munkelwitz (1993) proposed a more elaborate expression, but for moderate temperature ranges they showed that equations (2.16a,b) are adequate.

The MDRH (also known as the “eutonic point”) corresponds to the mixture with a composition that minimizes water activity. Below this point, a solid phase is thermodynamically favored. Consequentially, then RHD and MDRH points are used to determine when an aqueous phase is possible. The RHD values of various aerosol compounds as used in the SCAPE EQM, and partly in various other EQMs, are given in Table 2.3. The MDRH of various aerosol mixtures as used in the EQM ISORROPIA are given in Table 2.4.

**Table 2.3. Relative Humidities of Deliquescence (RHD) at 298.15 K and their temperature dependence as used in SCAPE**

Salt	RHD (298.15 K) x 100%	$\alpha^b$
NH <sub>4</sub> Cl	0.77	239
NH <sub>4</sub> NO <sub>3</sub>	0.61	852
(NH <sub>4</sub> ) <sub>2</sub> SO <sub>4</sub>	0.80	80
NH <sub>4</sub> HSO <sub>4</sub>	0.40 <sup>c</sup>	--
(NH <sub>4</sub> ) <sub>3</sub> H(SO <sub>4</sub> ) <sub>2</sub>	0.69 <sup>c</sup>	--
NaCl	0.75	25
NaNO <sub>3</sub>	0.74	304
Na <sub>2</sub> SO <sub>4</sub>	0.93 <sup>c</sup>	--
NaHSO <sub>4</sub>	0.52 <sup>c</sup>	--
KCl	0.84 <sup>d</sup>	179
KNO <sub>3</sub>	0.93 <sup>d</sup>	--
K <sub>2</sub> SO <sub>4</sub>	0.98 <sup>d</sup>	36
KHSO <sub>4</sub>	--	--
CaCl <sub>2</sub>	0.28 <sup>d</sup>	-1121
Ca(NO <sub>3</sub> ) <sub>2</sub>	0.49 <sup>d</sup>	-431
CaSO <sub>4</sub> · 2H <sub>2</sub> O	0.97 <sup>d</sup>	--
MgCl <sub>2</sub>	0.33 <sup>d</sup>	-1860
Mg(NO <sub>3</sub> ) <sub>2</sub>	--	--
MgSO <sub>4</sub>	0.86 <sup>d</sup>	-714

<sup>a</sup>  $\alpha$  in  $\ln RHD(T) = \ln RHD(T_0) - \alpha \left( \frac{1}{T} - \frac{1}{T_0} \right)$ , where  $T_0 = 298 \text{ K}$ . If no value is

given, temperature dependence is not considered for the species.

<sup>b</sup> RHD values are from Wexler and Seinfeld (1991) except otherwise indicated.

<sup>c</sup> Pilinis and Seinfeld (1987).

<sup>d</sup> refer to Kim and Seinfeld (1995), and the literature therein.

**Table 2.4. Mutual Deliquescence Relative Humidities (MDRH) at 298.15 K and their temperature dependence factors as used in ISORROPIA.**

Salt Mixture <sup>a</sup>	MDRH <sup>b</sup> (298.15 K) x100%	$\alpha^c$
NH <sub>4</sub> NO <sub>3</sub> , (NH <sub>4</sub> ) <sub>2</sub> SO <sub>4</sub>	0.60	932
NH <sub>4</sub> NO <sub>3</sub> , (NH <sub>4</sub> ) <sub>2</sub> SO <sub>4</sub> , Na <sub>2</sub> SO <sub>4</sub> , NH <sub>4</sub> Cl	0.50	3951
(NH <sub>4</sub> ) <sub>2</sub> SO <sub>4</sub> , Na <sub>2</sub> SO <sub>4</sub> , NH <sub>4</sub> Cl	0.54	71
(NH <sub>4</sub> ) <sub>2</sub> SO <sub>4</sub> , Na <sub>2</sub> SO <sub>4</sub>	0.76	71
NH <sub>4</sub> NO <sub>3</sub> , NH <sub>4</sub> Cl, Na <sub>2</sub> SO <sub>4</sub> , NaCl, NaNO <sub>3</sub>	0.50	3951
NH <sub>4</sub> Cl, Na <sub>2</sub> SO <sub>4</sub> , NaCl, NaNO <sub>3</sub>	0.54	2306
(NH <sub>4</sub> ) <sub>3</sub> H(SO <sub>4</sub> ) <sub>2</sub> , NaHSO <sub>4</sub> , Na <sub>2</sub> SO <sub>4</sub> , (NH <sub>4</sub> ) <sub>2</sub> SO <sub>4</sub>	0.36	3951
(NH <sub>4</sub> ) <sub>3</sub> H(SO <sub>4</sub> ) <sub>2</sub> , Na <sub>2</sub> SO <sub>4</sub> , (NH <sub>4</sub> ) <sub>2</sub> SO <sub>4</sub>	0.68	2306
(NH <sub>4</sub> ) <sub>3</sub> H(SO <sub>4</sub> ) <sub>2</sub> , NH <sub>4</sub> SO <sub>4</sub>	0.36	561
(NH <sub>4</sub> ) <sub>3</sub> H(SO <sub>4</sub> ) <sub>2</sub> , (NH <sub>4</sub> ) <sub>2</sub> SO <sub>4</sub>	0.68	262

<sup>a</sup> MRHD values as used in ISORROPIA (Nenes et al. 1998),

<sup>b</sup> source Potukuchi and Wexler (1995a, 1995b),

<sup>c</sup>  $\alpha$  in  $\ln RHD(T) = \ln RHD(T_0) - \alpha \left( \frac{1}{T} - \frac{1}{T_0} \right)$ , where  $T_0 = 298 \text{ K}$ .

The MDRH points are obtained from phase maps (e.g. Potukuchi and Wexler, 1995a,b). These maps cover the majority of all possible MDRH points. However, there are salt mixtures where MDRH information could not be found. Due to this lack of information, it is assumed for ISORROPIA that the salt mixture has the same MDRH of another mixture with known deliquescence properties. The values of the salt mixture system that most closely approximated this (i.e. most similar in composition) is then used. For example, the MDRH point for a NH<sub>4</sub>NO<sub>3</sub>-NH<sub>4</sub>Cl-Na<sub>2</sub>SO<sub>4</sub>-NaCl-NaNO<sub>3</sub> mixture is not known. The most similar NH<sub>4</sub>NO<sub>3</sub>-NH<sub>4</sub>Cl-NaCl-NaNO<sub>3</sub> system has, according to Potukuchi and Wexler (1995a,b), a MDRH of 50%. So this is assumed to be the MDRH of the mixture in question (Nenes et al., 1998).

## 2.6 Aqueous Phase

At relative humidities, above the deliquescence point, the electrolyte is present in an aqueous phase in the particles. If the RH is above the RHD of all species considered, no solid crystalline phase of water-soluble compounds is present. It is implicitly assumed here, as justified below, that the water activity in the aerosol is equal to the ambient relative humidity.

### 2.6.1 Water Activity

It is generally assumed that the ambient relative humidity (RH) is not influenced by the deliquescence of aerosol particles, because of the relatively large amount of water vapor in the atmosphere compared to the aerosol water mass. Under this assumption, and by neglecting the Kelvin effect, phase equilibrium between gas and aerosols implies that the water activity,  $a_w$ , is equal to the ambient relative humidity (Bassett and Seinfeld, 1983)

$$a_w = RH, \quad (2.17)$$

with RH expressed on a fractional (0-1) scale. In other words, phase equilibrium between water vapor and aerosols is maintained rather than phase equilibrium between aerosol precursor gases and aerosols, because of the much higher partial vapor pressure of water vapor.

➤ Thus, the concentration of electrolytes in the atmospheric aerosols changes with relative humidity. For instance, if the relative humidity increases, the concentration of solutes in the particle decreases, which can be shown as follows.

At constant temperature and pressure, the Gibbs-Duhem relation states

$$\sum_i n_i \cdot d\mu_i = 0. \quad (2.18)$$

For one solute in water, Eq. (2.18) reduces to  $n_1 \cdot d\mu_1 + n_w \cdot d\mu_w = 0$ .

Using  $\mu_i = \mu_i^0 + R \cdot T \cdot \ln a_i$  to replace the chemical potentials  $\mu_i$  with activities  $a_i$  gives

$$da_w = -(n_1 \cdot a_w) / (n_w \cdot a_1) \cdot da_1. \quad (2.19)$$

Activities  $a_i$  and mole numbers  $n_i$  are positive, so that an increase in water activity  $a_w$ , which corresponds to an increase in relative humidity (RH), must result in a decrease in activity and therefore molality  $m_i$  of the solute. The molality of an electrolyte is therefore zero if the water activity is one - the activity of pure water is defined as unity.

### 2.6.2 ZSR-Relation

Similarly to the molality of a single solute, the molality of a mixture of solutes changes with ambient relative humidity. To obtain the molality of a mixture of solutes, the total water content of the aerosols must be calculated. The calculation of the water content is hereby based on a mixing rule, which is used in most atmospheric aerosol modeling, i.e. the so-called ZSR relation named after Zdanovskii (1948), Stokes and Robinson (1966). The ZSR relation simply assumes that a mixture of single-solute solutions has the same water activity as each single-solute solution alone, because of  $a_w = RH$ . It is therefore a purely empirical relationship, which can be violated to some extent (Chen et al., 1973). Nevertheless, in most atmospheric applications it has been shown to be an excellent approximation (Cohen et al., 1987a,b; Kim et al., 1993b).

### 2.6.3 Aerosol Associated Water

The calculation of the total water content,  $W$ , which is associated with atmospheric aerosols in equilibrium with the ambient relative humidity, is based on:

1.  $N$  single-solute solutions with water activity  $a_w$ , where each containing  $n_i$  moles of the solute and  $W_i$  kilograms of water.
2. The definition of molality in the single-solute solutions,  $m_{i,ss} = n_i / W_i$  [mol/kg] from which  $W_i$  is calculated for each single-solute solution.
3. The total amount of water in the mixture is then obtained from  $W = \sum_i^N W_i = \sum_i^N n_i / m_{i,ss}$ .
4. The ZSR-relation is applied in step 3, assuming that the water activity of the mixture is equal to the water activity of all the single-solute solutions, i.e.  $m_i = m_{i,ss}(a_w)$ .

With the assumption that the ambient relative humidity (RH) is equal to the water activity  $a_w$ , i.e.  $m_i = m_{i,ss}(RH)$ , it follows that

$$W = \sum_i^N n_i / m_{i,ss}(RH). \quad (2.20)$$

If the number of moles of solute (in the aerosol) and the ambient relative humidity are known, the water content of the particles can be calculated with equation (2.20). Given the relative mole fractions of cations and anions (i.e. in EQMs the corresponding subdomains), it can be determined from phase-maps (i.e. in EQMs usually from RHD/MDRH curves) whether the given relative humidity is above the deliquescence relative humidity or below. If the relative humidity is below the deliquescence point, one or more solids form. Then, the relative mole fractions in the aqueous phase vary from their total value because the solid phases change the aqueous phase composition. Using the relative mole fractions of the aqueous phase, charge balance and the relative humidity, the water content can be calculated. Once the water content is known, the molalities of the electrolytes can be calculated using these concentrations and the corresponding activity coefficients of the multicomponent solution mixture. The activity coefficients are hereby usually evaluated with activity coefficient models (see below).

#### 2.6.4 Activity Coefficients

According to Eq. (2.10), activity coefficients are needed to calculate the equilibrium concentrations. Thus, several methods have been developed for the calculation of activity coefficients, e.g. the widely used ones of Bromley (1973), Pitzer and Mayorga (1973), and Kusik and Meissner (1978). More recent approaches have been developed (e.g. Clegg et al., 1992). These methods are also used in the EQMs to which we will refer in the following. For instance, the EQMs MARS (Saxena et al., 1986; Binkowski, 1991) and SEQUILIB (Pilinis and Seinfeld, 1987) use the Pitzer method for the calculation of binary activity coefficients, and the Bromley method for the calculation of multicomponent activity coefficients. SCAPE (Kim et al., 1993a,b; Kim and Seinfeld, 1995) has an option to use either of the three methods, while ISORROPIA (Nenes et al., 1998) makes use of all three methods depending on the aerosol composition. Comparisons of these methods are presented by Kim et al. (1993a,b) and Kim and Seinfeld (1995), in addition to Saxena and Peterson (1981).



Most of the methods that predict the activity coefficients of a multicomponent solution are empirical or semi-empirical, and typically use the activity coefficients of single-electrolyte solutions of the same ionic strength.

The multicomponent activity coefficients are calculated in various EQMs, as for instance in ISORROPIA (Nenes et al., 1998), using Bromley's formula

$$\log \gamma_{12} = -A_{\gamma} \cdot (z_1 \cdot z_2 \cdot I^{1/2}) / (1 + I^{1/2}) + (z_1 \cdot z_2) / (z_1 + z_2) \cdot [F_1 / z_1 + F_2 / z_2]. \quad (2.21a)$$

$\gamma_{12}$  is the activity coefficient of cation 1 and anion 2,  $A_{\gamma}$  is the Debye-Hückel constant, which has a value of  $0.511 \text{ kg}^{0.5} \text{ mol}^{-0.5}$  at 298.15 K. The parameters  $F_1$  and  $F_2$  are:

$$F_1 = Y_{21} \cdot \log \gamma_{12}^{\circ} + Y_{41} \cdot \log \gamma_{14}^{\circ} + Y_{61} \cdot \log \gamma_{16}^{\circ} + \dots + (A_{\gamma} \cdot I^{1/2}) / (1 + I^{1/2}) + \quad (2.21b) \\ \times [z_1 \cdot z_2 \cdot Y_{21} + z_1 \cdot z_4 \cdot Y_{41} + z_1 \cdot z_6 \cdot Y_{61} + \dots]$$

$$F_2 = X_{12} \cdot \log \gamma_{12}^{\circ} + X_{32} \cdot \log \gamma_{32}^{\circ} + X_{52} \cdot \log \gamma_{52}^{\circ} + \dots + (A_{\gamma} \cdot I^{1/2}) / (1 + I^{1/2}) + \quad (2.21c) \\ \times [z_1 \cdot z_2 \cdot X_{12} + z_3 \cdot z_2 \cdot X_{32} + z_5 \cdot z_2 \cdot X_{52} + \dots]$$

with the parameters  $Y_{21}$  and  $X_{12}$ :

$$Y_{21} = [(z_1 + z_2) / 2]^2 \cdot (m_2 / I) \quad (2.21d)$$

$$X_{12} = [(z_1 + z_2) / 2]^2 \cdot (m_1 / I) \quad (2.21e)$$

$I$  is the ionic strength of the solution, i.e.

$$I = 1 / 2 \cdot \sum_i (m_i \cdot z_i^2), \quad (2.22)$$

and  $z_i$  is the absolute charge of ionic species  $i$ .  $\gamma_{ij}^{\circ}$  is the mean ionic activity coefficient of the binary pair  $i$ - $j$  (binary activity coefficient) for a solution that contains only  $i$ - $j$  ions at the ionic strength of the multicomponent solution. In Equations (2.21a) to (2.21e), odd subscripts refer to cations, while even subscripts refer to anions.

The binary activity coefficients needed in Equations (2.21b) and (2.21c) are calculated from the relationship (Kusik and Meissner, 1978):

$$\log \gamma_{12}^{\circ} = z_1 \cdot z_2 \cdot \log \Gamma^{\nu} \quad (2.23a)$$

where

$$\Gamma^o = [1 + B \cdot (1 + 0.1 \cdot I)^q - B] \cdot \Gamma^* \quad (2.23b)$$

$$B = 0.75 - 0.065 \cdot q \quad (2.23c)$$

$$\log \Gamma^* = -0.5107 \cdot I^{1/2} / (1 + C \cdot I^{1/2}) \quad (2.23d)$$

$$C = 1 + 0.55 \cdot q \cdot \exp(-0.023 \cdot I^3) \quad (2.23e)$$

$q$  is a parameter specific for each salt.

Kim et al. (1993b) compared binary and multicomponent activity coefficients obtained with the above three estimation methods (Bromley, Pitzer, and Kusik-Meissner) with available experimental data. The conclusion was that binary coefficients should be calculated using the Kusik-Meissner method, while there was no conclusive preference for any method for multicomponent solutions. The reason for this lies in the fact that activity measurements for multicomponent systems are available for relatively low ionic activities (up to 6 M), while much higher ionic activities are found in aerosols (up to 30 M or more), especially when the ambient relative humidity is low.

- All common estimation methods for activity coefficients are based on the solute activity, i.e. the ionic strength of the solution, and therefore must be solved numerically iteratively. This can require many iterations, and therefore much computing time, if the solute activity is high, or when crystallization or evaporation occurs because of aqueous phase composition changes. This is the case if the relative humidities is in the deliquescence humidity range of salt solutes, i.e.  $RH=RHD$  or  $MDRH$  (see Section 2.9).

## 2.7 Gas/Aqueous Phase Equilibria

To give an example of a gas/aqueous phase equilibrium, we discuss the effect of condensation and evaporation of ammonium nitrate following Wexler and Potukuchi (1998). Ammonium nitrate is an electrolyte, volatile, and present in many urban aerosols. The equilibrium reaction is



The stoichiometric coefficients on the left-hand side of the reaction are each  $\nu_i = -1$ , while those on the right-hand side are both  $\nu_i = +1$ . The activity of each solute is  $a_i = m_i \cdot \gamma_i$ , and each vapor activity is  $a_i = p_i/p_o$ . Substituting these into the equilibrium equation (Eq. 2.10) gives

$$K_{AN} = (p_{NH_3} \cdot p_{HNO_3} / p_o^2) / (\gamma_{AN}^2 \cdot m_{AN}^2). \quad (2.25)$$

The equilibrium constant for aqueous ammonium nitrate is given in Table 2.2; other values are available from literature (Mozurkewich, 1993), as is the activity coefficient (Hamer and Wu, 1972).

Thus, if a solute such as ammonium nitrate condenses on an aqueous particle, the number of moles of ammonium nitrate in the particle increases. But as shown previously, the relative humidity fixes the single-solute molality of ammonium nitrate, therefore, as ammonium nitrate condenses, so must water (because of Eq. 2.20).

Conversely, if the relative humidity increases, the water activity increases in the particles, which leads to decreases in solute molality and associated decreases in surface partial pressure of ammonia and nitric acid. Thus, increasing relative humidity results in ammonia and nitric acid condensation.

- It should be noted (extending the discussion by Wexler and Potukuchi, 1998) that not only the relative humidity maintains the molality to remain constant, but also the aerosol activity remains constant at equilibrium, i.e. as long as no other processes such as crystallization or condensation of ammonium nitrate occurs which, however, changes the equilibrium condition. Consequently, activity coefficients must be related to RH. If this is true in general, this would allow a parameterization of activity coefficients. We will come back to this point in the next chapter, where a new method for the activity coefficient calculation will be introduced.

Equation (2.25) allows calculation of the surface partial pressures of volatile inorganics of the acidic ammonium-sulfate-nitrate-water system. The relevant parameters are the partial pressures,  $p_{NH_3}$  and  $p_{HNO_3}$ , i.e. the partial pressure product of ammonia and nitric acid, the equilibrium constant for the reaction,  $K_{AN}$ , the composition of the solutes,  $m_{AN}$  and the activity coefficient of ammonium nitrate,  $\gamma_{AN}$ . The partial pressure product is then obtained if all these values are inserted into Eq. (2.25). Generally, the partial pressure product of ammonium nitrate decreases during the phase-transitions of solid to aqueous as the relative humidity increases above the various relative humidities of deliquescence; above the upper RHD, i.e. if all salts are dissolved, it rapidly approximates zero; below the lowest RHD, where the particle completely effloresces, it reaches its maximum value.

However, phase diagrams, from which the deliquescence humidities are obtained, are only valid if it is assumed that the electrolytes are non-volatile. This is reasonable if the changes in ambient relative humidity are fast compared to the time-scales for evaporation or condensation of the electrolytes, but in general, this is not the case. The reason is that the condensation of volatile compounds, such as ammonium nitrate, also depends on the acidity (pH) of the particle. For instance, for regions where insufficient ammonia is present to neutralize particle sulfate — commonly the case in eastern Europe and eastern North America — the pH of the particles is low so that volatile compounds may not condense. The opposite cases, where the particle sulfate is completely neutralized by ammonia, permits volatile acids and ammonia to condense (e.g. to form ammonium nitrate) — a common occurrence in western North America and western Europe.

- Thus, we note that only the latter case has to be considered for the gas/aerosol partitioning — we can therefore assume that acidic particles remain in the aerosol phase regardless their actual composition. We will utilize this point at the development of our parameterization in the next chapter.

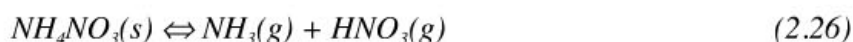
Note that it is implicitly assumed here, as by all air pollution modeling with EQMs, that all sulfate must be neutralized first by, for instance, ammonia, before surplus ammonia may react with nitric acid to allow for ammonium nitrate condensation. This is accounted for in EQMs by using the previously described domain structure (Section 2.4), for which certain assumptions and approximations are made (e.g. based on the fact that sulfuric acid is a stronger acid than nitric acid). The use of domains avoids the aforementioned problem of the use of phase-diagrams for volatile electrolytes, since volatile electrolytes are only permitted in EQMs if the aerosol acidity is sufficiently low, i.e. for certain domains (sulfate neutral or sulfate poor), which implicitly depend on the pH.

## 2.8 Solid Phase and Gas/Solid Phase Equilibria

Similar to the definition of the aqueous phase, EQMs determine the solid phase based on the deliquescence relative humidities of various aerosol compounds (Table 2.3, 2.4). If the relative humidity is below the deliquescence relative humidity of the salt considered, this electrolyte is treated as a solid crystal. When the RH is above the deliquescence point, the ions are saturated in solution. Nevertheless, crystallization has been observed in laboratory studies to occur at substantially lower relative humidities than the deliquescence relative humidity used in EQMs. In situ atmospheric studies have not yet been performed. However, full crystallization of particles will not occur if they are sufficiently acidic, which is accounted for in EQMs by the use of certain subdomains. For example, if the particle is composed of a mixture of ammonium sulfate and sulfuric acid, different salts or combinations of salts form, depending on the relative humidity and the ratio of ammonium to sulfate ions in the solution. When the ratio is 2, only ammonium sulfate forms. Between 2 and 1.5, a combination of ammonium sulfate and letovicite forms. At 1.5, only letovicite forms. Between 1.5 and 1 a combination of letovicite and ammonium bisulfate occurs, whereas at 1 only ammonium bisulfate forms. Finally, at ratios below 1, the particle never crystallizes completely; at low relative humidity it is composed of ammonium bisulfate crystal in equilibrium with hydrogen, ammonium, bisulfate and sulfate ions in an aqueous phase.

- It is therefore possible to simply parameterize the sulfate state, according to the ratio of ammonium to sulfate ion in the solution, rather than to explicitly treat the thermodynamics for this case, as it is presently done. We will also utilize this point by the formulation of our new simplified EQM (in the next chapter).

To give an example for a gas/solid phase equilibrium, i.e. particles that are composed only of crystalline phases of salts, we consider the case of ammonia and nitric acid:

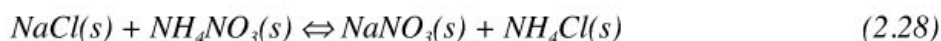


The activity of solid ammonium nitrate is 1, the stoichiometric coefficients are +1 for the vapors, and their activity is  $p_i/p_o$ . Using these with equation (2.5) gives

$$K_{AN} = p_{NH_3} \cdot p_{HNO_3} / p_o^2, \quad (2.27)$$

so that at a given temperature the presence of solid ammonium nitrate fixes the partial pressure product of ammonia and nitric acid vapors.

For a solid-solid equilibrium, however, such as the equilibrium of ammonium and sodium salts, i.e.



the activity of all the compounds is unity and equation (2.5) becomes  $K=1$ . Since this is not possible — the equilibrium equation cannot be used in this form for solid-solid reactions since the minimization of the Gibbs free energy must be applied differently.

The Gibbs free energy for the system composed of only solid phases is  $G = \sum_i n_i \cdot \mu_i^o$  and using the stoichiometry  $n_i = n_i^o + v_i \cdot \varepsilon$  gives

$$G = \sum_i n_i^o \cdot \mu_i^o + \varepsilon \sum_i v_i \cdot \mu_i^o, \quad (2.29)$$

$\mu_i^o$  are constants, so both summations on the right-hand side of Eq. (2.29) are constants and the Gibbs free energy is minimized when  $\varepsilon$  is either a minimum or maximum depending on the sign of  $\sum_i v_i \cdot \mu_i^o$ . The extreme values of  $\varepsilon$  are determined purely by stoichiometry and occur when one of the solids in the reaction is completely depleted. Thus, it is assumed that reacting solid salts are in equilibrium when one of them has been completely depleted in favor of formation of the other compounds.

Note that these assumptions, which are implicitly made for the solid state by air pollution modeling with EQMs, may not always be realistic. For instance, numerous laboratory observations have demonstrated that pure particles, that is, those that do not contain a pre-existing solid phase, do not crystallize until relative humidities are reached that are much below the efflorescence point (e.g. Rood et al., 1989). This is because the new solid phase must nucleate first, and this is not likely in homogeneous aqueous solutions until substantial supersaturations are achieved. These supersaturations have not been thoroughly explored in the atmosphere, so their occurrence there is not certain. However, in the atmosphere, many of the aerosol particles contain pre-existing solids, such as soot and crustal material, that provide heterogeneous nucleation sites for the formation of new phases. Heterogeneous nucleation typically does not require supersaturations as high as those required for homogenous nucleation.

This can have consequences for the aerosol size-distribution. Generally, the concentration of, for instance, ammonium nitrate in an aerosol particle increases as the relative humidity decreases until it saturates. If no pre-existing solid phase is present, continuing decreases in relative humidity would result for this pure particle in supersaturations of the ammonium nitrate in the solution, which result in partial pressures of ammonia and nitric acid over the particle that are higher than their equilibrium value for the solid phase. However, in the atmosphere populations of such particles usually occur. Some of them may have formed by binary nucleation of water and sulfuric acid, and therefore may not contain a pre-existing solid phase, whereas others may have been formed by condensation on a pre-existing solid. During transitions to low relative humidity, a solid phase of ammonium nitrate will nucleate in particles with a pre-existing solid phase and this solid ammonium nitrate will limit the partial pressure product of ammonia and nitric acid to its equilibrium value. In contrast, the particles without a pre-existing solid phase could supersaturate with ammonium nitrate and therefore exhibit a partial pressure product of ammonia and nitric acid that is above that for particles containing the solid phase. As a result, during transitions to low relative humidities, ammonium nitrate would evaporate from particles where it supersaturates and condense on ones where the solid phase forms. Thus relative humidity cycles, such as the diurnal one, might redistribute volatiles such as ammonium nitrate from particles without pre-existing solid cores to those with cores that facilitate formation of solid phases by heterogeneous nucleation. This is, however, not accounted for in present EQMs.

There are more uncertainties involved in the solid phase calculation. For instance, single component aerosols, such as those containing just ammonium sulfate are known to have a sharp change in phase state at the deliquescence point. Above this point the aerosol is aqueous and below it is a solid crystal. Multi-component aerosols do not show such simple behavior (Winkler, 1973; Winkler, 1988). Multicomponent aerosols are much more common in the atmosphere than just single component particles. Hence, the mutual deliquescence relative humidities (MDRH) must be considered to determine the solid aerosol phases (Table 2.4, Section 2.5).

- Note that only the EQM ISORROPIA (Nenes et al. 1998) treats MDRHs, while all other EQMs presented only consider RHDs of single salt compounds, and some of them do not even account for their temperature dependence (e.g. MARS and SEQUILIB). Since the RHD and MDRH are crucial to define the aqueous phase and subsequently the water content of the aerosol, this presents the largest uncertainty in air pollution modeling. To minimize errors, we will use MDRH points by the formulation of our new simplified EQM (in the next chapter).

Note further that it is assumed that the discussion of aqueous solutions or solid aerosols also applies to mixed phase aerosols, i.e. an aqueous solution containing solids which have been crystallized out of the aqueous phase. That is, aqueous phases are more dilute at higher relative humidity, the ZSR mixing rule can be applied to the aqueous phase to calculate the particulate mass of water, gas-particle equilibrium holds for both the solid and aqueous phases, and multiple, reacting solid phases are in equilibrium when one of the phases is depleted.

## 2.9 Solution Algorithm

Present EQMs use iterative schemes to calculate gas/aerosol partitioning for inorganic and volatile species, such as ammonium and nitrate. The reason is that the common calculation methods of the aerosol composition require information about the solute activity, which includes the aerosol associated water, and which determines the vapor pressure above the aerosol droplet. The solute activity depends on the activity and the activity coefficients of each component of the multicomponent solution, whereas each individual activity coefficient depends, in turn, on the solute activity of the aerosol droplet. Therefore iterative schemes are used to calculate activity coefficients and aerosol composition, which is illustrated in Figure 2.1.

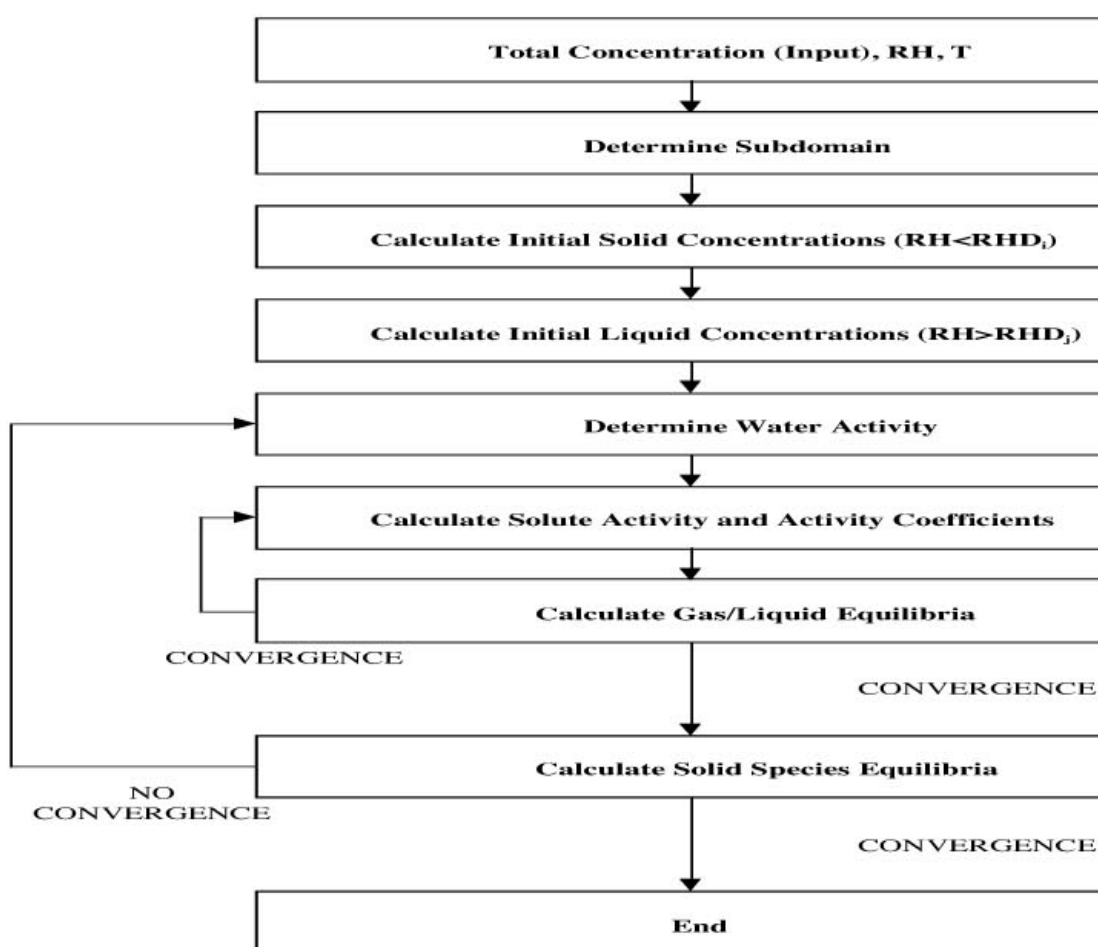


**Figure 2.1.** Schematic description of the solution algorithm of present EQMs.

The iteration procedure can be summarized as follows:

1. According to the anion/cation mole ratios (e.g.  $\text{NH}_4^+/\text{SO}_4^{2-}$ ) of the input concentrations the main domain is chosen, which determines the number and type of equilibrium reactions.
2. Depending on the mole ratio, relative humidity, and the deliquescence relative humidities (RHD), the subdomain is determined for the initial solid concentrations.

3. For each reaction, the molality of the binary solution (one solute and water) is determined for the initial liquid concentration from tabulated measurements; the molality  $m$  is hereby defined as the number of moles dissolved in 1000g of water.
4. The aerosol water content is calculated from the ZSR-relation
5. Binary and multicomponent activity coefficients are calculated from the initial concentrations and using the initial activity coefficients, the concentrations and the gas/aqueous equilibria are recalculated until convergence is reached for each reaction.
6. According to temperature and relative humidity and the actual aqueous concentrations, the solid species concentrations are recalculated until convergence is reached.
7. The final composition and the concentrations of the gas/liquid/solid aerosol phases are iterated until the results of all equilibrium reactions are stable in terms of pre-defined error bounds.

Thus, all EQMs need to calculate gas/aerosol partitioning, including activity coefficients, iteratively. This is a major disadvantage, not only computationally and with respect to global modeling. The reason is that the accuracy strongly depends on the stability of the numerical algorithms, which are usually solved iteratively. For instance, errors in iterative calculation of solid compounds can arise because of convergence problems which, however, affect the solute activity, and in turn the estimation of activity coefficients. Subsequently the gas/aqueous and solid equilibria are affected.

In order to minimize convergence problems, the number of iterations needed is determined by more complex EQMs (e.g. SCAPE and ISORROPIA) dynamically, i.e. by using error bounds rather than a fixed number of iterations (as is the case for SEQUILIB). This enhances not only the accuracy, it also speeds up the model under certain circumstances. Nevertheless, many iterations are often needed to calculate the gas-aerosol partitioning, strongly depending on the concentration domain, temperature and relative humidity, besides the chosen accuracy. Especially if the relative humidity is in the mutual deliquescence humidity range (or RHD range of single compounds), where crystallization of certain salt compounds occur, many iterations are needed. Even for a relatively high RH range (70-90%), which occurs widely and frequently in the atmosphere, many iterations are needed since phase-transition (liquid-solid) can occur, as for instance for sodium sulfate at RH=93% (298.15K).

- To illustrate the present situation, we apply the most recent, and in terms of computational performance, most sophisticated equilibrium model ISORROPIA to an arbitrary (but realistic) field of input concentrations (monthly mean values for January,  $3.75^\circ \times 3.75^\circ$  horizontal resolution, surface layer), and investigate the number of iterations needed to reach, for instance convergence for the activity coefficient calculations. This is shown in [Figure 2.2](#), plotted versus relative humidity for four different systems of aerosol composition: (I) ammonium and sulfate ( $\text{NH}_4\text{-SO}_4\text{-System}$ ); (II) ammonium and nitrate ( $\text{NH}_4\text{-NO}_3\text{-System}$ ); (III) ammonium, sulfate and



nitrate ( $\text{NH}_4\text{-NO}_3\text{-SO}_4\text{-System}$ ); (IV) ammonium, sulfate, nitrate and sea salt ( $\text{NH}_4\text{-NO}_3\text{-SO}_4\text{-Na-Cl-System}$ ). Each system refers to the same temperature and relative humidity variations and, therefore, represents only a different selection from the same input fields.

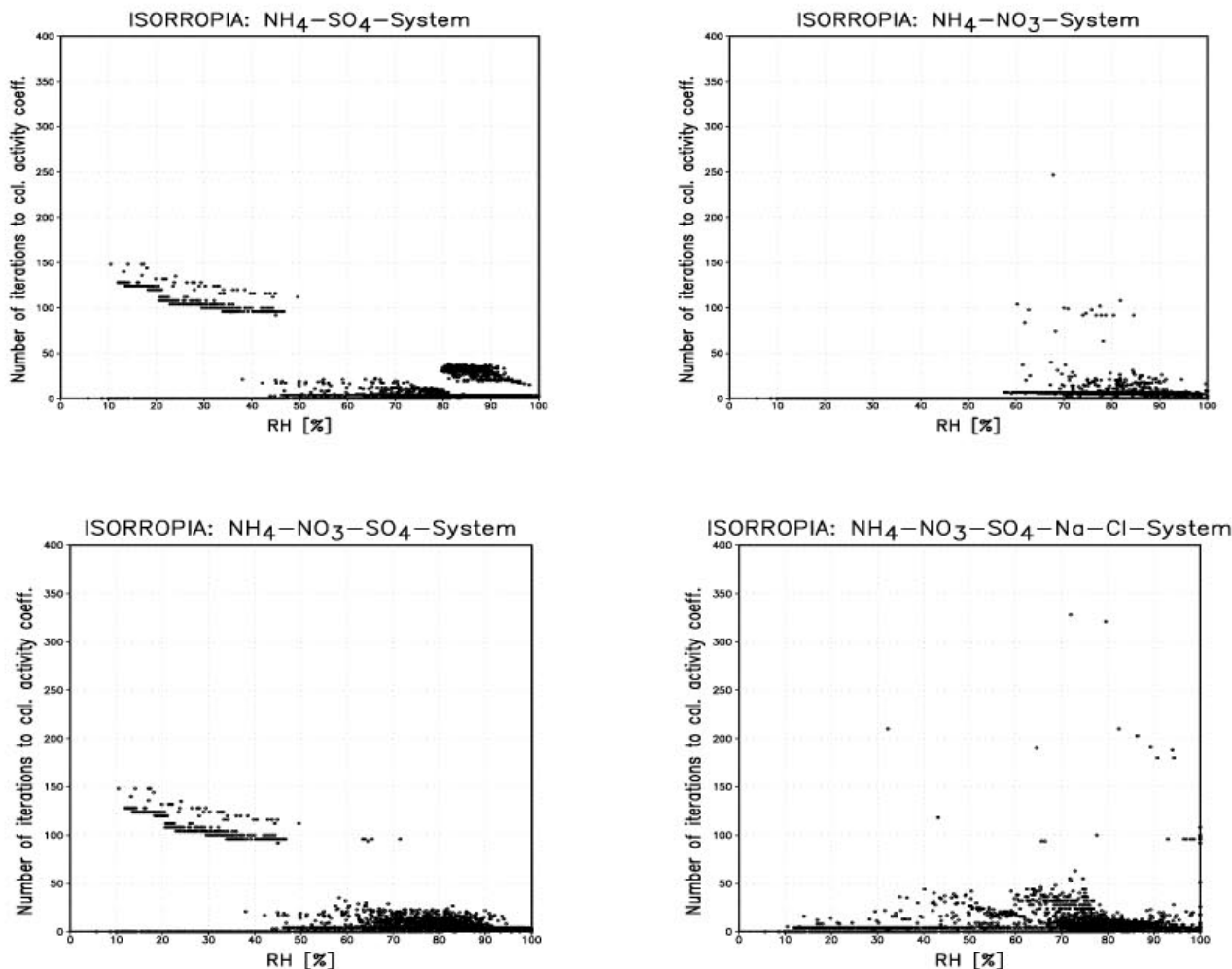


**Figure 2.2.** Number of iterations needed to reach convergence for the activity coefficient calculation. This is plotted versus relative humidity for four different cases of atmospheric aerosol compositions:  $\text{NH}_4\text{-NO}_3\text{-SO}_4$ ,  $\text{NH}_4\text{-SO}_4$ ,  $\text{NH}_4\text{-NO}_3$ ,  $\text{NH}_4\text{-NO}_3\text{-SO}_4\text{-Na-Cl}$ . Values are obtained from an application of the thermodynamic equilibrium model (ISORROPIA, Nenes et al. 1999) to global data, representing monthly mean values for January (one 3D-field  $3.75^\circ \times 3.75^\circ$  horizontal resolution, surface layer).

Figure 2.2 illustrates that the activity coefficient calculation depends on the aerosol composition and on relative humidity. Although for most cases less than 50 iterations are needed for the activity coefficient calculation, the number of iterations can exceed 300. Even for rather simple systems of aerosol composition, such as  $\text{NH}_4\text{-SO}_4$ - and  $\text{NH}_4\text{-NO}_3\text{-SO}_4$ , the number of iterations exceeds 100 for cases where solids co-exist with an aqueous solution. Note that each number represents one grid box. Thus, these numbers must be multiplied with the spatial and temporal resolution of a hosting model. It therefore becomes apparent that for large-scale applications the activity coefficient calculation can rapidly dominate the overall performance of an atmospheric/chemistry transport model (CTM). The same is true for or a general circulation model (GCM) (also indicated by Adams et al. 1999). Therefore, alternatives are needed for global modeling.

## Chapter III: A new Method and Equilibrium Model

As we have seen in the previous chapter, existing aerosol thermodynamic models that can calculate the aerosol composition and the aerosol associated water mass are too computationally expensive for global atmosphere/chemistry and climate modeling. Even the most optimized models would still require disproportionate amount of CPU time, compared to other processes in global models, and, thus, simplifications are needed. One option is to derive parameterizations from comprehensive models, which then can be alternatively used depending on the modeling tasks.

In the work leading to this thesis such an approach was initially followed, i.e. a parameterization for activity coefficients was derived from the most comprehensive thermodynamic gas/aerosol equilibrium model, the EQM SCAPE; see Metzger et al. (1999) for details. The parameterization is presented in the [Appendix](#). The main result of this work is that it shows that activity coefficients of atmospheric aerosols (calculated with EQMs) are strongly related to the relative humidity. The reason for this lies in the assumptions which are implicitly made by the calculation of the solute activity and aerosol associated water, and particularly in the definition of the water activity and application of the ZSR-relation. This activity coefficient - RH relationship yields, with non-linear curve fitting, for each activity coefficient ( $\gamma_i$ ) a function  $\Gamma_i(\text{RH})$ , which can be then used in any EQM to substitute the activity coefficient calculation method (those previously described in Chapter 2.6.4). The advantage of such an approach is, besides the reduction in computing time, that the model structure (e.g. domains and subdomains) does not need to be changed, so that gas/aerosol equilibria can be calculated as comprehensively as with a non-parameterized EQM. The differences in the accuracy then only depend on the quality of the polynomial fits. In general, differences are minimized if such fits are derived for each domain and subdomain (which, however, was omitted for the sake of simplicity).

Note that during the same time, where we have parameterized the SCAPE EQM, Nenes et al. (1998) developed ISORROPIA and provided an option to use pre-calculated activity coefficients for binary systems (based on the Kusik-Meissner method). Besides the fact that ISORROPIA was not available at that time, the use of pre-calculated sets of binary activity coefficients, which can speed up the model by a factor of 2 (Nenes et al. 1998), still requires too many iterations to solve gas/aerosol equilibria for global modeling (as illustrated in Chapter 2.9). The reason is that multicomponent activity coefficients must still be calculated iteratively.

This problem is overcome by the application of characteristic functions to calculate activity coefficients, as we have proposed in Metzger et al. (1999). More importantly, by using the relationship between activity coefficients and relative humidity, a completely new method can be developed, and consequently a new EQM, which then allows to calculate the gas/aerosol partitioning analytically and non-iteratively.

In the following we will develop such a new method (and EQM) from the same modeling assumptions as generally made for the EQMs presented (Chapter II). This new method is based on physical relations, such as the vapor pressure reduction and the generalization of Raoult's law. It implicitly explains the relationship between activity coefficients and relative humidity that is presented in Metzger et al. (1999). This relationship will be utilized to develop a new and simplified aerosol model, which calculates the gas/aerosol partitioning sufficiently fast and accurate for global modeling. Only the new method will be discussed in the following, since it is more fundamental than the above mentioned polynomial fitting procedure (which is summarized in [Appendix A](#)).

### 3.1 Implications of the General Assumptions

According to the assumptions generally made in air pollution modeling with EQMs (Chapter II), the solute activity of atmospheric aerosols depends on RH. The reason is that the solute activity depends on the water content of the aerosol particle, which in turn only depends for a given aerosol composition on the relative humidity since the water activity is fixed to RH. And since activity coefficients are needed only for aqueous aerosols (to determine the solute activity), we are able to theoretically derive, for atmospheric aerosols in thermodynamical equilibrium with the ambient relative humidity, a relationship between activity coefficients and RH.

The assumptions and solution algorithm of the equilibrium models presented can be summarized as follows (each point was discussed previously in Chapter II):

- (i) Thermodynamical and chemical equilibrium between the gas/liquid/solid aerosol phases (internally mixed), including the relative humidity (RH), i.e.  $K_{eq} = \gamma_i \cdot m$ .
- (ii) ZSR-relation; the total water content of a mixed solution aerosol is the sum of the water fractions associated with all binary solutions.
- (iii) Division of the concentration range into domains and subdomains, according to the anion/cation mole ratios, and the RHD/ MRHD regimes.
- (iv) Solid aerosol phase exists if the  $RH < RHD / MRHD$ .

From (i) it directly follows that the water activity of the aerosol equals the ambient relative humidity, i.e. (see Chapter 2.6.1)

$$a_w = rh, \quad (3.1)$$

which requires that the molality of the aerosol droplet remains constant for a given RH;  $rh = RH [\%] / 100$  is the fractional relative humidity [0-1].

This becomes more evident if we express the water activity in terms of the mole fraction of the aerosol water,  $x_w$ :

$$a_w = f_w x_w, \quad (3.2)$$

where  $f_w$  denotes the effective (rational) activity coefficient (Pruppacher & Klett, 1997).

The activity coefficient  $f_w$  is defined to account for the solution non-ideality, thus, for sufficiently dilute solutions  $f_w \rightarrow 1$  ( $rh \rightarrow 1$ ).

The mole fraction of the aerosol water expresses the ratio of water molecules ( $n_w$ ) to the total number of molecules in the solution, e.g. water and salt molecules ( $n_s$ ), i.e.

$$x_w = n_w / (n_s + n_w), \quad (3.3)$$

from which it directly follows that for a fixed RH any changes in the solute concentration due to evaporation/condensation or crystallization changes the water content of the aerosol, since  $a_w = x_w = \text{constant}$  (for sufficiently dilute solutions). Vice versa, if RH changes, the solute concentration must change to remain the water activity to be constant ( $a_w$  equals RH). We will see in the following that this also applies to non-ideal solutions, so that consequently activity coefficients are, for a given aerosol composition, a function of RH.

In other words, the vapor pressure reduction of an aerosol, containing an aqueous salt solution relative to a pure aqueous droplet, is - for a fixed RH - compensated by additional condensation of water vapor. For a given gas/liquid/solid equilibrium, a decrease in RH leads to an increase in the solute concentration. This can result in a supersaturation of the aqueous salt solution, by which individual salt compounds may crystallize out of the solution, or volatile compounds evaporate, especially if an increase in temperature occurs with a decrease in relative humidity - a consequence of the assumption that the water activity equals RH. However, according to Eq. (3.2 and 3.3), both  $f_w$  and  $x_w$  i.e.  $n_s$  must be calculated to determine the gas/aerosol partitioning.

### 3.2 Vapor Pressure Reduction and the Generalization of Raoult's Law

The link between the molality of an aqueous salt solution and the water activity is given by the vapor pressure reduction, which generally occurs by the solution of salts in water. For the so-called 'ideal' solutions, i.e. for a sufficiently dilute solution without interactions between solute molecules, this effect is described by Raoult's law. It states that the equilibrium vapor pressure of any component above the solution is proportional to its mole fraction in the solution, i.e.

$$P_{sat,s} / P_{sat,w} = x_w. \quad (3.4a)$$

To account for non-ideal solutions Eq. (3.4a) can be expressed in terms of activity coefficient, i.e.

$$p_{sat,s} / p_{sat,w} = f_w x_w, \quad (3.4b)$$

by which Eq. (3.4b) can be regarded as the generalization of Raoult's law to real salt solutions (Warneck, 1988; Pruppacher and Klett, 1997). Note that Eq. (3.4a) equals the Köhler-equation if the Kelvin-term ( $+2\sigma V_m / (RT \cdot r)$ ) would be included (Warneck, 1988). The radius increase of an atmospheric aerosol with relative humidity was first investigated by Köhler (1936) on the basis of thermodynamic principles, and later in detail by, for instance, Dufour and Defay (1963) and Pruppacher and Klett (1980).

The vapor pressure reduction can be expressed as

$$\Delta p_{sat} / p_{sat,w} = f_s x_s, \quad (3.4c)$$

with  $\Delta p_{sat} = p_{sat,w} - p_{sat,s}$ , and  $x_w + x_s = 1$ ;  $p_{sat,s}$  denotes the equilibrium vapor pressure over an aqueous salt solution at temperature  $T$ , and  $p_{sat,w}$  the equilibrium vapor pressure over an pure aqueous solution at the same temperature.  $f_s$  and  $f_w$  represent the effective activity coefficient of the salt compound, and the water activity coefficient of the aqueous solution, respectively. Both are used in conjunction with the mole fraction, while mean binary activity coefficients,  $\gamma_i, \gamma_w$ , are used with the molality. With the definition of molality  $m$ , i.e. number of moles of salt dissolved in 1000g of water, the mole fraction of the solute,  $x_s$ , can be expressed as  $x_s = n_s / (n_s + n_w) = m / (m + (1000/M_w)) = m / (m + 55.55)$ . The mole numbers,  $n_s$  and  $n_w$ , of the solute and water, respectively, can be replaced by the corresponding ratios of mass to molecular weight, from which the radius can be obtained:

$$m_{aerosol} = 4/3 \pi \bar{\rho} r^3 f_s x_s = n_s \bar{M}_s + n_w M_w = m_s + m_w, \quad (3.4d)$$

where  $r$  denotes the radius of the aerosol particle,  $\bar{\rho}$  and  $\bar{M}_s$  the average density and molecular mass of the solutes, respectively. The average density can be determined with the usual and quite realistic assumption (Hänel, 1976) of molar volume additivity,

$$\bar{\rho} = (m_s + m_w) / [m_s / \rho_s + m_w / \rho_w], \quad (3.4e)$$

➤ Note that Eq. (3.4b), i.e. the vapor pressure reduction, also applies to the condensation of volatile salts, such as ammonium nitrate, on for instance a pure water droplet. The reason is that an atmospheric aerosol, containing salt compounds, in equilibrium with relative humidity, the associated vapor pressure reduction is compensated by an additional condensation of water vapor, if the water activity is fixed to RH (as discussed previously). Thus, Eq. (3.1) equals Eq. (3.4a) and, therefore, Eq. (3.2) equals Eq. (3.4a), so that Eq. (3.4c) can be expressed in terms of relative humidity, from which it follows that for equilibrium, activity coefficients of atmospheric aerosols are related to relative humidity.

The physical explanation of Raoult's law is given by the osmotic pressure of solutes. Those results are summarized in van't Hoff's law (see physics textbook). From there it follows that the vapor pressure reduction, as the osmotic pressure, for sufficiently dilute solutions is directly proportional to concentration of the solute, but independent of its nature. To account for non-ideal solutions, e.g. the degree of ionic dissociation in electrolytes, the van't Hoff  $i$ -factor was used in earlier studies of osmotic pressure. Nowadays, the activity coefficient is used in conjunction with activities to account for non-ideal behavior of the solutions (Low, 1969a,b). The importance of the activity, however, is that it provides a direct measure of the equilibrium water vapor pressure over a real salt solution, or in other words, the generalization of Raoult's law to real solutions. This means that the inclusion of the activity coefficient allows to account for non-ideal behavior of highly concentrated solutions. Thus, with the generalized form of Raoult's law and the assumption that, for thermodynamical equilibrium, the water activity  $a_w$  of the aerosol is equal to RH, we have a relationship between activity coefficients and RH, which requires both that:

1. An increase of water activity due to growing relative humidity results in a decrease of the solute activity and therefore molality (see Chapter 2.6);
2. In turn, an increase of the solute lowers the vapor pressure above the solution, which leads to an additional condensation of water vapor until the vapor pressure reduction is compensated by the water vapor uptake. Hence, the increase of the water content in the aerosol maintains the molality to remain constant (see Chapter 2.7).

The consequence, however, because of equations (3.4a-c) is that activity coefficients change with RH, but not if the RH is fixed (as long as equilibrium is maintained). This is a direct result of the assumption that the water activity equals the relative humidity, and that the relative humidity is conservative with respect to aerosol formation processes ( $RH < 99\%$ ).

For atmospheric aerosols in thermodynamical equilibrium with ambient water vapor, the vapor pressure reduction that is associated with a certain amount of dissolved matter and the RH, i.e. water activity, are coupled. The same is true for the solute activity of binary solutions. In the following we will show that this is - under the above assumption ( $a_w = rh$ ) and the application of the ZSR-relation - true in general, so that the solute activity of real, mixed solutions, including activity coefficients depends on RH.

### 3.3 Relation between Aerosol Molality and Relative Humidity

Since we base our new method on the above considerations, we illustrate first the relation between the molality in the single-solute (ss), aqueous solutions of atmospheric aerosols and the relative humidity. These single-solute solutions are crucial for the equilibrium calculations. They are needed to calculate the water content of single-solute solutions (see Chapter 2.6.3). Based on the ZSR-relation (Chapter 2.6.2), the water content of an aerosol containing mixed solution is then calculated by which the solute activity and activity coefficients depend on the molality of single-solute aqueous solutions and their relation to RH.

The molality of single-solute solutions is calculated as follows. Assuming that the activity of the  $i$ -th solution contains  $n_i$  moles of solute  $i$  and  $W_i$  kilograms of water, and that the water activity equals the relative humidity (with the molality defined as  $m_{i,ss} = n_i/W_i$ ),  $m_{i,ss}(\text{RH}) = n_i/W_i(\text{RH})$ . Since single-solute solution molalities are essential for the equilibrium calculations, they have been measured and tabulated for various solutes and a wide range of relative humidities. Figure 3.1 shows the solution molality as a function of relative humidity [%] for various single solute solutions,  $m_{i,ss}(\text{RH})$ ,  $i=1, \dots, 5$ :  $\text{NH}_4\text{NO}_3$  (top),  $(\text{NH}_4)_2\text{SO}_4$  (middle),  $\text{H}_2\text{SO}_4$  (bottom) in the upper panel, and  $\text{NH}_4\text{HSO}_4$  (top) and  $(\text{NH}_4)_3\text{H}(\text{SO}_4)_2$  (bottom) in the lower panel. The red, thin solid lines will be discussed in Section 3.5. Although these solution molalities have been obtained from the thermodynamic data used in ISORROPIA, they are representative for all equilibrium models presented since the differences are rather small for single-solute solutions.

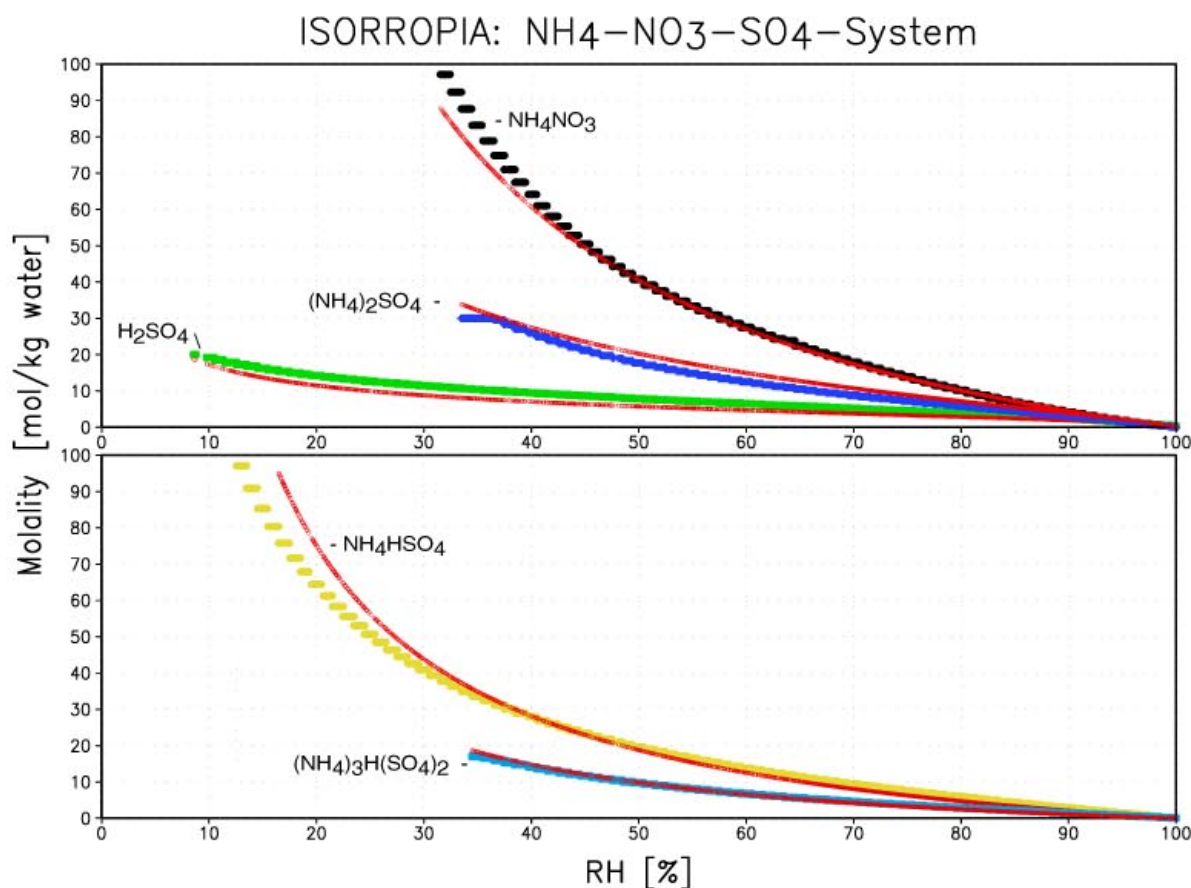


**Figure 3.1.** Solution molality as a function of relative humidity [%] for pure salt aerosols: The upper panel shows  $\text{NH}_4\text{NO}_3$  (black),  $(\text{NH}_4)_2\text{SO}_4$  (blue),  $\text{H}_2\text{SO}_4$  (green), the lower panel  $\text{NH}_4\text{HSO}_4$  (yellow) and  $(\text{NH}_4)_3\text{H}(\text{SO}_4)_2$  (light-blue). For comparison, the results of equation (3.6) are included (red, thin solid lines).

To obtain the molalities of multicomponent solutions, the ZSR mixing rule of solutes is used in equilibrium models (see Chapter 2.6.2). This ZSR relation assumes that the water activity of a mixed solution is equal to the water activity of all single-solute solutions, so that the water content associated with a mixed solution is simply the sum of the water content of all binary solutions, from which the molality of the mixed solution is obtained.

### 3.4 Relation between Aerosol Water and Relative Humidity

Before we focus on the total water content of the aerosol, which is crucial to calculate the solute activity and activity coefficients, we illustrate first the dependency of the water content of binary solutions, i.e. the fractions  $W_i$  (which corresponds to  $m_{i,ss}$ ), on RH. Note, this dependency will also hold for the total water content (because of the ZSR-relation). It is this relation (the dependence of  $W_i$ , i.e.  $W$  on RH) that is important for the solute activity and activity coefficient calculation, since it allows to simplify the present calculation - the discussion follows in Section 3.5.

Figure 3.2 shows the water fractions of single-solute solutions as a function of relative humidity, i.e. water activity. The upper panels show the water fractions of  $\text{NH}_4\text{NO}_3$ , and the lower panels the water fractions of  $\text{NH}_4\text{HSO}_4$  (top) and  $(\text{NH}_4)_2\text{SO}_4$  (bottom). The left panels represent the water fractions which have been obtained from equilibrium calculations with ISORROPIA using a fixed input concentration of  $1 \mu\text{mol}/\text{m}^3$  air; the right panels are based on  $1/2 \mu\text{mol}/\text{m}^3$  air. The temperature was fixed to 298.15 K, so that only the relative humidity varied. The black lines indicate the water fractions obtained by ISORROPIA. The red (thin) lines indicate the water fractions calculated with a formula, which will be derived in the following section. Note that each water fraction has been calculated independently.

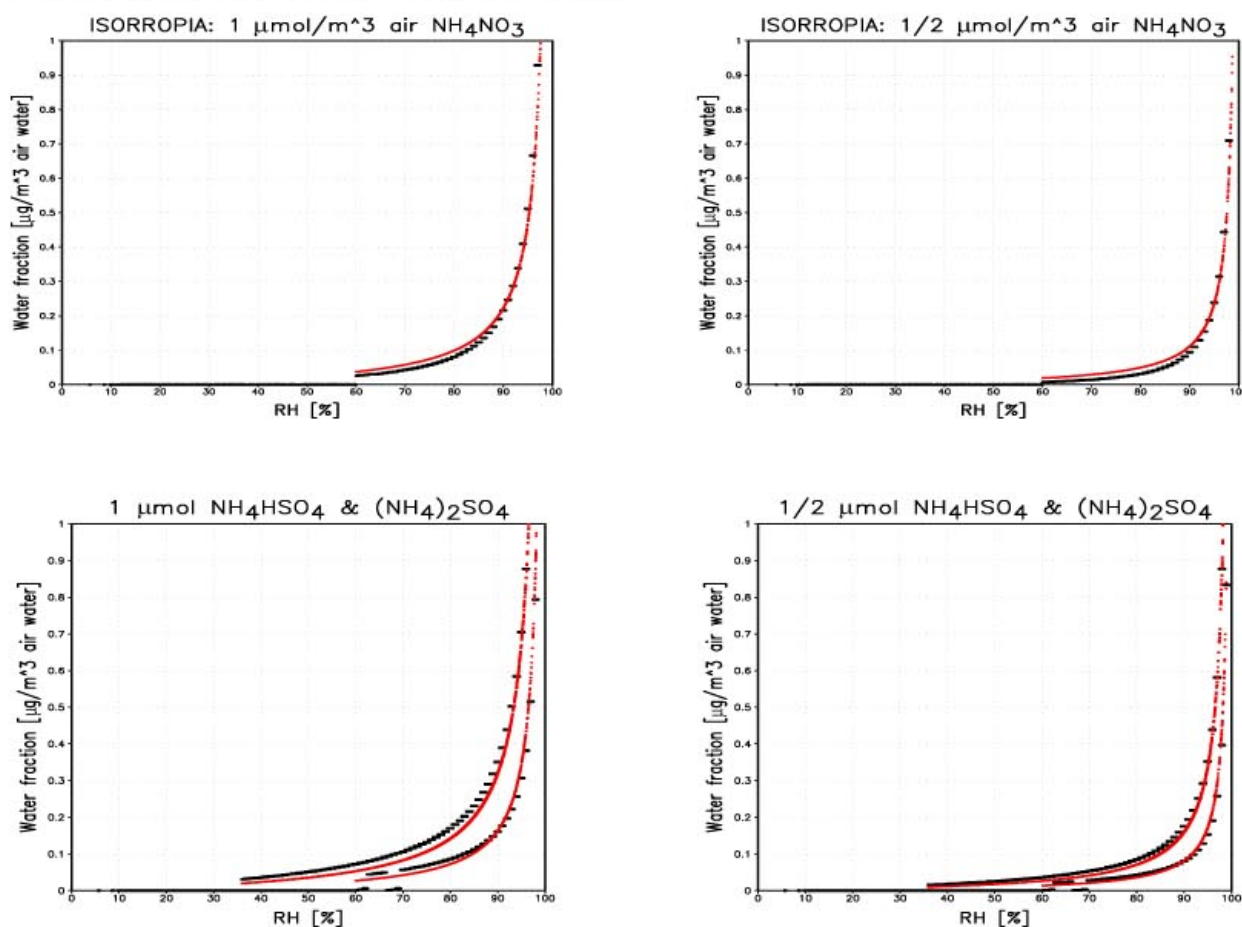


**Figure 3.2.** Water fractions of 3 electrolytes as a function of relative humidity at fixed temperature: Upper panels  $\text{NH}_4\text{NO}_3$ , lower panels  $(\text{NH}_4)_2\text{SO}_4$  (top) and  $(\text{NH}_4)\text{HSO}_4$  (bottom). The water fractions are shown for two concentrations  $1 \mu\text{mol}/\text{m}^3$  (left panels) and  $1/2 \mu\text{mol}/\text{m}^3$  air (right panels). For comparison, the results of equation (3.5b) are included (red, thin solid lines).



In general, the aerosol associated water is proportional to the number of moles of dissolved solute. Thus, the aerosol water decreases as the amount of dissolved matter decreases for a fixed relative humidity (comparing left and right panels), but steeply increases for a fixed amount of solute if the RH exceeds the model relative humidity of deliquescence (RHD). Below the RHD, the component is assumed to be pure solid. The RHD at 25°C of  $\text{NH}_4\text{NO}_3$  is approx. 0.6, that of  $\text{NH}_4\text{HSO}_4$  is slightly below 0.4, and of  $(\text{NH}_4)_2\text{SO}_4$  it is about 0.8 (the latter value differs somewhat from Figure 3.2, since ISORROPIA uses mutual deliquescence regions (see Chapter 2.5).

As expected, Figure 3.2 clearly illustrates that the aerosol water fraction of a single-solute solution is strongly related to the relative humidity. This relation is proportional to the solute concentration and depends on the type of solute (i.e. aerosol compound), and particularly on its hygroscopicity. Because of the ZSR-relation, we can expect the same relation for the aerosol associated water of mixed solutions, and consequently that the aerosol activity and activity coefficients are strongly related to RH. Thus, we will investigate in the following whether we can directly derive from theory the activity coefficients - RH relationship in a way, which allows to numerically simplify the gas/aerosol calculations without much loss of accuracy.

### 3.5 Parameterizations

To develop the new method we first consider the following hypothetical situation. An air parcel of humid, pristine air is in equilibrium with the environment at the dew point temperature  $T_d$ , where existing aerosol particles can be considered to be pure water droplets. The water activity of each aerosol droplet is equal to the relative humidity, in this case unity, so that the water vapor pressure above the aerosol droplet  $p_{w,0}$  is equal to the saturation vapor pressure  $p_{w,\text{sat}}$ . Each particle of the same size then contains the initial water mass  $W_0 = n_w M_w$ . As this air parcel moves along an atmospheric trajectory, it becomes contaminated with trace gases, say ammonia and nitric acid. We assume that the temperature and the relative humidity remain constant. After some time, the aerosol particles will equilibrate again with the environment, but now containing a certain amount of dissolved ammonium nitrate, and an additional amount of water, since the water activity is fixed to the relative humidity.

In this case,  $n_i$  mol of dissolved ammonium nitrate (=single-solute) will lead to the additional condensation of  $n_w$  mol of water. The mole fraction of water in the aerosol particle with single-solute  $i$  is  $x_w = n_w / (n_w + n_i)$  and that of the solute is  $x_i = n_i / (n_i + n_w)$ . For binary systems (one single-solute and water),  $x_w + x_i = 1$  ( $i=1$ ), and for sufficiently dilute solutions,  $x_w$  is equal to the water activity  $a_w$ , which is equal to the fractional relative humidity ( $\text{rh}=\text{RH}/100$ ). The total water mass of the aerosol particles is the sum of the initial water mass,  $W_0$ , and the increase in water mass,  $W_i$ , due to the condensation of additional water vapor that is associated with the condensation of the single-solute.

The total water mass is  $m_w = n_w \cdot M_w$ , with  $M_w$  the molecular weight of the  $n_w$  mol of water molecules, and the solute mass is  $m_i = n_i \cdot M_i$ , with  $M_i$  the molecular weight of the  $n_i$  mol of the single-solute ( $i$  denotes in the above example ammonium nitrate). The total aerosol mass is  $m = m_w + m_i$ . The partial mass of aerosol water and solute can be expressed in terms of the corresponding mole fractions,  $x_w$  and  $x_i$  to yield two equations

$$m_w = x_w \cdot m \quad (i)$$

and

$$m_i = x_i \cdot m \quad (ii)$$

which yield, upon substitution of  $m$  in (i) with (ii), an alternative expression for the water mass of the aerosol particles (according to Eq. 2.20, see next section), i.e.

$$W = n_w M_w = n_i M_i \cdot x_w / x_i. \quad (3.5a)$$

Note that for cases where the relative humidity is unity and  $n_i > 0$  actually an unlimited amount of water must condense to satisfy  $x_w = rh \cong 1$ . But these cases will not be discussed here, since the aqueous solution of the aerosol is sufficiently dilute to directly follow Raoult's law, and activity coefficients are not needed. Note further that the growth of atmospheric particles as a function of relative humidity, i.e. the relation between the saturation ratio and the wet size of the particle is given by the Köhler equation, i.e. the complete Eq. (3.4a) as mentioned earlier (see e.g. Pruppacher and Klett, 1997 for a discussion).

However, the water uptake by the aerosol is in any case a result of vapor pressure reduction above the solution due to the increased number of solute molecules. We can therefore express the mole fraction of the solute  $x_i$  in terms of the vapor pressure reduction  $\Delta p/p_{w,o}$ . Since  $\Delta p/p_{w,o}$  is compensated by the water uptake  $x_w = p_w/p_{w,o}$ , we can express  $\Delta p/p_{w,o}$  with  $\Delta p = p_{w,o} - p_w$  to yield  $1-rh$ ; this also follows from  $x_w + x_i = 1$ , with  $x_w$  equal to  $rh$ , if the binary solution is sufficiently dilute. Since the vapor pressure reduction is proportional to the total number of moles of dissolved matter, we must multiply  $\Delta p/p_{w,o}$  with the number of ions  $v_i = (v_i^+ + v_i^-)$  formed by dissociation of the solute, and correct  $v_i$  to account for non-ideal behavior of the system by including the activity coefficient. Note that in mixed and non-ideal solutions, the sum of mole fractions is  $f_w x_w + \sum_i f_i x_i = 1$ . Since the ZSR-relation is usually applied in aerosol modeling to calculate the total water mass from the water mass fractions of binary solutions, it is sufficient to consider only binary solutions in the next section. To correct for non-ideal solutions at lower relative humidities, we must, however, consider activity coefficients, for which we first use an arbitrary correction factor,  $f_i$ , which will be interpreted later (in Section 3.5.3).

### 3.5.1 Parameterization of Aerosol Water

The water content of the aerosol particles is  $W = n_w M_w$  [mol/kg], which we can express, according to the above discussion, as

$$W_i = n_i M_i / (1000 f_i v_i^{v_i} (1/rh-1)). \quad (3.5b)$$

To compare this analytical expression (Eq. 3.5b) with the calculation of the water mass fractions of single-solutes as used in EQMs (Eq. 2.20), we have included the results of Eq. (3.5b) in [Figure 3.2](#), marked in red (thin solid lines). To obtain the above water mass fractions (Section 3.4), we have used the following parameters: A dissociation number  $v_i = 2$  for ammonium nitrate ( $M_{\text{NH}_4\text{NO}_3}=80\text{g/mol}$ ), and ammonium bisulfate ( $M_{\text{NH}_4\text{HSO}_4}=115\text{g/mol}$ ), and  $v_i = 3$  for ammonium sulfate ( $M_{(\text{NH}_4)_2\text{SO}_4}=132\text{g/mol}$ ). For simplicity, we have assumed constant values, which did not depend on RH; and for all cases a correction factor  $f_i = 0.81$  (discussion follows in Section 3.5.3).

The comparison of the analytical expression (Eq. 3.5b) for the aerosol water fractions of single-solutes ([Figure 3.2](#), red, thin solid lines) shows overall excellent agreement with the values obtained from the equilibrium calculations with ISORROPIA ([Figure 3.2](#), black, thick lines). Nevertheless, the calculation of the water mass fractions with Eq. (3.5b) results, for the ammonium nitrate case, in a slightly increasing overestimation with decreasing relative humidity, and in a slight underestimation for the ammonium bisulfate and ammonium sulfate cases. These shifts arise, because we have assumed constant parameters of  $n_i$ ,  $v_i$ , and in particular  $f_i$ , for all values of RH. In contrast, EQMs explicitly calculate the equilibrium composition, i.e.  $n_i$  and, hence,  $W_i$  from Eq. (2.20), by which  $m_{i,ss}(\text{RH})$  is derived from tabulated measurements ([Figure 3.1](#)). Obviously, this leads to a slightly overestimation for aerosol compounds treated as volatile (in EQMs), such as ammonium nitrate, as RH decreases, but to an underestimation for non-volatile compounds such as ammonium bisulfate and ammonium sulfate. However, [Figure 3.2](#) shows that the aerosol water is for a fixed  $n_i$  a strong function of RH, for both Eq. (3.5b) and Eq. (2.20), because it is based on the molality scale, which depends for atmospheric aerosols on RH.

### 3.5.2 Parameterization of Aerosol Molality

Comparing equation (3.5b) with the definition of the molality of single-solute solutions,  $m_{i,ss}(\text{RH})= n_i / W_i(\text{RH})$  (used in Eq. 2.20), we can express  $m_{i,ss}(\text{RH})$  as

$$m_{i,ss}(\text{RH})= [(1000 \cdot f_i \cdot v_i^{v_i} \cdot (1/rh-1)) / M_i]^{z_i}, \quad (3.6)$$

if we include the charge carried by the ions of an ion pair, which is denoted by  $z_i$ .

Equation (3.6) allows us to reproduce the molalities of the single-solute solutions according to [Figure 3.1](#), if the previous parameters for  $v_i$  and  $M_i$  are used for  $\text{NH}_4\text{NO}_3$ ,  $(\text{NH}_4)_2\text{SO}_4$ , and  $\text{NH}_4\text{HSO}_4$ ; for the latter a value of  $1.5 \cdot v_i^{v_i}$ ; and the following parameters for  $v_i$  and  $M_i$  for  $\text{H}_2\text{SO}_4$  and

$(\text{NH}_4)_3\text{H}(\text{SO}_4)_2$ :  $v_i = 2$  and  $M_{\text{H}_2\text{SO}_4} = 98\text{g}$ ,  $v_i = 3$  with  $1/3 v_i^{v_i}$  and  $M_{(\text{NH}_4)_3\text{H}(\text{SO}_4)_2} = 115\text{g}+132\text{g}$ ;  $z_i = 1/2$  for  $\text{H}_2\text{SO}_4$ , and  $z_i = 3/4$  for  $(\text{NH}_4)_2\text{SO}_4$ , and unity  $z_i$  values for all other; and  $f_i$  for all electrolytes as above. The molalities obtained with the analytical expression (Eq. 3.6) are marked in red.

Thus, it follows from Figure 3.1 that, because of the definition of the molality in single-solute solutions and the water mass that is associated with atmospheric aerosols, both  $v_i$  and  $f_i$  are independent of the total number of dissolved molecules, i.e. the ion pair concentration.  $v_i$  is fixed, since complete dissociation is assumed for  $\text{RH} > \text{RHD}$ , while  $f_i$  is constant, because under equilibrium conditions the water mass increases with the ion pair concentration, so that the molality remains constant.

This implies that the correction factor  $f_i$  is a function of  $\text{RH}$  for a given molality. Assuming that  $f_i$  corrects for ion-ion interactions, it depends on the charge density of the solution, whereas the charge density is a function of ion charge and  $\text{RH}$  (the latter because  $\text{RH}$  determines the aerosol water). Since the aerosol water, i.e. water fractions increase as the ion pair concentration increases,  $f_i$  appears to depend to a first approximation for a given  $\text{RH}$  only on the ion charge, i.e. the composition of the solution but not on the concentration. If this can be generalized, this yields a non-iterative estimation method for activity coefficients.

### 3.5.3 Parameterization of Aerosol Activity Coefficients

Let us assume that  $f_i$  represents the ratio of the mean binary activity coefficient  $\gamma_{i\pm}$  of solute  $i$  (e.g. ammonium nitrate) and the corresponding water activity coefficient  $\gamma_w$ , according to the ratio of the mole fractions (Section 3.5). If we further express the molality of the ion pair in terms of the ratio of the water activity of the solution and  $\gamma_w$ , where we have to apply, for mixed solutions, the ZSR-relation to account for the water content of  $N$  single-solute solutions, then we can rewrite Eq. (3.5b) to yield an analytical expression for activity coefficients of a mixed solutions, i.e.

$$\gamma_{i\pm} = [ rh^N / (1000 / N \cdot (1-rh) + N) ]^{1/z_i^\pm} \quad (3.7)$$

$N$  accounts for the summation over  $N$  single-solute solutions. The activity coefficient of an ion-pair in the mixed solution is related to the activity coefficients of the corresponding ions by  $\gamma_{i\pm}^{z_i^\pm} = (\prod_{i+} \gamma_{i+}^{z_i^{+}} \cdot \prod_{i-} \gamma_{i-}^{z_i^{-}})$ , with  $z_i^\pm = 4 / Z$ . The ion pair charge per mol is  $Z = (\sum_+ z^+ + \sum_- z^-) / \sum n_{z^\pm}$ , with  $z^+ = e_+^{e^+}$  and  $z^- = e_-^{e^-}$ , where  $e^+$  and  $e^-$  denote the charge of the cation and anion, respectively.

Note that  $N$  represents a mean value, since the water mass fraction of the  $i$ -th ion pair in a mixed solution is given by the total water content of the aerosol divided by the number of ion pairs in the solution. The corresponding  $z_i^\pm$  values for major ion pairs used in various EQMs, e.g. SCAPE, are shown in Table 3.1.

**Table 3.1.**  $z_i^{\pm}$  values for ion pairs considered in various EQMs (e.g. SCAPE).

$Z_1^{\pm} = 4/Z$	Ion pair charge Z	Species			
4	$(1 \cdot 1^1 + 1 \cdot 1^1) / 2$	NH <sub>4</sub> NO <sub>3</sub>	NH <sub>4</sub> HSO <sub>4</sub>	NH <sub>4</sub> <sup>+</sup> , OH <sup>-</sup>	NaCl
		NaNO <sub>3</sub>	NaHSO <sub>4</sub>	H <sup>+</sup> , NO <sub>3</sub> <sup>-</sup>	KCl
		KNO <sub>3</sub>	KHSO <sub>4</sub>	H <sup>+</sup> , HSO <sub>4</sub> <sup>-</sup>	HCl
2	$(2 \cdot 1^1 + 1 \cdot 2^2) / 3$	(NH <sub>4</sub> ) <sub>2</sub> SO <sub>4</sub>	CaCl <sub>2</sub>	MgCl <sub>2</sub>	K <sub>2</sub> SO <sub>4</sub>
2.5	$(4 \cdot 1^1 + 1 \cdot 2^2) / 5$	(NH <sub>4</sub> ) <sub>3</sub> H(SO <sub>4</sub> ) <sub>2</sub>			
1	$(1 \cdot 2^2 + 1 \cdot 2^2) / 2$	CaSO <sub>4</sub>	MgSO <sub>4</sub>		

$z_i^{\pm} = 4/Z$ , and  $Z = (\sum_+ z^+ + \sum_- z^-) / \sum n_{z^{\pm}}$ , with  $z^+ = e_+^{c^+}$  and  $z^- = e_-^{c^-}$   
and (NH<sub>4</sub>)<sub>3</sub>H(SO<sub>4</sub>)<sub>2</sub> (letrovicite) = (NH<sub>4</sub>)<sub>2</sub>SO<sub>4</sub>\* NH<sub>4</sub>HSO<sub>4</sub>

According to Eq. (3.6), mean binary activity coefficients  $\gamma_{i\pm}$  can directly be derived from the definition of the molality in single-solute solutions, i.e.

$$\gamma_{i\pm} = [ 2 / (55.51 \cdot m_{i,ss}(RH) + 1) ]^{1/z_i^{\pm}} \quad (3.8)$$

To give an example, we have plotted in Figure 3.3 for the NH<sub>3</sub>-HNO<sub>3</sub>-H<sub>2</sub>SO<sub>4</sub>-system various activity coefficients versus RH. The upper panels show the activity coefficient of NH<sub>4</sub>NO<sub>3</sub>, and the lower panels the activity coefficient of (NH<sub>4</sub>)<sub>2</sub>SO<sub>4</sub>. The left panels show  $\gamma_{i\pm}$  calculated with ISORROPIA for two different ion pair concentrations, 1  $\mu$ mol (black) and 1/2  $\mu$ mol (yellow). The right panels show the activity coefficients as calculated with various equilibrium models and activity coefficient calculation methods for the 1  $\mu$ mol case: ISORROPIA (black), MARS (green), SCAPEa & Pitzer-method (blue), SCAPEb & K-M-method (yellow), SCAPEb & Bromley-method (light-blue), SEQUILIB (aqua). For comparison, the activity coefficients calculated with Eq. (3.7) is included using a value of N=1.5 for both activity coefficients (red solid line, right panels). The input concentration for the equilibrium calculations were fixed, similar to Figure 3.2, so that the relative humidity was the only variable, and scatter due to temperature dependence of the equilibrium constant and deliquescence point were avoided.

First of all, Figure 3.3 shows that the  $\gamma_{i\pm}$  is independent of the ion pair concentration for both NH<sub>4</sub>NO<sub>3</sub> and (NH<sub>4</sub>)<sub>2</sub>SO<sub>4</sub> (left panels), and that the activity coefficients calculated with equation (3.7) are within the range of the activity coefficients of all EQMs (right panels, red lines). Second, the  $\gamma_{i\pm}$  obtained from either equation (3.7) or (3.8) yield the same result, so that we have omitted the one of Eq. (3.8) for clarity. Third, the calculation of both activity coefficients (the  $\gamma_{i\pm}$  of NH<sub>4</sub>NO<sub>3</sub> and (NH<sub>4</sub>)<sub>2</sub>SO<sub>4</sub>) with Eq. (3.7) reproduces the activity coefficients within the range of results obtained by various different iterative schemes and various equilibrium models. This shows that the two activity coefficients shown can be expressed through each other. It further confirms our presumption that  $\gamma_{i\pm}$  depends on the charge-density in the solution, which is in turn a strong function of RH and ion charge.

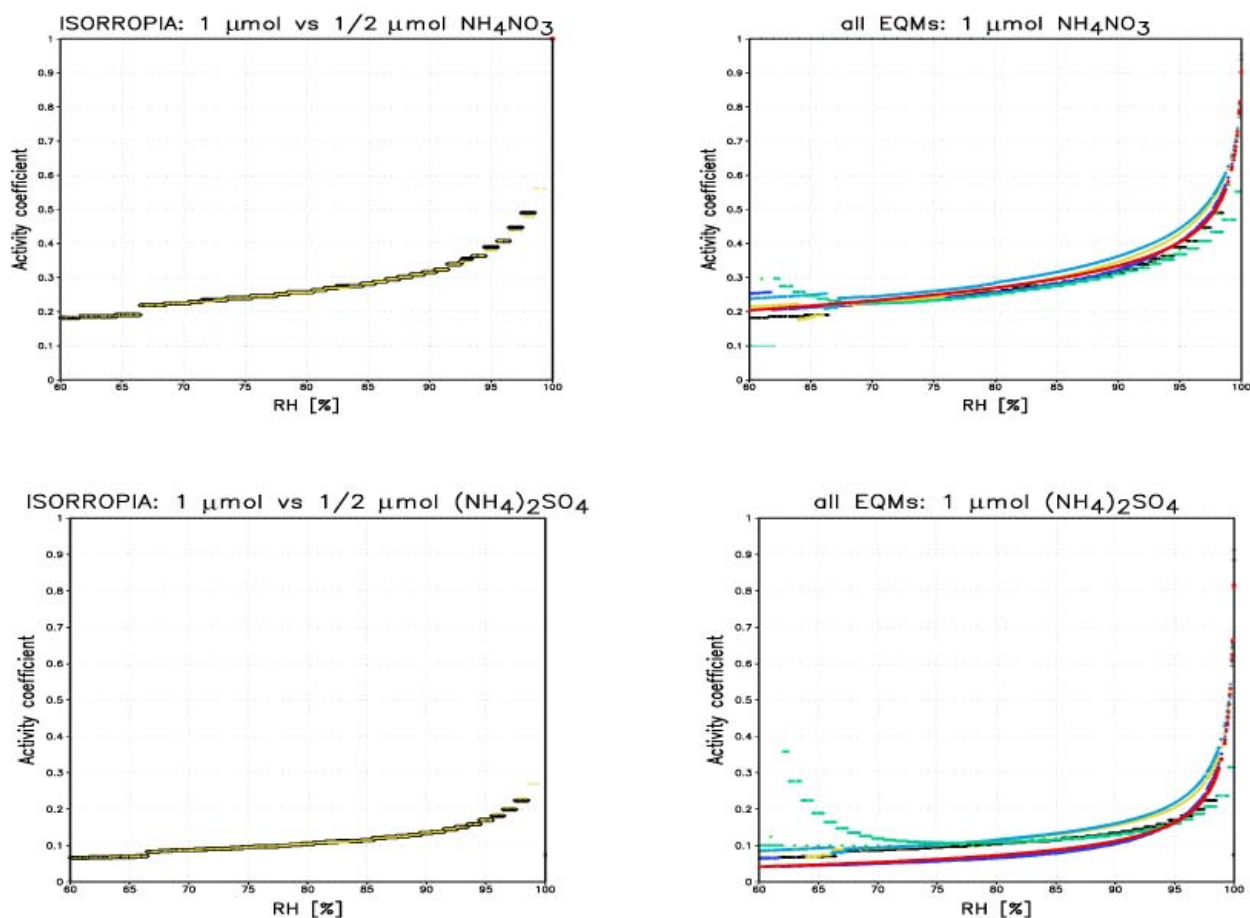


**Figure 3.3.** Mean binary activity coefficient vs. RH: top panels  $\gamma_{i\pm}$  of  $\text{NH}_4\text{NO}_3$ , bottom  $\gamma_{i\pm}$  of  $(\text{NH}_4)_2\text{SO}_4$ . Left panels shows the  $\gamma_{i\pm}$  for a 1  $\mu\text{mol}$  (black) vs. 1/2  $\mu\text{mol}$  (yellow) ion pair concentration (calculated with the EQM ISORROPIA), the right panels show the  $\gamma_{i\pm}$  for a 1  $\mu\text{mol}$  case and equilibrium calculations with various EQMs: ISORROPIA (black), MARS (green), SCAPEa & Pitzer-method (blue), SCAPEb & K-M-method (yellow), SCAPEb & Bromley-method (medium-blue), SEQUILIB (aqua), and Eq. (3.7) with  $N=1.5$  (red lines).

Thus, all activity coefficients used in the EQMs presented, can be obtained sufficiently accurately from each other using the following power function:

$$\gamma_i = \gamma_j^\xi \quad (3.9)$$

The corresponding exponents  $\xi = Z_i^\pm / Z_j^\pm$ ;  $Z_{i,j}^\pm = 4/Z$  are given in Table 3.1. Consequently, for atmospheric aerosol modeling only one activity coefficient needs to be known to derive an equilibrium state. For instance, the mean activity coefficient  $\gamma_i$  of  $\text{NH}_4\text{NO}_3$  can be approximated from that of  $\text{CaSO}_4$  through  $\gamma_i = \gamma_j^{0.25}$ , and  $\gamma_i$  of  $(\text{NH}_4)_2\text{SO}_4$  from  $\gamma_i$  of  $\text{NH}_4\text{NO}_3$  through  $\gamma_i = \gamma_j^2$ .

The types of activity coefficients used in the EQMs are shown in Figure 3.4, plotted as a function of relative humidity. The black lines represents the  $\gamma_{i\pm}$  of SCAPEa (Pitzer-method), the red thin lines Eq. (3.7). Generally, the activity coefficient departs for a given RH further from unity as the charge carried by the species increases. From top to bottom the types of activity coefficients represent the  $\gamma_{i\pm}$  of  $\text{NH}_4\text{NO}_3$ ,  $(\text{NH}_4)_3\text{H}(\text{SO}_4)_2$ ,  $(\text{NH}_4)_2\text{SO}_4$  and  $\text{CaSO}_4$ .

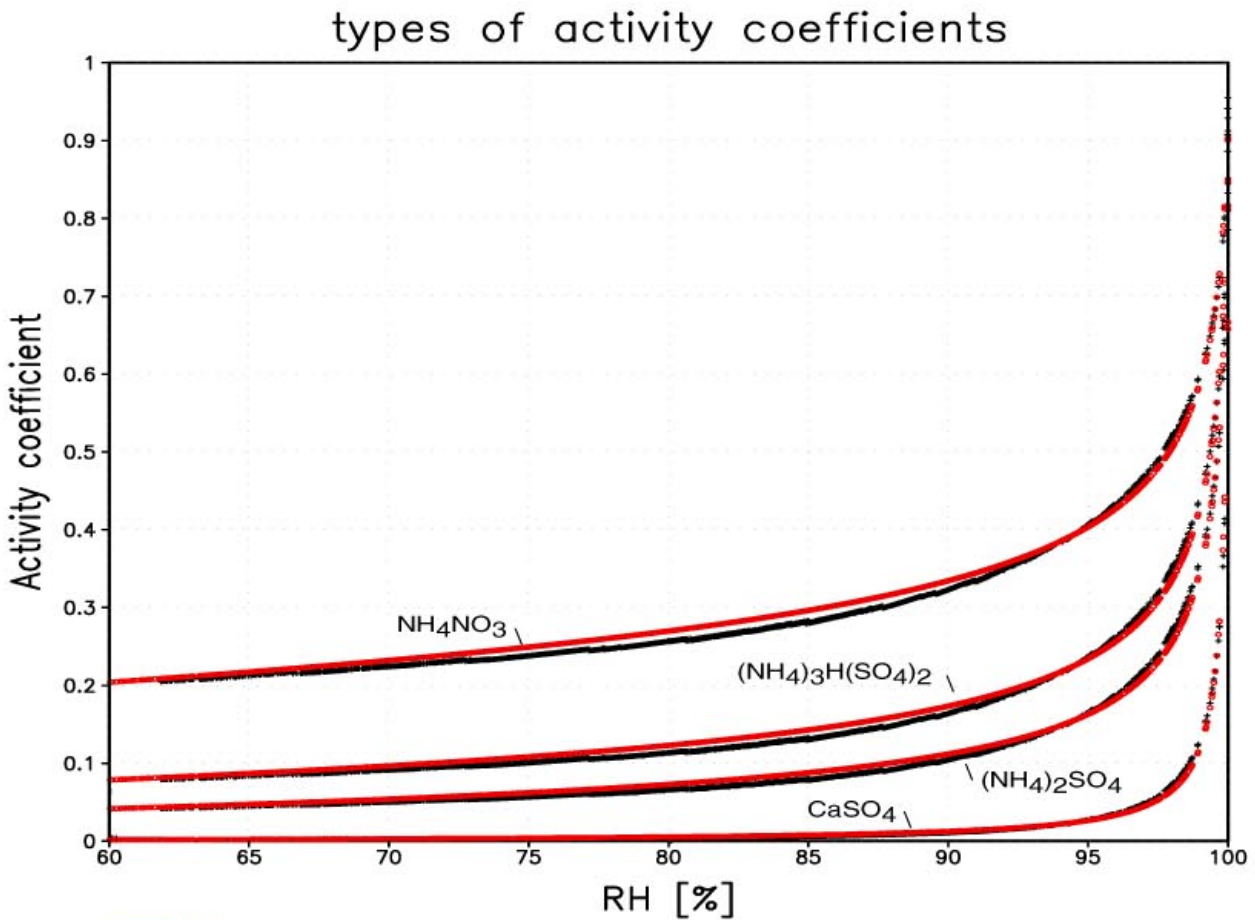


**Figure 3.4.** Effect of relative humidity on activity coefficients. The black lines represent the  $\gamma_{iz}$  of the EQM SCAPEa (Pitzer method), the red lines Eq. (3.7) with  $N=1.5$ . The types of activity coefficients used in EQMs are represented by the  $\gamma_{iz}$  of  $\text{NH}_4\text{NO}_3$ ,  $(\text{NH}_4)_3\text{H}(\text{SO}_4)_2$ ,  $(\text{NH}_4)_2\text{SO}_4$  and  $\text{CaSO}_4$ .

The  $\gamma_{iz}$  - RH relationship shows that the activity coefficients of salt solutes of an atmospheric aerosol (which is in equilibrium with the relative humidity) approaches one as the fractional relative humidity approaches one. Figure 3.4 further shows that differences between various activity coefficient estimation methods and Eq. (3.7) are rather small. Thus, these activity coefficients are basically a function of relative humidity, as is Eq. 3.7. The strong  $\gamma_{iz}$ -RH relationship can therefore be understood as a consequence of the increasing dilution of aerosols with increasing relative humidity, which is caused by the well-known equilibrium growth due to water uptake. Note that the  $\gamma_{iz}$ -RH relationship also holds for activity coefficients of mixed solutions (Figure 3.3), because of the ZSR-relation which is used in all EQMs to calculate the aerosol water.

Therefore all types of activity coefficients (according to Figure 3.4) used in the EQMs presented can be approximated with the above new method, i.e. an analytical activity coefficient calculation. Those results, i.e. obtained with Eq. (3.7), are within the range of results obtained with different numerical (iterative) activity coefficient calculation methods of various equilibrium models (according to Figure 3.3). Note that this is true in general, and not only for the case where the relative humidity is the only variable (both temperature and input concentration were up to now kept constant).

### 3.6 Sensitivities of the Activity Coefficient Calculation (ACC)

In this section we evaluate the  $\gamma_{\text{iz}}$  - RH relationship (Eq. 3.7) relative to various EQMs and activity coefficient calculation (ACC) methods. First, we show that the new method is applicable in general, for which we investigate the effects of temperature variations, various compositions, and different concentration domains on the  $\gamma_{\text{iz}}$ -RH relationship, using arbitrary (though realistic) input fields which represent a wide range of atmospheric conditions (see Chapter 4.2). Second, we will implement Eq. (3.7) into various EQMs and compare the results of such parameterized EQMs with their original versions; the equilibrium models used for this sensitivity study were presented in Chapter 2.1.

#### 3.6.1 ACC vs. Aerosol Concentrations and Temperature

To show the effect of input parameters on activity coefficients, the  $\gamma_{\text{iz}}$  of  $\text{NH}_4\text{NO}_3$  is plotted in [Figure 3.5](#) for various cases: Panel (a) shows, for reference,  $\gamma_{\text{iz}}$  of  $\text{NH}_4\text{NO}_3$  for the 1  $\mu\text{mol}$  case at a temperature fixed to 298.15 K (according to [Figure 3.3](#)); Panel (b) shows the same activity coefficient for a temperature variation and a concentration range, panel (c) the same for various aerosol compositions, including sea salt and mineral dust (discussion follows), and panel (d) for different domains. For comparison, the  $\gamma_{\text{iz}}$  obtained with Eq. (3.7) is included in all panels with a constant value of  $N=1.5$  (red, thin line). Note that the  $\text{NH}_4\text{NO}_3$  activity coefficient shown in panel (a) has been calculated with various equilibrium models and activity coefficient calculation methods: ISORROPIA (black), MARS (green), SCAPEa & Pitzer-method (blue), SCAPEb & K-M-method (yellow), SCAPEb & Bromley-method (light-blue), SEQUILIB (aqua), and that the  $\gamma_{\text{iz}}$  obtained with Eq. (3.7) ranges in-between the results obtained (as discussed above).

The comparison of panel (a) and (b) ([Figure 3.5](#)) further illustrates that temperature variations and a concentration range have a much weaker effect on  $\gamma_{\text{iz}}$  than different aerosol compositions (c), or different domains (d). The reason is that the concentration range cannot have a strong influence, since the water uptake is proportional to the total amount of dissolved matter (as discussed previously). Thus, only the temperature effect remains, which affects  $\gamma_{\text{iz}}$  mostly due to changes in aerosol composition when evaporation or crystallization occurs, i.e. when RH is in the mutual deliquescence humidity range. According to [Figure 3.5](#), the activity coefficient is most sensitive to the case of different aerosol compositions (c), or different domains (d), which will therefore be investigated in greater detail.



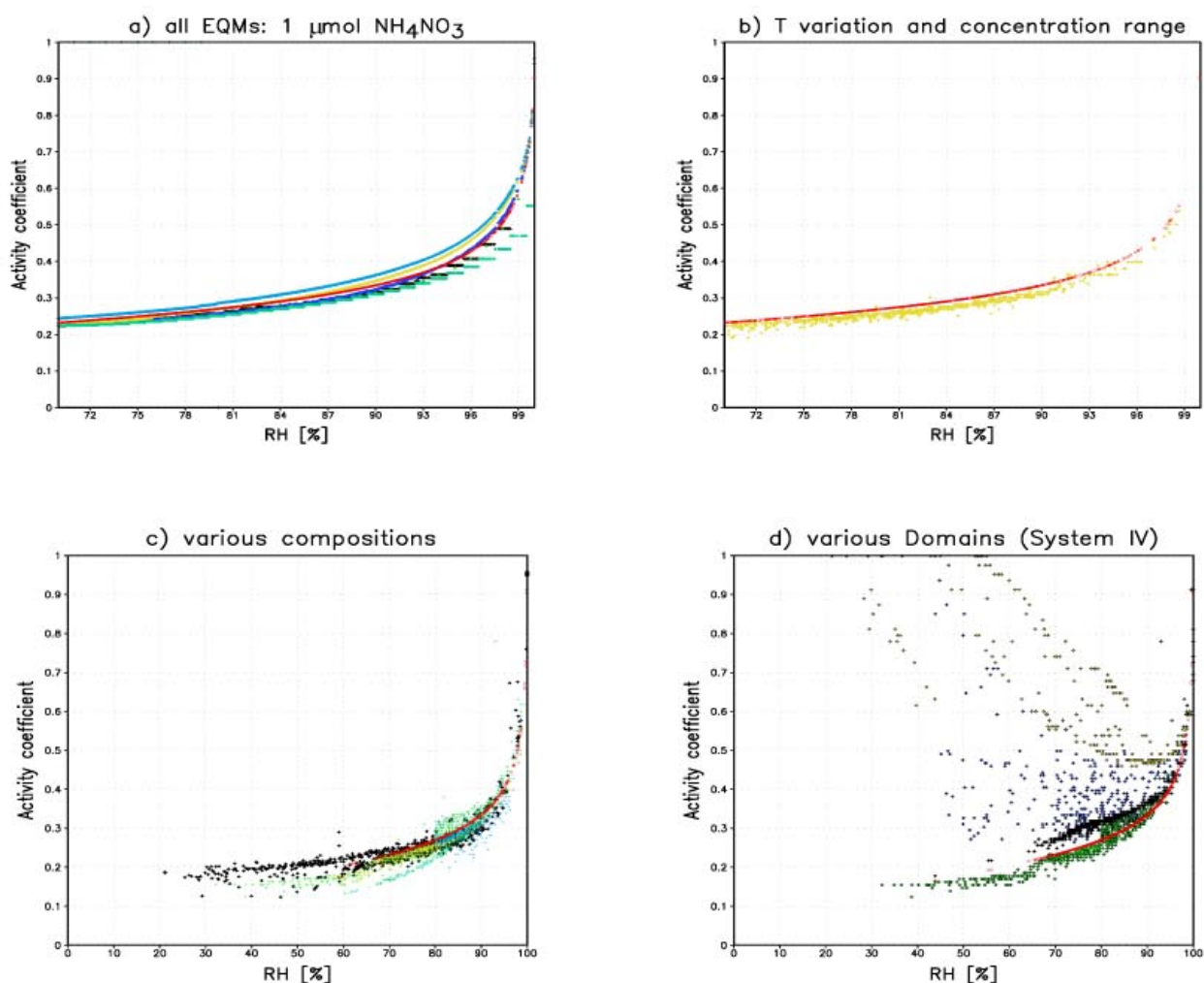


**Figure 3.5.** Effect of input parameters on the mean binary activity coefficient of  $\text{NH}_4\text{NO}_3$ . Panel (a) shows  $\gamma_{i\pm}$  for an ion pair concentration of  $1 \mu\text{mol NH}_4\text{NO}_3$  as a function of relative humidity [%] for equilibrium calculations with various EQMs (System III): ISORROPIA (black), MARS (green), SCAPEa and Pitzer-method (blue), SCAPEb and K-M-method (yellow), SCAPEb and Bromley-method (light-blue), SEQUILIB (aqua) (the references are given in Chapter 2.1). Panel (b) shows the sensitivity of  $\gamma_{i\pm}$  (ISORROPIA, System III) to temperature variations and a concentration range. Panel (c) shows the sensitivity of  $\gamma_{i\pm}$  to various compositions: System I =  $\text{NH}_3\text{-H}_2\text{SO}_4$  (light-blue), System II =  $\text{NH}_3\text{-HNO}_3$  (aqua), System III =  $\text{NH}_3\text{-HNO}_3\text{-H}_2\text{SO}_4$  (yellow), System IV = III + sea salt (green), System V = IV + mineral dust ( $\text{K}^+$ ,  $\text{Mg}^{2+}$ ,  $\text{Ca}^{2+}$ ) (black). System I-IV represents equilibrium calculations of ISORROPIA, System V of SCAPEa. Panel (c) includes temperature variations and a concentration range. Panel (d) shows  $\gamma_{i\pm}$  (ISORROPIA) for different domains of System IV: Domain 1 (black); Domain 2 (green); Domain 3 (blue); Domain 4 (yellow). For comparison, the result of equation (3.7) based on a constant value of  $N=1.5$  is included in each panel (red, thin lines).

### 3.6.2 ACC vs. Aerosol Compositions

To investigate the sensitivity of the activity coefficient to the case of different aerosol compositions, we define 5 different aerosol systems, representing: (I) ammonia and sulfuric acid ( $\text{NH}_3\text{-H}_2\text{SO}_4$ -System); (II) ammonia and nitric acid ( $\text{NH}_3\text{-HNO}_3$ -System); (III) ammonia, nitric acid and sulfuric acid ( $\text{NH}_3\text{-HNO}_3\text{-H}_2\text{SO}_4$ -System); (IV) system III + sea salt ( $\text{NH}_3\text{-HNO}_3\text{-H}_2\text{SO}_4\text{-Na-Cl}$ -System);

(V) system IV + mineral dust (K, Mg, Ca). Figure 3.6 shows the effect of composition on activity coefficients in detail, corresponding to panel (c) of Figure 3.5. Panel (a) shows  $\gamma_{\text{it}}$  of  $\text{NH}_4\text{NO}_3$  for system II (upper line) and of  $(\text{NH}_4)_2\text{SO}_4$  for system I (lower line), panel (b) shows both activity coefficients for system III, (c) for system IV, and (d) for system V (same order).

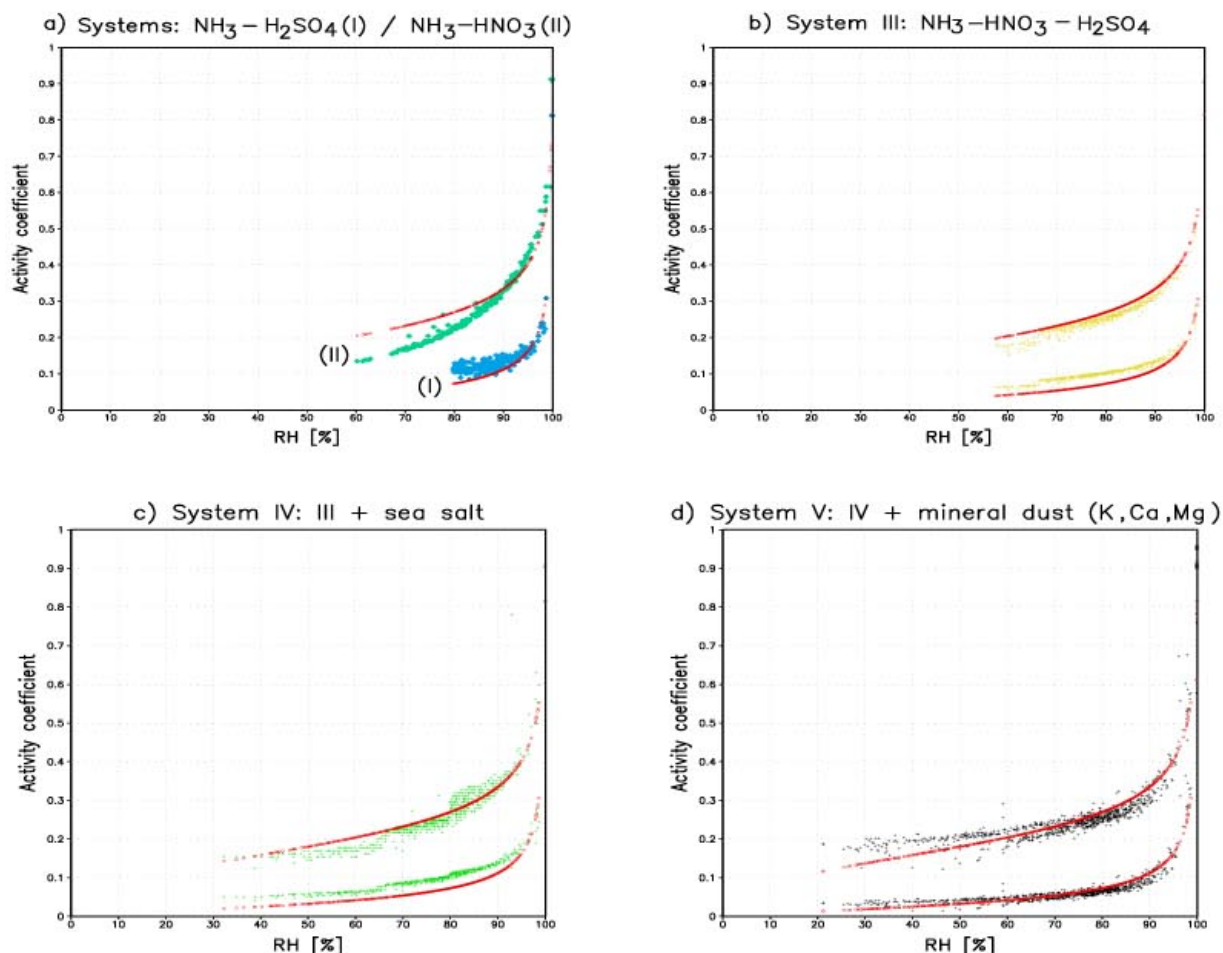


**Figure 3.6.** Effect of composition on activity coefficients of Figure 3.5c in detail.

First of all, the activity coefficients calculated with Eq. (3.7) reasonably matches all compositions, even though the parameter  $N$  is held constant ( $N=1.5$ , i.e. determined to best fit these various data). The comparison of panel a-d) (Figure 3.6) further illustrates the differences in the assumed deliquescence points of the different aerosol types: while a pure ammonium sulfate aerosol droplet (System I) deliquesces around a relative humidity of 80%, a pure ammonium nitrate aerosol droplet deliquesces at RH 60%. Aerosol droplets, which include sea salt already deliquesce around a RH of 30%, since magnesium chloride (part of the sea salt) is very hygroscopic. Therefore, water uptake can occur at a relatively low relative humidity. Subsequent deliquescence changes the composition of the aqueous droplet so that the relative strongest scatter occurs for system IV and V. In contrast, the activity coefficient calculated analytically with Eq. (3.7) does not show any scatter, since we have chosen for the sake of simplicity, a constant value of  $N$  (as mentioned above).

### 3.6.3 ACC vs. Aerosol Concentrations Domains

Figure 3.7 shows the effect of the use of different domains on calculated activity coefficients according to Figure 3.5 (d) in detail. Panel (a) shows  $\gamma_{\text{it}}$  of  $\text{NH}_4\text{NO}_3$  for various domains of System IV, and panel (c) of System V. Accordingly, panel (b) shows the  $\gamma_{\text{it}}$  of  $(\text{NH}_4)_2\text{SO}_4$  for various domains of System IV, and panel (d) of System V. The colors represent: Domain 1 (black) = cation rich; Domain 2 = sulfate neutral (green); Domain 3 = sulfate rich (blue); Domain 4 = sulfate very rich (yellow). For comparison, Eq. (3.7) is included for all cases with  $N=1.5$  (red line).

The relatively strongest deviations of the analytically and iteratively determined activity coefficients occur for domain 3 (i.e.  $2\text{NH}_4^+ < \text{SO}_4^{2-}$ ) and domain 4 ( $\text{NH}_4^+ < \text{SO}_4^{2-}$ ). The reason is that the activity coefficients obtained with Eq. (3.7) can only decrease with decreasing relative humidity, which describes very well the behavior of salt solutes, while deviations from this behavior occur for acidic solutions. Most, but not all, iterative methods predict, if a certain solute concentration is reached, even an unusual increase of the activity coefficients with increasing solute activity, i.e. decreasing relative humidity. Note that solutions with equal or similar ions behave generally more ideal than others. The behavior of activity coefficients obtained with EQMs probably reflects the much stronger ion-ion interactions of strong acidic solutions (Domain 3 and 4), i.e. those which contain sulfuric acid. However, to our knowledge, the calculation of any activity coefficients at high ionic strength is highly uncertain, because of the lack of validation, as mentioned earlier (see Chapter 2.6.4). This applies to strong acidic solutions as well as other solutions.

Fortunately, the deviation in the activity coefficient predictions for acidic aerosols has not much influence on the estimate of other aerosol properties such as the total particulate matter, or the gas/aerosol partitioning. The reason is that volatile species, such as ammonium nitrate, cannot be present in strong acidic solutions, because in these acidic solutions there is insufficient ammonia (or other cations) to neutralize the acidic aerosol particle which mostly consist of sulfuric acid (see discussion in Chapter 2.7). Therefore, and because all sulfate compounds are treated in all EQMs as non-volatile, gas/aerosol partitioning does then not occur. Furthermore, even the aerosol water is insensitive to the activity coefficient calculation for the case of acidic aerosols, because it only depends on the total amount of dissolved matter, which anyhow remains in the particulate phase since all species are then treated as non-volatile.

For instance, the strongest deviation occurs for sulfuric acid, i.e. Domain 4 (yellow) in panel (d) of Figure 3.5, and Figure 3.7, which have been calculated with the EQM ISORROPIA (System IV, upper panels). Note that the activity coefficient for ammonium nitrate is fictive, i.e. calculated although not used since ammonium nitrate cannot exist in this case, but it represents the behavior of the activity coefficient of sulfuric acid because of Eq. (3.9). However, for the acidic cases, the total amount of sulfuric acid is assumed to remain in the aqueous phase, regardless of the activity coefficient calculation, because of its strong hygroscopicity (there is no deliquescence considered,

as mentioned in Chapter 2.5). Because there are no other compounds present in this case, both total dry particulate matter and aerosol water can be obtained without loss of accuracy. The same is true for domain 3, in which a mixture of sulfuric acid and ammonium bisulfate can exist, since the amount of the latter can be determined by pure stoichiometry, i.e. the ammonium/sulfate ratio, as previously mentioned (Chapter 2.8).

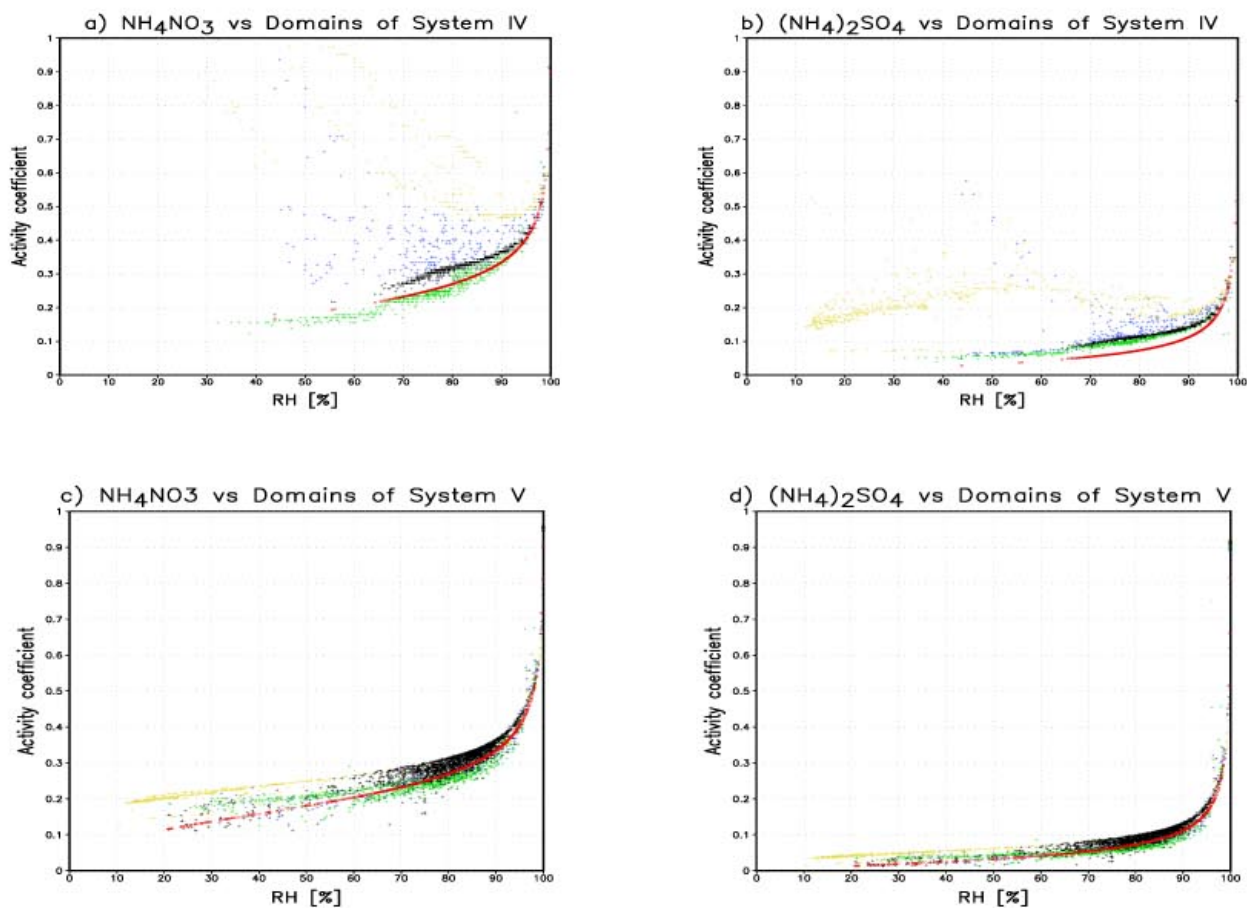


**Figure 3.7.** Effect of different domains on activity coefficients of Figure 3.5d in detail.

Besides the uncertainty in activity coefficients that is associated with the prediction of acidic aerosols with global models, their occurrence itself is highly uncertain. Especially, if one does not account for the total background aerosol mass, or processes such as nucleation, which becomes important for remote locations with a low aerosol load.

To illustrate the situation, the global distribution of concentration domains is shown in Figure 3.8. The domains for various systems of atmospheric aerosol compositions correspond to: (a) System I; (b) System III, (c) System IV, (d) System V (Section 3.6.2). Note that panel (a) shows the same global distribution of domains as panel (b), since ammonium is the only neutralization product for both the ammonia, sulfuric acid system (System I), and the ammonia, nitric acid, sulfuric acid system (System III). Panel (c) and panel (d) further illustrate that the global distribution of domain 3 and 4 reduces as the number of aerosol species considered increases (for a given model resolution).

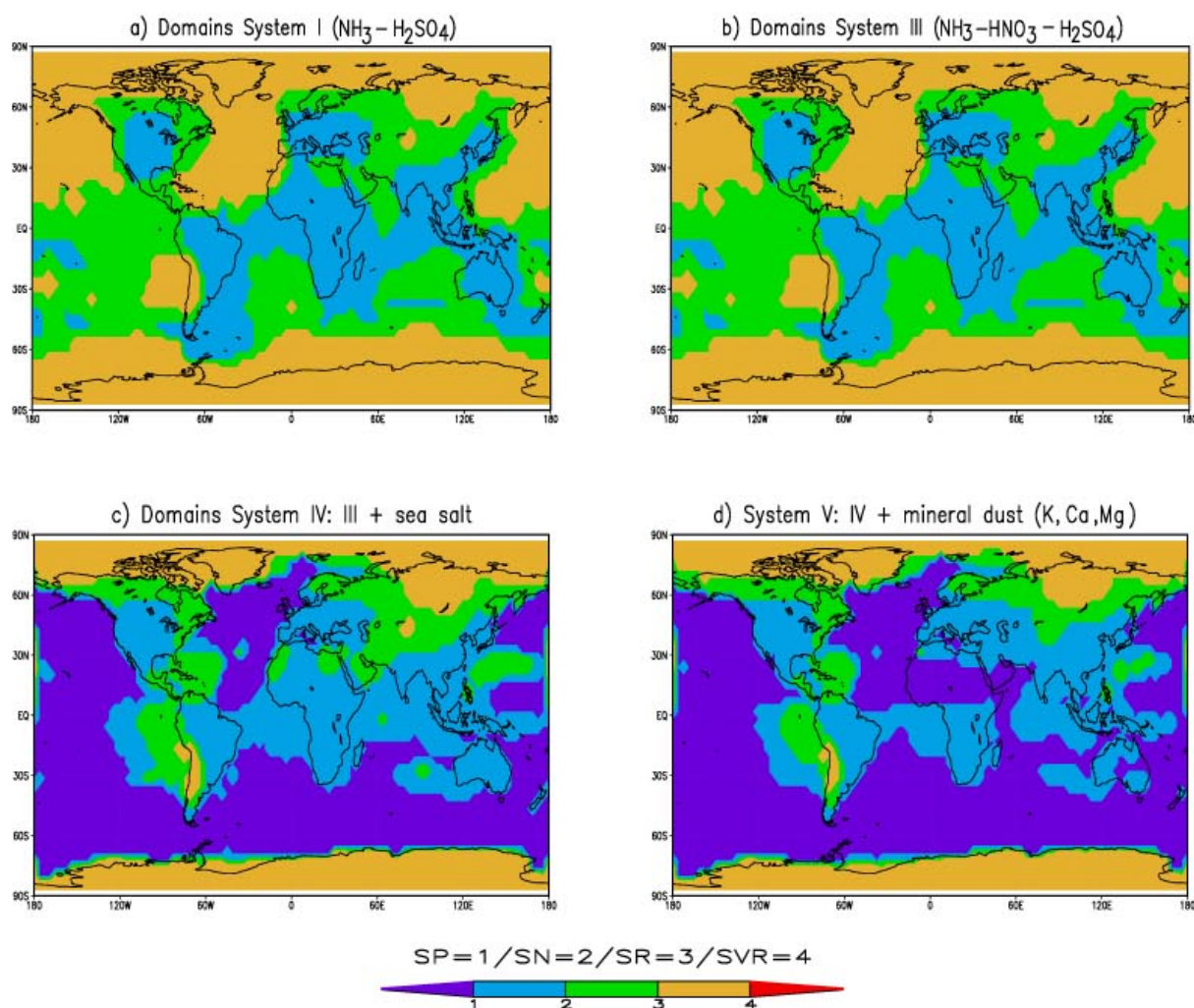


**Figure 3.8.** Domains for various systems of atmospheric aerosol compositions. The concentrations domains are abbreviated according to their definition in Chapter 2.4: SP = sulfate poor case (cation rich); SN = sulfate neutral case; SR = sulfate rich case; SVR = sulfate very rich case.

### 3.7 Non-iterative vs. iterative ACC Method

In this section we apply Eq. (3.7) to various EQMs and compare the non-iterative activity coefficient calculation method with original iterative schemes. In order to show the effect on the total particulate matter (PM) [ $\mu\text{g}/\text{m}^3$ ], we have plotted in Figure 3.9 scatter plots for each domain and various EQMs. Note that each equilibrium model has been modified so that the non-iterative (analytical) method, i.e. Eq. (3.7), substituted the original activity coefficient calculation (ACC) methods, and that the domain number was used for N.

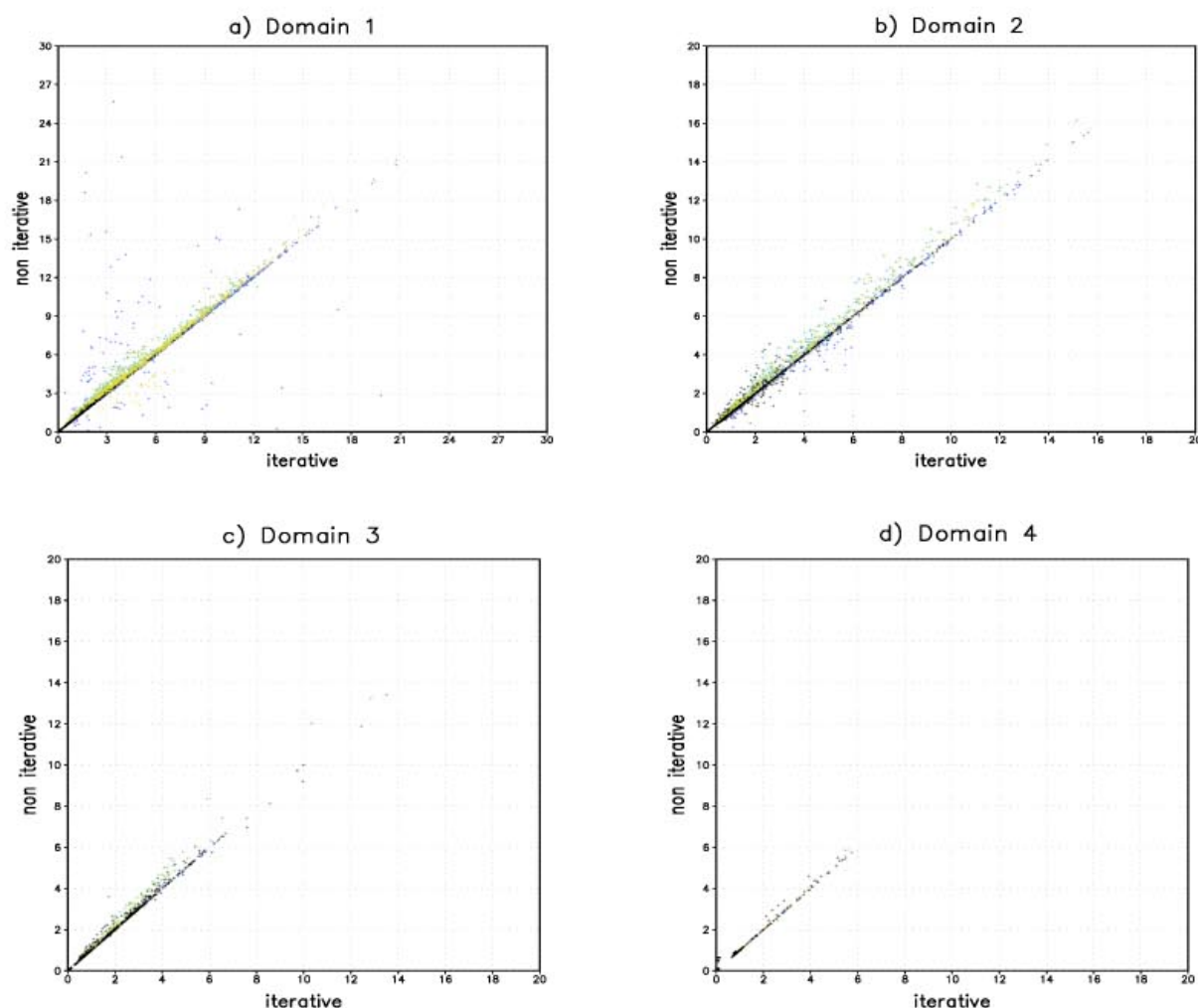


**Figure 3.9.** Scatter plots of total particulate matter (PM) in  $[\mu\text{g}/\text{m}^3]$  for various domains and equilibrium models: ISORROPIA (black), MARS (green), SCAPEa & Pitzer-method (blue), SCAPEb & K-M-method (yellow), SCAPEb & Bromley-method (medium-blue), SEQUILIB (aqua). Domain 1 represents System IV for ISORROPIA and System V for SCAPEa,b; Domain 2, 3 and 4 represent System III for all models.

Figure 3.9 shows that the use of iterative or non-iterative activity coefficient calculation methods do not strongly influence PM calculations. The relative strongest difference, however, occurs for the EQM SCAPEa & Pitzer-method (blue) for cases where sea salt is considered, which must be attributed to convergence problems for solid sodium chloride and sodium nitrate in the iterative scheme. Apart from that, differences are small for all other cases. Note that SCAPEb has similar difficulties when the Pitzer-method is used, which is why this combination was omitted. However, such difficulties are only limited to iterative schemes (original) and not to the non-iterative activity coefficient calculation, which we propose as an alternative for global modeling. Note that all EQMs compare rather well when the non-iterative method is used. This will be discussed in greater detail in the next chapter, where we compare various aerosol properties calculated with the above EQMs, using the parameterized and original versions. The comparison will also include a new and simplified equilibrium model, which is entirely based on the new method presented above and some additional simplifications. This new model will be described in the next section.

### 3.8 A new and simplified Gas/Aerosol Model (EQSAM)

Based on the results obtained with various equilibrium models, we will present in this section a new and simplified equilibrium model, which is based on additional simplifications allowing to calculate the equilibrium partitioning of major aerosol compounds completely non-iteratively. In this section we only discuss the ammonia, nitric acid, sulfuric acid and water system (System III), which represents typical pollution aerosol; however, the principles presented here can be easily extended to System IV or V.

#### 3.8.1 Schematic Description

The basic idea is that the activities of atmospheric aerosols in equilibrium with the environment are governed by the ambient relative humidity (RH). Since the water activity is fixed to RH, the solute molality is, for a given aerosol composition, mainly a function of RH; the molality depends on the water mass which solely depends on RH. This is approximately true for activity coefficients of salt solutes of binary and multicomponent solutions. The latter is a pure consequence of the ZSR-relation, since this relation, which is widely used in atmospheric chemistry modeling, simply assumes that the water content of a multicomponent solution is the sum of the water fractions of all binary solutions. The molality of binary solutions is obtained from tabulated measurements, by which the so-called single-solute molalities are functions of RH, and the same is true for mixed solutions because of the application of the ZSR-relation. Consequently, the activity coefficients of salt solutions, which are needed to calculate gas/aerosol equilibria, can be directly derived from specific RH-functions, as previously described. Using the domain structure, and taking into account that gas/aerosol equilibria are only possible for certain domains where sulfate is completely neutralized, we can analytically calculate the aerosol composition, including the aerosol associated water. The formulation of such an approach thus yields a new thermodynamic gas/aerosol partitioning model, called EQSAM (Equilibrium Simplified Aerosol Model).

A schematic overview of EQSAM is given in [Table 3.2](#), which can be described as follows (the number corresponds to the numbers in the table).

1. A subdivision of the input concentration into concentration domains, according to mole ratios is made (Chapter 2.4). This yields the number of reactions, order, and some domain specific parameters, which are subsequently used for the calculation of water activities and activity coefficients, i.e.  $N$  (in Eq. 3.7), and  $\Gamma$  (see next point).
2. Gas/aerosol partitioning is assumed to occur if sulfate is completely neutralized (Domain 2), so that semi-volatile ammonium nitrate can form. All ammonium sulfate salts and non-neutralized sulfate, i.e. sulfuric acid, are treated as non-volatile. In addition, sulfuric acid is assumed to remain in the aqueous phase regardless of its solute activity, i.e. the activity coefficients. This allows simplifications with respect to the explicit determination of the various sulfate states ( $\text{H}_2\text{SO}_4$ ,  $\text{HSO}_4^-$ ,  $\text{SO}_4^{2-}$ ), which are parameterized by  $\Gamma$  according to the ammonium/sulfate mole ratio (see Chapter 2.8).
3. The liquid/solid phase is determined according to the aerosol composition and the corresponding RHD or MRHD values for the mixed salt solution (using RHD/MRHD values of

ISORROPIA). Individual salts are subsequently treated as solid (or liquid) if the RH is below (or above) the temperature dependent RHD/MRHD values.

4. Activity coefficients are, if needed, directly calculated from Eq. (3.7) and Eq. (3.9).
5. The single-solute molality is obtained from RH-specific functions, i.e. Eq. (3.6).
6. Free ammonia is determined from the neutralization of total sulfate by total ammonia (total denotes the sum of gas and aerosol), using the parameter  $\Gamma$  to account for various ammonium sulfate salts.
7. Ammonium nitrate is determined from the equilibrium reaction of free ammonia and total nitric acid, using a temperature dependent equilibrium constant (as used in ISORROPIA).
8. In accord with all other EQMs, nitrate formation due to condensation on the aerosol droplet of non-neutralized  $\text{HNO}_3$  (and subsequent dissociation into  $\text{NO}_3^-$ ) at high relative humidities is accounted for, by using a parameterization, i.e. a specific RH and composition dependent function (fitted to values obtained from ISORROPIA).
9. Aerosol nitrate is the sum of ammonium nitrate and non-neutralized nitrate.
10. The residual gaseous nitric acid and ammonia, and the residual aqueous sulfuric acid are determined from the difference of total input concentration and particulate nitrate/ammonium and neutralized sulfate, output values are given in  $[\mu\text{mol}/\text{m}^3]$ .
11. According to the RHD/MRHD values, the solid/liquid concentrations of nitrate/ammonium and sulfate is determined, output values are given in  $[\mu\text{mol}/\text{m}^3]$ .
12. Nitrate/ammonium and sulfate are multiplied by their mole mass; the sum yields the wet and dry particulate matter (PM), output values are given in  $[\mu\text{g}/\text{m}^3]$ .
13. Total particulate matter is the sum of both wet and dry PM  $[\mu\text{g}/\text{m}^3]$ .
14. The total water content is determined with the ZSR-relation  $[\mu\text{g}/\text{m}^3]$ .
15. The radius increase due to water uptake ( $r_{inc}$ ) is determined from the total particulate matter including and excluding water (output).
16. The hydrogen ion concentration ( $H^+$ ) and the aerosol pH [log] are determined for the aqueous phase (output).
17. The ionic strength of the solution ( $I$ ) is determined for the aqueous phase [moles/kg].
18. The mole ratio of nitrate and sulfate is determined (output).
19. The gas-ratio ( $GR$ ) of residual  $\text{NH}_3$  and residual  $\text{HNO}_3$  is determined; values below 1 indicate that ammonia is limiting the ammonium nitrate formation; (note that this ratio is very sensitive to the aerosol calculations and therefore a good parameter for a model comparison) (output).
20. The degree of neutralization by ammonia is determined from the ratio of ammonium and total nitrate + sulfate (output).
21. The nitrate partitioning is given by the ratio of particulate nitrate and total nitrate, i.e. gas+aerosol (output).
22. The ammonium partitioning is given by the ratio of particulate ammonium and total ammonia, i.e. gas+aerosol (output).

Note that each point denoted with “(output)” is calculated only for diagnostic purpose and is not used in the aerosol module itself. However, some of these points (e.g. 16) might be subsequently used in an atmospheric/chemistry transport model.



Table 3.2. EQSAM (Equilibrium Simplified Aerosol Model).

1.	Domains:	$n\text{NH}_3 > 2 \text{tSO}_4$ $n\text{NH}_3 < 2 \text{tSO}_4$ $n\text{NH}_3 < \text{tSO}_4$	$\Leftrightarrow$ sulfate neutral $\Leftrightarrow$ sulfate rich $\Leftrightarrow$ sulfate very rich	$N=2$ $N=3$ $N=4$	$I=2$ $I=1.5$ $I=1$
2.		Domain: e.g. sulfate neutral: $\Rightarrow$ gas/aerosol partitioning Subdomains: various MDRHs (T)			
3.		e.g.: $\text{RH} < \text{RHD}_{\text{AN}}$ $\Leftrightarrow$ gas-solid equilibrium		e.g.: $\text{RH} > \text{RHD}_{\text{AN}}$ $\Leftrightarrow$ gas-liquid equilibrium	
4.		$\gamma_{\text{AN}} = 1$		$\gamma_{\text{AN}} = (\text{rh}^N / (1000/N \cdot (1-\text{rh}) + N))^{1/2}$	
5.		$q = (1000 \cdot v_i^{\text{vi}} \cdot (1/\text{rh} - 1) / M_i)^{n_i}$			
6.		$\text{NH}_3^{\text{F}} = \text{tNH}_3 - \Gamma \cdot \text{tSO}_4$			
7.		$K_{\text{AN}} = \gamma_{\text{AN}}^2 \cdot [\text{NH}_4\text{NO}_3] / [\text{NH}_3^{\text{F}}][\text{tHNO}_3]$ $\Rightarrow \text{NO}_3$			
8.		$n\text{NO}_3(\text{RH}) = f(\text{T}, \text{RH}, \text{N}, \text{HNO}_3)$			
9.		$\text{NO}_3 = \text{NO}_3 + n\text{NO}_3$			
10.		$\text{HNO}_3 = \text{tHNO}_3 - \text{NO}_3$ $\text{NH}_3 = \text{NH}_3^{\text{F}} - \text{NO}_3$ $\text{H}_2\text{SO}_4 = \text{tSO}_4 - \Gamma \cdot (\text{tNH}_3 - \text{NH}_3^{\text{F}})$			
11.		$\text{NO}_{3(\text{s})} = \text{tHNO}_3 - \text{HNO}_3$ $\text{NH}_{4(\text{s})} = \text{tNH}_3 - \text{NH}_3$ $\text{SO}_{4(\text{s})} = \text{tSO}_4$		$\text{NO}_{3(\text{aq})} = \text{tHNO}_3 - \text{HNO}_3$ $\text{NH}_{4(\text{aq})} = \text{tNH}_3 - \text{NH}_3$ $\text{SO}_{4(\text{aq})} = \text{tSO}_4 - \text{H}_2\text{SO}_4$	
12.		$\text{PM}_{(\text{s})} = 14 \cdot \text{NO}_{3(\text{s})} + 18 \cdot \text{NH}_{4(\text{s})} + 96 \cdot \text{SO}_{4(\text{s})}$		$\text{PM}_{(\text{aq})} = 14 \cdot \text{NO}_{3(\text{aq})} + 18 \cdot \text{NH}_{4(\text{aq})} + 96 \cdot \text{SO}_{4(\text{aq})} + 98 \cdot \text{H}_2\text{SO}_{4(\text{aq})}$	
13.		$\text{tPM} = \text{PM}_{(\text{s})} + \text{PM}_{(\text{aq})}$			
14.		$W = 0$		$W = \text{NO}_3 / a_{\text{NO}_3} + \text{NH}_4 / a_{\text{NH}_4} + \text{SO}_4 / a_{\text{SO}_4} + \text{H}_2\text{SO}_4 / a_{\text{H}_2\text{SO}_4}$	
15.		$\epsilon_{\text{nc}} = 1$		$\epsilon_{\text{nc}} = (W / \text{tPM} + 1)^{1/3}$	
16.		$\text{H}^* = 0$		$\text{H}^* = (2 \cdot \text{tSO}_4 + \text{NO}_{3(\text{aq})} - \text{NH}_{4(\text{aq})}) \cdot 1000 / W$ $\text{pH} = \log(\text{H}^*)$	
17.		$I = 0$		$I = 0.5 \cdot (\text{NH}_4 + \text{NO}_3 + \text{tSO}_4 \cdot 4) / W$	
18.		$R = \text{NO}_3 / \text{tSO}_4$			
19.		$\text{GR} = \text{NH}_3 / \text{HNO}_3$			
20.		$\text{DON} = 100 \cdot \text{NH}_4 / (\text{NO}_3 + 2 \cdot \text{tSO}_4)$			
21.		$\text{NO}_3 = 100 \cdot \text{NO}_3 / \text{tNO}_3$			
22.		$\text{NH}_4 = 100 \cdot \text{NH}_4 / \text{tNH}_3$			

## Chapter IV: Equilibrium Model Comparison

To compare the new thermodynamic gas/aerosol partitioning model, called EQSAM (Equilibrium Simplified Aerosol Model), with other EQMs in use, we present results of a model comparison for different modeling tasks, using various equilibrium models as presented in Chapter II. Since SCAPE has the option to choose various activity coefficient calculation methods (ACCM), i.e. the Pitzer Method (PM), Kusik-Meissner Method (KM), or Bromley Method (BM), we will use either of them for the model comparison to investigate the differences caused by different ACCMs. The different SCAPE models will be termed according to the ACCM used: SCAPEa-PM, SCAPEb-KM, SCAPEb-BM. Note that unfortunately not all versions were numerically stable under all conditions, therefore only combinations have been used which yield reliable results. The comparison includes all parameterized EQM versions (denoted with the suffix '-P'), in which the original ACCMs have been replaced by the same method used in EQSAM (the activity coefficient - RH relationship, as described in Chapter III).

The model comparison includes:

1. Box-model calculations, in which all EQMs are applied to an artificial set of input data, using fixed concentrations and temperature, so that the results (differences) can be studied as a function of relative humidity (RH).
2. Global offline calculations, where all EQMs are applied to global chemistry fields ( $10^{\circ}\times 7.5^{\circ}$ ) as produced with a tracer transport model (TM3) and ECMWF meteorology, using monthly mean values for January 1997 at surface level; this allows a study of the differences for a wide range of realistic atmospheric conditions, i.e. temperature, relative humidity and various aerosol precursor concentrations.
3. Global online calculations, for which EQSAM and ISORROPIA have been incorporated into the TM3 model, so that differences can be quantified for calculations of gas/aerosol partitioning for different model time steps and model layers, including feedback between the gas and cloud phase chemistry.

### 4.1 Box-model Calculations

To explore the errors introduced by using EQSAM, relative to the more complex models in use, we compare the models first for three artificial cases of selected input concentrations of the ammonium/sulfate/nitrate/water-system, which corresponds to three different concentration domains, i.e. ammonium/sulfate ratios. The results will be shown as function of RH (10-95%) with input concentrations [ $\mu\text{mol}/\text{m}^3$ ] for the gas/liquid/solid equilibrium partitioning fixed to:

- $t\text{SO}_4 = 0.6 / 0.3 / 0.1$  (for domain=4/3/2)
- $t\text{NH}_3 = 0.4$
- $t\text{NO}_3 = 0.1$

where the prefix  $t$  denotes the total gas and aerosol concentration. The temperature was fixed to  $T=20^{\circ}\text{C}$  for all calculations. Considering our ultimate goal of global modeling, we focus in the comparison on the gas/aerosol partitioning, the degree of neutralization, the total particulate matter, and the aerosol associated water mass, i.e. the radius increase due to water uptake.

The results of the model comparison for the nitrate and ammonium partitioning, and the degree of neutralization are shown in [Figure 4.1](#); each panel and domain shows the results as a function of RH (10-95%). Domain 4 represents the so-called 'sulfate very rich' case ( $2\text{NH}_4^+ < \text{SO}_4^{2-}$ ), where insufficient ammonia is available to neutralize sulfate, so that sulfuric acid exists in the aerosol phase. Domain 3 represents accordingly the 'sulfate rich' case ( $\text{NH}_4^+ < \text{SO}_4^{2-}$ ), where still insufficient ammonia is present to neutralize sulfate, but not enough to neutralize the sulfuric acid; ammonium sulfate and/or bisulfate exist in the solid and/or aqueous phase. Domain 2 represents the complementary cases with sufficient ammonia to neutralize sulfate, and potentially available nitric acid to allow for ammonium nitrate formation. Since ammonium nitrate is the only volatile salt considered, gas/aerosol partitioning can only occur for Domain 2, by which the ammonium nitrate salt may be crystalline or deliquescent depending on relative humidity and aerosol composition. Note that all models account for little nitrate formation at high relative humidities for Domain 3 & 4, which can be attributed to an RH dependent  $\text{HNO}_3$  uptake on aerosols, which increases with RH because the aerosol radius increases and the solute concentration decreases due to the strong uptake of water vapor by acidic aerosols.

The comparison shows that nitrate and ammonium partitioning is predicted for all domains by all models and all versions with differences smaller than a few percent. While nitric acid partitions almost completely into nitrate only at relative high humidities above 90%, and only for domain 2, ammonia remains independently from RH in the aerosol phase, if sulfate is not completely neutralized by ammonium (Domain 3 & 4). Only for the case of surplus ammonia (Domain 2), ammonia partitioning occurs by RH dependent ammonium nitrate formation. Note that EQSAM nicely follows our reference model ISORROPIA, which is presently the most sophisticated model in terms of accuracy and computational performance. MARS, on the other hand, is the simplest of all equilibrium models, and shows the largest deviations from other models predictions. Remarkably, all parameterized EQM versions (denoted with a suffix '-P') are also able to predict the gas/aerosol partitioning and show only small deviations from their original versions; a few deviations shows SEQUILIB-P because it does not dynamically determine the number of iterations needed to solve the gas/aerosol partitioning and activity coefficients (see Section 4.2.1). Note that the iterative structure of the parameterized EQMs was kept unchanged to minimize errors not associated with the ACCM itself. Especially in the mutual deliquescence range where many iterations are need to calculate solid species, the use of fixed iteration numbers can lead to errors, Nevertheless, even SEQUILIB-P and MARS-P reproduce the results of the original versions for almost all cases.

These results satisfy our assumption that the complex ACCMs can be parameterized for large-scale applications without much loss of accuracy; especially if the iterative structure of the original EQM is adjusted. Therefore, our alternative, non-iterative ACCM can be expected to not significantly affect aerosol properties which are particularly important for global modeling: the total particulate matter and the aerosol associated water, and subsequently, the radius increase due to water uptake. These properties are shown in Figure 4.2. In accord with the previous discussion, the relative strongest differences between all models occur for the sulfate poor case (Domain 2). Nevertheless, differences are overall rather small, and EQSAM follows closely ISORROPIA for all cases. Note that the uptake of aerosol water is strongest for the 'sulfate very rich case', where sulfuric acid exists in the aerosol phase, which causes water uptake at relative humidities below 10%; a deliquescence relative humidity is not considered for this case.

For the other cases water uptake can only take place if the relative humidity exceeds the lowest deliquescence relative humidity of the corresponding salt solution, i.e. the lower limit of the mutual deliquescence relative humidity range. Although water uptake is strongest for the free sulfuric acid case, the radius increase due to water uptake is not. The reason is that aerosol properties such as the radius increase is a) proportional to both the ratio of total wet particulate matter (including aerosol associated water mass) and the total dry particulate matter (to a power of 1/3 to obtain the radius from mass); and b) the aerosol water mass is proportional to the total particulate matter (Chapter 3.4). Consequently, the main differences in water uptake and radius increase are confined to the relative humidity range where solid particles can form. However, this is also the range where the main differences between all models occur, since the aqueous phase is determined for equilibrium calculations that include gas/liquid/solid partitioning, by the relative humidity of deliquescence (RHD), for which different assumptions are made. For instance, ISORROPIA uses temperature dependent mutual deliquescence ranges for salt mixtures (Nenes et al. 1998), which are also partly used in EQSAM. All other models only use RHD values for individual salts, which generally leads to a solid particle formation at higher relative humidities. Additionally, MARS and SEQUILIB do not even account for the temperature dependence of the RHDs.

As a result we note that the different deliquescence humidities that are used in various EQMs are the main cause of uncertainty associated in the prediction of aerosol water with EQMs. To a lesser extent, uncertainties in the prediction of the solute concentration are responsible that some EQMs predicts solids while other do not. The latter includes differences in the activity coefficient calculation and the numerical stability for reaching convergence in iterative processes, and also the differences which are associated if the original ACCM is replaced by our activity coefficient - relative humidity relationship.

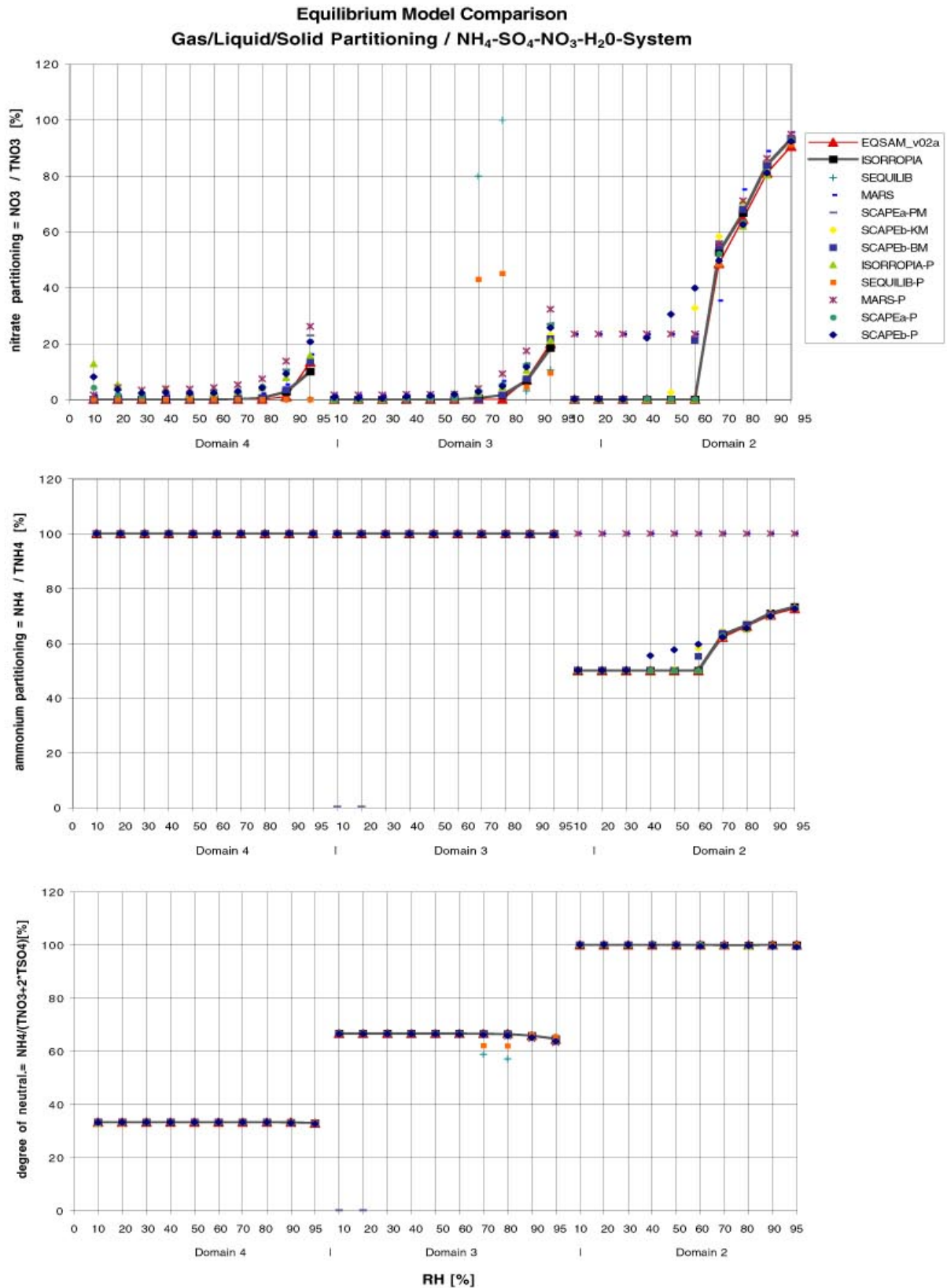


**Figure 4.1.** Comparison of equilibrium calculations with the equilibrium simplified aerosol model (EQSAM), various EQMs in use (ISORROPIA, SEQUILIB, MARS, SCAPEa-PM, SCAPEb-KM, SCAPEb-BM), and their parameterized versions (-P). Results are shown for each domain as a function of relative humidity (10-95%) and are given in percentage for nitrate- (top) and ammonium- (middle) partitioning, and the degree of neutralization (bottom). The domains (ammonium/sulfate ratios) are: Domain 4 = sulfate very rich ( $2\text{NH}_4^+ < \text{SO}_4^{2-}$ ); Domain 3 = sulfate rich ( $\text{NH}_4^+ < \text{SO}_4^{2-}$ ); and Domain 2 = sulfate poor case ( $\text{NH}_4^+ > \text{SO}_4^{2-}$ ).

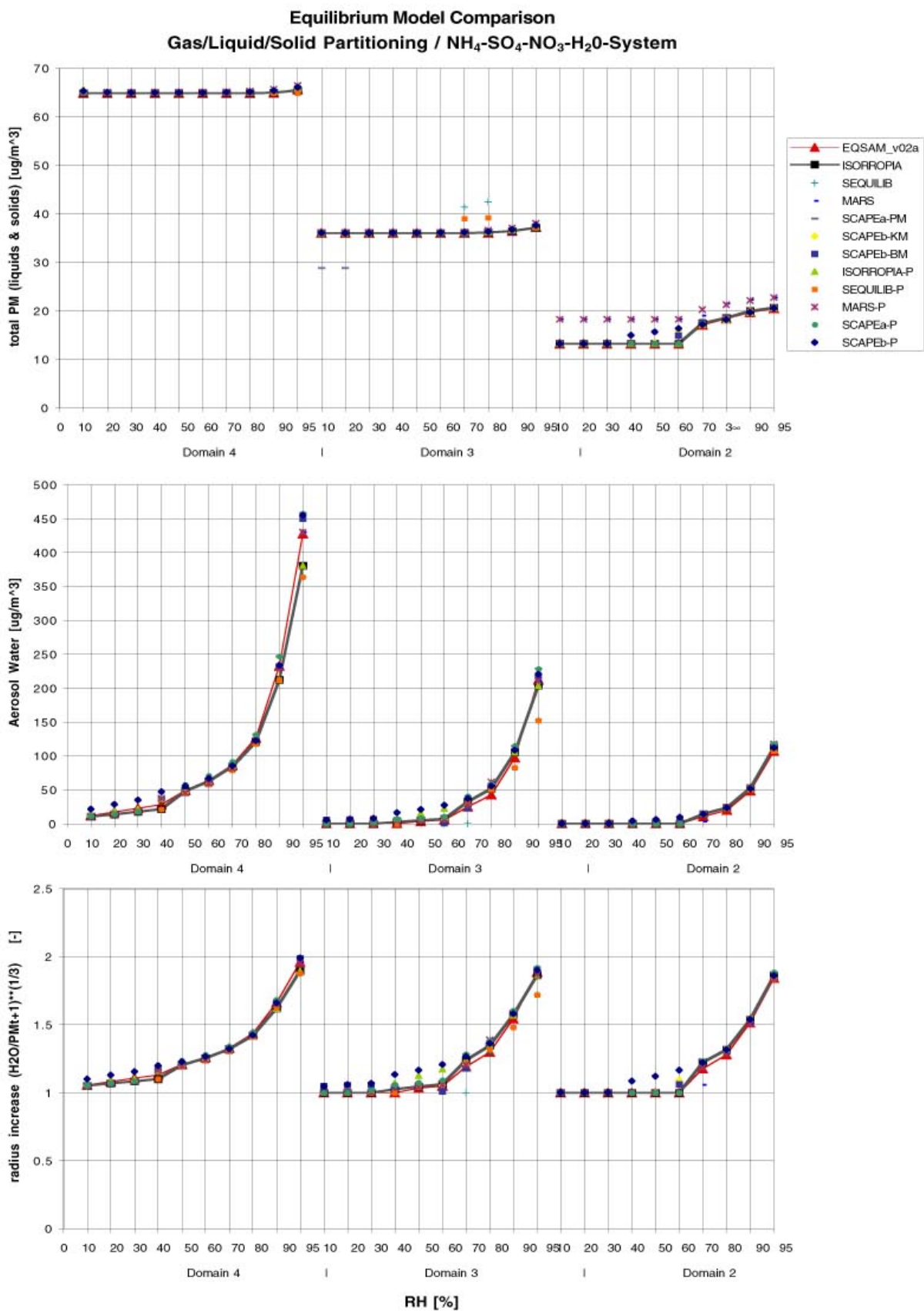


**Figure 4.2.** Comparison of equilibrium calculations of Figure 4.1 continued. Results are shown for the total particulate matter (top), the aerosol-associated water (middle), and the radius increase due to water uptake (bottom).

As noted in Chapter I, many salts may exhibit hysteresis in the atmosphere, that is that they do not crystallize at the same RH at which they deliquesce. Instead, these compounds remain in a metastable supersaturated aqueous phase, rather than form solids after they have been wet. This effect is probably not negligible for hygroscopic particles at mid-latitudes or marine environments, where the relative humidity exceeds at least diurnally the deliquescence points of the salts of interests (see also Chapter 6.1.3).

To quantify the differences for the aerosol associated water for the two cases, we have plotted in Figure 4.3 the aerosol water based on metastable aerosols, in addition to the aerosol water based on the gas/liquid/solid partitioning of Figure 4.2 (middle). Note that the maxima in Figure 4.3 are the same as before but they have been cut off to highlight the differences which occur in the lower part and that only the results of EQSAM and ISORROPIA are included, since the other models do not allow metastable aerosols.

The main result is that differences between both models are negligible compared to the differences in the total amount of aerosol water, which is associated with the two different treatments of the gas/aerosol partitioning. Also the absolute difference between both models is, at least for the case considered, acceptable for global modeling applications.

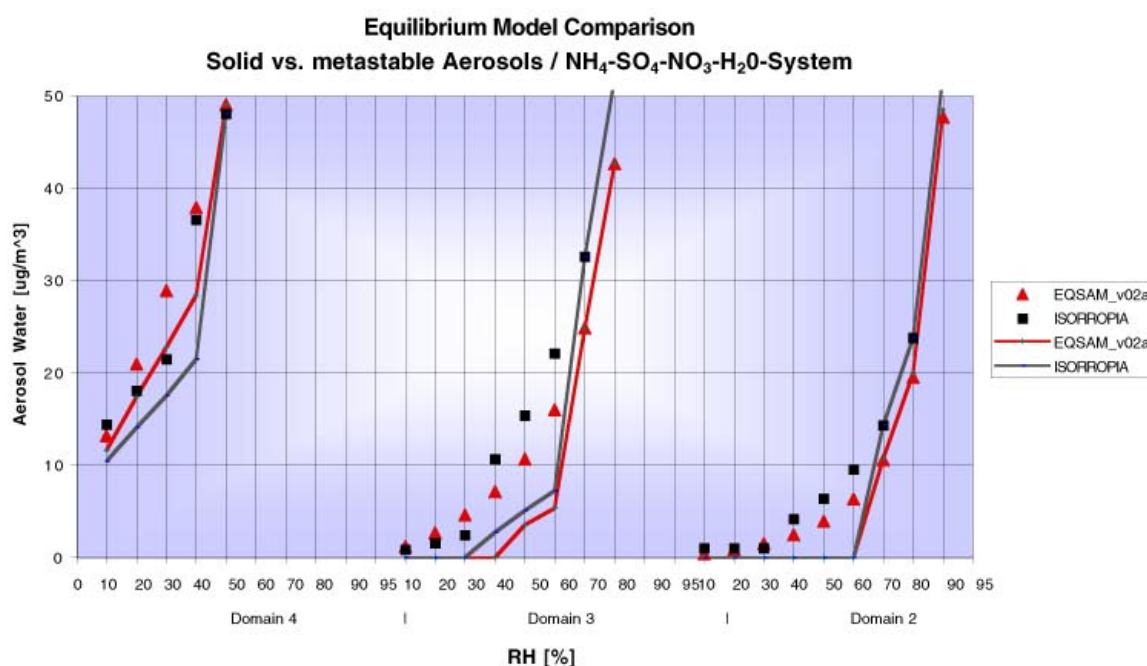


**Figure 4.3.** Comparison of equilibrium calculations of Figure 4.2 (middle) supplemented for EQSDAM/ISORROPIA by the results of the aerosol associated water based on metastable aerosols (indicated by triangles and squares, respectively). Note that the maxima have been cut off since they remained unchanged.

To quantify the relative errors for more cases, i.e. different temperatures and aerosol concentrations, we investigate in the next section the relative errors associated in the prediction of various aerosol properties by applying the models to global CTM fields.

## 4.2 Global Offline Calculations

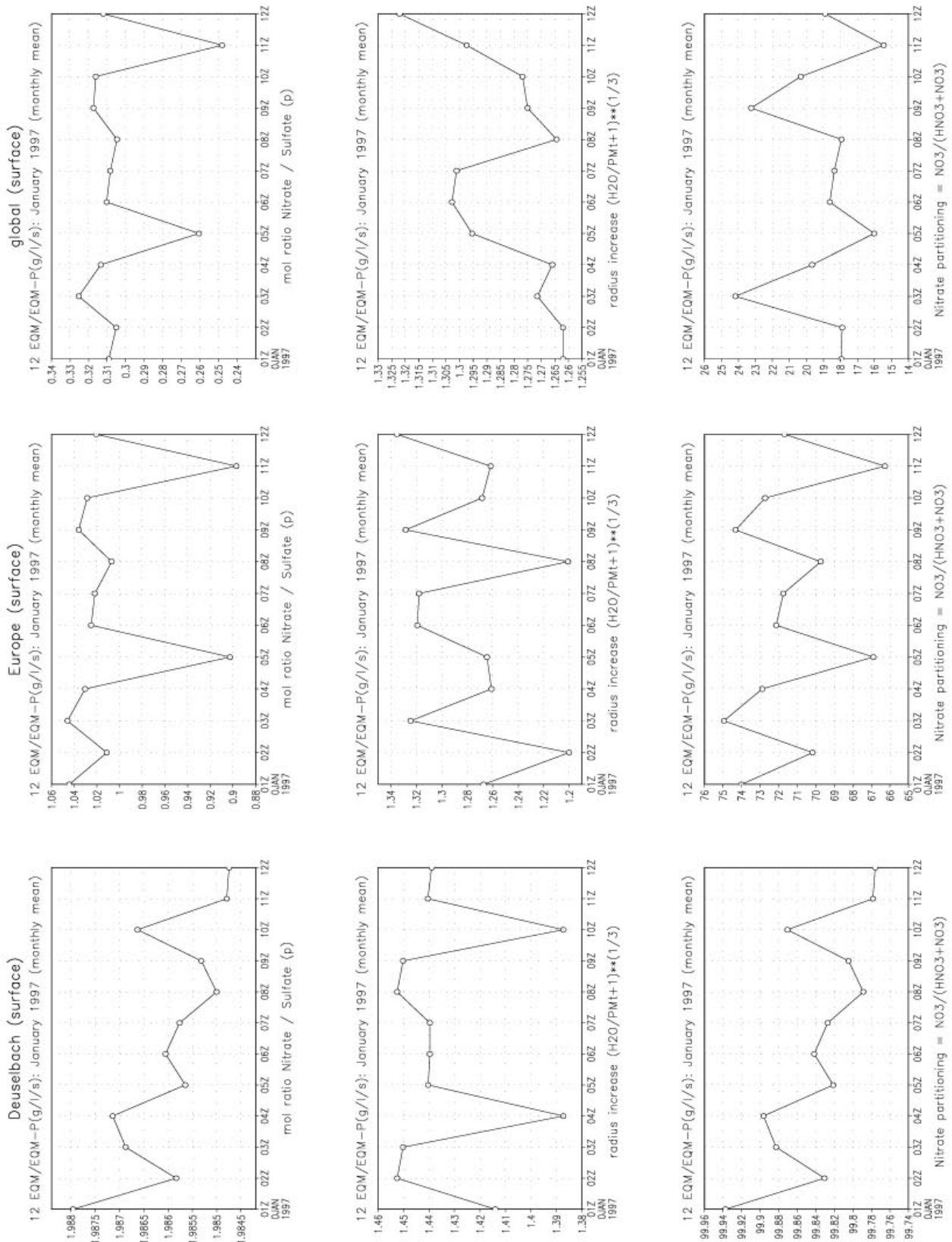
To extend the previous comparison to a wide range of realistic atmospheric conditions, we apply all EQMs to global chemistry fields ( $10^{\circ} \times 7.5^{\circ}$ ) of a tracer transport model (TM3 and ECMWF meteorology), using monthly mean values for January 1997 at the surface level. The global fields were calculated with the chemistry transport model TM3 (Dentener et al., 1999, Houweling et al., 1998; and Lelieveld and Dentener, 2000).

Figure 4.4 shows the results of the gas/liquid/solid equilibrium calculations of all EQMs (including all versions) for the mol ratio of aerosol nitrate and sulfate (upper panels), the aerosol radius increase due to water uptake (middle panels), and the nitrate partitioning (lower panels) for a location in Germany (left), a regional average over Europe (middle), and the global average (right); for January 1997 at surface level. Each point corresponds to one model, i.e. from left to right (01Z to 12Z): EQSAM, ISORROPIA, SEQUILIB, MARS, SCAPEa-PM, SCAPEb-KM, SCAPEb-BM, ISORROPIA-P, SEQUILIB-P, MARS-P, SCAPEa-P, SCAPEb-P.

First, the results of EQSAM are within the range of all EQMs. Second, all parameterized EQMs are close to their original versions, even for the global averages. This indicates that the iterative ACCMs can be safely substituted for global calculations by our non-iterative parameterization; the effect on the gas/aerosol partitioning is rather small for all models, and in particular smaller than the differences which are associated with different EQMs. Accordingly, the two different iterative ACCMs applied to the SCAPEb EQM yields consistent results, as indicated by the comparison of the results of SCAPEb-KM (point 06Z) and SCAPEb-BM (point 07Z).

In addition, the comparison of the results for the point location in Germany with the results of the regional and global average further shows that the differences between EQSAM and ISORROPIA are smallest for the global average. This indicates that the results of both models are also in good agreement (or even better) for locations outside of Europe, which means that the results of both models are comparable for a wide range of atmospheric conditions. Also the differences for the single gridbox are small; about a thousandth for the nitrate-sulfate mol ratio and the nitrate partitioning, and a few percent for the radius increase. The absolute values for this location furthermore indicate that the monthly mean nitric acid is predicted to partition completely into the aerosol phase under northern hemispheric winter conditions, so that the aerosol nitrate concentrations are twice as high as the sulfate concentrations. On the regional scale, the mean nitrate concentration is comparable to the sulfate concentration, which is associated with a considerable nitrate partitioning of about 70% for Europe. Although these values are much less for the global average, approximately 20% for the nitrate partitioning and of about 33% for the nitrate/sulfate mol ratio, they do indicate that the gas/aerosol partitioning is not negligible on global scale.





**Figure 4.4.** Comparison of equilibrium calculations with the equilibrium simplified aerosol model and various EQMs in use, including their parameterized versions (-P). Left to right (01Z to 12Z): EQSAM, ISORROPIA, SEQUILIB, MARS, SCAPEa-PM, SCAPEb-KM, SCAPEb-BM, ISORROPIA-P, SEQUILIB-P, MARS-P, SCAPEa-P, SCAPEb-P. Shown are the mol ratio of aerosol nitrate and sulfate (upper panels), the aerosol radius increase due to water uptake (middle panels), and the nitrate partitioning [%] (lower panels) for a location in Germany (left), a regional average over Europe (middle), and the global average (right); for January 1997 at surface level.

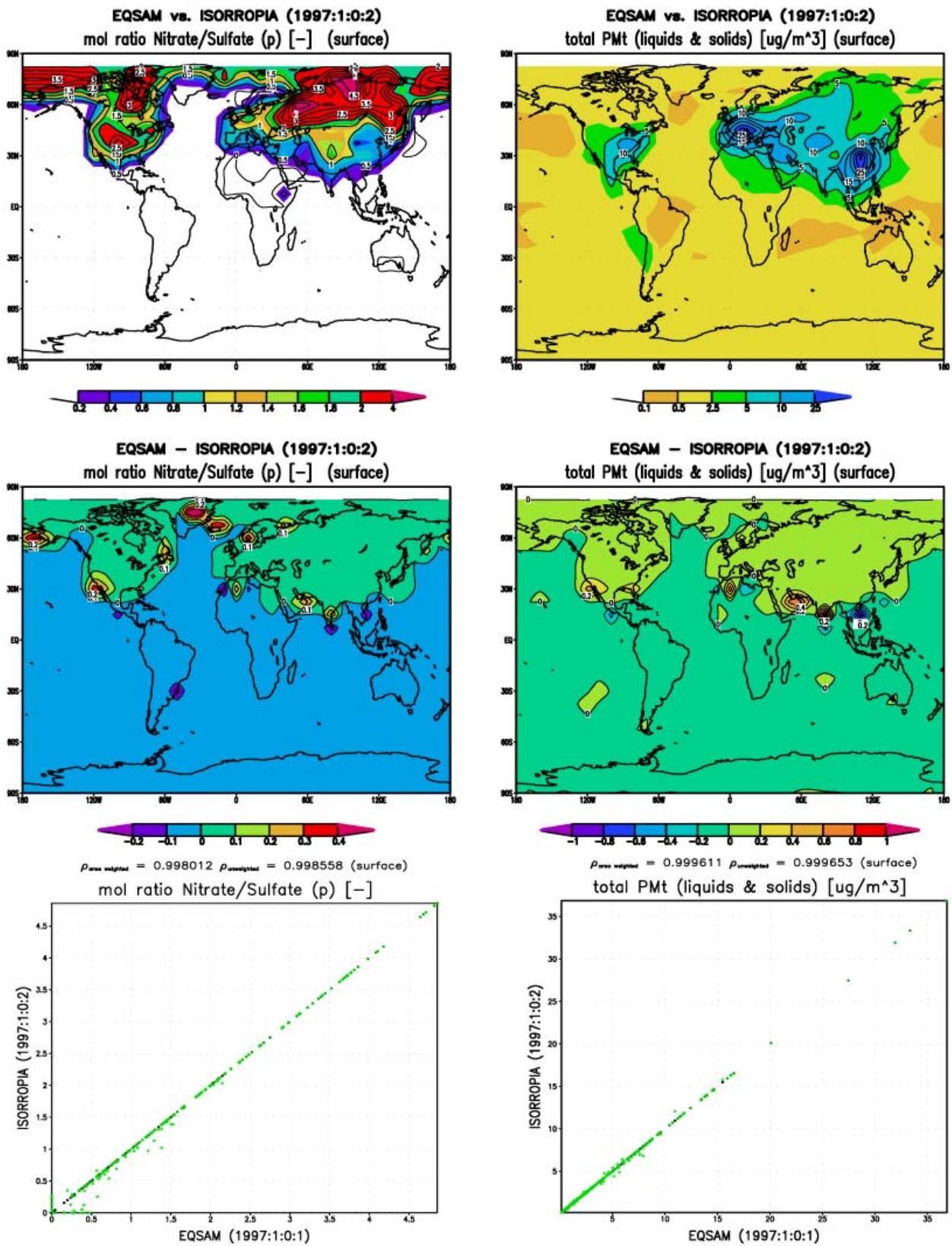


**Figure 4.5a.** Comparison of EQSAM with ISORROPIA. Shown are the mol ratio of aerosol nitrate and sulfate (left) and the total particulate matter (right). The upper panels show the global pattern (shaded EQSAM, contour ISORROPIA), the middle panels show the corresponding difference of EQSAM-ISORROPIA, and the lower panels show the scatter, including the regionally weighted and unweighted correlations coefficients; for January 1997 at surface level.

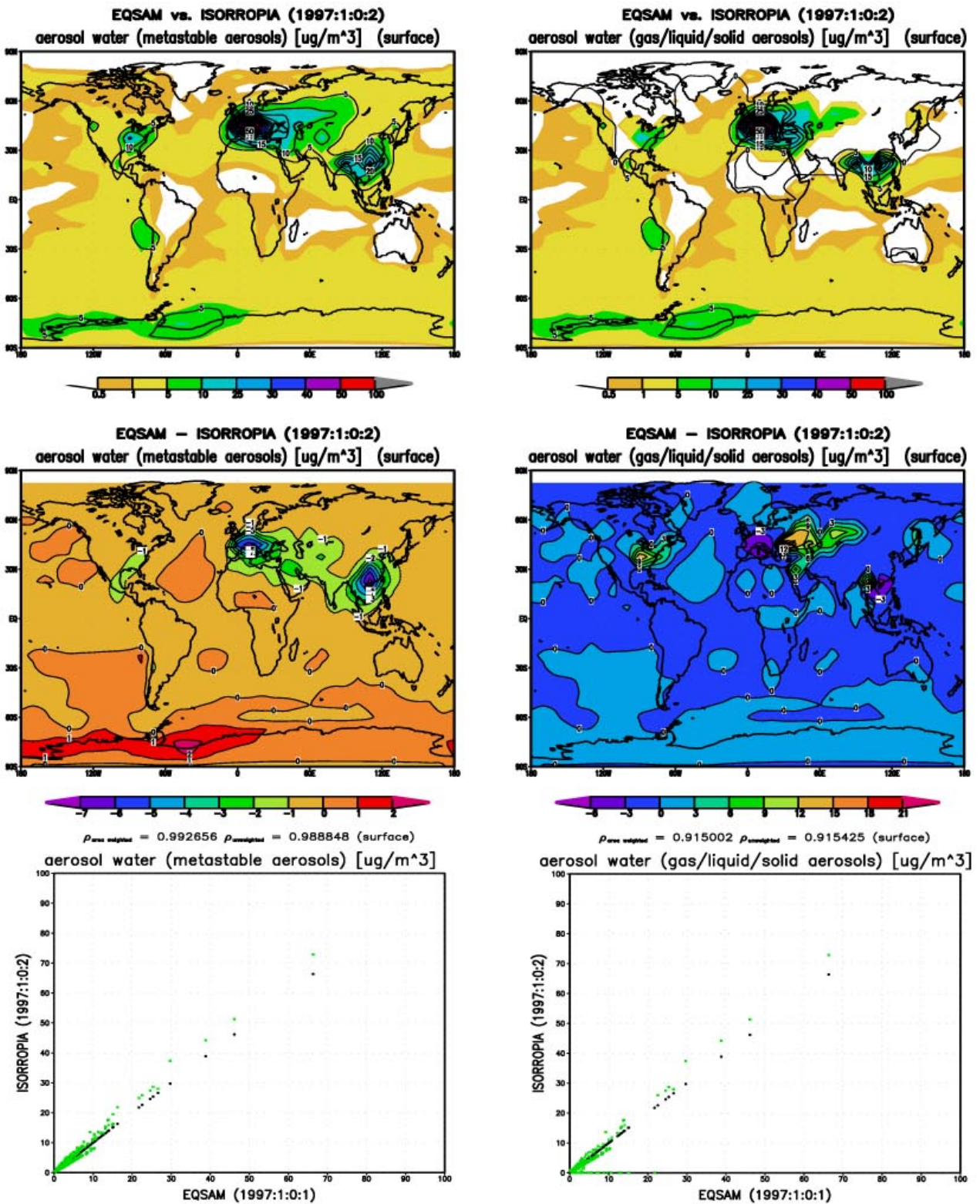


**Figure 4.5b.** Comparison of EQSAM with ISORROPIA. Shown are the aerosol associated water which corresponds to the calculation of metastable aerosols (left), and which corresponds to the gas/liquid/solid equilibrium partitioning (right). The upper panels show the global pattern (shaded EQSAM, contour ISORROPIA), the middle panels show the corresponding difference of EQSAM-ISORROPIA, and the lower panels show the scatter, including the regionally weighted and unweighted correlations coefficients; for January 1997 at surface level. Note that the contour lines differ for the left and right panels.

To investigate these differences in greater detail, we have plotted in [Figure 4.5a](#) the global patterns (upper panels) as predicted by EQSAM (shaded) and ISORROPIA (contour) for the nitrate/sulfate mol ratio (left panels) and the total particulate matter (right panels); the middle panels show the corresponding difference of EQSAM-ISORROPIA, and the lower panels a scatter plot, including the gridbox area-weighted (left) and unweighted (right) correlation coefficients for January 1997 at surface level. Note that the gridbox area-weighted correlation coefficient accounts for the decrease of the gridbox area with increasing latitude. If both differ than this indicates that they are non-zero values at northern latitude, e.g. that gas/aerosol partitioning occurs; the absolute difference additionally indicates the relative importance of the northern latitudes.

[Figure 4.5b](#) shows the same for the aerosol water, which corresponds to the calculation of metastable aerosols (left) in comparison to the one associated with the full gas/liquid/solid equilibrium partitioning (right).

In accord with the previous discussion, differences are overall rather small, and they are mainly restricted to locations with extreme atmospheric conditions, e.g. high temperatures and low relative humidities. These are the conditions where hygroscopic aerosols may form solids. Those predictions, however, strongly depend on the assumptions made about the deliquescence points, as mentioned before. Although EQSAM uses the mutual deliquescence relative humidities as used in ISORROPIA, not all MDRHs/RHDs are used for all salt mixtures. Note that this explains most of the differences, which are basically restricted to the occurrence of solids; both solute concentration and solid aerosol concentrations compare rather well (not shown). This also becomes evident from the comparison of the scatter plots of the aerosol water ([Figure 4.5b](#)). In contrast to the one based on metastable aerosols (left panels), the one based on the gas/liquid/solid equilibrium partitioning (right panels) shows zero values, indicating that EQSAM predicts for some locations aerosol water while ISORROPIA does not. Nevertheless, this effect is rather small and mainly limited to arid locations at mid-latitudes, as indicated by the difference plots and the regionally weighted and unweighted correlation values. Furthermore, for these dry cases the solute activity is usually high and likely to exceed the range for which the activity coefficient calculation methods are tested (i.e. 30M for the Pitzer method), so that the results of ISORROPIA and the other EQMs may also be questioned.

For this reason, i.e. the uncertainties that are associated with the calculations of solids, and because of the hysteresis effect of aerosols, it is probably appropriate to limit global calculations to metastable aerosols rather than to include the calculation of solids, unless hysteresis is explicitly calculated. Adams et al (1999) therefore used the metastable approach; they coupled ISORROPIA to the Goddard Institute for Space Studies general circulation model II (GISS-GCM II-prime) to calculate the gas/aerosol partitioning online, using pre-described  $\text{HNO}_3$ -fields from the Harvard CTM. Besides the fact that they could therefore only treat nitrate aerosol as a diagnostic tracer, i.e. no feedback of the nitrate partitioning on the gas-phase chemistry, they had to spend roughly three

quarters of the total processor time for the thermodynamic equilibrium calculations by ISORROPIA (this would have been much more if solids had been calculated).

#### 4.2.1 CPU-time

Table 4.1 shows the CPU time for all EQMs for two different platforms (discussion follows). The parameterized versions are included, although they have not been optimized in terms of CPU time, to minimize errors not related to the activity coefficients as mentioned before. Thus, only the ACCMs have been substituted by our parameterization, while the iterative structure was kept unchanged (except for ISORROPIA-P and SCAPEa-P, where some modifications were made). Nevertheless, MARS and SCAPEb also show a gain in computing time, caused by the fact that less iterations are needed to reach convergence, if the activity coefficients are determined non-iteratively (the number of iterations needed only depend on the pre-described convergence criteria). This is not the case for SEQUILIB, since a fixed number of iteration is used for all cases. However, the largest gain in computational performance is achieved with EQSAM. The computational burden is of about 2-3 orders less compared to the non-parameterized EQMs. Since EQSAM calculates the gas/liquid/solid aerosol partitioning completely non-iteratively, it indicates the lower boundary for the CPU-time usage, although it is numerically not yet optimized. Note that the average CPU-time usage strongly depends, for iterative models, on the atmospheric conditions, i.e. the number of cases where solids must be calculated. For the same reason it depends on the assumptions made on the gas/aerosol partitioning (metastable or gas/liquid/solid aerosols). Also the hardware architecture on which the computations are performed can have a strong impact on the computational burden, as shown by the results presented in Table 4.1; the left side shows the computing times for the calculations performed on a personal computer (Macintosh PowerBook G3) with a 250MHz CPU running under Mac OS 9, and the right side for the same calculations performed on a supercomputer infrastructure of a CRAY- C916/121024 / UNICOS 10.0.0.2. The columns show the computational burden, i.e CPU seconds for 8640 gridboxes.

From this comparison it becomes apparent that the EQMs in use are naturally not suited for present generation of supercomputers, which are based on vector architectures such as the CRAY-C916, because they are purely scalar and too complex for vectorization. While global modeling is presently restricted to supercomputers because of the large amount of data needed and produced, the present use of vector architectures prohibits actually the application of models such as the EQMs. Although all EQMs in use were developed for incorporation in larger air-quality models, they are all numerically not very efficient since the gas/aerosol partitioning is solved iteratively. This is certainly also a drawback on the next generation supercomputers, which might use scalar architectures.

Because pure scalar models generally have a poor performance on a vector computer, it is not very surprising that even a personal computer outperforms a supercomputer (by a factor of 4 or so), and

even for the most sophisticated EQM, ISORROPIA. In contrast the simplified model EQSAM shows a better performance on a vector machine (by a factor of 3 or so for the version including solids, and up to 3 orders of magnitude for the reduced version excluding solids), due to the possibility for vectorization. Thus, the gain in computing time even increases for global applications, especially on vector architectures, and potentially also for parallel architectures (although not yet tested) where all scalar models show a better performance, due to the fact that EQSAM solves the gas/aerosol partitioning completely non-iteratively.

**Table 4.1. CPU times.**

Platform	Mac Pb-G3 (250MHz)	Cray-C916
CPU seconds (burden <sup>1</sup> )		
<b>Gas/liquid/solid aerosol partitioning:</b>		
EQSAM	0.94	0.31
ISORROPIA	14	60
SEUILIB	105	64
MARS	8	12
SCAPEa-PM	52	49
SCAPEb-KM	40	181
SCAPEb-BM	38	172
ISORROPIA-P	1.5	2.7
SEUILIB-P	116	92
MARS-P	3.7	5.3
SCAPEa-P	7.0	28
SCAPEb-P	31	85
<b>Metastable aerosols:</b>		
EQSAM	0.93	0.28
EQSAM <sup>2</sup>	0.88	0.0048
ISORROPIA <sup>3</sup>	3.1	9.7
ISORROPIA-P	1.7	3.3

<sup>1</sup> Number of gridboxes = 8640 (values are rounded)

<sup>2</sup> reduced version of EQSAM (code without solids to allow for better vectorization)

<sup>3</sup> double precision was omitted on the CRAY for ISORROPIA (ISORROPIA-P) to achieve better performance

For instance, for a one year integration on a coarse grid (10°x7.5°) with 19 vertical levels and a 2 hours time-step for the chemistry/equilibrium calculations (gas/liquid/solid partitioning), which already yields a total number of calls to the equilibrium routine in the order of millions (71.90208E+06), the computational burden for EQSAM on the CRAY would be about 43 minutes, compared to 139 hours needed for ISORROPIA, and of about 6 hours for the parameterized version

(ISORROPIA-P). Note that these numbers give the lower limit; the actual burden of a real integration usually consumes, for iterative models, more computing time, due to the dependence of the solid calculations on the atmospheric condition as mentioned before (these numbers were based on monthly mean values for January 1997). However, the same calculations with the EQM SCAPEb would add up to 400 hours CPU-time, which is why ISORROPIA is already regarded as accurate and fast. Nevertheless, our comparison shows that for global applications alternatives are desired – in spite of increasing computing power. Especially for climate calculations, where hundreds of years of simulations must be performed, a parameterization is needed. Even if the gas/aerosol calculations are limited to the metastable aerosols, the computational burden for ISORROPIA remains too high, i.e. of about 22.5 hours per year, which is a factor 10 more compared to the entire atmospheric/chemistry transport model (TM3) consumption of computing time for this resolution; this is about 650 CPUs/month or ~2 hours per year, without the thermodynamic gas/aerosol calculations. The reduced version of EQSAM without the option for solid calculation only adds 3.5 CPUs per month (40s/a), because of the better ability for vectorization.

### 4.3 Global Online Calculations

In the previous subsections we have shown that the results of the aerosol calculations based on the simplified equilibrium model were in the range of the results of various EQMs in use. To extend the comparison to global modeling, i.e. to test the stability of the previous results by integration over time, and to account for various altitudes, we will compare results of EQSAM and ISORROPIA in so-called online calculations. For these calculations, both equilibrium models were incorporated into the atmospheric/chemistry transport model TM3 (Dentener et al., 1999, Houweling et al., 1998; and Lelieveld and Dentener, 2000), so that the gas-phase and cloud chemistry could be calculated online with the ammonium/sulfate/nitrate/water equilibrium calculations, on a  $10^\circ \times 7.5^\circ$  horizontal resolution, 19 vertical levels and a 2hr-time step for the chemistry and equilibrium calculations. Note that these calculations consist of a fully dynamical treatment of aerosol species with respect to transport and deposition processes, which includes feedbacks with the chemistry calculations (the TM3 model will be described in the next Chapter). In accord with Adams et al. (1999) we focus on metastable aerosols.

Results are presented in [Figure 4.6](#) for July 1997, showing time series of the surface mol ratio of total transported aerosol nitrate and sulfate (upper panels), the column aerosol radiative forcing of nitrate (middle panels) and sulfate (lower panels) for a location in Germany (left), a regional average over Europe (middle), and the global average (right), as calculated with EQSAM. In addition, the differences between these results and those obtained by using ISORROPIA are included in each panel (EQSAM - ISORROPIA). Note that the aerosol direct radiative forcing was calculated online by implementing the method of Van Dorland et al. (1997) in TM3.

Figure 4.6 demonstrates that the relative errors introduced by the simplified equilibrium model are also rather small for the online equilibrium calculations. The differences are largest for the surface mol ratio of aerosol nitrate and sulfate for the single location in Germany, which can be attributed to differences in the nitrate partitioning, which in turn is strongest in summer. The time series show a strong contrast between the day and night values, which illustrates that the aerosol calculations very much depend on both temperature and relative humidity. The latter affects the nitrate formation mainly due to the dependency of the activity coefficients on RH, which enhances the ammonium nitrate formation in the aqueous phase compared to the solid phase. To a much smaller extent due to  $\text{HNO}_3$  uptake on aerosol, as this is discussed previously. More important is the temperature dependency of the ammonium nitrate equilibrium constant, which shows the largest effect on the nitrate formation for this location in July, due the largest day-night temperature contrast. This effect, however, decreases as the area increases over which is averaged. Furthermore, the high surface ratios indicate that aerosol nitrate exceeds regionally those of sulfate; even during northern summer nights at the model surface, nitrate to sulfate mol ratios of up to 10 or more are predicted. During day and on a regional scale (Europe) nitrate and sulfate concentrations are still comparable, while for the global average, nitrate is not important. Note that this picture differs for other seasons, since nitrate concentrations are generally higher in wintertime, due to the temperature dependent nitrate partitioning, in contrast with sulfate (see next chapter).

Differences in the aerosol radiative forcings (Figure 4.6) are even smaller than differences in the surface mol ratios, although the radiative forcings are based on the vertical integral (the differences are almost zero and therefore difficult to distinguish from the minimum values which occur at night and which are therefore also zero). Thus, the relative errors associated with the simplified equilibrium calculations are negligible for aerosol properties, such as the direct aerosol radiative forcing (note the different scale for the aerosol radiative forcing of sulfate). Nevertheless, we do not want to stress the values of the absolute forcing, because we do not account for the effect of aerosol species other than the ammonium salts (sulfate and nitrate). We rather use here the aerosol forcing as an optimal variable to quantify the relative differences, i.e. uncertainties associated with the aerosol calculations, since the forcing depends on various aerosol properties (e.g. column nitrate and sulfate, total particulate matter, aerosol water), as well as their interaction with the various meteorological and geophysical parameters (e.g. cloud cover, solar constant, solar-zenith angle, i.e. effective daylight, albedo). However, the global average aerosol radiative forcing is about  $-0.3 \text{ W/m}^2$ , which is within the range given by IPCC (Figure 1.1).



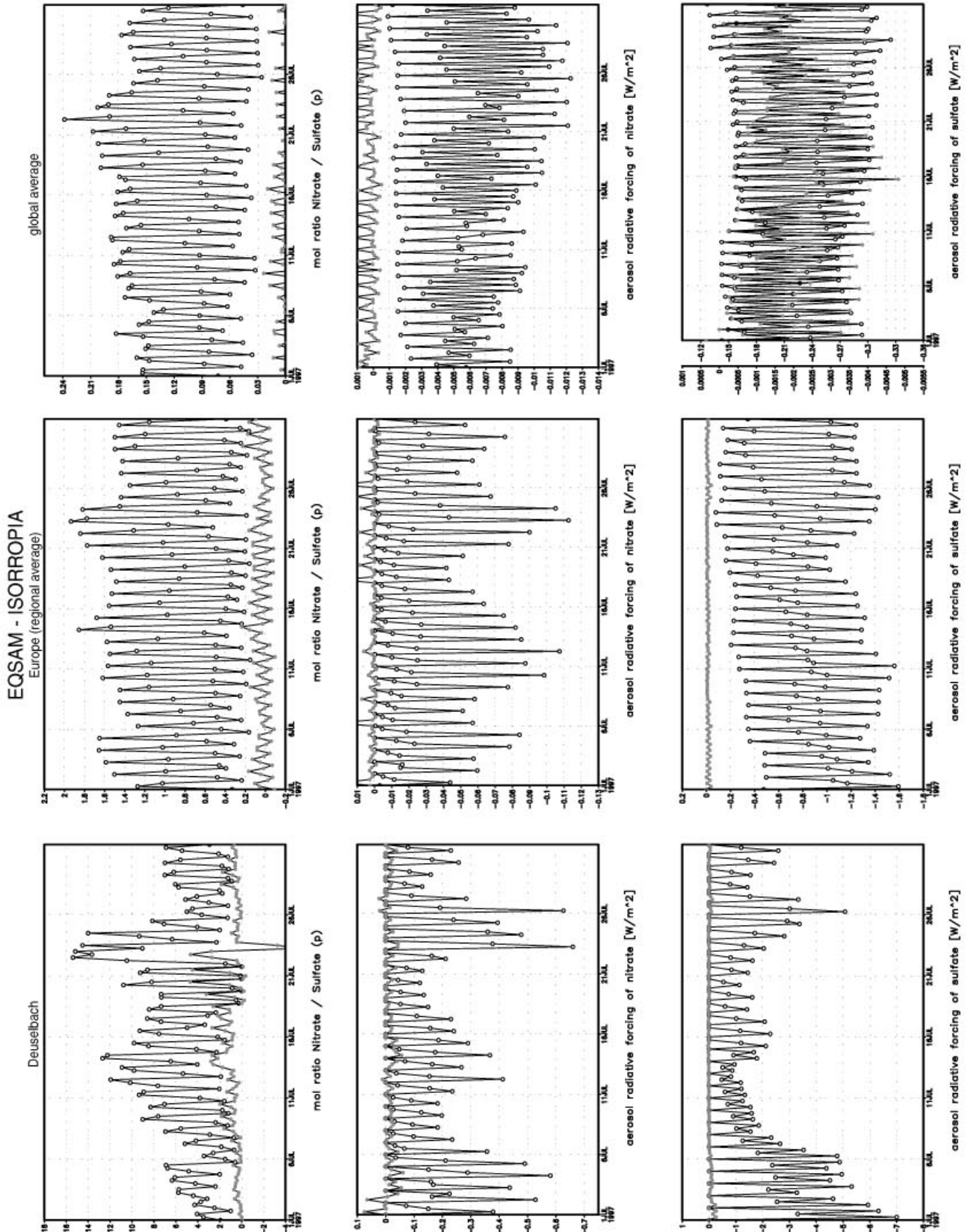


**Figure 4.6.** Online equilibrium calculations (metastable aerosols) with EQSAM: Time series for July 1997 of the surface mol ratio of total transported aerosol nitrate and sulfate (upper panels), the column aerosol radiative forcing of nitrate (middle panels) and sulfate (lower panels) for a location in Germany (left), a regional average over Europe (middle), and the global average (right). In addition, the differences between these results and those obtained by using ISORROPIA are included in each panel and marked in light grey (EQSAM - ISORROPIA). Note that the differences are almost zero and therefore difficult to distinguish from the minimum values which are also zero. Note further the different scale for the aerosol radiative forcing of sulfate.

## Chapter V: Global Gas/Aerosol Partitioning Modeling

From measurements and theory it is well known that aerosol distributions exhibit a strong spatial and temporal variability. This variability is caused by both the non-uniform distribution of the sources of aerosols and aerosol precursor gases, and the ever-changing atmospheric conditions, where the synoptic weather fluctuation controls much of the variability. This fluctuation partly determines the aerosol precursor emission and deposition processes, which determine the atmospheric residence time of the aerosol particles and the potential for long-range transport. Furthermore, aerosol formation is governed by meteorological parameters, such as the temperature, and relative humidity, which are all highly variable at various time-scales, regions and altitudes. Especially the aerosol formation from trace gases (gas-to-particle conversion) explicitly depends on all these parameters, as well as the presence of pre-existing aerosol particles or cloud droplets, so that the gas/aerosol partitioning is likely to exhibit not only a strong diurnal variability, but also an annual cycle.

In this chapter, we will investigate the spatial and temporal distribution of aerosol patterns with a global atmosphere chemistry transport model (TM3), described in Section 5.1. We focus on the annual cycle of the gas/aerosol partitioning for 1997 (Section 5.2.1), global aerosol patterns for January and July 1997 (monthly means) (Section 5.2.2), space-time variability, i.e. GMT 6hr vs. 18hr averages (Section 5.2.3), zonal distributions (Section 5.2.4), and the feedback of the aerosol calculations on chemistry (Section 5.2.5). In addition, we analyze the aerosol budgets with a focus on the annual cycle at various altitudes. All results in this chapter are obtained from global aerosol calculation with the aerosol version of the atmosphere chemistry tracer model (TM3), using EQSAM as previously described (Chapter III). The results are, unless otherwise stated, based on the coarse model resolution (CG,  $10^\circ \times 7.5^\circ$  grid, 19 vertical levels); the results of the vertical distributions (Section 5.2.4) and the comparison with measurements (Chapter VII) are partly based on the highest model resolution (VG,  $2.5^\circ \times 2.5^\circ$ , 31). The aerosol calculations are limited to the ammonium/sulfate/nitrate/water-system for which we have assumed submicron particles (bulk approach).

### 5.1 Atmosphere/Chemistry Transport Model (TM3)

An increasing number of global CTMs and GCMs are nowadays capable to simulate sources and sinks of aerosols. Langner and Rodhe (1991) were among the first to perform a global simulation of sulfate aerosols. Many more modelers followed (e.g. Pham et al., 1995; Feichter et al., 1996; Chin et al., 1996; Roelofs et al., 1998). Also for other aerosol species like organic aerosols (Liousse et al., 1996), black carbon (Cooke and Wilson, 1996), dust aerosols (Tegen and Fung, 1994), sea salt aerosol (Gong et al., 1997) and nitrate aerosols (Metzger et al., 1999; Adams et al., 1999), three-dimensional global model studies have become available. For sulfate aerosols, the confidence in model results is largest. Model results for other aerosol components are associated with large uncertainties, largely attributed to the lack of measurements available for validation. However, also the modeling of the sulfur cycle remains uncertain.

The main reasons for this are the irregularly spaced and highly variable sources of the sulfate precursor  $\text{SO}_2$  and the strong dependence of  $\text{SO}_2$  oxidation and aerosol scavenging on cloud and precipitation processes. The concentration distribution of  $\text{SO}_2$ , in addition, strongly depends on dry deposition at the surface, since the deposition velocities vary considerably depending on surface characteristics and local meteorology. As a result the lifetime of  $\text{SO}_2$  and sulfate is short ( $\pm 1$ -10 days). Due to the limited resolution and due to rather crude parameterizations of the above mentioned processes, current models have difficulties to simulate the observed variability of sulfate correctly.

From the COSAM (COmparison of large scale atmospheric Sulfate Aerosol Models) workshop (Barrie et al., 2000; Lohmann et al., 1999; Roelofs et al., 2000), in which about 10 global models participated, it was concluded that the difference in results for sulfur components among the different models is large. Most of the differences originated from the treatment of cloud and precipitation processes. Model results for sulfate were on average within 20% of the observed concentrations at remote sites while  $\text{SO}_2$  was overestimated by as much as a factor 2. Reported results from model-measurement comparisons for sulfur species thus indicate that the processes controlling the sulfate aerosol cycle are not fully understood or at least not sufficiently accurately modeled yet. In this chapter the TM3 model, as originally described by Houweling et al. (1998), is extended with the chemical cycles of sulfur and reduced nitrogen species. A schematic overview of the TM3 model as used in this work is presented in Figure 5, illustrating the coupling of the aerosol module with various other modules of TM3. The modules will be briefly described in the following sections.

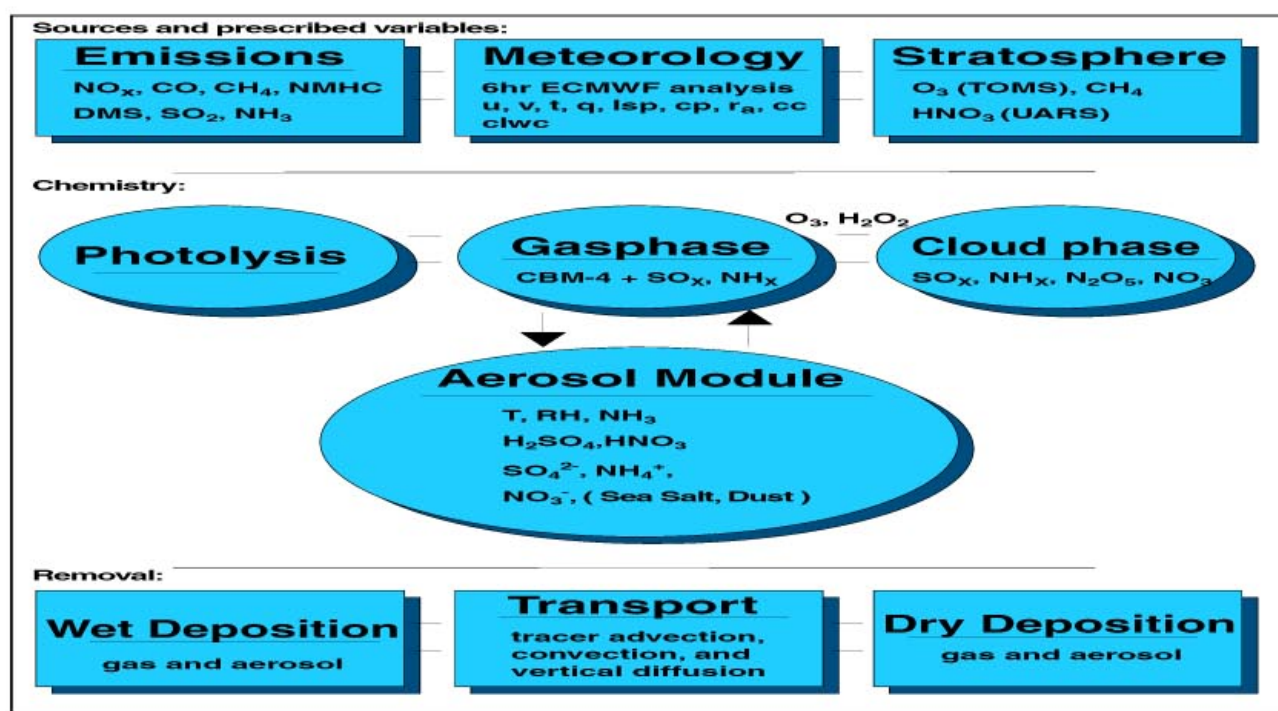


Figure 5. Schematic overview of the aerosol version of TM3.

Recent changes to the model as described by Jeuken (2000) are also included in this aerosol version of TM3. The new description of the boundary layer turbulent diffusion, for instance, improves the transport of SO<sub>2</sub> surface emissions to the free troposphere. The improved wet scavenging scheme also has a strong impact on simulated aerosol concentrations. In the last chapter (Chapter VII) it is therefore investigated to what extent the TM3 model with its additional improvements is able to reproduce the large observed variability.

### 5.1.1 Tracer Transport Processes

The TM3 offline chemistry transport model has gradually evolved from the TM2 model as developed by Heimann (1995). In TM3 the chemical continuity equation is solved:

$$\partial\mu/\partial t = -\vec{v} \cdot \vec{\nabla} \mu + (\partial\mu/\partial t)_{conv} + (\partial\mu/\partial t)_{diff} + S, \quad (5.1)$$

with  $\mu$  the tracer mixing ratio which is advected by the three-dimensional wind field and transported by parameterized convection and turbulent diffusion.  $S$  is the net source term that can be subdivided in emissions, chemical production or destruction, and the loss by precipitation scavenging processes or by dry deposition at the surface

$$S = S_{emis} + S_{chem} + S_{scav} + S_{depo}. \quad (5.2)$$

Three-dimensional tracer transport in the model is accounted for by advection for the resolved motions and by convection and vertical diffusion for the unresolved motions (the sub-grid scale). The advection of tracers in the model is calculated with the slope scheme of Russell and Lerner (1981). The sub-grid scale convection fluxes are calculated using the scheme of Tiedtke (1989). A new boundary layer scheme similar to the scheme used in the ECMWF model (Beljaars and Viterbo, 1998) has been implemented. For stable atmospheric conditions, we use a local formulation based on Louis et al. (1982), and for unstable conditions a non-local formulation based on Holtslag and Boville (1993). In addition, the time resolution has been increased from 6 to 3 hours. This new vertical diffusion scheme has been tested in TM3 by comparing surface and profile measurements of the radio nuclide radon (<sup>222</sup>Rn) with model output (Jeuken, 2000). It was concluded that due to the better temporal resolution of 3 hours instead of 6 used for the new scheme the diurnal cycle in radon surface concentrations is much better resolved by the model. In addition, also the absolute concentrations were better simulated with the new diffusion scheme but were still somewhat overestimated by the model indicating that mixing remains underestimated. The effect on the aerosol concentration will be discussed in Chapter 6.3.

### 5.1.2 Meteorological Data

To accurately calculate the gas/cloud phase and aerosol chemistry in the model, we prescribe three-dimensional meteorological input fields, including cloud cover and the cloud liquid and ice water content from the European Center of Medium Weather Forecast (ECMWF).

Since wet processes are of major importance for the chemistry of sulfate and nitrate aerosols, accurate cloud fields are crucial. The global mean cloud cover is close to 60%. The global average volume fraction of clouds in the troposphere is 7-8% and about 10% of the tropospheric air mass is contained in cloud systems. Together with the fact that chemical reactions in clouds are often much faster than in the gas phase, these numbers illustrate the importance of clouds for tropospheric chemistry (Lelieveld and Crutzen, 1991). The distribution of clouds influences the chemistry in the model in three ways:

1. Clouds provide an efficient reaction volume for aqueous phase reactions. The concentrations of dissolved species in the water droplets depend on the liquid water content, i.e. relative humidity and temperature, also influencing the acidity of the droplet, and the water in the droplets in turn depend on the dissolved species and its acidity.
2. Large cloud droplets are removed as rain, returning particulate matter and dissolved gases to the surface.
3. Clouds also have a strong interaction with radiation, reflecting large parts of the short-wave radiation back to space, increasing the radiation intensity above the cloud, and decreasing it below the cloud. Photo-dissociation of chemical species in this way strongly depends on the cloud distribution. We have implemented the photolysis parameterization of Krol and Van Weele (1997), which takes into account the radiative effects of clouds in the photochemistry.

In fact, only few offline models contain such accurate cloud information. Often a climatological cloud distribution is prescribed (Pham et al., 1995; Langner and Rodhe, 1991) and sometimes part of the hydrological cycle is calculated online (Rasch et al., 1997) or strongly parameterized (Benkovitz et al., 1994; Kasibhatla et al., 1997). Climate models predict a climatological cloud distribution, but have the advantage of a better time resolution of the cloud fields. A higher resolution in time than 3 or 6 hours in our model can be important for the often very efficient chemical reactions in clouds. Since TM3 uses offline calculated cloud fields, there is no feedback of calculated aerosol mass on cloud formation, and no cloud-aerosol interaction at present.

### 5.1.3 Emissions

Anthropogenic emissions of  $\text{NO}_x$ ,  $\text{NH}_3$ ,  $\text{SO}_2$  have been taken from the historical Emission Database for Global Atmospheric Research (EDGAR), available on a  $1^\circ \times 1^\circ$  grid (Olivier, 1996). Van Aardenne et al. (1999) have estimated trends in these emissions, based upon demographical, economical, agricultural and technological developments during the past century. The time resolution of the database is 10 years until 1970 and 5 years hereafter until 1990. After 1990 we have extrapolated the 1990 emission data based on the increase of energy consumption (Dentener, personal comm., 2000) to which we refer in the following as EDGAR<sup>D</sup>. The seasonal variation in  $\text{NO}_x$  and  $\text{SO}_2$  emissions is based upon the Global Emission Inventory Activity (GEIA) database valid for 1985 (Benkovitz et al., 1996). The GEIA database distributes the emissions over two

layers, below and above 100m height. Volcanic sulfur emissions have been estimated by Andres and Kasgnoc (1998). They distinguish between continuously and sporadically erupting volcanoes. DMS emissions are obtained by combining the oceanic surface concentrations compiled by Kettle et al. (1999) with turbulent air-sea exchange coefficient calculated by using the parameterization by Liss and Merlivat (1986). For DMS land-emissions and SO<sub>2</sub> natural emissions, we use the estimates of Spiro et al. (1992). All other emissions are described in Houweling et al. (1998). For Europe we optionally use SO<sub>2</sub> emissions from the CORINAIR (COre INventory AIR) project (see Chapter 6.2 for the effect on aerosol). In contrast with the global EDGAR<sup>D</sup> data, reported CORINAIR emissions take into account the changes in emission factors, e.g. changes in the conversion factors from fossil fuel use by electric power generation to SO<sub>2</sub> emissions. While the total of SO<sub>2</sub> emissions for Europe in the EDGAR<sup>D</sup> database is 22 Tg S, it is only 12 Tg S in the CORINAIR database. Both databases will also be used in Chapter VII and provide interesting insights in the effect of emission reduction on the aerosol abundance.

#### 5.1.4 Chemistry

The sulfur cycle is coupled to the chemistry version of TM3, and is described by Houweling et al. (1998). The chemistry module calculates the background tropospheric CH<sub>4</sub>-O<sub>3</sub>-HO<sub>x</sub>-NO<sub>x</sub> chemistry and the chemistry of non-methane hydrocarbons (NMHC's), using a modified version of the widely used Carbon Bond mechanism (Gery et al., 1989). To calculate photolysis rates we use the scheme adapted from Krol and Van Weele (1997) consistently with local cloud cover and ozone columns (Lelieveld and Dentener, 2000). We have added the gas and cloud phase reactions of SO<sub>2</sub>, DMS, NH<sub>3</sub>, SO<sub>4</sub><sup>2-</sup> and NH<sub>4</sub><sup>+</sup> (Dentener and Crutzen, 1994). For a complete list of all other gas phase reactions we refer to Houweling et al. (1998).

SO<sub>2</sub> and its oxidants H<sub>2</sub>O<sub>2</sub> and O<sub>3</sub> are dissolved into the cloud droplet according to their Henry's Law equilibrium. For SO<sub>2</sub> an effective Henry's law constant is used, taking into account dissociation into HSO<sub>3</sub><sup>-</sup> and SO<sub>3</sub><sup>2-</sup>, effectively allowing more SO<sub>2</sub> to dissolve. Both the dissociation equilibrium and rate coefficients are pH dependent. Ignoring the contribution of weak acids and bases the pH is calculated from the concentration of strong acids and bases:

$$[H^+] = 2[SO_4^{2-}]_a + [MSA]_a - [NH_4^+]_a + [HNO_3]_g + [NO_3^-]_a. \quad (5.3)$$

where subscripts *a* and *g* indicate dissolved aerosol and gaseous species respectively. For pH > 4.3 also the dissociation of the weak acids SO<sub>2</sub> and CO<sub>2</sub> as well as the base NH<sub>3</sub> are taken into account. With the concentration of H<sup>+</sup> being known, the effective Henry's law coefficient for SO<sub>2</sub> can be calculated.

In many models the sulfur cycle is coupled with offline calculated fields of OH, H<sub>2</sub>O<sub>2</sub> and O<sub>3</sub> (Feichter et al., 1996; Langner and Rodhe, 1991). In some models the H<sub>2</sub>O<sub>2</sub> concentration is allowed to gradually recover after reaction with SO<sub>2</sub>. However, in reality the recovery of H<sub>2</sub>O<sub>2</sub> depends on the local chemistry regime. Lohmann et al. (1999) conclude that models that calculate

the chemistry of the oxidants online are better able to simulate measured instantaneous profiles of SO<sub>2</sub> and sulfate. Roelofs et al. (1998) also conclude that coupling between sulfur chemistry and photochemistry gives a somewhat better agreement with observations. However, the average overestimation of SO<sub>2</sub> levels is less in models with prescribed oxidant fields (Koch et al., 1999). In this work all oxidants are explicitly calculated.

Following Dentener and Crutzen (1993) we calculate heterogeneous reaction rates of N<sub>2</sub>O<sub>5</sub> on pre-existing aerosol surface, resulting in the formation of HNO<sub>3</sub>(g). Since the aerosol in our model is MSA and ammonium-sulfate/nitrate only, we might underestimate the rate of this reaction. Most other sulfur-cycle models do not model ammonia, but assume that a fixed fraction of sulfate is neutralized by ammonium. Ammonium, however, can have a strong, spatially variable feedback on the sulfur cycle via the calculation of the pH and is therefore included in our model.

### 5.1.5 Aerosol Module

To be able to calculate the gas/aerosol partitioning of the ammonia/sulfate/nitrate/water system, we have added a simplified thermodynamical equilibrium model (EQSAM) to TM3 (Chapter 3.8). EQSAM describes the equilibrium partitioning between aerosol precursor gases such as NH<sub>3</sub>, H<sub>2</sub>SO<sub>4</sub>, HNO<sub>3</sub>, and HCl and liquid and solid aerosol phases for major inorganic aerosol compounds, e.g. ammonium, sulfate, nitrate, sea salt, and mineral dust. Usually EQMs are complex models in which the gas/aerosol partitioning and the estimation of activity coefficients need to be calculated iteratively, therefore demanding large computing resources (Chapter 4.2.1). Based on fundamental physical relations, an alternative method has been introduced, which allows one to calculate the gas/aerosol partitioning sufficiently fast and accurate for global modeling (Chapter III). The method is based on the fact that, for atmospheric aerosols in thermodynamical equilibrium with the ambient air, the solute activity, and hence the activity coefficient calculation, is governed by the aerosol associated water. The latter depends only on the relative humidity and the type and number of moles of dissolved matter, which are determined in certain concentration domains based on the mole ratio of the solute concentration. This mole ratio is associated with different aerosol compositions, and can denote, for instance, a “sulfate rich” domain (i.e. NH<sub>4</sub><sup>+</sup> < 2SO<sub>4</sub><sup>2-</sup>), a “sulfate very rich” domain (i.e. NH<sub>4</sub><sup>+</sup> < SO<sub>4</sub><sup>2-</sup>), or a “sulfate poor domain” (i.e. NH<sub>4</sub><sup>+</sup> > 2SO<sub>4</sub><sup>2-</sup>), according to the definition in Chapter 2.4. Based on the domain and the relative humidity, the amount of aerosol associated water and corresponding activity coefficients are directly derived by utilizing the generalized Raoult's law. The activity coefficients and various aerosol properties calculated non-iteratively with the new method and the simplified equilibrium module (EQSAM), compare well with those obtained with common iterative methods of various EQMs (Chapter III and IV).

### 5.1.6 Dry Deposition

Dry deposition is a major sink for soluble or reactive trace gases like SO<sub>2</sub> and NH<sub>3</sub>. Especially in wintertime, when low H<sub>2</sub>O<sub>2</sub> concentrations limit SO<sub>2</sub> oxidation, it will be the dominant sink for SO<sub>2</sub>.

We use the “resistance in series” dry deposition scheme as described by Ganzeveld et al. (1998), which contains a fairly detailed description of surface characteristics. The deposition velocity can be written as the reciprocal of the aerodynamic resistance, the quasi-laminar boundary layer resistance, and the surface resistance. The surface resistance of  $\text{SO}_2$  strongly depends on snow cover and surface wetness. For sulfate and nitrate aerosol the deposition velocity is dependent on two parameterized size distributions, one for land and one for oceans, and further depends on the wind velocity which may increase the contact surface area over ocean when the sea roughness increases.

Most meteorological surface fields, for example, the aerodynamic resistance are calculated from ECMWF data. Vegetation descriptions are derived from a global ecosystem database (Olson et al., 1983). Variables like snow cover and surface wetness are prescribed by ECHAM4 climatological data (Claussen et al., 1994). According to Van der Hurk et al. (1999), in wooded areas the snow-covered fraction is substantially smaller than one. We correct the ECHAM snow cover for this effect by allowing a maximum snow cover of 70% over vegetated surfaces.

### 5.1.7 Wet Deposition

Generation of synoptic precipitation is calculated in TM3 from the cloud liquid and ice content, using the same formulations as in the operational ECMWF weather forecast model (Tiedtke, 1993). In-cloud scavenging of gases and aerosols is calculated according to these local precipitation rates, using a first order loss approach (e.g. Guelle et al., 1997a,b).  $\text{HNO}_3$  is assumed to be completely soluble, and is scavenged in a cloud with the same rate as cloud water is converted into precipitation. The scavenging rate for any other gaseous specie is scaled to the scavenging rate of  $\text{HNO}_3$  according to its Henry equilibrium constant (Dentener and Crutzen, 1993). Following Roelofs and Lelieveld (1995), the mass transfer of gases to the cloud droplets is taken into account as well. Below cloud scavenging of gases is calculated as the product of the mass transfer coefficient and the dimensionless rain liquid water content divided by the rain droplet radius (Roelofs and Lelieveld, 1995). To calculate this radius and the rain liquid water content we use the empirical formulas proposed by Mason (1971). The mass transfer coefficient is calculated as a function of the Schmidt and Reynolds numbers (e.g. Seinfeld, 1986). The same scaling with respect to  $\text{HNO}_3$  is applied to below-cloud scavenging rates.

For below-cloud scavenging of accumulation mode aerosols we adopt a scavenging efficiency of  $0.05 \text{ mm}^{-1}$ , taken from Dana and Hales (1991), for a log-normal background aerosol distribution with  $r=0.13\mu\text{m}$ ,  $\sigma=1.9$  (Jaenicke, 1988) and a frontal rain spectrum with a geometric mean droplet radius  $R_g$  of 0.02 cm with  $\sigma=1.86$ . It should be noted that the scavenging coefficient is strongly dependent on the actual choice of  $r$  and  $\sigma$ . For below-cloud scavenging of  $\text{SO}_2$  we assume that the maximum scavenging rate (i.e. the rate of  $\text{HNO}_3$  scavenging) is only limited by the amount of  $\text{H}_2\text{O}_2$  in the falling rain with a pH below 5, assuming fast reaction of  $\text{H}_2\text{O}_2$  and S(IV). Above pH=5 the below-cloud scavenging rate of  $\text{SO}_2$  is equal to the scavenging rate of  $\text{HNO}_3$ , assuming that



oxidation by  $O_3$  effectively removes  $S(IV)$ . By keeping track of the amount of  $H_2O_2$  and  $H^+$  scavenged in the grid cells above, the below cloud-scavenging rate of  $SO_2$  is calculated. This simplified method probably presents an upper limit for the below cloud scavenging of  $SO_2$  since it assumes that the reactions and dissociation processes are fast compared to the time scales of existence of rain droplets.

The removal of tracers in convective clouds has been parameterized as a function of the updraft mass flux (Balkanski et al., 1993). In this method, scavenging is directly coupled to the intensity of convection assuming 100% efficiency for deep and 50% for shallow (precipitating) convective clouds.

## 5.2 Aerosol Distributions

### 5.2.1 Gas/Aerosol Partitioning

To investigate the temporal variability of gas/aerosol partitioning, we focus on a single gridbox in Germany ( $10^\circ E$ ,  $50^\circ N$ ). For this location (near Deuselbach) we discuss time series (for 1997) of various surface variables relevant to the gas/aerosol partitioning calculations.

Figure 5.1a shows the meteorological parameters temperature [ $^\circ C$ ], relative humidity [%], and pressure [hPa]. Figure 5.1b shows the surface mass ratio of aerosol nitrate and sulfate, and the dry aerosol fraction, i.e. dry particulate matter / total particulate matter; the latter includes the aerosol associated water mass. Figure 5.1c shows the corresponding nitrate and ammonium partitioning [%], and Figure 5.1d the degree of neutralization [%] and the gas ratio of residual ammonia and nitric acid. The timestep is 6 hours. According to Figures 5.1a-d, the diurnal and annual cycle of the gas/aerosol partitioning can be characterized as follows.

At low temperatures ( $<10^\circ C$ ) and at high relative humidities ( $>70\%$ ) (Figure 5.1a), i.e. the northern hemispheric winter season (November-April), nitric acid is predicted to partition completely into the aerosol phase (Figure 5.1c, top). This results in a significant amount of nitrate aerosol compared to sulfate, by which the surface mass of nitrate is, in the winter season, four times that of sulfate, with comparable nighttime concentrations in summer (Figure 5.1b, top). During summer days, the nitrate fraction can be very low, especially for days where less than 10% gaseous nitric acid partitions into the aerosol phase (Figure 5.1c, top). The reason is that for hot days, ammonium nitrate can not be formed during day, since the partial pressures of ammonia and nitric acid do not exceed the high values of the temperature dependent ammonium nitrate equilibrium constant. Additionally, ammonium nitrate, which might be formed during night, is not stable during day (i.e. at higher temperatures), because ammonium nitrate is (semi-) volatile. Furthermore, the ammonium nitrate formation depends on the availability of ammonia, which is partly controlled by the presence of sulfate. If sulfate is present, then ammonium nitrate formation is assumed to take place only if sulfate is completely neutralized by ammonia. In addition, since the sulfate concentration strongly

depends on the photochemical oxidation of sulfur dioxide, sulfate concentrations are highest during day and in summer. Thus, the ammonium nitrate concentrations are highest at cold atmospheric conditions, i.e. during night and winter.

The ammonium partitioning on the other hand, does not show such a strong seasonal cycle (Figure 5.1c, bottom). The reason is that ammonia partitions into the aerosol phase only if it can neutralize either nitric acid or sulfuric acid. While the neutralization of nitric acid by ammonia is more important during winter months or during night (to form ammonium nitrate), ammonia also neutralizes sulfuric acid, i.e. sulfate during day and during summer. This is illustrated by the ammonium fraction relative to the aerosol mass of nitrate and sulfate, i.e.  $\text{NH}_4^+ / (\text{NO}_3^- + 2\text{SO}_4^{2-})$  in  $[\mu\text{gN}/(\mu\text{gN} + \mu\text{gS})]$ , since values are only of about 75% during summer, and for some summer days only of 50% due to the high sulfate concentrations (Figure 5.1d, top). During winter, the ammonium fraction is usually much higher (up to 90 %); the remaining percent are associated with the nitric acid uptake on wet aerosol at high RHs. This indicates that in winter nitric acid limits the nitrate aerosol formation rather than ammonia, while the opposite is true for the summer; this is also indicated by the high values of the gas ratio ( $\text{NH}_3/\text{HNO}_3$ ) in the winter season and their absence in the summer season (Figure 5.1d, bottom). It should be noted that we did not account for a seasonal cycle of the ammonia emissions in these model calculations, due to the lack of information, which would be needed globally.

A seasonal cycle also appears for the predicted aerosol water, which is associated with the dry particulate matter (Figure 5.1b, bottom). In the winter, up to 80% of the average aerosol mass is predicted to be water. Although in summer the fraction is much lower, 50% of the aerosol mass is water. Nevertheless, due to the diurnal cycle, also a water fraction of 90% or more can occur. Since high water fractions are always associated with high RH values, which often occur at least diurnally (Figure 5.1a, middle), it is important to account for the aerosol water in all aerosol calculations.

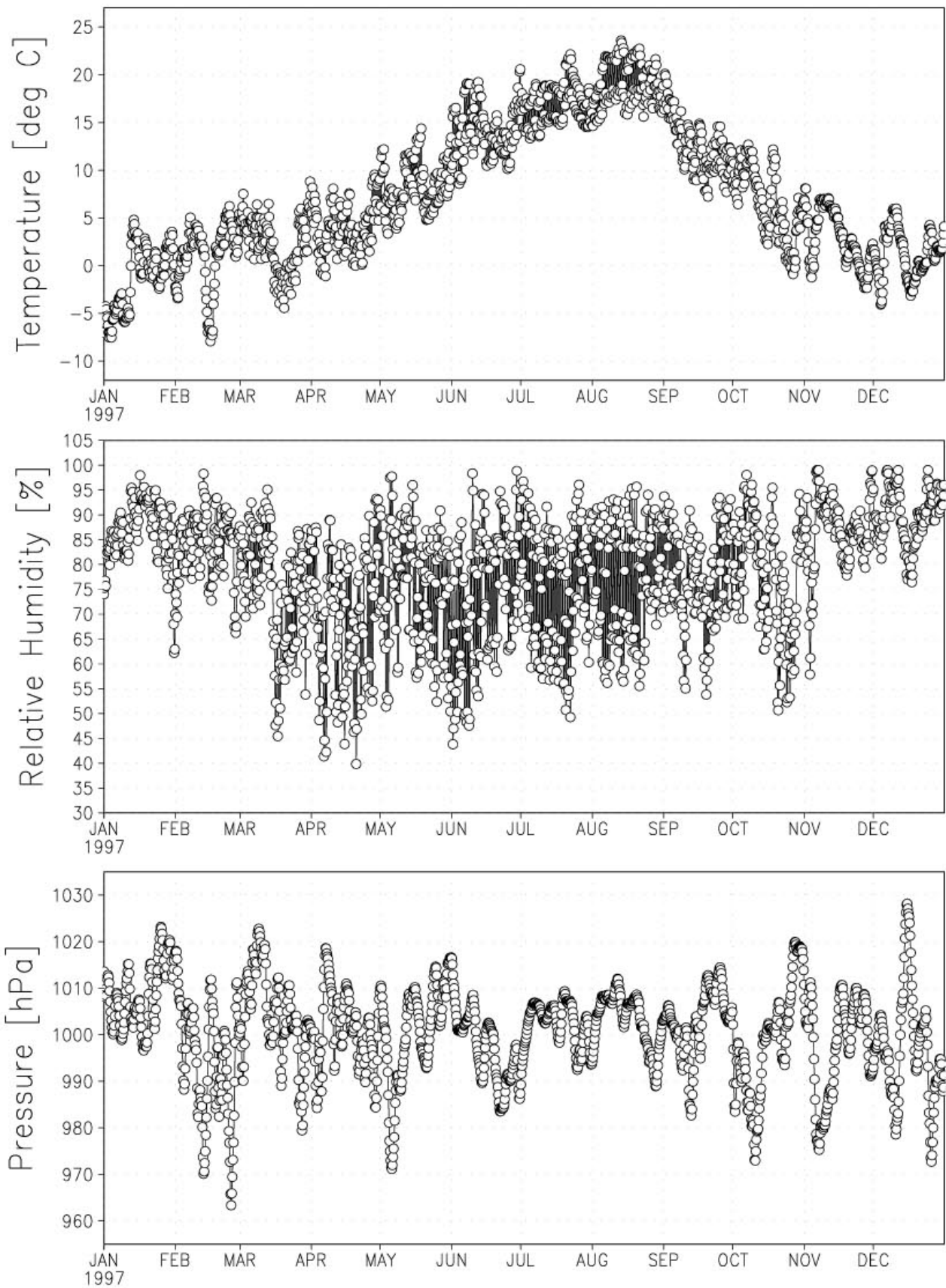


**Figure 5.1a.** Time series (for the year 1997) of various surface variables relevant to the gas/aerosol partitioning calculations. Meteorological parameters for a single gridbox in Germany (10°E, 50°N): Temperature [°C], relative humidity [%], and pressure [hPa].

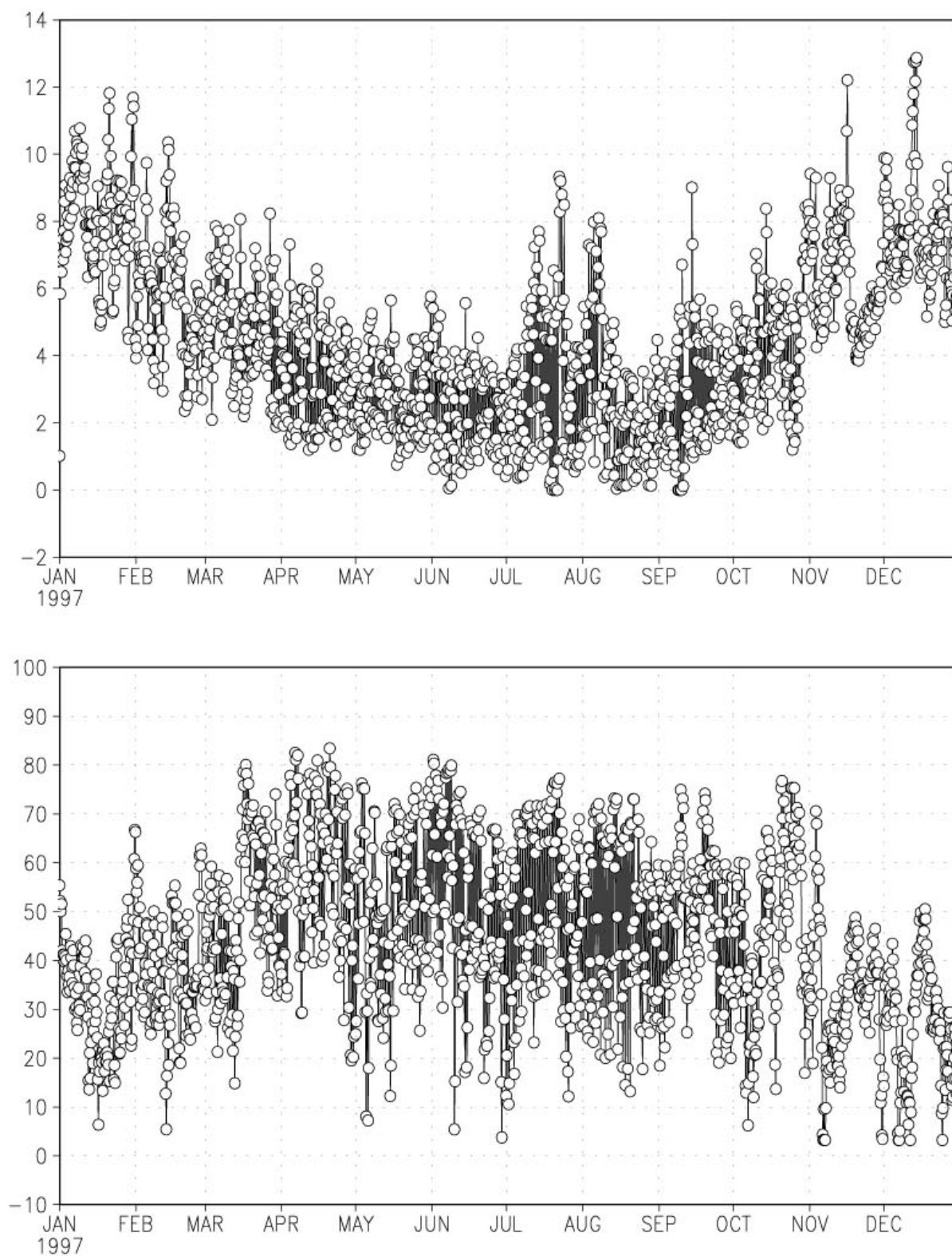


**Figure 5.1b.** Time series (for the year 1997) of the surface mass ratio of aerosol nitrate and sulfate (top), and dry aerosol fraction (bottom), i.e.  $PM/(PM+H_2O)$  [%], for a single gridbox in Germany ( $10^\circ E, 50^\circ N$ ).

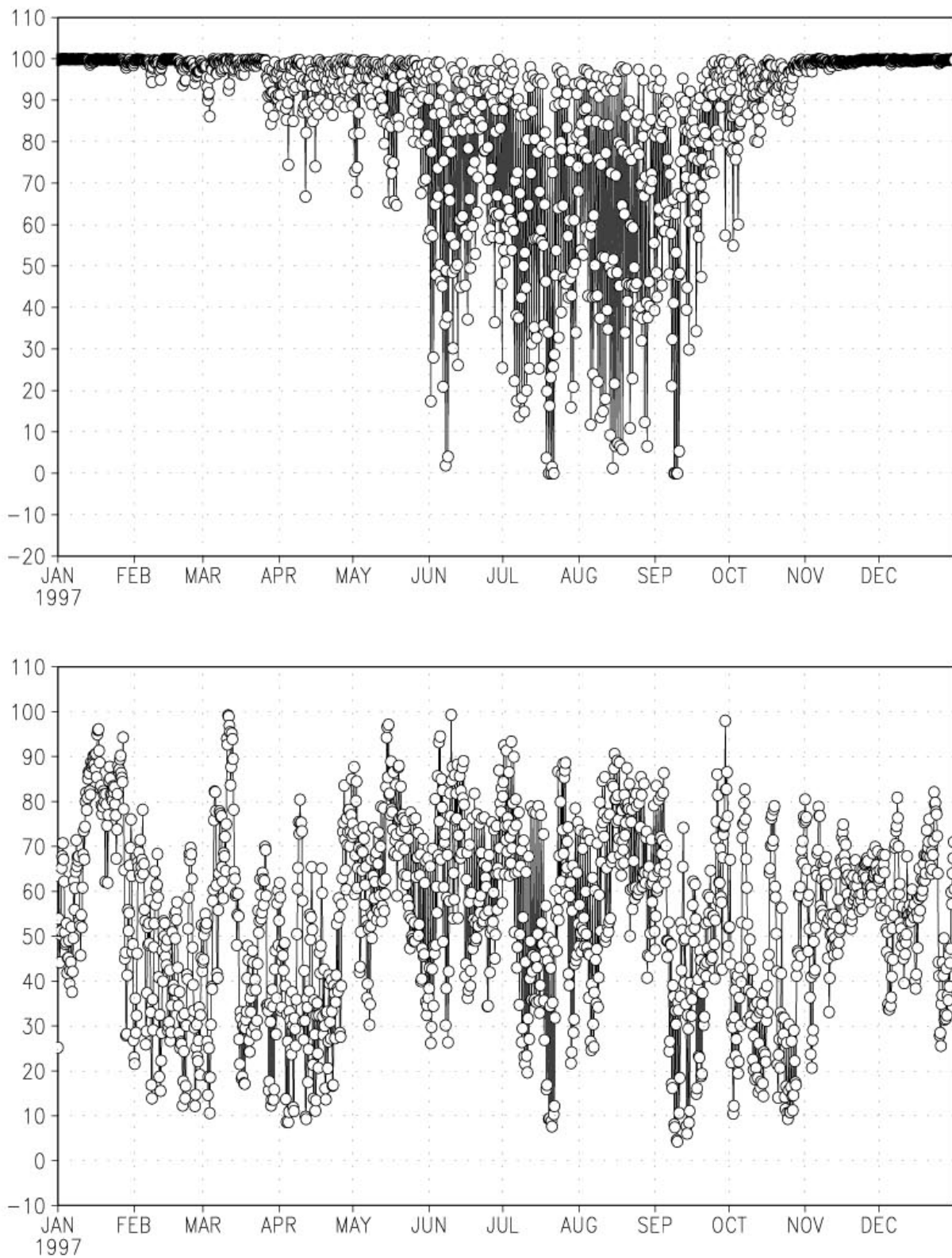


**Figure 5.1c.** Time series (year 1997) of the corresponding nitrate (top) and ammonium partitioning (bottom) [%], i.e.  $\text{NO}_3^-/(\text{HNO}_3+\text{NO}_3^-)$  and  $\text{NH}_4^+/(\text{NH}_3+\text{NH}_4^+)$ , respectively (single gridbox, Germany,  $10^\circ\text{E}$ ,  $50^\circ\text{N}$ ).

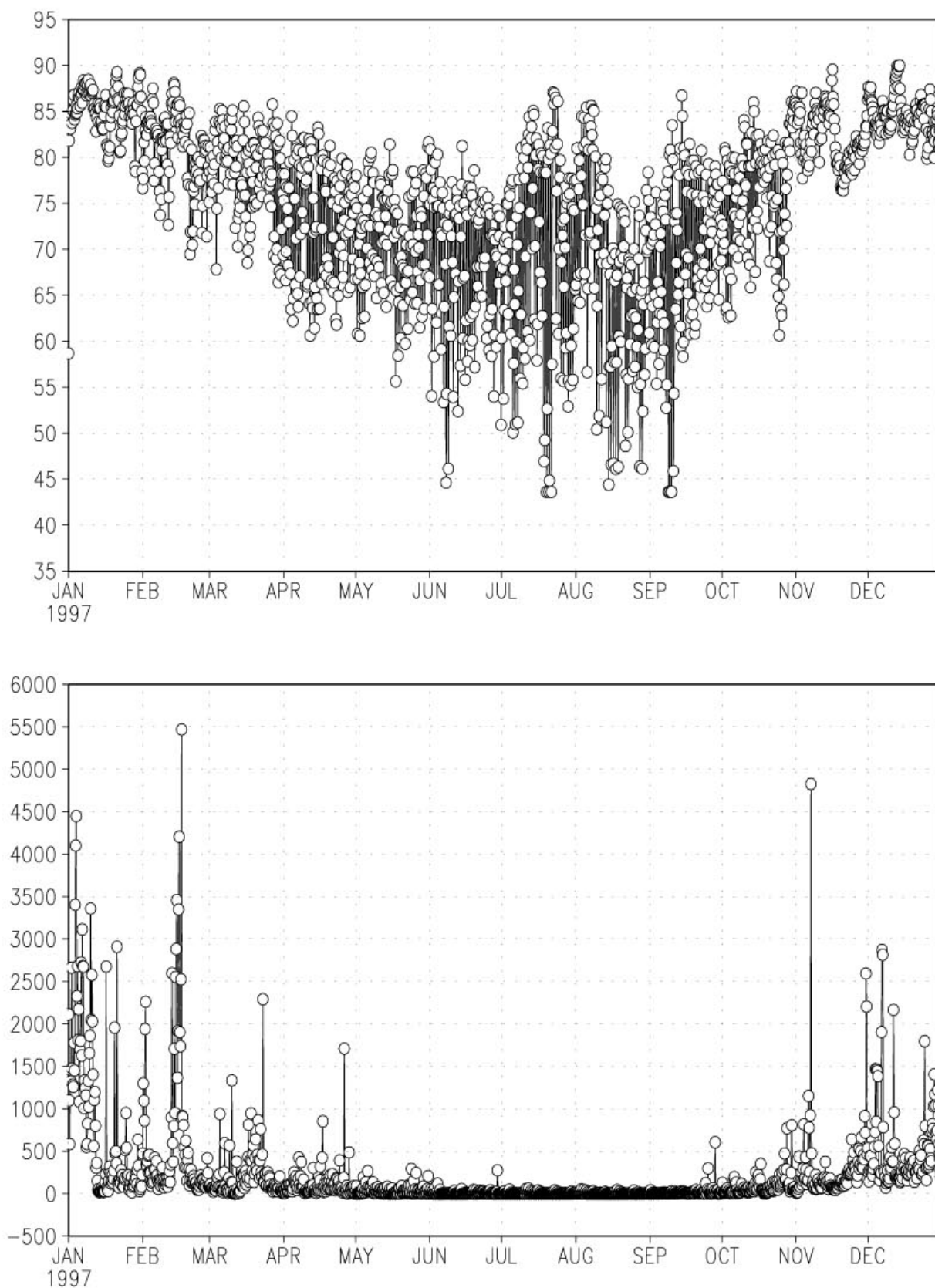


**Figure 5.1d.** Time series (year 1997) of the corresponding ammonium fraction (top) [%], i.e.  $\text{NH}_4^+(\text{NO}_3^- + 2\text{SO}_4^{2-})$  in  $[\mu\text{gN}/(\mu\text{gN} + \mu\text{gS})]$ , and the gas ratio (bottom) of residual ammonia and nitric acid [mol/mol], i.e.  $\text{NH}_3/\text{HNO}_3$  (single gridbox, Germany,  $10^\circ\text{E}$ ,  $50^\circ\text{N}$ ).

### 5.2.2 Global Aerosol Patterns

To investigate the spatial aerosol distributions we discuss global aerosol patterns, focusing on monthly means of January and July 1997. [Figure 5.2a](#) shows the surface mole fraction of aerosol nitrate, relative to the sum of nitrate and sulfate, [Figure 5.2b](#) shows the vertically integrated total particulate aerosol mass (burden) [ $\mu\text{g}/\text{m}^2$ ], [Figure 5.2c](#) the associated aerosol water (burden) [ $\mu\text{g}/\text{m}^2$ ], and [Figure 5.2d](#) the total (direct) aerosol radiative forcing of sulfate and nitrate [ $\text{W}/\text{m}^2$ ].

The comparison of the monthly mean aerosol distribution of January and July shows ([Figure 5.2a](#)) that in January for most regions of the northern hemisphere more than 50% of the nitrate and sulfate surface mass is explained by nitrate, while in summer, a similar fraction is only predicted for a few regions, i.e. western Europe, and parts of the eastern USA. Accordingly, the same is true for the southern hemisphere, where such high fractions are predicted only in winter (i.e. July) for industrialized regions of South Africa, Brazil, and South Australia. Especially during the northern hemispheric winter, a large amount of nitric acid partitions into the aerosol phase, which is in accord (although at some location lesser) with the previously discussed single grid-box in Germany. The vertically integrated total particulate matter ([Figure 5.2b](#)) does not reflect such a strong seasonal variability, apart from some regions. East Asia shows a three times higher total aerosol mass in January compared to July, while the opposite is true for the Mediterranean region, Arabia, and parts of North Africa, where higher values are predicted in July. Obviously, the high aerosol load in winter over Central Europe, which extends in winter over parts of Russia, is shifted southwards in summer. Similarly, the high aerosol load, which occurs in winter over the eastern US, extends across the Atlantic in summer.

Since we have not considered sea salt or mineral dust aerosol, which might significantly contribute to the total aerosol mass at remote sites, long-range transport largely explains the redistribution of the global aerosol patterns. However, the fact that the variability of the total aerosol mass (burden) is generally much less compared to the surface mole fraction of aerosol nitrate, indicates that most of the nitrate aerosol mass resides in the lower atmosphere, i.e. in the planetary boundary layer where most of the variability occurs. Consequently, this indicates that most of the vertical aerosol burden is made up by sulfate in our model simulations. Sulfate is treated as non-volatile so that it resides in the aerosol phase regardless of the meteorological conditions.

Nevertheless, the associated aerosol water ([Figure 5.2c](#)) does show a seasonal variability, even vertically integrated. While peaks of the aerosol water mass are predicted to be higher in winter for the region of Europe and Asia, more aerosol water is predicted for the eastern US in July. In addition, a larger region is then covered by high aerosol water, which extends across the Atlantic to Europe in summer. Similarly, during the southern hemispheric summer (January), large aerosol water amounts are predicted over the South Pacific region, and part of Antarctica, which is not the case during the local wintertime. This further indicates that long-range transport of the aerosol species partly redistributes the global aerosol patterns. Note that the predicted amount of aerosol water was limited to a RH=99% to exclude clouds.

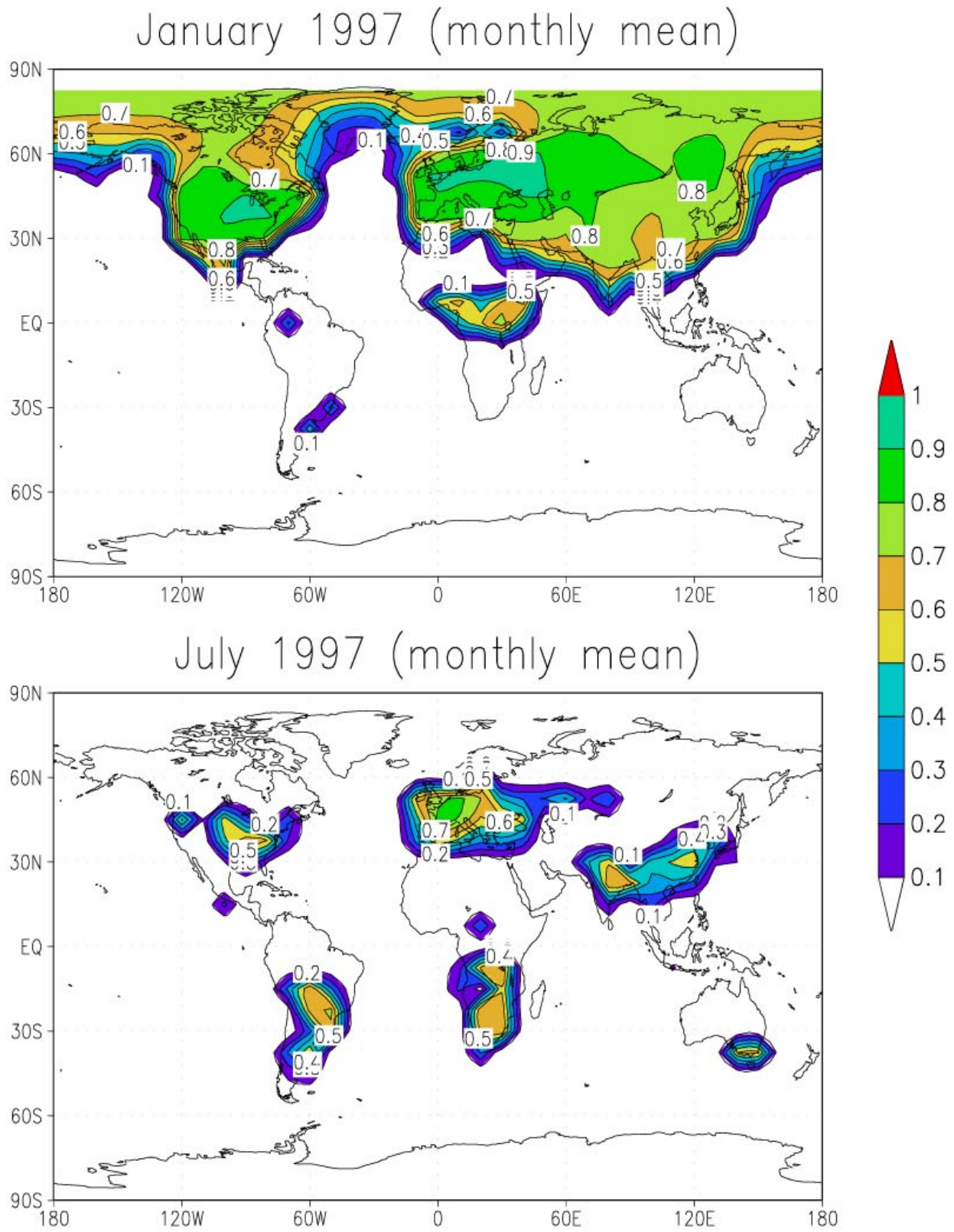


**Figure 5.2a.** Surface mole fraction of aerosol nitrate relative to the sum of nitrate and sulfate, i.e.  $\text{NO}_3^-/(\text{SO}_4^{2-}+\text{NO}_3^-)$ .



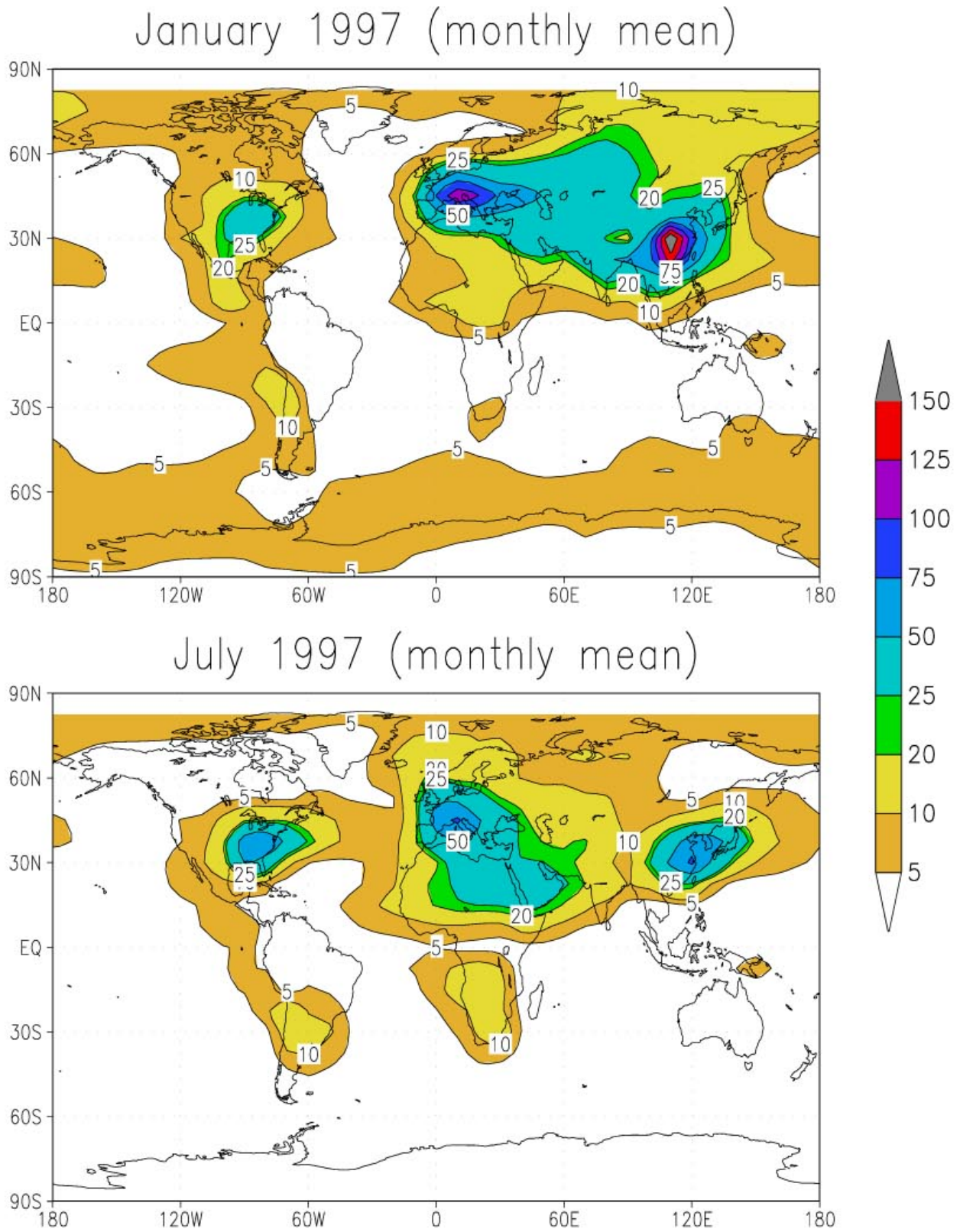


**Figure 5.2b.** Total particulate aerosol mass vertically integrated (burden) [ $\mu\text{g}/\text{m}^2$ ].

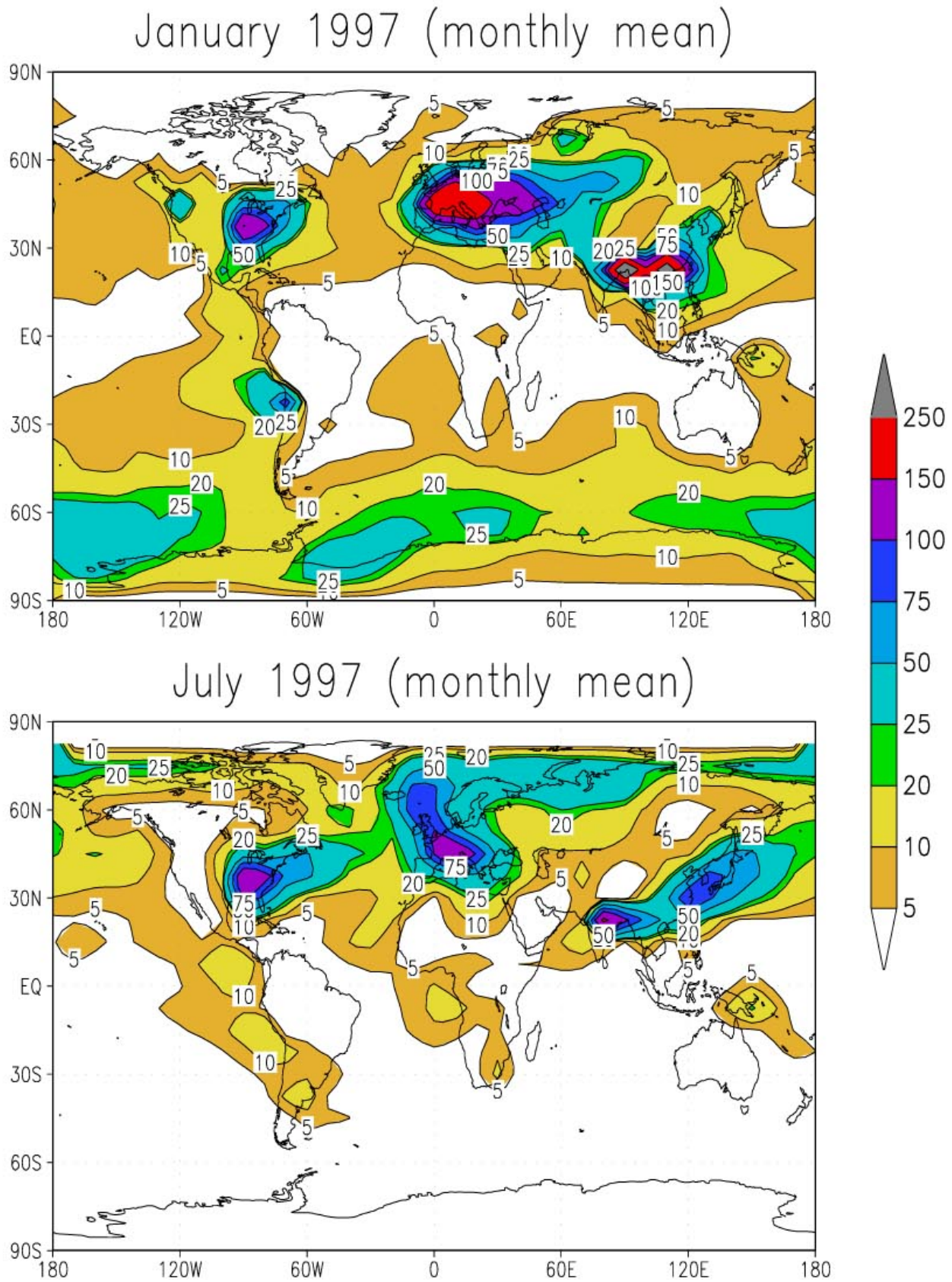


Figure 5.2c. Aerosol associated water (burden) [ $\mu\text{g}/\text{m}^2$ ].

### 5.2.3 Space-Time Variability

To investigate the time variability of the spatial aerosol distributions we discuss in this section two different representations of the previously shown global aerosol patterns for July 1997: an average over all values obtained at both 6:00 and 18:00 hrs Greenwich mean time (GMT). [Figure 5.3a](#) shows, accordingly, the surface mole fraction of aerosol nitrate, [Figure 5.3b](#) the total particulate aerosol mass vertically integrated (burden) [ $\mu\text{g}/\text{m}^2$ ], [Figure 5.3c](#) the associated aerosol water mass (burden) [ $\mu\text{g}/\text{m}^2$ ], and [Figure 5.3d](#) shows the total (direct) aerosol radiative forcing of sulfate and nitrate [ $\text{W}/\text{m}^2$ ].

The diurnal variability is nicely illustrated by the large variability of the surface mole fraction of aerosol nitrate ([Figure 5.3a](#)). While during early morning (6hr GMT) nitrate clearly dominates the surface aerosol mass relative to sulfate in large parts of Europe (the nitrate mole fraction exceeds 0.8), this is not the case during early evening (18hr GMT), by which only for Central Europe, including the region of the Netherlands, comparable mean concentrations of nitrate and sulfate are predicted. Even more striking are the daily variations over South Africa. There, the nitrate mole fractions are less than 0.1 in the evening, while fractions exceed 0.8 during early morning. However, other regions of the world are at these times less affected, but would show similar fluctuations if other time slices would have been considered.

Similar to the less pronounced seasonal variability of the total vertically integrated aerosol mass, the diurnal cycle is also less pronounced ([Figure 5.3b](#)). Nevertheless, significant differences are found over Europe where the total aerosol load is twice as high in the morning compared to the evening. This further indicates the strong regional impact of the gas/aerosol partitioning. Especially because the higher aerosol load is associated with additional aerosol water, which is twice as high in the morning (values exceed  $100 \mu\text{g}/\text{m}^2$ ) compared to the evening (and twice as high as the total dry aerosol mass).

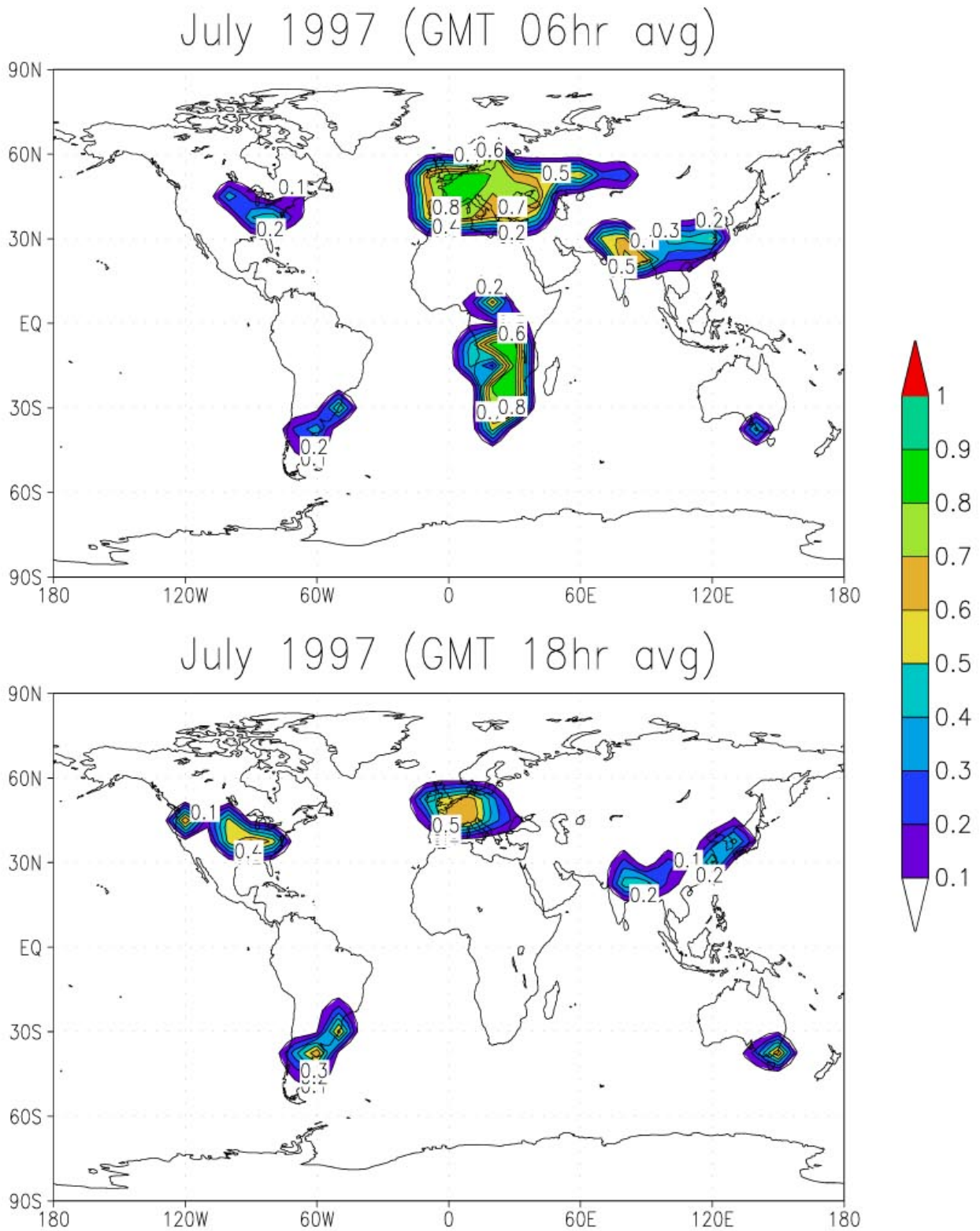


**Figure 5.3a.** Surface mole fraction of aerosol nitrate relative to the sum of nitrate and sulfate, i.e.  $\text{NO}_3^-/(\text{SO}_4^{2-}+\text{NO}_3^-)$ .

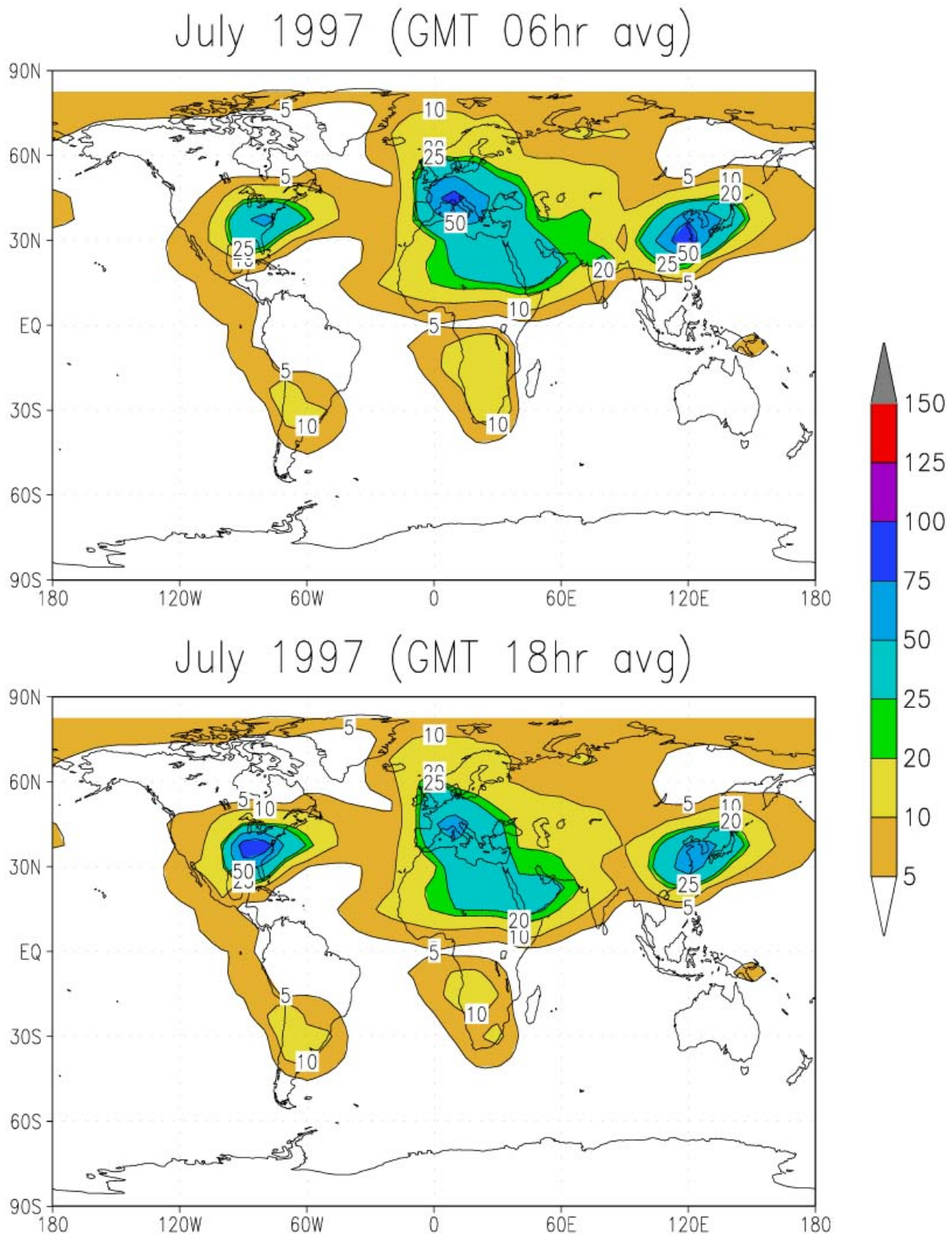


**Figure 5.3b.** Total particulate aerosol mass vertically integrated (burden) [ $\mu\text{g}/\text{m}^2$ ].

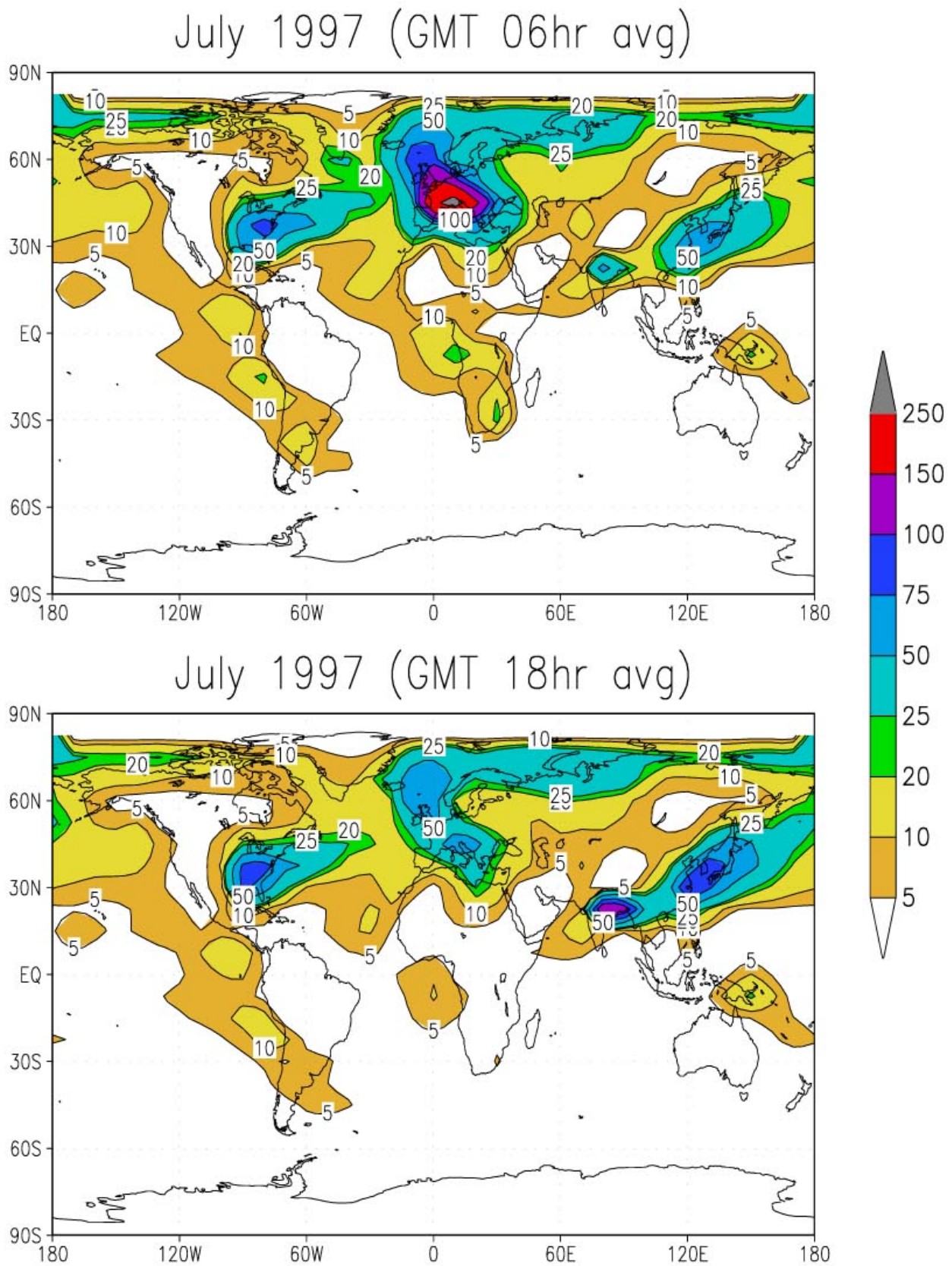


Figure 5.3c. Aerosol associated water (burden) [ $\mu\text{g}/\text{m}^2$ ].

### 5.2.4 Zonal Distributions

In the previous sections we have investigated the spatial and temporal variability of global aerosol patterns. In this section, we will investigate the corresponding large scale vertical distributions of various aerosol compounds. First, however, we show the vertical-time variability of various aerosol properties exemplary for the previously discussed single gridbox in Germany (50°N and 10°E).

Figure 5.4a shows the vertical-time distribution (Hovmöller representation) of the mass ratio of nitrate and sulfate (top), the total dry particulate matter (middle), and the associated aerosol water mass (bottom). According to the annual cycle of the nitrate partitioning (Section 5.2.1), the vertical dispersion of nitrate is limited to the northern hemispheric winter season. During summer (June–September) nitrate aerosol is confined to the surface model layer. The reason is that in summer insufficient ammonia is available to neutralize sulfate (as concluded previously). Because sulfate concentrations are highest in summer, nitric acid can only be neutralized by ammonia near the emission sources, which are mostly confined to the surface. However, the total dry particulate matter and the aerosol water show a highly variable vertical distribution at all times due to the high sulfate concentrations in summer; the 5  $\mu\text{g}/\text{m}^3$  contour line reaches on average up to 750 hPa for the dry aerosol mass, and up to 550 hPa for the aerosol water.

Nevertheless, our model results indicate that ammonium nitrate aerosol might be present even in summer at higher altitudes. Model results of the high resolution run (2.5°x2.5°x31 levels) predict an ammonium nitrate concentration of roughly 50 pptv at 200 hPa (approx. 0.3  $\mu\text{g}/\text{m}^3$ ), with a corresponding nitrate mole fraction of about 0.5 (relative to the sum of nitrate and sulfate) for the region of Germany, i.e. 50°N and 6°E (zonal cross-section) in summer (August, monthly mean) (Figure 5.4b). Note that we have omitted the nitric acid uptake on aerosol for this model run, so that the only possibility to form nitrate is the neutralization by ammonia. Because insufficient ammonia is available in summer in Europe, due to a maximum abundance of sulfate concentrations, the only possibility to allow for ammonium nitrate in the free troposphere is by long-range transport from Asia, i.e. over North India around the Himalaya. There, ammonia is emitted at relatively high altitudes. Even more important may be the fact that the surface emitted trace gases such as ammonia, are efficiently transported to the free troposphere by convection associated with the Indian monsoon (and particularly the dry north-westerlies). This is illustrated by the zonal cross-section of ammonia, nitric acid, and aerosol nitrate at 80°E in Figure 5.4c, and the global distribution of aerosol nitrate and ammonia at approx. 270 hPa in Figure 5.4d. It should be noted that, for the same reason, trace gases originating from the surface are transported upwards to the free troposphere at other locations under similar conditions. However, the strongest effect will certainly prevail at the Himalayas, not only because it is the world highest mountains, also because of the huge air pollution in Asia and the extreme atmospheric conditions, especially during the monsoon season. Note that in other regions upward air movements are often associated with wet scavenging processes, which rather remove the aerosol than enhance the upward transport in to the free troposphere. Only the unique geographical and atmospheric conditions around the Himalaya seems to favor this situation.

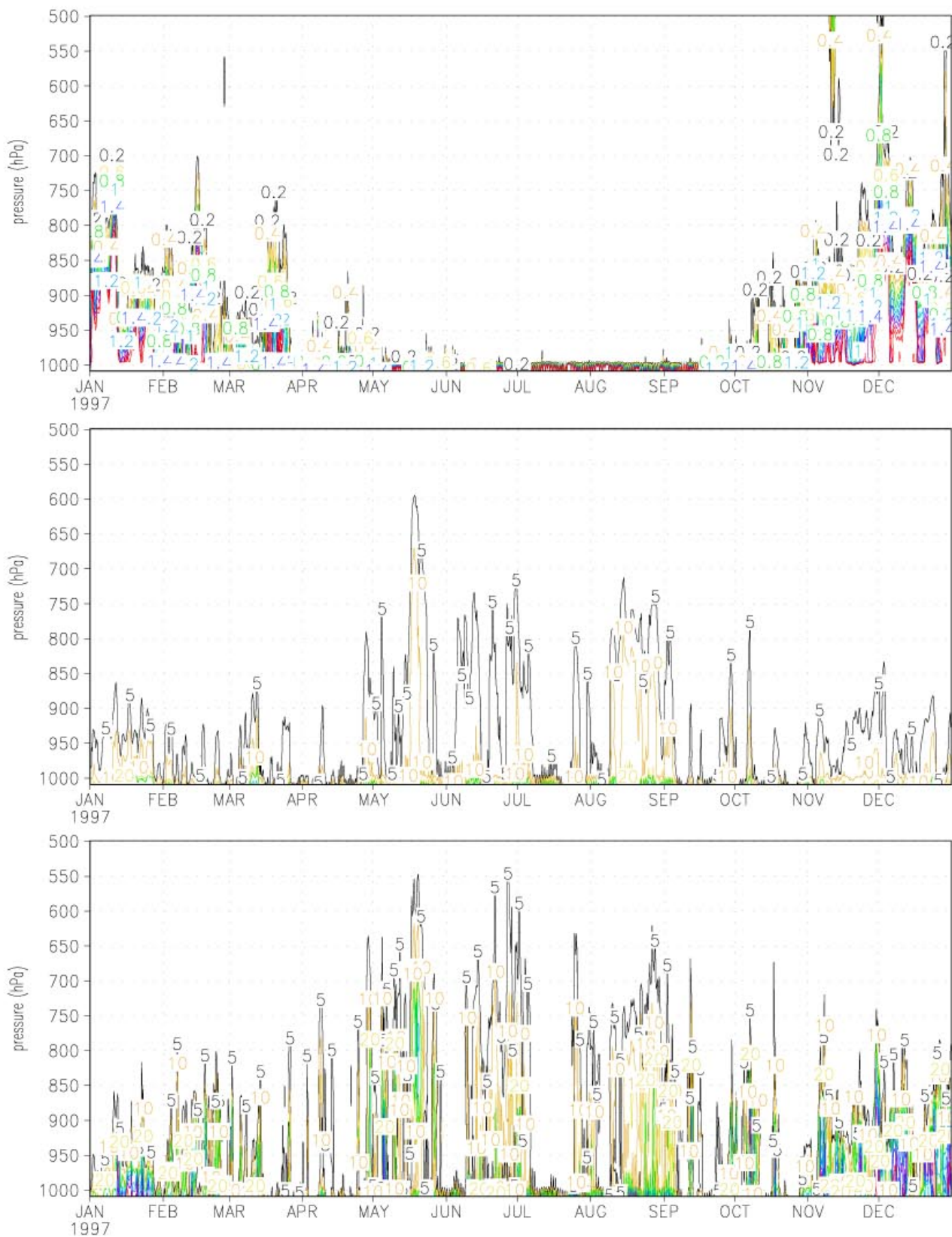


**Figure 5.4a.** Vertical-time distribution for 1997 (Hovmöller representation) of the mass ratio of nitrate and sulfate (top), the total dry particulate matter (middle), and the associated aerosol water mass (bottom) for a single gridbox in Germany (50°N and 10°E).



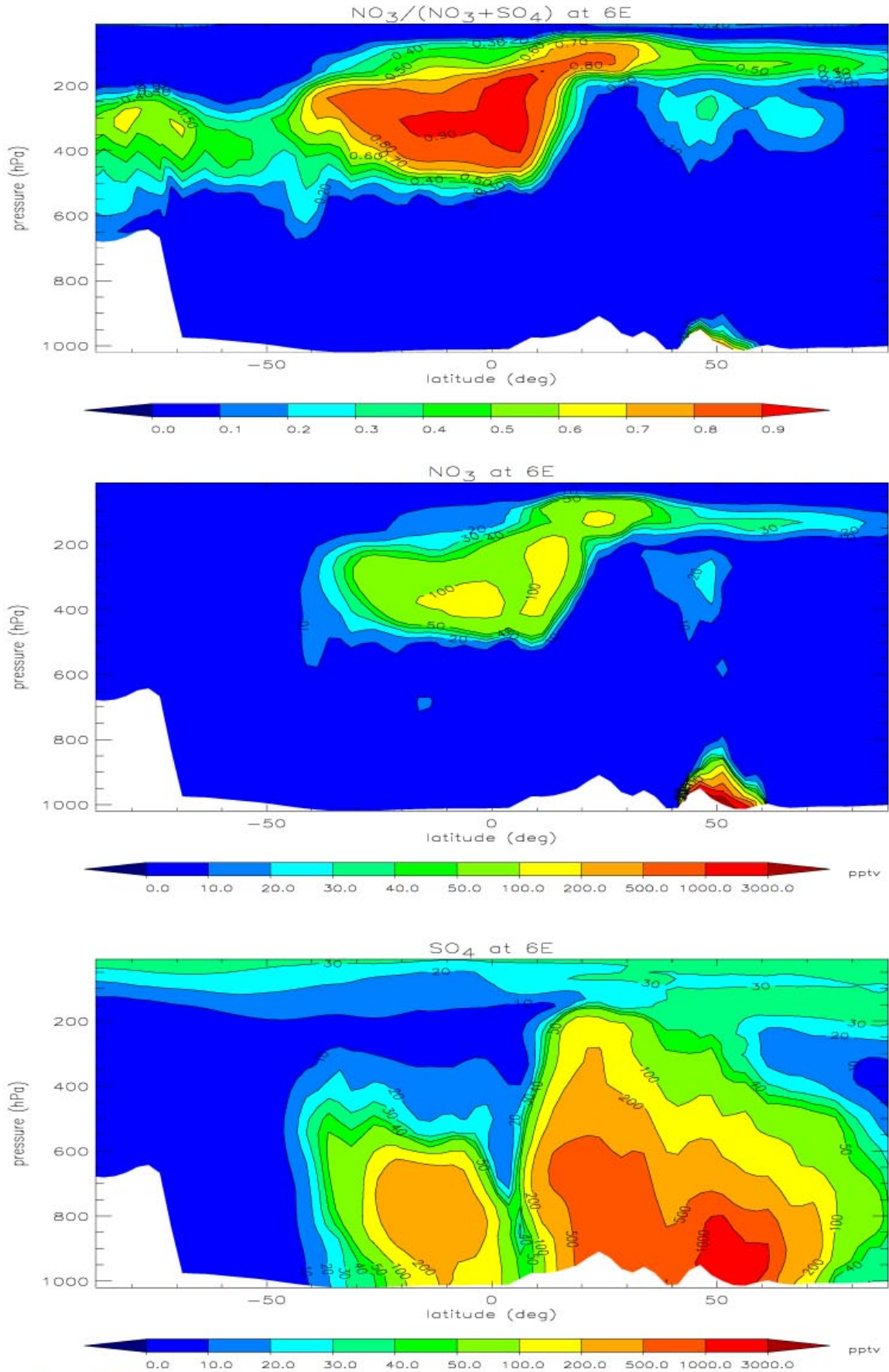


**Figure 5.4b.** Zonal cross-section 6°E for August 1997 (monthly mean). Nitrate mole fraction (top), aerosol nitrate (middle), and aerosol sulfate (bottom). White colors denote orography.

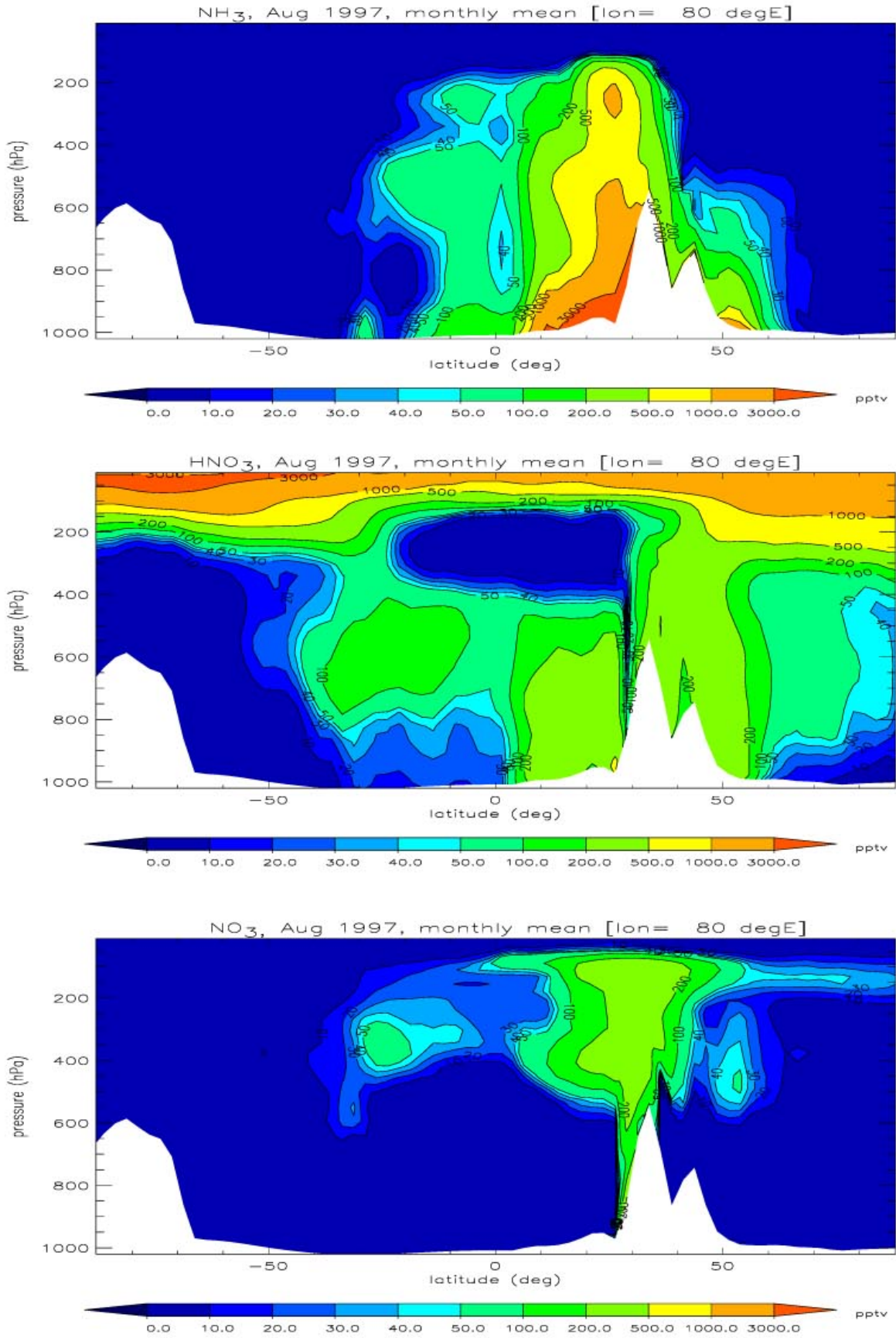
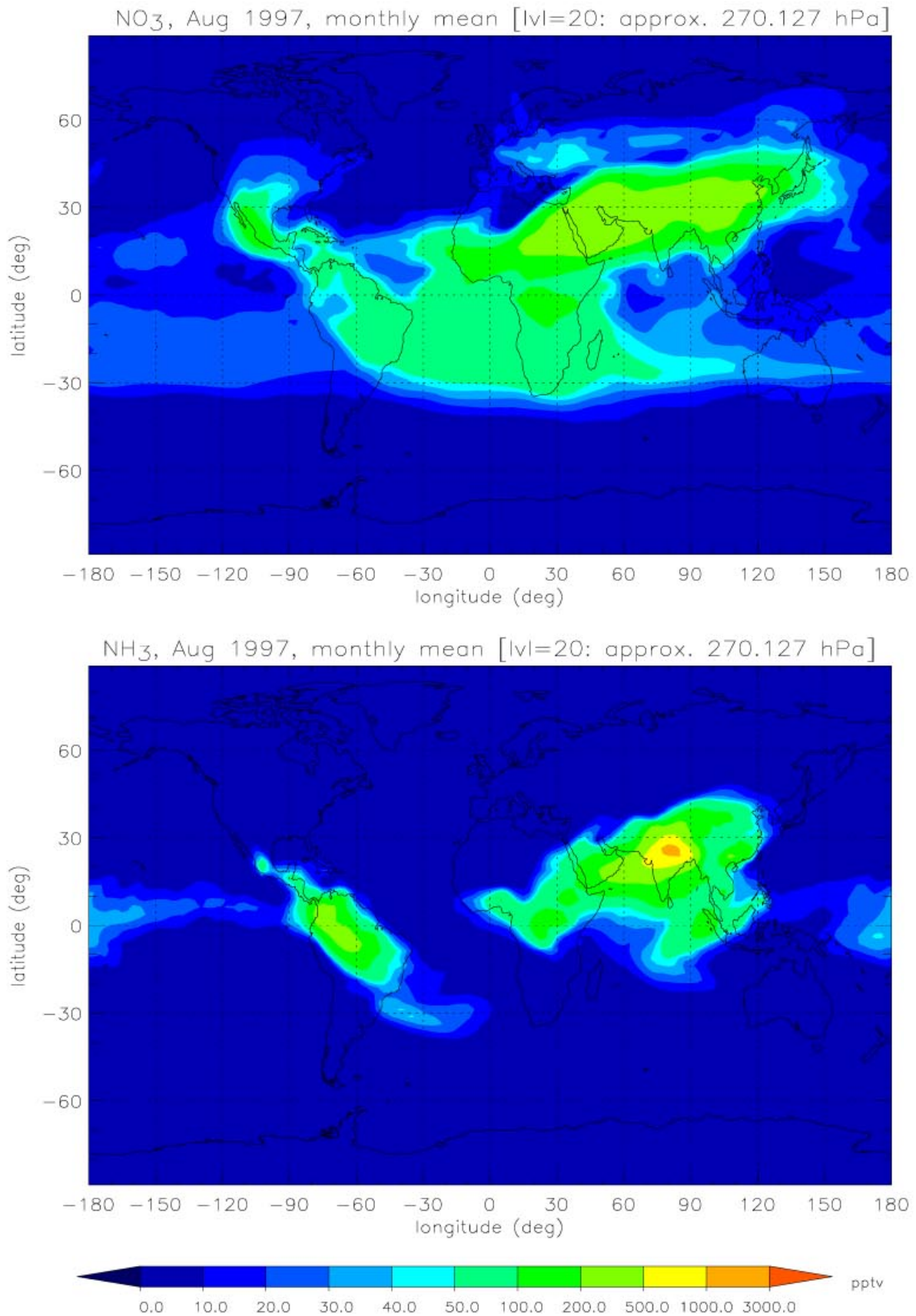


Figure 5.4c. Zonal cross-section at 80°E for August 1997 (monthly mean). Ammonia (top), nitric acid (middle), and aerosol nitrate (bottom). White colors denote orography.



**Figure 5.4d.** Global distribution of aerosol nitrate (top) and ammonia (bottom) at approx. 270 hPa for August 1997 (monthly mean).

According to [Figure 5.4c](#), ammonium nitrate can form above 500 hPa at 30°S-60°N. Associated with the localized ammonium nitrate formation is a nitric acid depletion around 300-200 hPa, and 30°S-30°N. Nitric acid has partitioned completely into the aerosol phase, indicating that the ammonium nitrate formation is limited rather by nitric acid than by ammonia. Subsequently, ammonium nitrate is widely distributed at approx. 270 hPa as shown in [Figure 5.4d](#). Ammonia, on the other hand, is less widely distributed at the same model level, as a result of the shorter atmospheric residence time, which is of the order of 1-2 days compared to approx. 1 week for ammonium nitrate. Therefore, the ammonium nitrate concentrations extend toward Europe so that even at 50°N and 6°E comparable nitrate and sulfate concentrations occur, of the order of 50-100 pptv ([Figure 5.4b](#)). According to the assumptions made, ammonium nitrate is also vertically concentrated at regions where the sulfate concentrations are low, i.e. approximately between 400 and 200 hPa in the southern hemisphere over Africa. Conversely, sulfate is in summer widely distributed over the Northern Hemisphere, not only at the surface layer, but also at higher altitudes.

### 5.2.5 Feedback on Chemistry

The previous sections have shown that nitric acid, under cold conditions with excess ammonia present, partitions completely into the aerosol phase, so that regionally nitrate aerosol can contribute significant to the total aerosol mass. Furthermore, long-range transport in our model simulations causes the global re-distribution of ammonium nitrate, especially at higher altitudes at 200 hPa. Thus, to estimate the feedback on the air-chemistry associated with the gas/aerosol partitioning, we compare in this section the model results of the aerosol run (ar) with those of a reference simulation (base run=br) without gas/aerosol partitioning only accounting for sulfate aerosols. The differences are expressed in percent, i.e.  $c (br-ar)/br*100$ .

[Figure 5.5a](#) shows the global changes [%] for vertically integrated ammonia (burden), for nitric acid (burden), and for ozone (burden) in January 1997 (monthly mean). Accordingly, [Figure 5.5b](#) shows the changes in monthly mean zonal averages, July 1997. Positive differences indicate higher concentrations in the base run, and indicate for instance, for the global ammonia distribution, the ammonia partitioning in percent during the aerosol run. Most significant are the changes for ammonia with values exceeding 80% at mid to high latitudes, and over the subtropical Atlantic. This indicates that in these locations ammonia partitions almost completely into the aerosol phase if gas/aerosol partitioning is considered. Changes are much smaller for HNO<sub>3</sub>, mainly because of the overall much higher nitric acid concentration in the stratosphere (vertical integral).

Changes in ammonia include changes in the horizontal and vertical distribution, partly caused by the global re-distribution as discussed previously. Such changes might be caused by the fact that particulate ammonium (aerosol) is less efficiently removed from the atmosphere compared to gaseous ammonia. The longer residence time of ammonium allows for long-range transport, so that ammonium nitrate can even act as a source of ammonia if the atmospheric conditions favor

evaporation, i.e. if ammonium nitrate is thermodynamically not stable. For instance, ammonium nitrate that has been formed during night or at colder locations might be destroyed after transport during day, and therefore adds to ammonia remote from the original ammonia source.

Furthermore, the higher ammonium concentration increases the aerosol and cloud pH, by which the latter can enhance oxidation processes, which may be relevant to atmospheric chemistry. For instance, the oxidation of sulfur dioxide is enhanced if the cloud pH increases due to additional ammonium that results from the gas/aerosol partitioning. Note that we have accounted by the aerosol run for various ammonium sulfate salts as previously discussed (e.g. Chapter 3.8), in contrast to the base run where we have assumed all sulfate to be neutralized in form of ammonium bisulfate only. This can lead to higher sulfate concentrations compared to the case where the gas/aerosol partitioning is omitted. Additionally, an increase in the aerosol surface can reduce the  $N_2O_5$  formation, which can lead to  $O_3$  destruction involving the  $NO_3$  radical; most likely because we assume that aerosol nitrate does not photolyzes. Therefore, changes in ozone are positive, although overall small, which indicates a small ozone reduction if gas/aerosol partitioning is considered. Note that the area of largest changes corresponds to the previously discussed horizontal distribution of ammonium nitrate, i.e. at 270 hPa (see [Figure 5.4d](#)), also indicated by the zonal distribution shown in [Figure 5.5b](#).

Base Run vs Aerosol Run, January 1997

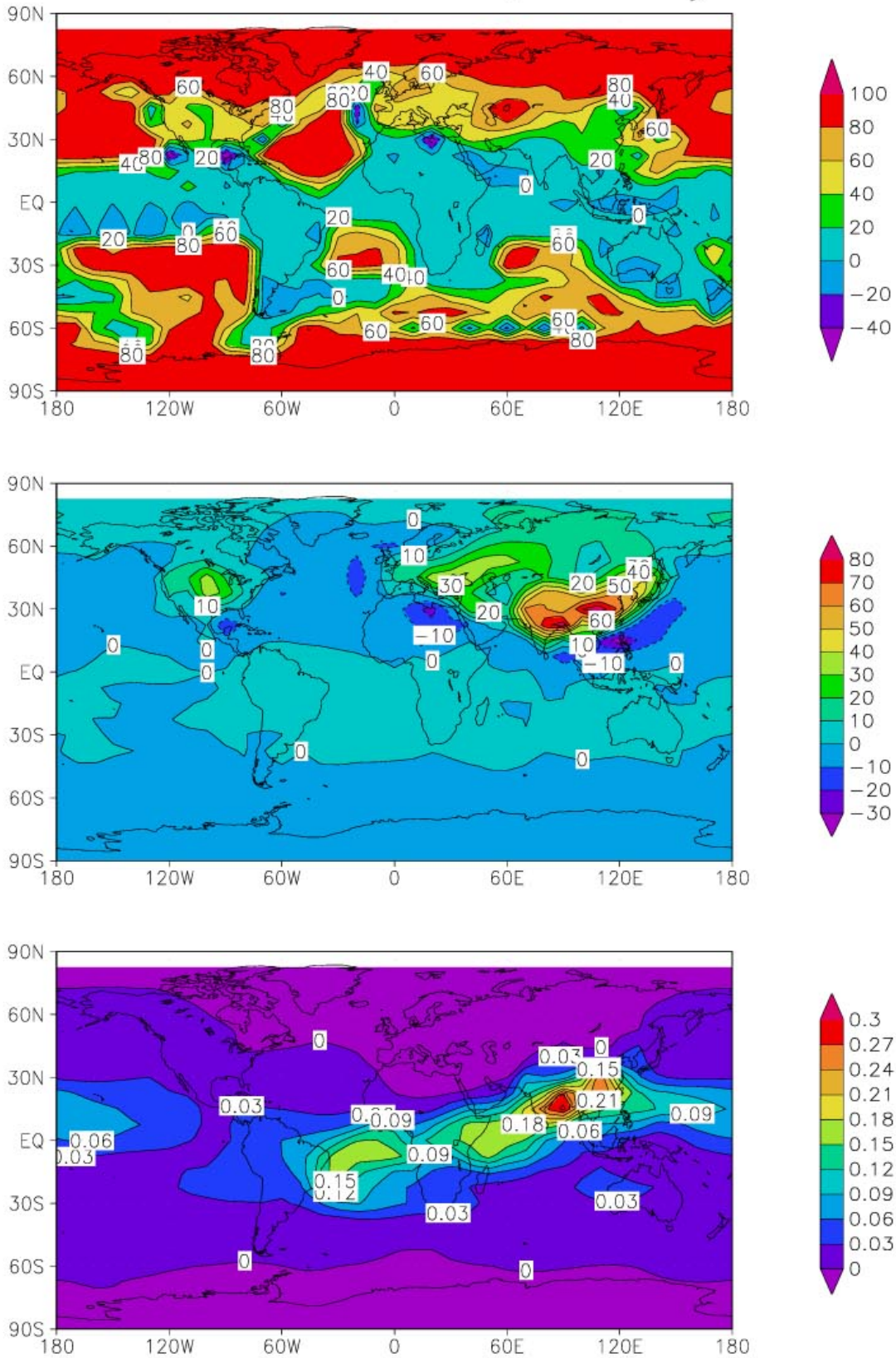


**Figure 5.5a.** Global changes in [%] for vertically integrated (burden) ammonia (top), nitric acid (middle), and ozone (bottom) for January 1997 (monthly mean).

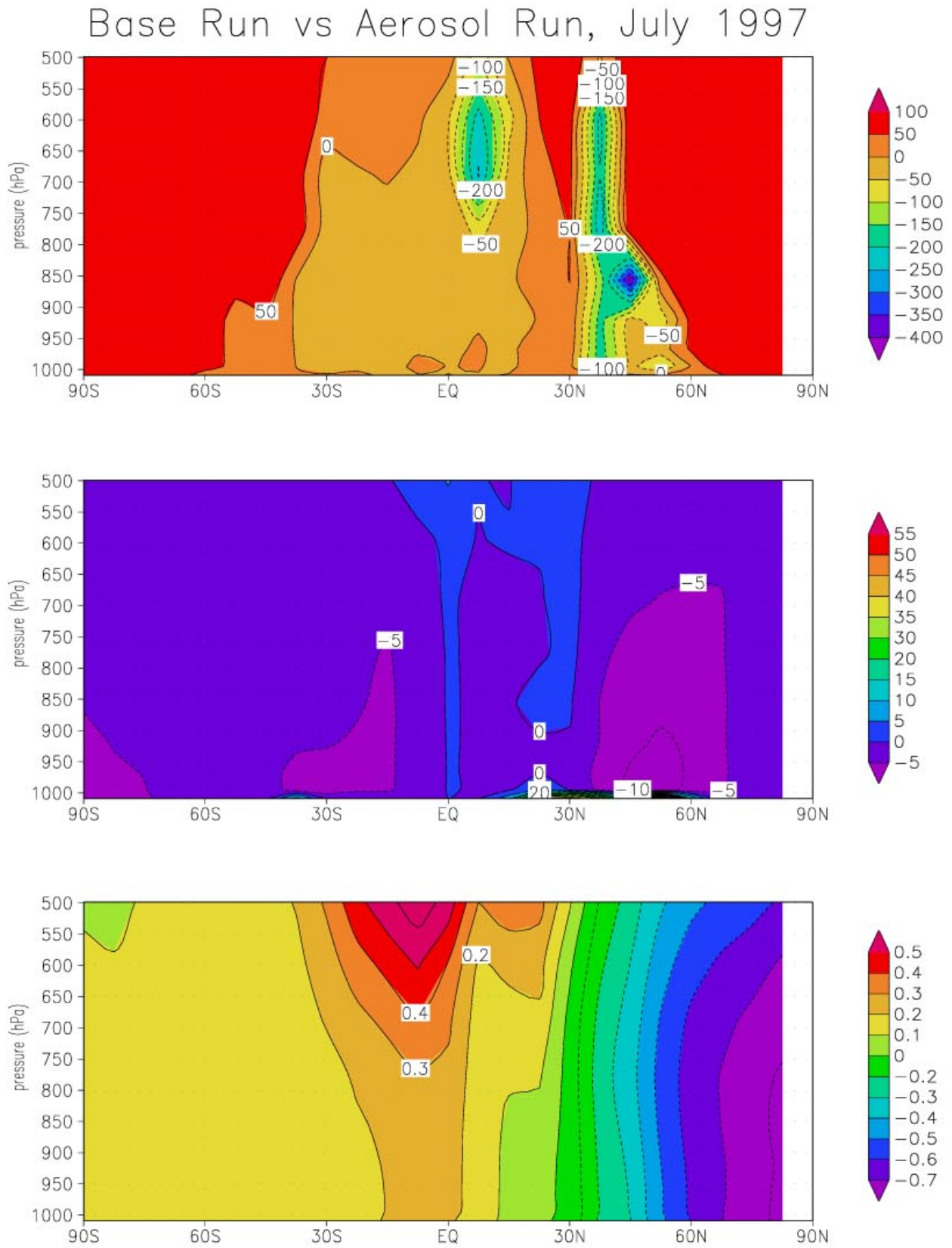


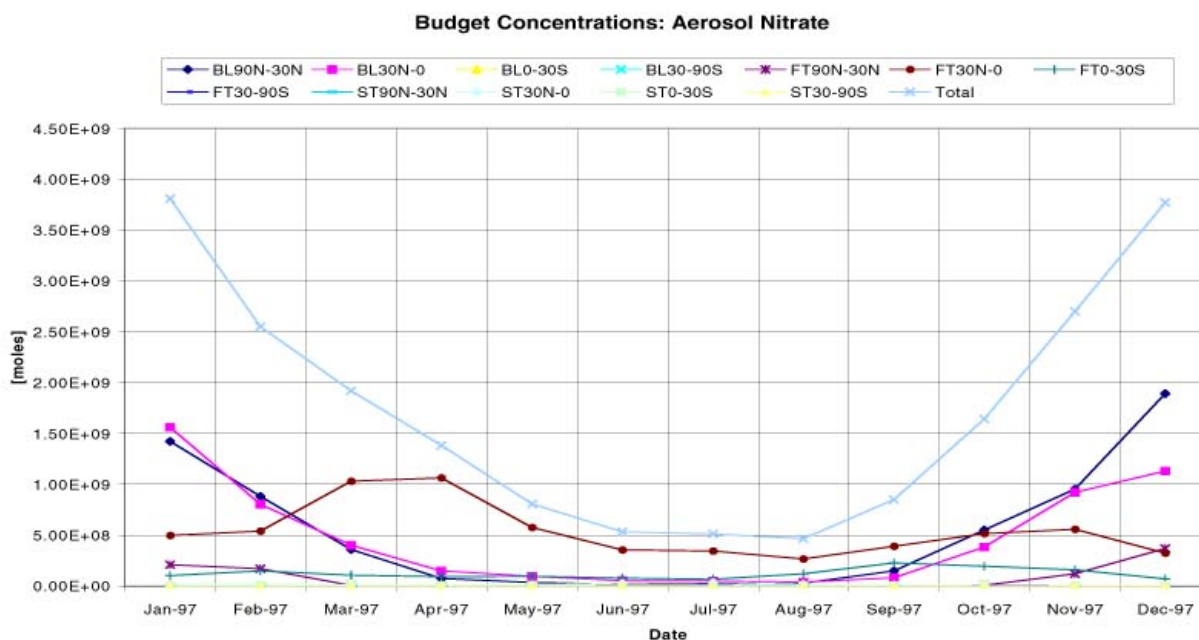
**Figure 5.5b.** Global changes in [%] for the zonal averages (up to 500 hPa) of ammonia (top), nitric acid (middle), and ozone (bottom) for July 1997 (monthly mean).

### 5.3 Aerosol Budgets

In this section, we discuss the global budgets from our model calculations. First, we focus on the annual variability of nitrate and sulfate aerosol compounds for which we have summarized various budget values in the planetary boundary layer (BL90N-30N, BL30N-0, BL0-30S, BL30-90S), the free troposphere (FT90N-30N, FT30N-0, FT0-30S, FT30-90S, FT90N-30N), and the stratosphere (ST30N-0, ST0-30S, ST30-90S), as well as the total burden. Second, we discuss the feedback of the aerosol calculations on chemistry. Note that the budgets are given in  $10^9$  moles, which must be multiplied by the mol mass of sulfate and nitrate aerosol, i.e. 96 and 62 [g/mol], respectively.

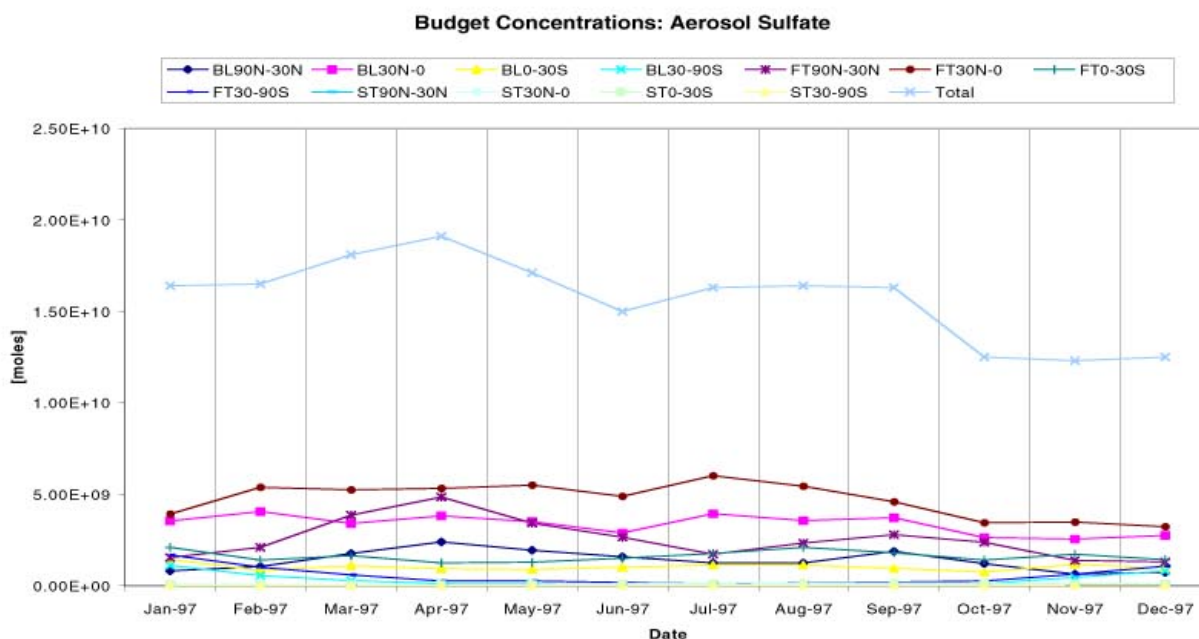
#### 5.3.1 Annual Cycle

Figure 5.6a shows the aerosol nitrate budget for 1997, and Figure 5.6b the same for sulfate. The comparison between both figures illustrates that nitrate aerosol exhibits a strong seasonal cycle, even considering the global amount, while sulfate does not show a pronounced seasonal cycle because large amounts of sulfate reside in the free troposphere where less variability occurs. Although the sulfate budget values are more than an order of magnitude higher than the nitrate ones, the latter adds significantly to the aerosol mass for northern hemispheric wintertime, i.e. from October until April/May. While in this season, the total mass is basically explained by the northern hemispheric boundary layer, the free troposphere (FT30N-0) explains most of the total budget from March until November. The same is true for sulfate. This indicates that long-range transport is quite important for aerosol compounds (as discussed previously).



**Figure 5.6a.** Budgets concentrations of aerosol nitrate for the year 1997 representing the planetary boundary layer (BL90N-30N, BL30N-0, BL0-30S, BL30-90S), the free troposphere (FT90N-30N, FT30N-0, FT0-30S, FT30-90S, FT90N-30N), and the stratosphere (ST30N-0, ST0-30S, ST30-90S), and the total burden.





**Figure 5.6b.** Budgets concentrations of aerosol sulfate for the year 1997 representing the planetary boundary layer (BL90N-30N, BL30N-0, BL0-30S, BL30-90S), the free troposphere (FT90N-30N, FT30N-0, FT0-30S, FT30-90S, FT90N-30N), and the stratosphere (ST30N-0, ST0-30S, ST30-90S), and the total burden.

### 5.3.2 Feedback on Chemistry

To estimate the influence of the gas/aerosol partitioning on the global atmosphere chemistry calculations, we summarize the changes [%] in the budget concentrations for the aerosol run compared to the base run. Considering gas/aerosol partitioning leads to the following changes of the budget concentrations for January 1997, PBL, 90N-30N: -49% for  $\text{NH}_3(\text{g})$ , +33% for  $\text{NH}_4(\text{a})$ , +11.7% for  $\text{SO}_4^{2-}(\text{a})$ , -22% for  $\text{HNO}_3(\text{g})$ , -4.3% for  $\text{SO}_2(\text{g})$ , -5% for  $\text{N}_2\text{O}_5(\text{g})$ , <1% for  $\text{O}_3$ ,  $\text{NO}_x(\text{g})$ ,  $\text{H}_2\text{O}_2(\text{g})$ ,  $\text{NO}_3^-(\text{g})$ . Note that changes are smaller in July 1997.

The relatively large numbers for the aerosol budgets indicate that gas/aerosol partitioning can significantly affect atmospheric chemistry calculations regionally. For instance, up to approx. 50% of the ammonia occurs on average in the aerosol phase in the northern hemispheric BL (90N-30N). This leads, due to differences in the turnover time, to an (non-linear) increase of particulate ammonium by approx. 33%. Subsequently, the sulfate concentration is affected, which increases by 11.7% due to an increase of the aerosol pH, which leads to an enhanced oxidation of  $\text{SO}_2$ . Therefore, the  $\text{SO}_2$  concentrations decrease by approx. 4.3%. Accordingly,  $\text{N}_2\text{O}_5$  decreases by approx. 5%, while changes for other gases are less than 1%. Nevertheless, all values differ on regional scales, where (over Europe in winter), for instance, nitric acid partitions completely into the aerosol phase, while on average  $\text{HNO}_3$  is only reduced by approx. 22% (only because of the formation of ammonium nitrate). It should also be noted that these numbers partly depend on the assumptions made in our gas/aerosol modeling, as well as on the representation of the model physics of the atmospheric chemistry model, e.g. the boundary layer and the model resolution. In the next chapter, we will therefore present gas/aerosol partitioning sensitivities.

## Chapter VI: Gas/Aerosol Partitioning Sensitivities

In this chapter we compare the differences that are associated by using different equilibrium models (discussed in Chapter IV) with the differences inherent from the assumptions made about the aerosol state and the representation of the model physics. First we quantify the differences for total aerosol radiative forcing, according to Chapter 4.3. We investigate the dependence of aerosol forcing on modeling assumptions, considering (R1) sulfate only calculations, (R2) equilibrium calculations based on gas/liquid/solid aerosol partitioning, (R3) those based on metastable aerosols, and (R4) those which include the hysteresis effect of aerosols (see Chapter IV for the definitions). Subsequently we quantify the differences in the aerosol concentrations associated with various model resolutions and the old and new boundary layer mixing scheme (see Chapter V).

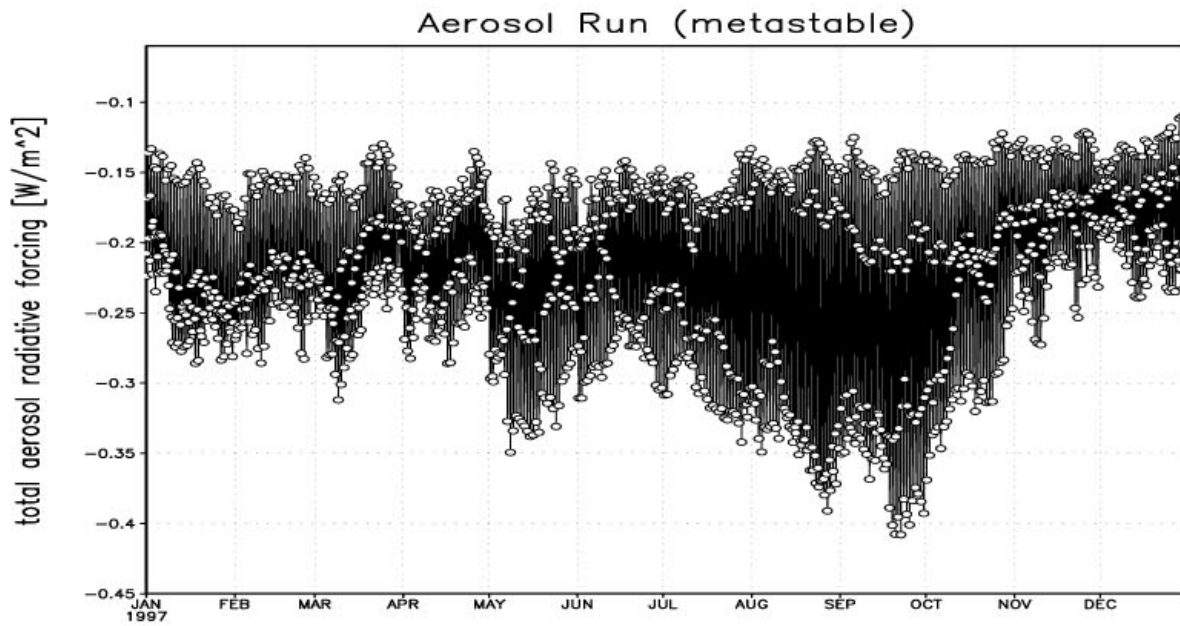
### 6.1 Dependence on Modeling Assumptions

To investigate the relevance of gas/aerosol partitioning for global calculations, we quantify the difference between the aerosol run (assuming R3, i.e. metastable aerosols) and the reference run (R1) where gas/aerosol equilibrium was neglected. The latter represents the sulfate-only-calculations, such as those represented in previous aerosol calculations in climate studies (e.g. IPCC, 1996). Although gas/aerosol partitioning has been neglected, our reference run is to some extent more accurate than previous studies, since we have explicitly calculated the aerosol water associated with sulfate aerosols. The differences between R1 and R3 are, therefore, not that large as they would have been according to these previous studies that apply a constant factor for the aerosol water associated with sulfate aerosols.

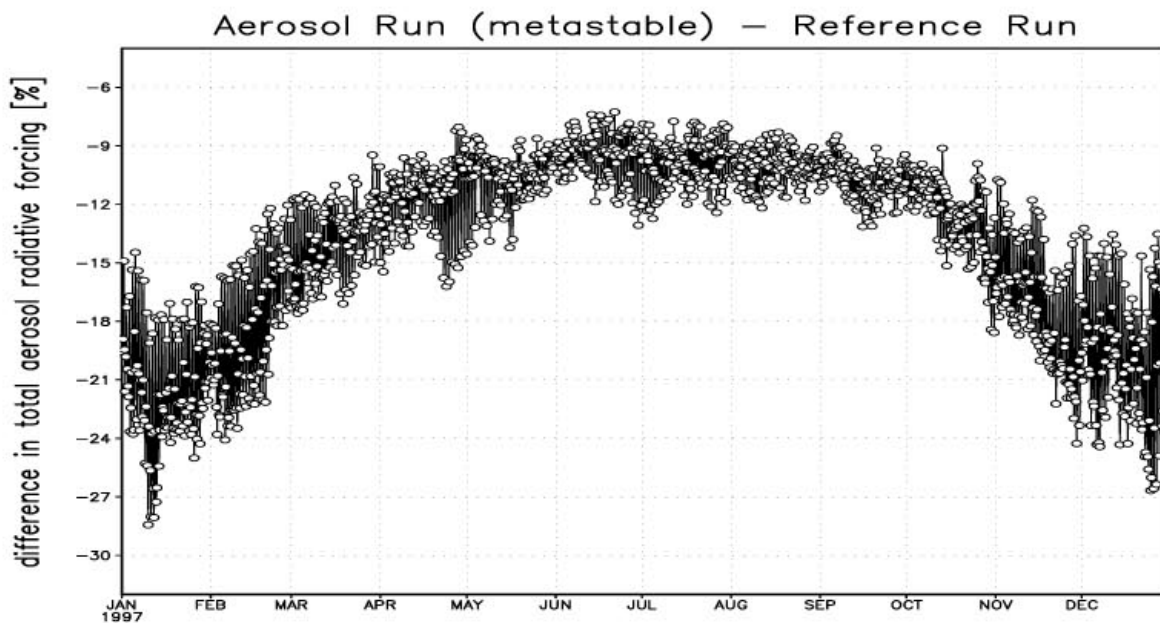
#### 6.1.1 Aerosol Run (metastable) vs. non-Aerosol (Reference) Run (Sulfate-only)

Figure 6.1a shows the global average aerosol radiative forcing for the year 1997 by the column aerosol as calculated with EQSAM (assuming metastable aerosols). Figure 6.1b shows the relative difference [%] for the aerosol run (R3) and the reference run (R1). The difference is largest in the northern winter season (October-April), where the total aerosol radiative forcing of the reference run is about 25% less compared to the aerosol calculations. Thus, neglecting the gas/aerosol partitioning leads to a considerable underestimation of the total aerosol radiative forcing, even on a global scale. The difference is largest in the northern winter since aerosol nitrate adds an equal amount in aerosol mass compared to sulfate. In summer, much less nitric acids partitions into the aerosol phase because ammonium nitrate is less stable at higher temperatures (because of the temperature dependent ammonium nitrate equilibrium constant), and because of the higher sulfate concentrations (mainly because of the enhanced photochemical oxidation of SO<sub>2</sub>).

However, in our simulations we did not consider other aerosol species such as sea salt or mineral dust. Thus, in regions with substantial sea salt or dust loadings the actual forcing and the associated seasonally might be quite different, although in other regions the considered ammonium/sulfate/nitrate/water-system may already explain a large fraction of the total aerosol mass. Consequently, we do not focus on the absolute radiative forcing, and only use the forcing as an optimal parameter to estimate differences, in accord with Chapter 4.3.



**Figure 6.1a.** Total column aerosol radiative forcing [ $\text{W}/\text{m}^2$ ] (global average) for 1997 as calculated with TM3 / EQSAM (metastable aerosols); R3.



**Figure 6.1b.** Difference between the aerosol calculations with TM3 / EQSAM (metastable aerosols) and the so-called sulfate-only calculations with TM3 for the total column aerosol radiative forcing [%] for 1997 (global); R3-R1.

### 6.1.2 Aerosol Run: metastable vs. solids

In the previous section we have assumed wet aerosols (metastable) which remain in the aqueous phase, although they might be solids if the relative humidity is sufficiently low. To quantify the relative differences in the total direct aerosol radiative forcing associated by explicitly calculating gas/liquid/solid equilibrium partitioning as previously discussed (Chapter IV), we have plotted in

Figure 6.2 the corresponding difference (R3-R2). Because of the high fraction of aerosol nitrate, differences are largest in the northern winter season, i.e. in the range of 5% lower (forcing globally integrated) if full equilibrium calculations are considered. Although this global value is not high, the effect can locally be considerably stronger, as the results of Chapter IV indicate (e.g. Figure 4.5b, comparing upper left and upper right panels).

There are many uncertainties associated with the calculation of solids. For instance, deliquescence relative humidities have only been investigated for single-salt compounds and certain mixed-salts as discussed in Chapter 2.5. Thus, the deliquescence behavior of various aerosol mixtures present in the atmosphere is unknown. Similar uncertainties are associated with the assumptions made on the aerosol shape, since aerosol particles are mostly modeled as spherical droplets, which most likely is a wrong assumption for crystalline solids, e.g. affecting aerosol optical properties.

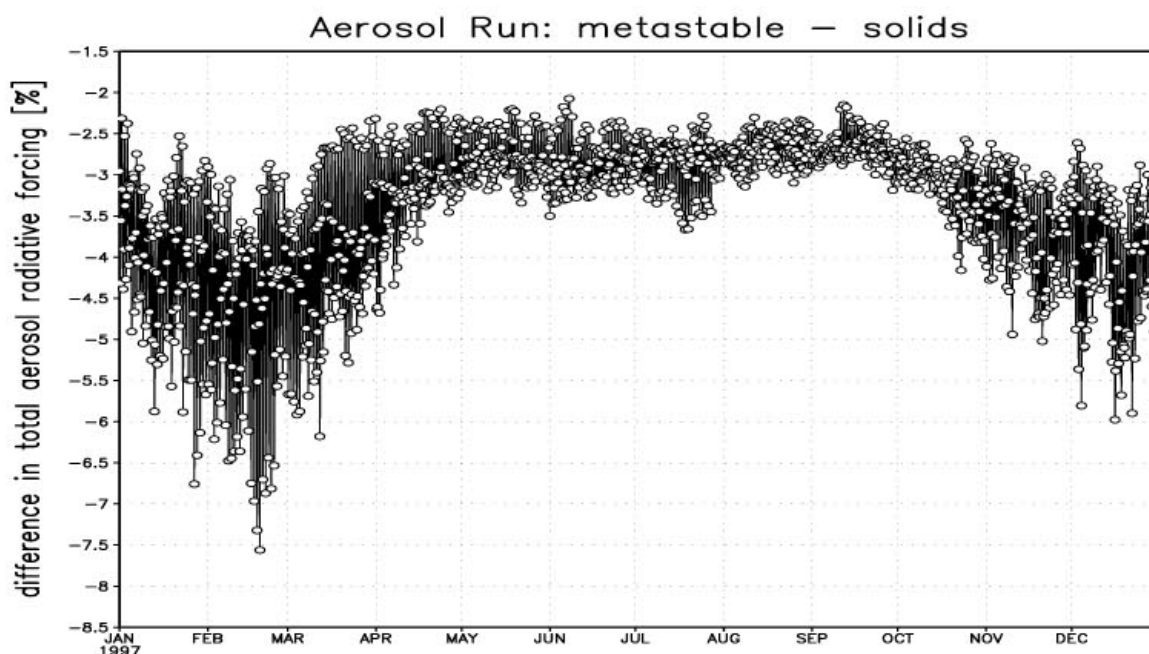


**Figure 6.2.** Difference between the aerosol calculations with TM3 / EQSAM assuming metastable aerosols and gas/liquid/solid equilibrium partitioning for the total column aerosol radiative forcing [%] for 1997 (global); R3-R2.

### 6.1.3 Aerosol Run: metastable vs. hysteresis

We have estimated in the previous section the differences between aerosol calculations including and excluding solids. For the latter we have simply assumed supersaturated aerosol compounds, which remain in the aqueous phase regardless of the actual relative humidity. Since on average more water is associated with the particles, this yields a somewhat larger aerosol radiative forcing. In reality in the atmosphere aerosol particles exhibit hysteresis, which is known to occur for many particles as noted in Chapters I, IV. Hysteresis means that at decreasing RH, the aqueous salt solution exists in a supersaturated state until it crystallizes, which is often far below the

deliquescence relative humidity. At increasing RH dry particles remain solid until they deliquesce at higher RH (the RHD) (Charlson et al., 1978; Tang, 1980). For instance, the crystallization RH of  $(\text{NH}_4)_2\text{SO}_4$  is about 39%, that of  $\text{NH}_4\text{HSO}_4$  is about 2% (Tang and Munkelwitz, 1994), and of  $\text{NH}_4\text{NO}_3$  about 10% (ten Brink, 1996); the RHD is about 60% for  $\text{NH}_4\text{NO}_3$  and 80% for  $(\text{NH}_4)_2\text{SO}_4$ , (see Chapter 2.5). Thus, the conditions in which solid aerosols can exist describe the lower branch of the hysteresis curve, while metastable aerosols represent the upper branch (see Figure 4.3).

To investigate the hysteresis effect on the aerosol radiative forcing, we have plotted in Figure 6.3 the differences [%] relative to metastable aerosols (R3-R4)). For simplicity we have assumed that metastable aerosols remain in the aqueous phase regardless of the actual relative humidity, while we have accounted for the full gas/liquid/solid aerosol partitioning (based on mutual deliquescence relative humidities) for the lower branch of the hysteresis curve. To keep track of the history of the aerosol water, we have added a tracer that is assigned an arbitrary value of 2 if aerosol water is associated, and a value of 1 for the case of a dry aerosol particle. After one transport time step a new mixing state of dry and wet particles is obtained. Metastable aerosols were considered for cases where this history value was above 1.5, reflecting that aerosol associated water is, after transport, present in more than 50% of the grid box considered. For the other case, i.e. a value below 1.5, the gas/solid partitioning was considered, if, additionally, the actual RH was below the mutual deliquescence relative humidity. Although we realize that this diagnostic procedure is not formally correct (a Lagrangian rather than a Eulerian approach would be needed), it provides a good approximation of the hysteresis effect. Thus, consideration of hysteresis (R4) results in an estimate of the aerosol radiative forcing in-between that of metastable aerosols (R3), which gives the upper bound, and that of the previously shown solid aerosols, which gives the lower bound.

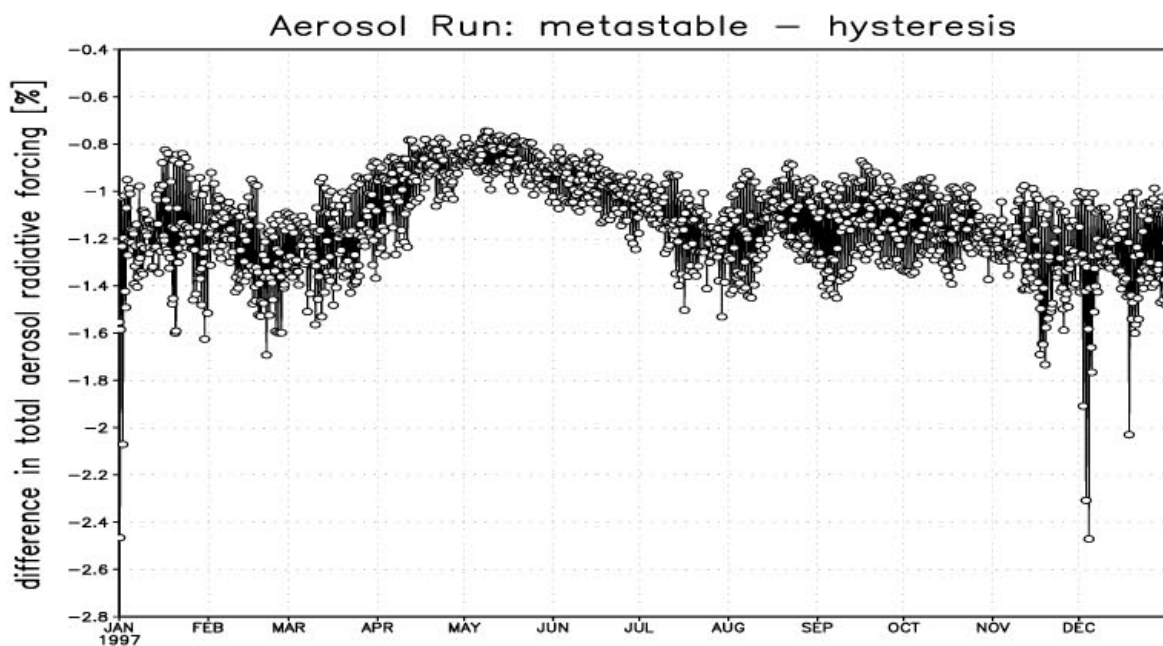


**Figure 6.3.** Difference between the aerosol calculations with TM3 / EQSAM assuming metastable aerosols and hysteresis (including the full gas/liquid/solid equilibrium partitioning) for the total column aerosol radiative forcing [%] for 1997 (global); R3-R4.

Indeed, the differences in Figure 6.3 (R3-R4) are only of the order of 1-2 percent, and smaller than the differences of between metastable aerosols and gas/liquid/solid equilibrium partitioning (R3-R2) shown in Figure 6.2. Negative values again indicate a weaker forcing associated with hysteresis aerosol compared to metastable aerosols. The lack of seasonal dependence indicates that hysteresis is not confined to the boundary layer. This indicates that hysteresis is important when aerosol particles are transported to dry regions, e.g. upward, since at higher altitudes the RH is low so that solid formation at thermodynamic equilibrium becomes important. However, the over-all effect on the forcing is globally rather small for the aerosol species considered.

These estimates provide indications of the relative importance of the uncertainty associated with the assumptions made on the aerosol state. Because the crystallization RH values are all much below the RH generally encountered in the planetary boundary layer, and because the RH frequently (e.g. diurnally) exceeds the deliquescence relative humidities (RHD) of tropospheric aerosols at night, it is most likely that it is sufficient for global modeling purposes to assume for humid regions, that aqueous salt solutions remain in a supersaturated (metastable) state during day, unless hysteresis is considered explicitly.

## 6.2 Dependence on the Model Version (TM3)

In this section we estimate the influence of the tracer transport model physics and resolution on the aerosol calculations. We compare for the aerosol sulfate and nitrate budget concentrations the effect of the model resolution and the representation of the boundary layer scheme, i.e. old vs. new; the latter scheme basically yields an enhanced but more realistic vertical mixing compared to the old one (see Chapter 5.1). Analogous to Chapter 5.3, we focus here on the planetary boundary layer (PBL) at 90N-30N, and on global budgets for August 1997. The differences, which are associated with the TM3 model, are additionally compared with those associated with the choice of the thermodynamical model (EQSAM or ISORROPIA), and the choice of the emission inventory used (EDGAR<sup>D</sup> or CORINAIR). They will be viewed in the context of the seasonal variability of the aerosol nitrate budget concentrations (August or December). The model resolutions of TM3 are: coarse grid (CG)  $\Leftrightarrow 10.00^\circ \times 7.50^\circ \times 19$ ; fine grid (FG)  $\Leftrightarrow 5.00^\circ \times 3.75^\circ \times 19$ ; very fine grid (VG)  $\Leftrightarrow 2.50^\circ \times 2.50^\circ \times 31$ ; (longitude by latitude by vertical levels).

### 6.2.1 Resolution and Boundary Layer

Table 6.1 summarizes approximated differences in aerosol nitrate budget concentrations [%], which is based on a more comprehensive comparison of aerosol and aerosol precursor gases budgets. For instance, the seasonal variation in the emission budgets of NO<sub>x</sub> and SO<sub>2</sub> (summer vs. winter) provides a large variation in the input data of the thermodynamic gas/aerosol routine (EQSAM). While differences between the EDGAR<sup>D</sup> and CORINAIR emission inventory are globally not large, because the CORINAIR inventory is limited to Europe. Deposition budgets, however, depend

---

EDGAR<sup>D</sup> denotes our extrapolation of the EDGAR emission inventory of 1990 to 1997 for SO<sub>2</sub>

strongly on the model resolution (not shown). For instance, nitrate and sulfate dry depositions strongly decrease with increasing model resolution, while the dry and wet depositions are significantly higher if the old boundary layer mixing scheme is used. Thus, enhanced vertical mixing associated with the new scheme leads to significantly less wet and dry deposition of aerosol nitrate and sulfate in the PBL (90N-30N), which is approximately of the order of the seasonal variability (not shown). Consequently, the same is true for the concentrations in the PBL. Globally, however, the aerosol nitrate concentrations increase significantly when the new boundary layer scheme is used (shown in Table 6.1), while sulfate concentrations decrease because of the enhanced removal of SO<sub>2</sub> which is also associated with stronger vertical mixing due to enhanced dry deposition (not shown). Comparing these variations, differences caused by the aerosol modules are small and only detectable for nitrate aerosol.

**Table 6.1. Approximated differences in aerosol nitrate budget concentrations [%].**

Total (global):	
+ 5	for CORINAIR vs. EDGAR <sup>D</sup> ,
+ 9	for EQSAM vs. ISORROPIA
+ 77	for new vs. old Boundary Layer Scheme
+ 33	for VG vs. CG
+ 32	for VG vs. FG
- 83	for August vs. December (FG)
PBL 90N-30N:	
- 4	for CORINAIR vs. EDGAR <sup>D</sup> ,
- 9	for EQSAM vs. ISORROPIA
- 210	for new vs. old Boundary Layer Scheme
+ 83	for VG vs. CG
+ 47	for VG vs. FG
- 4560	for August vs. December (FG)

In summary, differences in the aerosol nitrate concentrations are associated with:

- the seasonal cycle, especially in the PBL;
- the difference from change in boundary layer mixing schemes is of the same order as the differences associated with the seasonal cycle, mainly because dry removal of SO<sub>2</sub> is enhanced by stronger vertical mixing, which leads to less sulfate, and subsequently to more ammonium nitrate;
- model resolution; nitrate concentrations increase with the model resolution due to lower sulfate concentrations;
- the thermodynamical representation, which are of the same order as the differences associated with the use of different emission databases (EDGAR<sup>D</sup> or CORINAIR).

## Chapter VII: Comparison with Ground-based Measurements

In this chapter, we evaluate the aerosol calculations by comparing model results with various measurements at different sites in Europe. The results are obtained in close cooperation with Dr. Ad Jeuken, who developed and validated the sulfur cycle representation of TM3, essential for the gas/aerosol partitioning calculations.

To evaluate the predicted aerosol composition with ground-based measurements, and to estimate the influence of differences in the emission data bases on the aerosol concentrations, we compare in the following the aerosol sulfate and nitrate concentrations with measurements obtained at various EMEP sites in Europe. In addition, we use measurements performed at the Dutch Energy Research Center at Petten (53°N, 5°E) and at a few other measurement sites in the Netherlands. We focus on the period of August 1997, for which we have detailed data. To be able to represent variability on time scales of a day or less, these model simulations have been performed at the highest available resolution of TM3, which is 2.5° by 2.5° and 31 layers in the vertical. Model concentrations of  $\text{SO}_4^{2-}$ ,  $\text{NO}_3^-$ ,  $\text{NH}_4^+$ ,  $\text{NH}_3$ ,  $\text{SO}_2$ , and  $\text{HNO}_3$  are sampled every two hours at the locations of the measurement sites. This includes 6 sites in the Netherlands and an additional 200 sites from the EMEP network. It must be noted that not all sites measured all species over the entire period. Especially for ammonia and aerosol nitrate only few measurements are available. Following Jeuken (2000), we will compare two model simulations with measurements, namely one based on the EDGAR<sup>D</sup> emission inventory to which we refer as A4, and one based on the CORINAIR emission inventory (see Chapter 5.1) to which we refer as model experiment A5.

### 7.1 Sulfate/Nitrate at Petten (The Netherlands)

To compare simulated daily variability of sulfate and nitrate, we focus here on one site, i.e. Petten in the Netherlands, for which we have a relatively detailed set of measurements available, kindly provided by Dr. Harry ten Brink (ECN). In [Figure 7.1a,b](#), we compare instantaneous model values with measurements (left) and the average daily cycle (right) for August 1997; [Figure 7.1a](#) shows sulfate, and [Figure 7.1b](#) shows nitrate.

The day-to-day variability of sulfate and nitrate are rather well simulated. The correlation between both model runs and the observations are 0.78 (A4) and 0.71 (A5) for sulfate using the EDGAR<sup>D</sup> and the CORINAIR emission databases, respectively, and 0.41 (A4) and 0.42 (A5) for nitrate, respectively. Although both simulations, A4 and A5, underestimate the sulfate levels for Petten by approx. 25% and 50%, respectively, the episodic nature of elevated sulfate concentrations is well simulated by the model. While sulfate does not show a very pronounced diurnal cycle in the simulations and measurements ([Figure 7.1a](#), right panel), the simulated cycle of nitrate seems to be somewhat too strong at this location ([Figure 7.1b](#)).

---

EDGAR<sup>D</sup> denotes our extrapolation of the EDGAR emission inventory of 1990 to 1997 for  $\text{SO}_2$



The daytime concentrations appear to be more strongly underestimated (up to 50%) in the afternoon. This could reflect the influence of local sources, because this particular measurement site is at a rural location influenced by local agriculture, so that we may expect that this particular site is not always representative for the particular model grid. Our model resolution represents a scale of  $\approx 200$  km, which also includes part of the North Sea, hence diluting pollution from the Netherlands over a large grid box. However, it is also possible that coarse mode particles and in particular sea salt influence this site; Petten is located near the North Sea. Thus, local winds, and in particular the sea breeze, which is strongest in summer during afternoon, might transport coarse mode sea salt particles over land, so that nitrate formation might be enhanced; larger (pre-existing) particles generally favor condensation especially those including a solid core (see discussion in Chapter 2.8). Because alkaline particles are not yet considered in the aerosol module, we could also have underestimated the nitrate formation in these model runs for this reason.

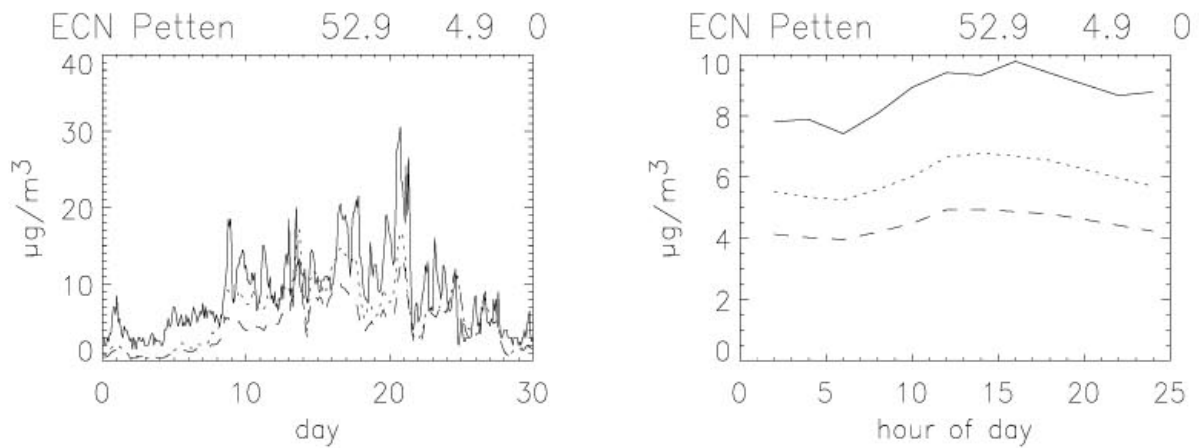


**Figure 7.1a.** Comparison of instantaneous model values and measurements of  $\text{SO}_4^{2-}$  for Petten (The Netherlands) and the average diurnal cycle for August 1997. The solid line represents the observations, the dotted line the model run A4, and the dashed line A5. Correlation is 0.78 and 0.71, the average difference is 2.2 and 4.2  $\mu\text{g}/\text{m}^3$  for A4 and A5 respectively. Times are in GMT.

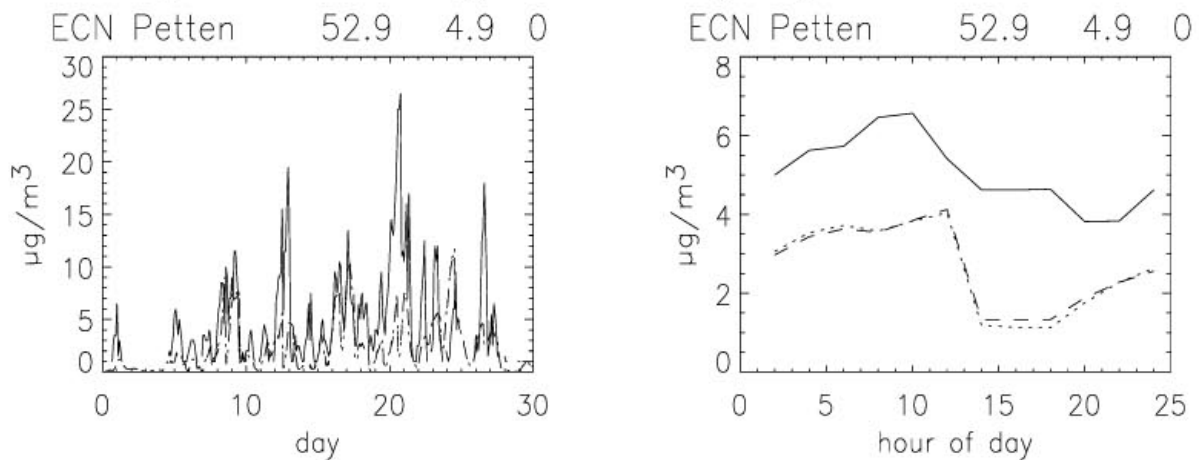


**Figure 7.1b.** Comparison of instantaneous model values and measurements of  $\text{NO}_3^-$  for Petten (The Netherlands) and the average diurnal cycle for August 1997. The solid line represents the observations, the dotted line the model run A4, and the dashed line A5. Correlation is 0.41 and 0.42, the average difference is 2.6 and 2.6  $\mu\text{g}/\text{m}^3$  for A4 and A5 respectively. Times are in GMT.

## 7.2 Ammonium/Sulfate/Nitrate at various EMEP stations

To further evaluate the aerosol predictions, we compare the aerosol concentrations of ammonium, sulfate, and nitrate with measurements at various European sites of the EMEP network. [Figure 7.2a](#) shows a selection of EMEP stations where  $\text{SO}_4^{2-}$  has been measured. Sites were chosen to illustrate different European regions. In general, episodic peak values are captured by both model simulations, although this is not always the case for the aerosol precursor gas of sulfate,  $\text{SO}_2$ , as shown by Jeuken (2000). He concluded that modeled  $\text{SO}_2$ , even using CORINAIR emissions, are in most cases too high and in particular in the region of the British Islands. However, at the eastern part of the European domain, e.g. in Russia, the agreement between model simulation A5 (using CORINAIR emissions) and the measurements is rather good for  $\text{SO}_2$  (not shown). Despite the overestimated  $\text{SO}_2$  concentrations at other sites, the agreement is much better for modeled and observed sulfate concentrations, although  $\text{SO}_4^{2-}$  is a reaction product of  $\text{SO}_2$ . Both model runs (A5 and A4) simulate the day-to-day variability as well as the absolute magnitude of the  $\text{SO}_4^{2-}$  concentrations rather well. Even at sites where  $\text{SO}_2$  was overestimated by a factor of 5 (e.g. Langenbrugge, Tange) sulfate is within 10 to 20% of the observations. The best agreement is clearly obtained with simulation A5. This indicates that the CORINAIR  $\text{SO}_2$  emission inventory for Europe, which is with 12 Tg S about half that of EDGAR<sup>D</sup>, yields more realistic results.

To quantify potential effects such as the decrease of the  $\text{SO}_2$  emissions due to the successful air pollution abatement in western Europe, and to provide information on model behavior, we compare both model runs (A4 and A5) with the observations. We have calculated the average difference (observation – model) and the correlation between both model runs and observation for all available EMEP measurements in [Table 7.1](#). The numbers also indicate that the agreement with observations improves when the CORINAIR emissions are used. For instance, on average model simulation A5 overestimates the measurements with  $2.7 \mu\text{g}/\text{m}^3$  and A4 with  $4.0 \mu\text{g}/\text{m}^3$ , both with a large variability between the sites. The correlation between model and measurements also slightly improves by using the CORINAIR emissions, but the value of 0.39 is still rather low.

Total ammonia (sum of ammonium and ammonia) is measured at about 24 sites; four of them are shown in [Figure 7.2b](#). Although  $\text{NH}_x$  is difficult to model due to the short lifetime and the spatially and temporally heterogeneous sources of ammonia, the agreement between model and observations is quite good (see also [Table 7.1](#)); mainly because the ammonium concentrations are strongly correlated with sulfate. Thus these results provide some confidence in the quality of the  $\text{NH}_3$  emission inventory.

**Table 7.1.** Correlations and average differences (observation-model) [ $\mu\text{g}/\text{m}^3$ ] based on daily averages for all available EMEP stations for August 1997.  $\text{tNO}_3$  denotes the sum of  $\text{NO}_3^-$  and  $\text{HNO}_3$ , and  $\text{NH}_x$  the sum of  $\text{NH}_3$  and  $\text{NH}_4^+$ .

	Correlation			Average difference(O-M)	
	N	A4	A5	A4	A5
$\text{SO}_2$	1868	0.36	0.39	$-4.2 \pm 5.4$	$-2.7 \pm 4.3$
$\text{SO}_4^{2-}$	2059	0.56	0.58	$-0.3 \pm 1.8$	$0.0 \pm 0.8$
$\text{NH}_x$	956	0.66	0.66	$-0.5 \pm 1.7$	$-0.40 \pm 1.7$
$\text{tNO}_3$	884	0.60	0.61	$-0.5 \pm 0.9$	$-0.5 \pm 0.9$
$\text{NO}_3^-$	401	0.66	0.66	$0.3 \pm 0.3$	$0.3 \pm 0.3$

According to our model simulations, approximately 50% of ammonia partitions on average into the aerosol phase over the European continent at surface level (Chapter 5.2). However, co-located ammonia and ammonium measurements are needed to identify the fraction of ammonia in  $\text{NH}_x$ , especially because of its importance for the pH of cloud water; aqueous phase reaction rates strongly depend on the pH and therefore on the  $\text{NH}_4^+$  concentrations, e.g. influencing the  $\text{SO}_2$  oxidation to  $\text{SO}_4^{2-}$ .

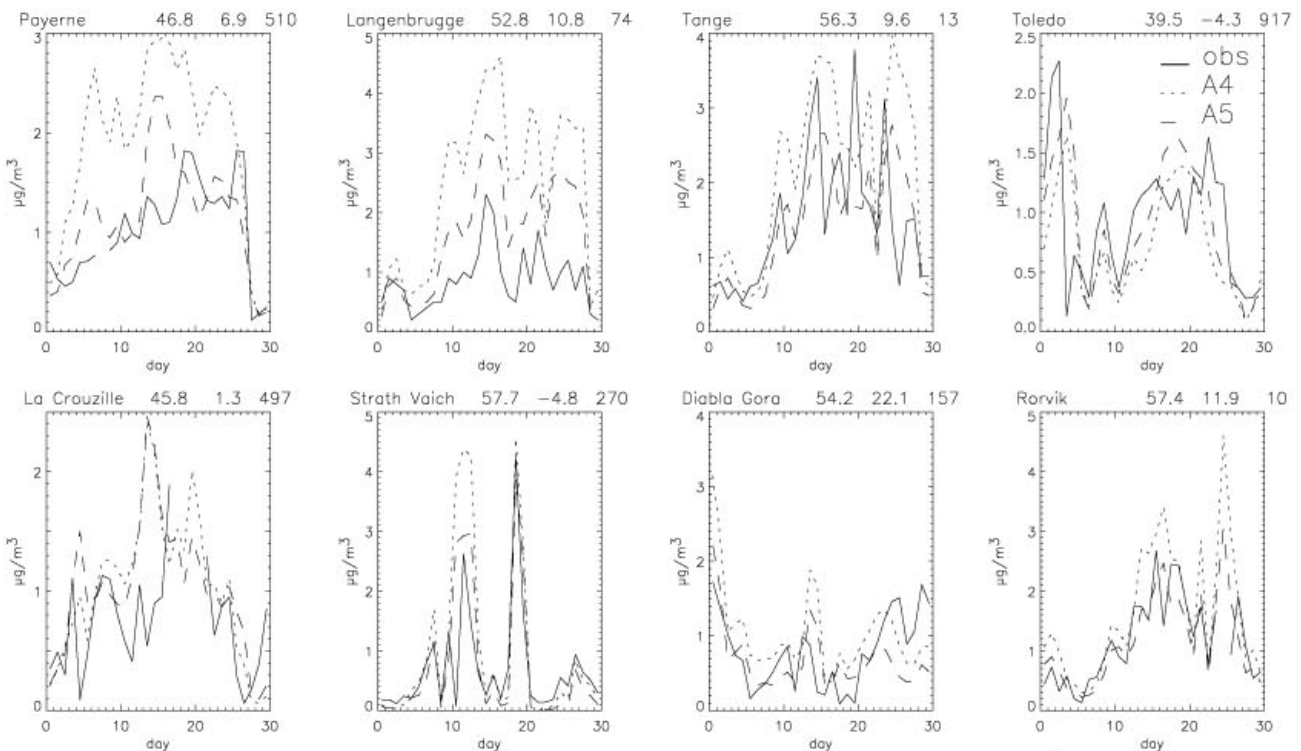


**Figure 7.2a.** Comparison of daily averaged model values and measurements of  $\text{SO}_4^{2-}$  for several EMEP sites (August 1997).

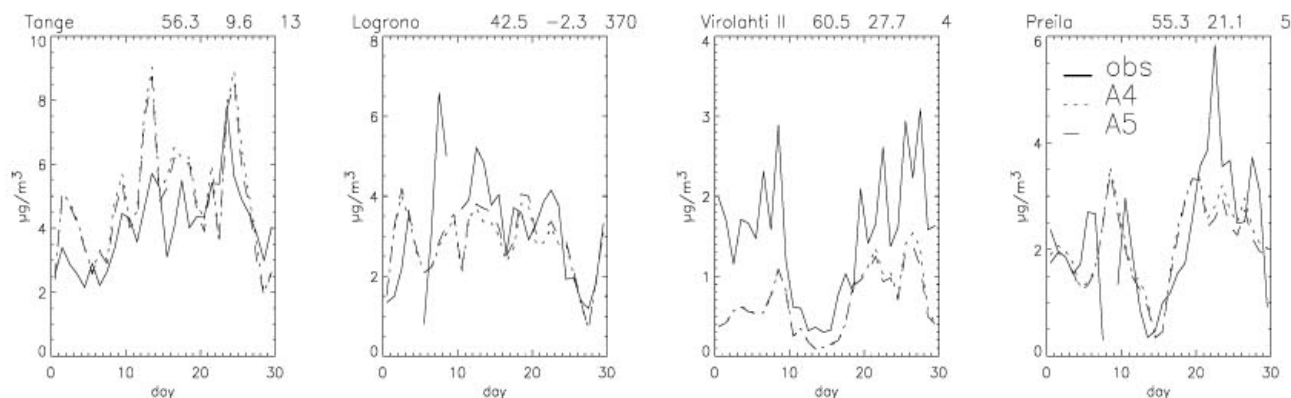


**Figure 7.2b.** Comparison of daily averaged model values and measurements of  $\text{NH}_4^+ + \text{NH}_3$  for several EMEP sites (August 1997).

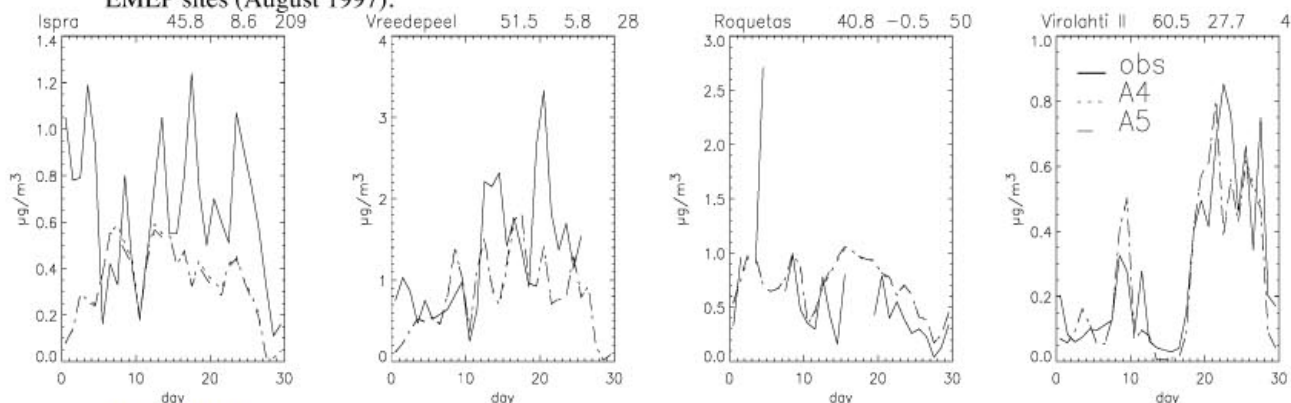


**Figure 7.2c.** Comparison of daily averaged model values and measurements of  $\text{NO}_3^-$  for the EMEP sites Ispra (Italy) and Vreedepeel (Netherlands), and of total nitrate ( $\text{HNO}_3 + \text{NO}_3^-$ ) for Roquetas (Spain) and Virolahti II (Finland).

In Chapter V we have seen that nitrate may constitute a large fraction of the TM3 aerosol concentration (nitrate + sulfate) over large parts of Europe at the surface. To compare our model predictions with observations at various EMEP sites, we show in Figure 7.2b results for particulate nitrate. It should be noted here that aerosol nitrate is difficult to measure, because it is (semi-) volatile. Only more recent and sophisticated sampling methods using thermodenuder (as used in Petten) account for the evaporation loss that is associated with conventional filter samplers. Similarly, as already noted, aerosol nitrate is relatively difficult to model since its formation strongly depends on humidity, temperature, and the concentrations of other aerosol species, in particular on sulfate and ammonia. For instance, if the ammonia concentrations do not exceed the sulfate concentrations, nitrate can not partition into the aerosol. Note that for these calculations, the nitrate formation was restricted to  $\text{NH}_4\text{NO}_3$ , which is only formed in our model if sufficient ammonia is available to neutralize both sulfuric acid and nitric acid. Note that the  $\text{HNO}_3$  uptake on aerosol at high relative humidities (as mentioned in Chapter IV) was neglected for this comparison. For Ispra in Italy, and Vreedepeel in the Netherlands, aerosol nitrate is in reasonable agreement with the observations. The comparison for total nitrate ( $\text{HNO}_3 + \text{NO}_3^-$ ) is rather good for Roquetas in Spain and Virolahti II in Finland, while at the Eastern European sites the agreement is much less (not shown). Note that in all cases the difference between model simulations A4 and A5 is small. In average (Table 7.1), particulate nitrate is too low, while the sum of nitrate plus nitric acid is too high compared to the observations at the 8 sites that measure the sum of these components.

### 7.3 Closing Remarks

The comparison with various measurements at different sites shows that the predicted aerosol nitrate concentrations are on average too low. Because  $\text{HNO}_3$  is not predicted to partition completely into the aerosol phase in summer (see Chapter V), this indicates that the availability of  $\text{HNO}_3$  does not limit the formation of nitrate aerosol. It rather seems from our model results and this comparison that enhanced nitrate formation due to the condensation of  $\text{HNO}_3$  on sea salt or mineral dust particles, or  $\text{HNO}_3$  uptake on wet aerosol, is important for some regions. For instance, considering sea salt can also lead to more ammonium nitrate if ammonia limits the nitrate formation, i.e. for cases with insufficient ammonia to neutralize sulfate, because sulfate rather reacts with sea salt so that surplus ammonia can neutralize nitric acid to form ammonium nitrate.

In addition, an extended comparison that includes American sites of the EMEFS network yields contradictory results, i.e. that we rather overpredict the observed aerosol mass. While for a few sites aerosol nitrate and ammonium concentrations are too high compared to the observations, the wet deposition seems to be underestimated for these species, especially for Europe, although the precipitation is simulated well. Furthermore, the comparison of the aerosol run with the base run (excluding gas/aerosol partitioning calculations) yields an improvement for the wet deposition rather than for the modeled aerosol concentrations, except for the USA where the latter improves as well. Note that the aerosol precursor gases  $\text{NO}_x$  and  $\text{SO}_2$  are in rather good agreement with all observations for different model simulations and modeling periods.

Also a classification of the measurement sites according to different aerosol types (polluted continental, remote continental, or marine) did not clarify this picture. It rather seems that the global modeling the gas/aerosol partitioning needs to involve more aerosol species. This is also supported by the results of a comparison of model and satellite derived aerosol optical depth (AOD) (Jeuken, 2000). For instance, to obtain good agreement a constant factor of 0.2 needed to be added to the model AOD, as mentioned in Chapter 5.1.8. Without speculating about the origin and the uncertainty in this number, the fact of the huge discrepancy between modeled and observed AOD indicates the uncertainty range of the aerosol calculations (and potentially of the interpretation of the satellite observations as well). Nevertheless, both occurrence and variability in the AOD were in rather good agreement for Europe, indicating that the main features, i.e. aerosol patterns, are captured well by the model.

## Chapter VIII: Discussion and Conclusions

At the core of this thesis is the development of a simplified method to routinely calculate gas/aerosol partitioning of multicomponent aerosols and aerosol associated water within global atmospheric chemistry (CTM) or climate models (GCM). Multicomponent aerosol mixtures which are composed out of ammonium/sulfate/nitrate and water are very common in the atmosphere. However, up to recently they were not accounted for in CTMs or GCMs. The problem is that with conventional approaches the calculation of mixed aerosols requires a complex thermodynamical treatment, because of the various aerosol states. For instance, mixed aerosols that include volatile compounds can partition between the aerosol and the gas phase. Additionally, most aerosol compounds partition between the liquid and solid aerosol phases, which is important for the amount of aerosol associated water and the aerosol optical properties. Especially the aerosol radiative forcing, which is of crucial importance for the assessment of “Global Warming” with climate models (e.g. IPCC, 1996) depends very much on physical properties such as the aerosol associated water (e.g. Pilinis et al., 1995). However, these properties depend highly non-linear on the aerosol composition, which in turn depends on the gas/liquid/solid aerosol partitioning.

Thus, thermodynamic models are required and must be implemented in global atmospheric chemistry models if aerosol composition, including aerosol associated water, needs to be calculated. Unfortunately, all models introduced in Chapter I, designed to determine the aerosol composition and associated water mass, are unfeasible for global modeling, since the computing time needed easily exceeds the actual computational burden of the hosting CTM or GCM. Even the simpler thermodynamic models, which assume equilibrium between the various aerosol states and the ambient air, are not directly suited for global applications because of their iterative structure, as outlined in Chapter II.

In Chapter III, a simplified method is developed to calculate the equilibrium gas/aerosol partitioning within global models. This method is based on physical relations such as the vapor pressure reduction and the generalization of Raoult’s law. Due to this simplification aerosol composition and aerosol associated water mass can be calculated analytically. A numerical and therefore expensive iterative solution of the gas/aerosol partitioning is thus avoided, considerably speeding up the equilibrium calculations. Crucial for the method is the insight that the aerosol activity, including activity coefficients, is basically determined by the aerosol associated water, which in turn depends mainly on the relative humidity. Using the assumptions usually made in aerosol modeling, analytical functions for the aerosol associated water (Eq. 3.5) and activity coefficients (Eq. 3.7) have been derived theoretically.

These functions allow one to calculate the water fractions of binary solutions (which are usually obtained from laboratory measurements and then used in thermodynamic equilibrium models (EQMs) to calculate the molality and the water content of mixed solutions, see Chapters II and III), and the activity coefficients of various salt compounds relevant to atmospheric aerosols. Subsequently, these functions have been applied to various EQMs, i.e. by replacing the original

iterative activity coefficient calculation methods with the analytical and, hence, non-iterative method using Eq. (3.7), while keeping all other calculations unchanged. The comparison of aerosol properties such as the total particulate matter and the aerosol associated water mass showed a good agreement, indicating that the most important aerosol properties for global modeling can be accurately reproduced with the simplified activity coefficient calculation method. The only exception where the simplified method fails is the prediction of activity coefficients of highly acidic solutions, i.e. of unneutralized sulfuric acid in the aerosol. Fortunately, this has no influence on the calculation of particulate matter and the aerosol associated water, since regardless of the activity coefficients, and because of its high hygroscopicity and sufficiently low vapor pressure, sulfuric acid can be regarded to remain in the aqueous phase, which is generally assumed. Because the aerosol water mass only depends on the dry aerosol mass (which does not change unless the aerosol becomes neutralized) aerosol water is not affected in this case. As mentioned in Chapter II, volatile vapors can not be present in a very acidic solution, so that in this case gas/aerosol and liquid/solid partitioning does not occur. To simplify calculations, concentration domains are used to account for typical aerosol mixtures as outlined in Chapter 2.4.

Based on these results a new thermodynamic gas/aerosol partitioning model has been developed, called EQSAM (Equilibrium Simplified Aerosol Model), presented in Chapter III. EQSAM only utilizes analytical expressions for the calculation of the gas/liquid/solid aerosol states, considerably reducing the computational burden that is normally associated with these types of calculations. The equilibrium model comparison presented in Chapter IV shows that the results of EQSAM are consistent with several EQMs, including the state-of-the-art EQM ISORROPIA, for various aerosol properties and modeling applications. In addition, the results of a box-model comparison show that the assumption on the aerosol state, i.e. that the particles remain in a metastable supersaturated aqueous phase or partition between the liquid/solid phases, has a much stronger effect on the aerosol associated water compared to the differences between EQSAM and ISORROPIA. Generally, the main differences between various EQMs are associated with the determination of the aqueous phase, because this strongly depends on the assumption made on the deliquescence behavior of various salt compounds, i.e. whether deliquescence humidities of multicomponent salts (MDRH) are considered (as it is the case for ISORROPIA and EQSAM), or only deliquescence humidities of single salt compounds (RHD), and their temperature dependence (Chapter III and IV).

In Chapter V, we have performed gas/aerosol partitioning calculations with EQSAM, which has been coupled to an atmospheric chemistry transport model (TM3). The main results are that gas/aerosol partitioning is important in certain regions, seasons and times of day. For instance, the mean surface gaseous nitric acid concentration is predicted to partition completely into the aerosol phase during northern hemispheric winter over large parts of Europe, while this is not the case for the reference run, which excluded gas/aerosol partitioning. This effect is much less pronounced in summer, because of the temperature dependence of the ammonium nitrate equilibrium constant and the much higher sulfate concentrations; the latter is mainly a result of the enhanced photochemical

oxidation of sulfur dioxide in summer. Nevertheless, also during the summer nights, up to 100 percent of nitric acid is predicted to partition into the aerosol phase. While in summer ammonium nitrate might not be stable during day, because of the higher daytime temperature, aerosol nitrate leads at least during morning and night to a considerable increase in aerosol associated water mass, due to the higher aerosol load. However, due to the predicted diurnal variability of the total aerosol load (including aerosol associated water), time averages must be interpreted with care, as illustrated by monthly mean averages and the corresponding time averages for 6 hr and 18 hr (GMT).

To estimate the uncertainties associated with the gas/aerosol partitioning calculations, we have quantified the differences associated with various assumptions and model parameters in Chapter VI. The conclusions are that the uncertainties associated with the simplified aerosol model, i.e. the difference between the results of EQSAM and the recently developed EQM ISORROPIA, are relative small compared to the effects of different assumptions on the aerosol state, e.g. considering partitioning between gas/liquids (metastable), gas/liquid/solids, or hysteresis (combination of both). The comparison further shows that uncertainties associated with the calculation of aerosol nitrate with EQSAM relative to ISORROPIA, are relatively small and of the same order as uncertainties associated with the use of different SO<sub>2</sub> emission inventories, which might be used for TM3. Differences are of the order of 5-10% for the budget concentrations in summer (August). These are rather small compared to the uncertainties associated with the choice of model resolution or boundary layer mixing scheme. For instance, in the planetary boundary layer (PBL), the use of a more realistic turbulent mixing scheme may lead to twice as high nitrate concentrations, while the model resolution has an effect of about 50-80%. These uncertainties, however, should be viewed in the light of the very high seasonal variability, which can be orders of magnitudes higher, especially for the huge contrast in the predicted nitrate aerosol concentrations in the summer and winter PBL. Since there is little variation in winter, mainly due to the lower temperature that thermodynamically favors aerosol formation of (semi-) volatile compounds such as ammonium nitrate, and the much higher sulfate concentrations in summer, uncertainties in aerosol calculations are largest in summer.

The comparison of the differences associated with the use of different SO<sub>2</sub> emission inventories further illustrates that the effect of air-pollution abatements, e.g. an 50% reduction of the European SO<sub>2</sub> emission inventory, is less effective in reducing aerosol concentrations than expected. The reason is that sulfate aerosol formation is mostly limited by the photo-oxidation of SO<sub>2</sub>, while aerosol nitrate remains unaffected for most of western Europe, because ammonia is not limiting the ammonium sulfate aerosol formation so that sufficient ammonia is available to react with nitric acid to form aerosol nitrate. However, in cases where ammonia does limit the ammonium sulfate aerosol formation, a decrease in the sulfate concentrations, for instance, due to a decrease in SO<sub>2</sub>, can increase the aerosol nitrate concentrations because excess ammonia reacts with nitric acid to form ammonium nitrate. This could occur in summer (especially during night, while during day ammonium nitrate might not be thermodynamically stable at higher temperatures), or over eastern



Europe (where sulfate concentrations are predicted to be higher than nitrate concentrations for the entire year). Over western Europe, during winter, the surface concentrations of aerosol nitrate are higher than those of sulfate by a factor of 2 or more, so that a decrease in the sulfate concentrations (e.g. due to a decrease in  $\text{SO}_2$ ) does not have a large effect on the aerosol nitrate concentrations, and the total particulate matter (including aerosol associated water).

Another interesting result of the aerosol calculations is that, because of gas/aerosol partitioning, anthropogenically produced trace gases, such as ammonia, might be more widely distributed as a result of the longer residence time of accumulation mode aerosols; the atmospheric residence time of total ammonia ( $\text{NH}_x = \text{NH}_3 + \text{NH}_4$ ) is assumed to be 1-2 days while ammonia in the form of ammonium nitrate has an average residence time of about 1 week, because it is less effectively removed by dry deposition. For instance, our results show that at a model layer about 200-300 hPa ammonium nitrate can be widely distributed, although ammonium nitrate is not predicted to form at higher altitudes in summer, due to an insufficient amount of ammonia above the surface model level to completely neutralize all sulfate. Whereas ammonia is emitted at relatively high altitudes in the northern region of the Indian Himalayas, because of the high wind velocities (and particularly the dry north-westerlies) during the Indian monsoon, ammonia can be transported into the free troposphere where it is predicted to neutralize nitric acid that is present in higher amounts than sulfate. An extended plume of ammonium nitrate is therefore predicted to exist in the free troposphere, which may be transported as far as Europe.

Although it is difficult to say to which extent these model simulations are realistic - because of lacking aircraft measurements for validation - the results indicate that long-range transport of aerosols might occur over thousands of kilometers. If our simulations are realistic, then especially the Indian-Ocean region might be important as a source of anthropogenic air pollutants that can be carried upward in the free troposphere and then transported by jetstreams far away from their sources, because of the huge local air-pollution and the extreme atmospheric conditions. This topic therefore deserves further attention.

The comparison of all uncertainties (Chapter IV and VI) and the comparison of the aerosol calculations with measurements (Chapter VII) shows that the uncertainties associated with thermodynamical parameters, such as the exact representation of activity coefficients, are least important for global modeling. Instead, it is more important to fully account for all aerosol compounds. Although the comparison with measurements is preliminary, mainly because it only represents a snap-shot of the present model development (inclusion of other aerosol compounds and a "zoom"-version are in progress) it seems that the implementation of other aerosol compounds is necessary to obtain a better agreement with measurements, especially at remote sites, while for anthropogenically polluted sites in Europe, where ammonium nitrate is important, the comparison is already remarkably good.

Additionally, there are various other aspects which need to be addressed in the future, or which can be improved. The inclusion of more aerosol compounds (e.g. sea salt, mineral dust, and organic compounds) is one. Also the explicit calculation of the size-distribution from the actual aerosol mass (including aerosol associated water) is needed. At present different size distributions are prescribed for the dry deposition module only. Another aspect is the consistent use of the aerosol parameters throughout all atmospheric chemistry modules, including aerosol thermodynamics, dry and wet deposition, and heterogeneous chemistry. Additionally, it is further desirable to routinely account for the various aerosol states, and in particular for the hysteresis effect of aerosols. Although our results have shown that the difference between the assumptions of metastable aerosols and hysteresis are rather small for the total aerosol (direct) radiative forcing (globally integrated), they are certainly larger for dry regions, such as the free troposphere. In these regions, the amount of aerosol water might influence the local chemistry much stronger than the global direct radiative forcing by aerosols.

It should be also noted that the application of any EQM to the global atmosphere is always associated with uncertainties, because of the assumptions on which these models (including EQSAM) are based. These assumptions are thermodynamical equilibrium, which implies that the water activity of the aerosol equals the ambient relative humidity (justified because of the much higher partial pressure of water vapor compared to the partial pressure of atmospheric vapors), and the so-called ZSR-relation, which simply assumes that the total aerosol associated water is the sum of the water fractions of all single-solute solutions. In addition, the aerosols are assumed to be internally mixed, and occur in the sub-micron size range (bulk approach).

These assumptions may be valid for inorganic salt compounds if the aerosol modeling is limited to the ammonium/sulfate/nitrate/water-system (as we did). These assumptions are, however, no longer valid if additional particles such as sea-salt or mineral dust are considered. Especially the latter particles often provide a pre-existing solid core that favors condensation; heterogeneous nucleation is generally thermodynamically favored. They therefore can diurnally redistribute (semi-) volatile compounds such as ammonium nitrate from smaller particles to larger ones (those including a solid core) as the relative humidity decreases (see Chapter 2.8).

Furthermore, the equilibrium approach might be insufficient for the coarse mode particles, such as sea salt and mineral dust, since the equilibration times are considerable longer for larger particles (because of the smaller surface-to-volume ratio), possibly exceeding the timescales over which transport and chemistry are calculated (about 1 hour in our study). Especially in remote and less polluted regions, or regions exposed to cold atmospheric conditions, the equilibrium approach may not be satisfied. In these locations, also nucleation might become important, which is, however, not considered in EQMs nor in EQSAM because condensation is predominant in the polluted atmosphere and nucleation mode particles add only little to the total aerosol burden.

One also has to keep in mind the limitations of the hosting atmospheric chemistry and climate models. The efforts to achieve high accuracy for the aerosol calculations should balance with the efforts spent on describing other uncertain processes. One should therefore not automatically assume that the results of complex models such as ISORROPIA, incorporated in large-scale models, are always valid on a global scale, since other processes may determine the real uncertainty, or the assumptions on which the complex model is based may not hold under all circumstances. Nevertheless, complex models such as ISORROPIA are needed to develop and validate simpler models such as EQSAM. Our simplified method (EQSAM) should be understood as an initial step for further development, which will include other aspects that are important for global modeling, e.g. a hybrid approach, i.e. a combination of equilibrium assumptions with a full dynamical treatment for remote cases with a low aerosol load, or coarse particles.

## Appendix

As mentioned in Chapter III, prior to the development of an alternative method for the activity coefficient calculation (ACC) and the development of a new thermodynamic gas/aerosol partitioning model, called EQSAM (Equilibrium Simplified Aerosol Model), an empirical functional fit of activity coefficients,  $\gamma_i$ , to more comprehensive ACC already provides an important improvement in the simplification of equilibrium calculations (see Metzger, 1999). An alternative method was simultaneously developed by Nenes et al. (1998) for use in the EQM ISORROPIA, based on pre-calculated sets of binary activity coefficients.

While the method used by Nenes et al. (1998) has the disadvantage that activity coefficients of mixed solutions must still be calculated iteratively (see Chapter 2.6.4), pre-calculated sets of  $\gamma_i$  values, which apply to mixed solutions, and which could be pre-defined for a range of RH and used in look-up tables has the disadvantage that look-up tables are generally more suited for small data sets. Therefore, we initially preferred polynomial fits to pre-calculated sets of  $\gamma_i$  which have been calculated with SCAPEa using the Pitzer-method. To cover a wide range of atmospheric conditions including a large set of different concentration domains at different temperatures and relative humidities, we have applied SCAPE to global input fields (similar to those used in Chapter 4.2) with monthly mean values of temperature, RH, ammonia, sulfuric and nitric acid, sea salt and dust for the month January. Representing each activity coefficient of the global set as a function of the corresponding relative humidity shows that the activity coefficients of atmospheric aerosols in equilibrium with the ambient relative humidity mainly depend on RH.

Based on this  $\gamma_i$  - RH relationship we have derived with non-linear curve fitting characteristic functions for each type of activity coefficient shown in Figure 3.4, i.e.

$$\Gamma_i(RH) = a_{i,0} + a_{i,1} \cdot RH + \exp(a_{i,2} \cdot (RH - 100) - a_{i,3}), \quad (A1)$$

where  $a_{i,0}$ ,  $a_{i,1}$ ,  $a_{i,2}$ ,  $a_{i,3}$  denote the unknown coefficients of the polynomial fit (Eq. A1), and  $RH$  the relative humidity [%]. The non-linear curve fitting procedure has been applied to all  $\gamma_i$  values in the same manner. However, it appeared that the activity coefficients used in SCAPE could be classified according to the charge and the number of moles of ions considered, so that only four<sup>1</sup> polynomials  $\Gamma_i(RH)$  were used to obtain the activity coefficients needed in SCAPE. This classification of activity coefficients is shown in Table 3.1 (see Chapter 3.5.3). The unknown coefficients used in Eq. (A1) are given in Table A1.

<sup>1</sup> Using Eq. (3.9) only one polynomial is needed.

**Table A1. Coefficients of the polynomial fit used in Eq. (A1).**

	$a_{i,0}$	$a_{i,1}$	$a_{i,2}$	$a_{i,3}$
i=1	0.160000	0.001600	0.340000	0.554000
i=2	0.013000	0.001100	0.770000	0.175000
i=3	0.047000	0.001100	0.490000	0.175000
i=4	0.000000	0.000091	1.110000	0.100000

Note that all fits, i.e. the  $\Gamma_{i=1}$  (RH) functions are derived from a global set of activity coefficients that consists of 4608 independent equilibrium calculations. However, a dependency of the  $\Gamma_{i=1}$  (RH) functions on the concentration domains is omitted here, but is accounted for in the analytically derived activity coefficient calculation method, i.e. Eq. (3.7) by using different values of the parameter N (see Chapter 3.5.3).

The advantage of using  $\Gamma_i$ (RH) functions based on pre-calculated sets of  $\gamma_i$  values (or analytical functions such as Eq. 3.7) is that if such a pre-calculated set comprises all activity coefficients of all species and reactions as considered in the EQM, e.g. SCAPE (Table 2.2), the equilibrium can be calculated not only much faster with the parameterization but also as comprehensive as with the non-parameterized equilibrium routine by explicitly calculating activity coefficients. The differences then only depend on the accuracy of the estimation method for the  $\gamma_i$  values which are not pre-described, i.e. on the quality of the polynomial fits (or for Eq. 3.7 on N).

## List of Acronyms

<i>ACCM</i>	Activity Coefficients Calculation Method
<i>KM</i>	Kusik-Meissner Method
<i>PM</i>	Pitzer Method
<i>BM</i>	Bromley Method
<i>CCN</i>	cloud condensation nuclei
<i>CORINAIR</i>	COre INventory AIR
<i>COSAM</i>	COmparison of large scale atmospheric Sulfate Aerosol Models
<i>CPUs</i>	computing time units per second
<i>CRAY</i>	Super Computer using vector architecture
<i>CTM</i>	atmospheric/Chemistry Transport Model
<i>ECMWF</i>	European Center of Medium Weather Forecast re-analysis project (ERA).
<i>ECN</i>	Dutch Energy Research Center
<i>EDGAR</i>	Emission Database for Global Atmospheric Research
<i>EDGAR</i>	our extrapolation of the EDGAR emission inventory of 1990 to 1997 for SO <sub>2</sub>
<i>EMEFS</i>	Emission data base of North America prepared under the co-sponsorship of the United States Environmental Protection Agency, the Atmospheric Environment Service, Canada, the Ontario Ministry of Environment, the Electric Power Research Institute, and the Florida Electric Power Coordinating Group
<i>EMEP</i>	Emission data of Europe in the framework of the European Measuring Project
<i>EQM</i>	thermodynamic gas/aerosol EQUilibrium Model
<i>-P</i>	suffix denotes parameterized EQM versions
<i>EQMs:</i>	
<i>EQSAM</i>	Equilibrium Simplified Aerosol Model (this work)
<i>EQUIL</i>	Equilibrium Model (Basset and Seinfeld, 1983)
<i>KEQUIL</i>	Equilibrium Model considering the Kelvin effect (Basset and Seinfeld, 1984)
<i>MARS</i>	Equilibrium Model (Saxena et al., 1986; Binkowski, 1991)
<i>SEQUILIB</i>	Equilibrium Model (Pilinis and Seinfeld, 1987)
<i>SCAPE</i>	Equilibrium Model: Simulating Composition of Atmospheric Particles at Equilibrium: version a (Kim et al., 1993ab, Kim and Seinfeld, 1995); version b (Meng et al. 1998)
<i>ISORROPIA</i>	Equilibrium Model (Greek: equilibrium) (Nenes et al. 1999)
<i>IPCC</i>	Intergovernmental Panel on Climate Change
<i>FT</i>	Free Troposphere
<i>GCM</i>	General Circulation Model (climate model)
<i>GEIA</i>	Global Emission Inventory Activity
<i>GISS</i>	Goddard Institute for Space Studies
<i>GMT</i>	Greenwich mean time
<i>GOME</i>	Global Ozone Monitoring Experiment
<i>GPC</i>	Gas-to-Particle Conversion
<i>MADM</i>	Multicomponent Aerosol Dynamic Model (Pilinis et al., 2000)
<i>Mac OS9</i>	Macintosh Operating System
<i>NMHC's</i>	Non-Methane Hydrocarbons
<i>PBL</i>	Planetary Boundary Layer
<i>PM</i>	Particulate Matter
<i>ST</i>	Stratosphere
<i>TM3</i>	atmospheric/chemistry Transport Model (version 3)
<i>CG</i>	Coarse Grid ⇔ Resolution 10° x 7.50° by 19 vertical levels
<i>VG</i>	Very Fine Grid ⇔ Resolution 2.5° x 2.50° by 31 vertical levels
<i>FG</i>	Fine Grid ⇔ Resolution 5.0° x 3.75° by 19 vertical levels
<i>UNICOS</i>	UNIX Cray Operating System
<i>ZSR</i>	relation to calculate water content of mixed aerosols; Zdanovskii (1948), Stokes and Robinson (1966)

## List of Symbols

### Chapter II:

$a_w$	water activity
$a_i$	activity of species $i$
$A_\gamma$	Debye-Hückel constant
$C_p^o$	standard molar heat capacity at constant pressure
$\varepsilon$	reaction coordinate [-1, 1]
$G$	Gibbs free energy
$G^o$	Gibbs free energy at a standard state, e.g. T=298.15 K, P=1023 hPa
$H$	standard molar enthalpy
$H^o$	standard molar enthalpy at a standard-state
$i$	compound $i$
$I$	ionic strength of the solution
$K$	equilibrium constant
$L_{solvent}$	latent heat of vaporization of water in the saturated solution
$L_{solute,i}$	latent heat of fusion of salt $i$
$m_i$	molality, i.e. the concentration of the solution
$M_w$	molar mass of water
$M_s$	molar mass of a salt compound
$m_{i,ss}$	molality of single-solute aqueous solution of solute $i$
$MDRH$	mutual deliquescence relative humidity (multicomponent salt particles)
$n_i$	number of moles
$n_i^o$	initial amount of compound $i$
$p$	pressure
$p_i$	partial pressure of the compound $i$
$p_w$	ambient partial pressure of water
$p_s$	saturation vapor pressure of water
$R$	universal gas constant
$RHD$	relative humidity of deliquescence (single salt particles)
$RH$	percentage relative humidity [%]
$rh$	fractional relative humidity [0-1]
$R_{SO_4}$	sulfate ratio
$R_{Na}$	sodium ratio
$S$	entropy
$T$	temperature
$T_o$	standard state temperature
$U$	internal energy
$V$	volume
$W_i$	amount of water corresponding to single solute $i$
$W$	total amount of water in the mixture
$\gamma_{ij}$	mean binary activity coefficient of the $i$ - $j$ ion pair
$\gamma_{12}$	activity coefficient of cation 1 and anion 2
$z_i$	absolute charge of ionic species $i$
$\mu_i$	chemical potential
$\mu_i^o$	chemical potential at a standard state
$\mu_w$	chemical potential of water
$\nu_i$	stoichiometric coefficient of compound $i$
$\nu_i$	dissociation number of salt compound $i$
$\Delta$	total change
$\prod$	product
$\sum$	summation
$\ln$	natural logarithm
$exp$	exponentiation

**Chapter III:**

$a_w$	water activity
$e_+$	charge of the cation
$e_-$	charge of the anion
$f_w$	rational activity coefficient of water (of an aqueous salt solution)
$f_s$	rational activity coefficient of a salt solute
$K_{AN}$	equilibrium constant of ammonium nitrate for the reaction (formation)
$m_{aerosol}$	total aerosol mass
$m_s$	mass of the salt compound
$m_w$	mass of the aerosol water
$m_{AN}$	molality of ammonium nitrate
$n_w$	number of water molecules
$n_s$	number of salt molecules
$p_o$	Atmospheric pressure
$p_{sat,s}$	equilibrium vapor pressure of a volatile salt compound over an aqueous salt solution
$p_w$	equilibrium vapor pressure of water vapor over an aqueous salt solution
$p_{sat,w}, p_{w,o}$	equilibrium vapor pressure over an pure aqueous solution
$p_{HNO_3}$	vapor pressure of nitric acid
$p_{NH_3}$	vapor pressure of ammonia
$pH$	potentia Hydrogenia: $-\log[H^+]$
$PM_{wet}$	wet Particulate Matter
$PM_{dry}$	dry Particulate Matter
$PM$	total Particulate Matter (wet + dry)
$r$	aerosol radius
$V_m$	mol volume
$W_o$	initial water mass of the particle
$x_w$	mole fraction of the aerosol water
$x_s$	mole fraction of the salt solute
$Z$	ion pair charge
$\Delta p_{sat}$	vapor pressure reduction
$\Gamma$	parameter for the various sulfate states
$\rho$	density
$\rho_s$	density of the salt compound
$\rho_w$	density of the aerosol water
$\sigma$	surface tension
$\gamma_{AN}$	activity coefficient of ammonium nitrate
$\gamma_{ij}^o$	mean ionic activity coefficient of the binary pair $i-j$ (binary activity coefficient) for a solution that contains only $i-j$ ions at the ionic strength of the multicomponent solution
$\xi$	exponent of activity coefficient

**Chapter V:**

$^{222}Rn$	radio nuclide radon
$S$	net source term
$S_{emis}$	source term of emissions
$S_{chem}$	source term of chemical production or destruction
$S_{scav}$	loss of a tracer by precipitation scavenging processes
$S_{depo}$	loss of a tracer by dry deposition at the surface
$t$	time
$\vec{v}$	velocity
$\mu$	tracer-mixing ratio



**General:**

$H_2O_2$	hydrogen per-oxide
$CO_2$	carbon dioxide (gas)
$CH_4$	methane (gas)
$O_3$	ozone (gas)
$SO_2$	sulfur dioxide
$NO_x$	nitrogen oxides (NO+NO <sub>2</sub> )
$H_2O(g)$	water vapor (gas)
$H_2SO_4(g)$	sulfuric acid (gas)
$HNO_3(g)$	nitric acid (gas)
$NH_3(g)$	ammonia (gas)
$HCl(g)$	hydrogen chloride (gas)
$H_2O(aq)$	water (aqueous)
$H^+(aq)$	hydrogen ion (aqueous)
$NH_4^+(aq)$	ammonium ion (aqueous)
$Na^+(aq)$	sodium ion (aqueous)
$Ca^{++}(aq)$	calcium ion (aqueous)
$Mg^{++}(aq)$	magnesium ion (aqueous)
$K^+(aq)$	potassium ion (aqueous)
$OH^-(aq)$	hydrogen oxide ion (aqueous)
$NO_3^-(aq)$	nitrate ion (aqueous)
$Cl^-(aq)$	chloride ion (aqueous)
$SO_4^{2-}(aq)$	sulfate ion (aqueous)
$HSO_4^-(aq)$	bisulfate ion (aqueous)
$(NH_4)_3H(SO_4)_2(s)$	letovicite (solid)
$(NH_4)_2SO_4(s)$	ammonium sulfate (solid)
$NH_4HSO_4(s)$	ammonium bisulfate(solid)
$NH_4NO_3(s)$	ammonium nitrate (solid)
$NH_4Cl(s)$	ammonium chloride (solid)
$Na_2SO_4(s)$	sodium sulfate (solid)
$NaHSO_4(s)$	sodium bisulfate(solid)
$NaCl(s)$	sodium chloride (solid)
$NaNO_3(s)$	sodium nitrate (solid)
$KNO_3(s)$	potassium nitrate (solid)
$KCl(s)$	potassium chloride (solid)
$KHSO_4(s)$	potassium bisulfate (solid)
$K_2SO_4(s)$	potassium sulfate (solid)
$Ca(NO_3)_2(s)$	calcium nitrate (solid)
$CaCl_2(s)$	calcium chloride (solid)
$CaSO_4(s)$	calcium sulfate (solid)
$Mg(NO_3)_2(s)$	magnesium nitrate (solid)
$MgCl_2(s)$	magnesium chloride (solid)
$MgSO_4(s)$	magnesium sulfate (solid)
$tSO_4$	total sulfate = $H_2SO_4(g) + SO_4^{2-}(aq)$
$tNH_3$	total ammonia = $NH_3(g) + NH_4^+(aq)$
$tNO_3$	total nitrate = $HNO_3(g) + NO_3^-(aq)$

## List of Figures

**Figure 1.1.** Uncertainty in climate change caused by aerosols..... 2

**Figure 1.2.** Emissions of SO<sub>2</sub> and NO<sub>x</sub> in Hamburg, Germany..... 5

**Figure 2.1.** Schematic description of the solution algorithm of present EQMs..... 30

**Figure 2.2.** Number of iterations needed to reach convergence for the activity coefficient calculation. This is plotted versus relative humidity for four different cases of atmospheric aerosol compositions: NH<sub>4</sub>-NO<sub>3</sub>-SO<sub>4</sub>, NH<sub>4</sub>-SO<sub>4</sub>, NH<sub>4</sub>-NO<sub>3</sub>, NH<sub>4</sub>-NO<sub>3</sub>-SO<sub>4</sub>-Na-Cl. Values are obtained from an application of the thermodynamic equilibrium model (ISORROPIA, Nenes et al. 1999) to global data, representing monthly mean values for January (one 3D-field 3.75° x 3.75° horizontal resolution, surface layer) ..... 32

**Figure 3.1.** Solution molality as a function of relative humidity [%] for pure salt aerosols: The upper panel shows NH<sub>4</sub>NO<sub>3</sub> (black), (NH<sub>4</sub>)<sub>2</sub>SO<sub>4</sub> (blue), H<sub>2</sub>SO<sub>4</sub> (green), the lower panel NH<sub>4</sub>HSO<sub>4</sub> (yellow) and (NH<sub>4</sub>)<sub>3</sub>H(SO<sub>4</sub>)<sub>2</sub> (light-blue). For comparison, the results of equation (3.10) are included (red, thin solid lines) .. 38

**Figure 3.2.** Water fractions of 3 electrolytes as a function of relative humidity at fixed temperature: Upper panels NH<sub>4</sub>NO<sub>3</sub>, lower panels (NH<sub>4</sub>)<sub>2</sub>SO<sub>4</sub> (top) and (NH<sub>4</sub>)HSO<sub>4</sub> (bottom). The water fractions are shown for two concentrations 1 μmol/m<sup>3</sup> (left panels) and 1/2 μmol/m<sup>3</sup> air (right panels). For comparison, the results of equation (3.5) are included (red, thin solid lines) ..... 39

**Figure 3.3.** Mean binary activity coefficient vs. RH: top panels  $\gamma_{\pm}$  of NH<sub>4</sub>NO<sub>3</sub>, bottom  $\gamma_{\pm}$  of (NH<sub>4</sub>)<sub>2</sub>SO<sub>4</sub>. Left panels shows the  $\gamma_{\pm}$  for a 1 μmol (black) vs. 1/2 μmol (yellow) ion pair concentration (calculated with the EQM ISORROPIA), the right panels show the  $\gamma_{\pm}$  for a 1 μmol case and equilibrium calculations with various EQMs: ISORROPIA (black), MARS (green), SCAPEa & Pitzer-method (blue), SCAPEb & K-M-method (yellow), SCAPEb & Bromley-method (medium-blue), SEQUILIB (aqua), and Eq. (3.7) with N=1.5 (red lines).....45

**Figure 3.4.** Effect of relative humidity on activity coefficients. The black lines represent the  $\gamma_{\pm}$  of the EQM SCAPEa (Pitzer method), the red lines Eq. (3.7) with N=1.5. The types of activity coefficients used in EQMs are represented by the  $\gamma_{\pm}$  of NH<sub>4</sub>NO<sub>3</sub>, (NH<sub>4</sub>)<sub>3</sub>H(SO<sub>4</sub>)<sub>2</sub>, (NH<sub>4</sub>)<sub>2</sub>SO<sub>4</sub> and CaSO<sub>4</sub> ..... 46

**Figure 3.5.** Effect of input parameters on the mean binary activity coefficient of NH<sub>4</sub>NO<sub>3</sub>. Panel (a) shows  $\gamma_{\pm}$  for an ion pair concentration of 1 μmol NH<sub>4</sub>NO<sub>3</sub> as a function of relative humidity [%] for equilibrium calculations with various EQMs (System III):

ISORROPIA (black), MARS (green), SCAPEa and Pitzer-method (blue), SCAPEb and K-M-method (yellow), SCAPEb and Bromley-method (light-blue), SEQUILIB (aqua) (the references are given in Chapter 2.1). Panel (b) shows the sensitivity of  $\gamma_{\pm}$  (ISORROPIA, System III) to temperature variations and a concentration range. Panel (c) shows the sensitivity of  $\gamma_{\pm}$  to various compositions: System I = NH<sub>3</sub>-H<sub>2</sub>SO<sub>4</sub> (light-blue), System II = NH<sub>3</sub>-HNO<sub>3</sub> (aqua), System III = NH<sub>3</sub>-HNO<sub>3</sub>-H<sub>2</sub>SO<sub>4</sub> (yellow), System IV = III + sea salt (green), System V = IV + mineral dust (K<sup>+</sup>, Mg<sup>2+</sup>, Ca<sup>2+</sup>) (black). System I-IV represent equilibrium calculations of ISORROPIA, System V of SCAPEa. Panel (c) includes temperature variations and a concentration range. Panel (d) shows  $\gamma_{\pm}$  (ISORROPIA) for different domains of System IV: Domain 1 (black); Domain 2 (green); Domain 3 (blue); Domain 4 (yellow). For comparison, the result of equation (3.7) based on a constant value of N=1.5 is included in each panel (red, thin lines) .....48

**Figure 3.6.** Effect of composition on activity coefficients of Figure 3.5c in detail .....49

**Figure 3.7.** Effect of different domains on activity coefficients of Figure 3.5d in detail .....51

**Figure 3.8.** Domains for various systems of atmospheric aerosol compositions. The concentration domains are abbreviated according to their definition in Chapter 2.4: SP = sulfate poor case (cation rich); SN = sulfate neutral case; SR = sulfate rich case; SVR = sulfate very rich case.....52

**Figure 3.9.** Scatter plots of total particulate matter (PM) in [μg/m<sup>3</sup>] for various domains and equilibrium models: ISORROPIA (black), MARS (green), SCAPEa & Pitzer-method (blue), SCAPEb & K-M-method (yellow), SCAPEb & Bromley-method (medium-blue), SEQUILIB (aqua). Domain 1 represents System IV for ISORROPIA and System V for SCAPEa,b; Domain 2, 3 and 4 represent System III for all models.....53

**Figure 4.1.** Comparison of equilibrium calculations with the equilibrium simplified aerosol model (EQSAM), various EQMs in use (ISORROPIA, SEQUILIB, MARS, SCAPEa-PM, SCAPEb-KM, SCAPEb-BM), and their parameterized versions (-P). Results are shown for each domain as a function of relative humidity (10-95%) and are given in percentage for nitrate- (top) and ammonium- (middle) partitioning, and the degree of neutralization (bottom). The domains (ammonium/sulfate ratios) are: Domain 4 = sulfate very rich (2:NH<sub>4</sub><sup>+</sup><SO<sub>4</sub><sup>2-</sup>); Domain 3 = sulfate rich (NH<sub>4</sub><sup>+</sup><SO<sub>4</sub><sup>2-</sup>); and Domain 2 = sulfate poor case (NH<sub>4</sub><sup>+</sup>>SO<sub>4</sub><sup>2-</sup>) .....60

**Figure 4.2.** Comparison of equilibrium calculations of Figure 4.1 continued. Results are shown for the total particulate matter (top), the aerosol-associated water (middle), and the radius increase due to water uptake (bottom) .....61

- Figure 4.3.** Comparison of equilibrium calculations of **Figure 4.2** (middle) supplemented for EQSDAM/ISORROPIA by the results of the aerosol associated water based on metastable aerosols (indicated by triangles and squares, respectively). Note that the maxima have been cut off since they remained unchanged ..... **62**
- Figure 4.4.** Comparison of equilibrium calculations with the equilibrium simplified aerosol model and various EQMs in use, including their parameterized versions (-P). Left to right (01Z to 12Z): EQSAM, ISORROPIA, SEQUILIB, MARS, SCAPEa-PM, SCAPEb-KM, SCAPEb-BM, ISORROPIA-P, SEQUILIB-P, MARS-P, SCAPEa-P, SCAPEb-P. Shown are the mol ratio of aerosol nitrate and sulfate (upper panels), the aerosol radius increase due to water uptake (middle panels), and the nitrate partitioning [%] (lower panels) for a location in Germany (left), a regional average over Europe (middle), and the global average (right); for January 1997 at surface level ..... **64**
- Figure 4.5a.** Comparison of EQSAM with ISORROPIA. Shown are the mol ratio of aerosol nitrate and sulfate (left) and the total particulate matter (right). The upper panels show the global pattern (shaded EQSAM, contour ISORROPIA), the middle panels show the corresponding difference of EQSAM-ISORROPIA, and the lower panels show the scatter, including the regionally weighted and un-weighted correlations coefficients; for January 1997 at surface level ..... **65**
- Figure 4.5b.** Comparison of EQSAM with ISORROPIA. Shown are the aerosol associated water which corresponds to the calculation of metastable aerosols (left), and which corresponds to the gas/liquid/solid equilibrium partitioning (right). The upper panels show the global pattern (shaded EQSAM, contour ISORROPIA), the middle panels show the corresponding difference of EQSAM-ISORROPIA, and the lower panels show the scatter, including the regionally weighted and un-weighted correlations coefficients; for January 1997 at surface level. Note that the contour lines differ for the left and right panels ..... **66**
- Figure 4.6.** Online equilibrium calculations (metastable aerosols) with EQSAM: Time series for July 1997 of the surface mol ratio of total transported aerosol nitrate and sulfate (upper panels), the column aerosol radiative forcing of nitrate (middle panels) and sulfate (lower panels) for a location in Germany (left), a regional average over Europe (middle), and the global average (right). In addition, the differences between these results and those obtained by using ISORROPIA are included in each panel and marked in light grey (EQSAM - ISORROPIA). Note that the differences are almost zero and therefore difficult to distinguish from the minimum values which are also zero. Note further the different scale for the aerosol radiative forcing of sulfate..... **72**
- Figure 5.** Schematic overview of the aerosol version of TM3. .... **74**
- Figure 5.1a.** Time series (for the year 1997) of various surface variables relevant to the gas/aerosol partitioning calculations. Meteorological parameters for a single gridbox in Germany (10°E, 50°N): Temperature [°C], relative humidity [%], and pressure [hPa] ..... **82**
- Figure 5.1b.** Time series (for the year 1997) of the surface mass ratio of aerosol nitrate and sulfate (top), and dry aerosol fraction (bottom), i.e.  $PM/(PM+H_2O)$  [%], for a single gridbox in Germany (10°E, 50°N) ..... **83**
- Figure 5.1c.** Time series (year 1997) of the corresponding nitrate (top) and ammonium partitioning (bottom) [%], i.e.  $NO_3^-/(HNO_3+NO_3^-)$  and  $NH_4^+/(NH_3+NH_4^+)$ , respectively (single gridbox, Germany, 10°E, 50°N) ..... **84**
- Figure 5.1d.** Time series (year 1997) of the corresponding ammonium fraction (top) [%], i.e.  $NH_4^+/(NO_3^-+2SO_4^{2-})$  in  $[\mu gN/(\mu gN+\mu gS)]$ , and the gas ratio of residual ammonia and nitric acid [mol/mol], i.e.  $NH_3/HNO_3$  (single gridbox, Germany, 10°E, 50°N) ..... **85**
- Figure 5.2a.** Surface mole fraction of aerosol nitrate relative to the sum of nitrate and sulfate, i.e.  $NO_3^-/(SO_4^{2-}+NO_3^-)$  ..... **87**
- Figure 5.2b.** Total particulate aerosol mass vertically integrated (burden)  $[\mu g/m^2]$  ..... **88**
- Figure 5.2c.** Aerosol associated water (burden)  $[\mu g/m^2]$  ..... **89**
- Figure 5.3a.** Surface mole fraction of aerosol nitrate relative to the sum of nitrate and sulfate, i.e.  $NO_3^-/(SO_4^{2-}+NO_3^-)$  ..... **91**
- Figure 5.3b.** Total particulate aerosol mass vertically integrated (burden)  $[\mu g/m^2]$  ..... **92**
- Figure 5.3c.** Aerosol associated water (burden)  $[\mu g/m^2]$  ..... **93**
- Figure 5.4a.** Vertical-time distribution for 1997 (Hovmöller representation) of the mass ratio of nitrate and sulfate (top), the total dry particulate matter (middle), and the associated aerosol water mass (bottom) for a single gridbox in Germany (50°N and 10°E) ..... **95**
- Figure 5.4b.** Zonal cross-section 6°E for August 1997 (monthly mean). Nitrate mole fraction (top), aerosol nitrate (middle), and aerosol sulfate (bottom). White colors denote orography ..... **96**
- Figure 5.4c.** Zonal cross-section at 80°E for August 1997 (monthly mean). Ammonia (top), nitric acid (middle), and aerosol nitrate (bottom). White colors denote orography ..... **97**
- Figure 5.4d.** Global distribution of aerosol nitrate (top) and ammonia (bottom) at approx. 270 hPa for August 1997 (monthly mean) ..... **98**

- Figure 5.5a.** Global changes in [%] for vertically integrated (burden) ammonia (top), nitric acid (middle), and ozone (bottom) for January 1997 (monthly mean) **101**
- Figure 5.5b.** Global changes in [%] for the zonal averages (up to 500 hPa) of ammonia (top), nitric acid (middle), and ozone (bottom) for July 1997 (monthly mean) ..... **102**
- Figure 5.6a.** Budgets concentrations of aerosol nitrate for the year 1997 representing the planetary boundary layer (BL90N-30N, BL30N-0, BL0-30S, BL30-90S), the free troposphere (FT90N-30N, FT30N-0, FT0-30S, FT30-90S, FT90N-30N), and the stratosphere (ST30N-0, ST0-30S, ST30-90S), and the total burden..... **103**
- Figure 5.6b.** Budgets concentrations of aerosol sulfate for the year 1997 representing the planetary boundary layer (BL90N-30N, BL30N-0, BL0-30S, BL30-90S), the free troposphere (FT90N-30N, FT30N-0, FT0-30S, FT30-90S, FT90N-30N), and the stratosphere (ST30N-0, ST0-30S, ST30-90S), and the total burden..... **104**
- Figure 6.1a.** Total column aerosol radiative forcing [ $\text{W}/\text{m}^2$ ] (global average) for 1997 as calculated with TM3 / EQSAM (metastable aerosols); R3..... **106**
- Figure 6.1b.** Difference between the aerosol calculations with TM3 / EQSAM (metastable aerosols) and the so-called sulfate-only calculations with TM3 for the total column aerosol radiative forcing [%] for 1997 (global); R3-R1 ..... **106**
- Figure 6.2.** Difference between the aerosol calculations with TM3 / EQSAM assuming metastable aerosols and gas/liquid/solid equilibrium partitioning for the total column aerosol radiative forcing [%] for 1997 (global); R3-R2 ..... **107**
- Figure 6.3.** Difference between the aerosol calculations with TM3 / EQSAM assuming metastable aerosols and hysteresis (including the full gas/liquid/solid equilibrium partitioning) for the total column aerosol radiative forcing [%] for 1997 (global); R3-R4 ..... **108**
- Figure 7.1a.** Comparison of instantaneous model values and measurements of  $\text{SO}_4^{2-}$  for Petten (The Netherlands) and the average diurnal cycle for August 1997. The solid line represents the observations, the dotted line the model run A4, and the dashed line A5. Correlation is 0.78 and 0.71, the average difference is 2.2 and 4.2  $\mu\text{g}/\text{m}^3$  for A4 and A5 respectively. Times are in GMT **112**
- Figure 7.1b.** Comparison of instantaneous model values and measurements of  $\text{NO}_3^-$  for Petten (The Netherlands) and the average diurnal cycle for August 1997. The solid line represents the observations, the dotted line the model run A4, and the dashed line A5. Correlation is 0.41 and 0.42, the average difference is 2.6 and 2.6  $\mu\text{g}/\text{m}^3$  for A4 and A5 respectively. Times are in GMT **112**
- Figure 7.2a.** Comparison of daily averaged model values and measurements of  $\text{SO}_4^{2-}$  for several EMEP sites (August 1997)..... **114**
- Figure 7.2b.** Comparison of daily averaged model values and measurements of  $\text{NH}_4^+ + \text{NH}_3$  for several EMEP sites (August 1997)..... **115**
- Figure 7.2c.** Comparison of daily averaged model values and measurements of  $\text{NO}_3^-$  for the EMEP sites Ispra (Italy) and Vreedepeel (Netherlands), and of total nitrate ( $\text{HNO}_3 + \text{NO}_3^-$ ) for Roquetas (Spain, 40.81, -0.5, 50) and Virolahti II (Finland, 60.52, 27.68, 4) ..... **115**

## List of Tables

<b>Table 1.1.</b> Natural and anthropogenic aerosol production rates (estimates) .....	<b>4</b>
<b>Table 2.1.</b> Comparison of Chemical Components in Equilibrium Models .....	<b>12</b>
<b>Table 2.2.</b> Equilibrium relation constants used in SCAPE .....	<b>16</b>
<b>Table 2.3.</b> Relative Humidities of Deliquescence (RHD) at 298.15 K and their temperature dependence as used in SCAPE .....	<b>20</b>
<b>Table 2.4.</b> Mutual Deliquescence Relative Humidities (MDRH) at 298.15 K and their temperature dependence factors as used in ISORROPIA. ....	<b>21</b>
<b>Table 3.1.</b> $z_i^{\pm}$ values for ion pairs considered in various EQMs (e.g SCAPE).....	<b>44</b>
<b>Table 3.2.</b> EQSAM (Equilibrium Simplified Aerosol Model).....	<b>56</b>
<b>Table 4.1.</b> CPU times .....	<b>69</b>
<b>Table 6.1.</b> Approximated differences in aerosol nitrate budget concentrations [%] .....	<b>110</b>
<b>Table 7.1.</b> Correlations and average differences (observation-model) [ $\mu\text{g}/\text{m}^3$ ] based on daily averages for all available EMEP stations for August 1997. $t\text{NO}_3$ denotes the sum of $\text{NO}_3^-$ and $\text{HNO}_3$ , and $\text{NH}_x$ the sum of $\text{NH}_3$ and $\text{NH}_4^+$ .....	<b>114</b>
<b>Table A1.</b> Coefficients of the polynomial fit used in Eq. (A1) .....	<b>APP-2</b>

## Bibliography

- Adams, P. J., J. H. Seinfeld, and D. M. Koch, Global concentrations of tropospheric sulfate, nitrate, and ammonium aerosol simulated in a general circulation model, *J. Geophys. Res.*, *104*, 13,791, 1999.
- Allen A. G., Harrison R. M., and Erisman J. Field measurements of the dissociation of ammonium nitrate and ammonium chloride aerosols. *Atmos. Environ.* *23*, 1591-1599, 1989.
- Andres, R. J., and A. D. Kasgnoc, A time-averaged inventory of aerial volcanic sulfur emissions, *J. Geophys. Res.*, *103*, 25,251-25,261, 1998.
- Balkanski, Y. J., D. J. Jacob, G. M. Gardner, W. C. Graustein, and K. K. Turekian, Transport and residence times of tropospheric aerosols inferred from a global three-dimensional simulation of 210 Pb, *J. Geophys. Res.*, *98*, 20,573-20,586, 1993.
- Barrie, L. A., and many others, A comparison of large scale atmospheric sulphate aerosol models (COSAM), overview and highlights., *Tellus B*, submitted, 2000.
- Bassett, M. E., and J. H. Seinfeld, Atmospheric equilibrium model of sulfate and nitrate aerosols, *Atmos. Environ.*, *17*, 2237-2252, 1983.
- Bassett, M. E., and J. H. Seinfeld, Atmospheric equilibrium model of sulfate and nitrate aerosols II. Particle size analysis, *Atmos. Environ.*, *18*, 1163-1170, 1984.
- Beljaars, A. C. M., and P. Viterbo, Role of the boundary layer in a numerical weather prediction model, in Clear and cloudy Boundary layers, edited by A. A. M. Holtslag and P. G. Duynkerke, pp. 85-110, Koninklijke Nederlandse Akademie van Wetenschappen, 1998.
- Benkovitz, C. M., C. M. Berkowitz, R. C. Easter, S. Nemesure, R. Wagener, and S. E. Schwartz, Sulfate over the North Atlantic and adjacent continental regions: Evaluation for October and November 1986 using a three-dimensional model driven by observation-derived meteorology, *J. Geophys. Res.*, *99*, 20,725-20,756, 1994.
- Benkovitz, C. M., M. T. Scholtz, J. Pacyna, L. Tarrason, J. Dignon, E. C. Voldner, P. A. Spiro, J. A. Logan, and T. E. Graedel, Global gridded inventories of anthro-pogenic emissions of sulfur and nitrogen, *J. Geophys. Res.*, *101*, 29,239-29,253, 1996.
- Binkowski, F. S., MARS-8 Source Code, U.S. EPA, Research Triangle Park, 1991.
- Bromley, L. A., Thermodynamic properties of strong electrolytes in aqueous solutions, *A.I.Ch.E.J.*, *19*, 313-320, 1973.
- Charlson, R. J., D. S. Covert, T. V. Larson, and A. P. Waggoner, Chemical properties of tropospheric sulfate and nitrate aerosol, *Atmos. Environ.*, *12*, 39-53, 1978.
- Charlson, R. J., Lovelock, J. E., Andreae, M. o., and Warren, S.G. oceanic phytoplankton, atmospheric sulfur, cloud albedo and climate. *Nature* *326*, 655 661, 1987.
- Charlson, R. J., and M. L. T. Wigley, Sulfate aerosol and climatic change: industrial emissions of sulfur form particles that may be reflecting solar radiation back into space, thereby masking the greenhouse effect over some parts of the Earth, *Sci. American*, *270*, 48-57, 1994.
- Charlson, R. J., and J. Heintzenberg, Aerosols as a cause of uncertainty in climate forecasts, Report of the Dahlem Workshop on Aerosol Forcing of Climate, Berlin 1994, April 24-29 (ed. R. J. Charlson and J. Heintzenberg), Wiley & Sons, Chichester, 1-10, 1995.
- Chen H., Sangster J., Teng T. T., and Lenzi F. A general method for predicting the water activity of ternary aqueous solutions from binary data. *Canadian J. of Chem. Eng.* *51*, 234 241, 1973.
- Chin, M., D. J. Jacob, G. M. Gardner, M. S. Foreman-Fowler, and P. A. Spiro, A global three-dimensional model of tropospheric sulfate, *J. Geophys. Res.*, *101*, 22,869-22,889, 1996.
- Claussen, M., U. Lohmann, E. Roeckner, and U. Shulzweida, A global data set of land-surface parameters, *Tech. Rep. 135*, Max-Planck Insitut für Meteorologie, Hamburg, 1994
- Clegg, S. L., K. S. Pitzer, and P. Brimblecombe, Thermodynamics of multicomponent, miscible, ionic solutions. II. Mixture including unsymmetrical electrolytes, *J. Phys. Chem.*, *96*, 9470-9479, 1992.
- Clegg, S. L., P. Brimblecombe, and A. S. Wexler, A thermodynamic model of the system  $H^+NH_4^+Na^+SO_4^{2-}NO_3^-Cl^-H_2O$  at 298.15 K, *J. Phys. Chem.*, *102*, 2155-2171, 1998a.
- Clegg, S. L., P. Brimblecombe, and A. S. Wexler, A thermodynamic model of the system  $H^+NH_4^+Na^+SO_4^{2-}NO_3^-CL^-H_2O$  at tropospheric temperatures, *J. Phys. Chem.*, *102*, 2137-2154, 1998b.
- Cohen M. D., Flagan R. C., and Seinfeld J. H. Studies of concentrated electrolyte solutions using the electrodynamic balance. 1. Water activities for single electrolyte solutions. *J. Phys. Chem.*, *91*, 4563 4574, 1987a.

- Cohen M. D., Flagan R. C., and Seinfeld J. H. Studies of concentrated electrolyte solutions using the electrodynamic balance. 2. Water activities for mixed electrolyte solutions. *J. Phys. Chem.*, *91*, 4575-4582, 1987b.
- Cooke, W. F., and J. J. N. Wilson, A global black carbon aerosol model, *J. Geophys. Res.*, *101*, 19,395-19,409, 1996.
- Dana, M. T., and J. M. Hales, Statistical aspects of the washout of polydisperse aerosols, *Atmos. Environ.*, *10*, 45-50, 1991.
- Dassios, G. M. and S. N. Pandis, Mass accommodation coefficient of ammonium nitrate, *Atmos. Environ.*, *33*, 2999-3003, 1999.
- Denbigh, K., The principles of chemical equilibrium, *4th ed. Cambridge University Press, Cambridge, Great Britain.*, 1981.
- Dentener, F., and P. J. Crutzen, Reaction of N<sub>2</sub>O<sub>5</sub> on tropospheric aerosols: Impact on the global distributions of NO<sub>x</sub>, O<sub>3</sub> and OH, *J. Geophys. Res.*, *98*, 7149-7163, 1993.
- Dentener, F., and P. J. Crutzen, A global 3D model of the ammonia cycle, *J. Atmos. Chem.*, *19*, 331-369, 1994.
- Dentener, F. J., J. Feichter, and A. Jeuken, Simulation of the transport of Rn<sup>222</sup> using online and off-line models at different horizontal resolutions: a detailed comparison with measurements, *Tellus*, *51B*, 573-602, 1999.
- Diederer, H., R. Guicherit, and J. Hollander, Visibility reduction by air pollution in the Netherlands, *Atmos. Environ.*, *19*, 377-383, 1985.
- Dufour, L., and R. Defay, Thermodynamics of Clouds, *Academic Press, New York*, 1963.
- EMEP, Transboundary acidifying air pollution in Europe, *Tech. Rep. MSC-W Status Report 1998 - Part 1*, EMEP/MS-CW, NMI, Oslo, Norway, 1998.
- Feichter, J., E. Kjellström, H. Rodhe, F. Dentener, J. Lelieveld, and G.-J. Roelofs, Simulation of the tropospheric sulfur cycle in a global climate model, *Atmosph. Environ.*, *30*, 1693-1707, 1996.
- Ganzeveld, L., J. Lelieveld, and G.-J. Roelofs, Dry deposition parametrization of sulfur oxides in a chemistry and general circulation model, *J. Geophys. Res.*, *103*, 5679-5694, 1998.
- Gery, M. W., G. Z. Whitten, J. P. Killus, and M. Dodge, A photo-chemical kinetics mechanism for urban and regional scale computer modeling, *J. Geophys. Res.*, *94*, 925-956, 1989.
- Gong, S. L., L. A. Barrie, J. Prospero, D. L. Savoie, G. P. Ayers, J.-P. Blanchet, and L. Spacek, Modeling seasalt aerosol in the atmosphere, part 2: Atmospheric concentrations and fluxes, *J. Geophys. Res.*, *102*, 3819-3830, 1997.
- Guelle, W., Y. J. Balkanski, J. E. Dibb, M. Schulz, and F. Dulac, Wet deposition in a global size-dependent aerosol transport model: 1. comparison of a 1 year 210 Pb simulation with ground measurements, *J. Geophys. Res.*, *103*, 11, 429-11, 445, 1997a.
- Guelle, W., Y. J. Balkanski, J. E. Dibb, M. Schulz, and F. Dulac, Wet deposition in a global size-dependent aerosol transport model: 2. influence of the scavenging scheme on 210 Pb vertical profiles, surface concentrations and deposition, *J. Geophys. Res.*, *103*, 28, 875-28, 891, 1997b.
- Hamer W. J. and Wu Y.-C. osmotic coefficients and mean activity coefficients of univalent electrolytes in water at 25°C. *J. Phys. Chem. Ref Data*, *1*, 1047-1099, 1972.
- Hayami, H., C. H. Song, L. L. Chen, and G. R., Carmichael, Modeling aerosol composition at Cheju Island, Korea, *Measurements and modelling in environmental pollution., Billerica, MA, Wageningen Pers*, 141-149, 1997.
- Hayami, H., and G. R. Carmichael, Analysis of aerosol composition at Cheju Island, Korea, *Atmos. Environ.*, *31*, 3429-3439, 1997.
- Hayami, H., and G. R. Carmichael, Factors influencing the seasonal variation in particulate nitrate at Cheju Island, Korea, *Atmos. Environ.*, *32*, 1427-1434, 1998.
- Hänel G., The properties of atmospheric aerosol particles as functions of the relative humidity at thermodynamic equilibrium with the surrounding moist air. *Adv. Geophys. Res.* *19*, 73-188., 1976.
- Heimann, M., The global atmospheric tracer model tm2, Tech. Rep. Technical Report 10, *Deutsches Klima Rechenzentrum, Modellbetreuungsgruppe, Hamburg*, 1995.
- Heintzenberg, J., Fine particles in the global troposphere, A review. *Tellus*, *41B*, 149-160, 1989.
- Hildemann, L. M., Russell, A. G. and Cass, G. R., Ammonia and nitric acid concentrations in equilibrium with atmospheric aerosols, Experiment vs. Theory. *Atmos. Environ.* *18*, 1737-1750, 1984.
- Holtslag, A. A. M., and B. A. Boville, Local versus nonlocal boundary-layer diffusion in a global climate model, *J. Climate*, *6*, 1825-1842, 1993.

- Houweling, S., F. J. Dentener, and J. Lelieveld, The impact of non-methane hydrocarbon compounds on tropospheric photochemistry, *J. Geophys. Res.*, *103*, 10673-10696, 1998.
- IPCC, (Ed.: Houghton, J. T., L. G. Meira Filho, B. A. Callander, N. Harris, A. Kattenburg, K. Maskell, J. A. Lakeman), Climate change 1995: the science of climate change, Contribution of Working Group I to the Second Assessment Report of the Intergovernmental Panel on Climate Change, *New York, Cambridge University Press*, 572 p., 1996.
- Jaenicke, R., Landolt Börnstein, Numerical Data and functional Relationships in Science and Technology, New Series Vol. 4, Meteorology Sub. Vol. B, *Physical and Chem. Properties of Air*, p391, G. Fischer, Ed., Springer, 1988.
- Jacobson, M. Z., A. Tabazadeh, and R. P. Turco, Simulating equilibrium within aerosols and non-equilibrium between gases and aerosols, *J. Geophys. Res.*, *101*, 9079-9091, 1996.
- Jacobson, M. Z., Studying the effects of calcium and magnesium on size-distributed nitrate and ammonium with EQUISOLV II, *Atmos. Environ.*, *33*, 22, 3635-3649, 1999.
- Jeuken, A., Evaluation of chemistry and climate models using measurements and data assimilation, *Koninklijk Nederlands Meteorologisch Instituut (KNMI), - Technische Universiteit Eindhoven, ISBN 90-386-0987-6, Ph.D. Thesis*, 2000.
- Kasibhatla, P., W. L. Chameides, and J. S. John, A three-dimensional global model investigation of seasonal variations in the atmospheric burden of anthropogenic sulfate aerosols, *J. Geophys. Res.*, *102*, 3737-3759, 1997.
- Kettle, A. J., M. O. Andreae, and many others, A global database of sea surface dimethylsulfoxide (DMS) measurements and a procedure to predict sea surface DMS as a function of latitude, longitude and month, *Global Biogeochem. cycles*, *13*, 399-444, 1999.
- Khlystov, A., Cloud forming properties of ambient aerosol in the Netherlands and resultant shortwave radiative forcing of climate, *Landbouwwuniversiteit Wageningen, The Netherlands, Ph.D. Thesis*, 1998.
- Kiehl, J. T., and B. P. Briegleb, The relative roles of sulfate aerosols and greenhouse gases in climate forcing, *Science*, *260*, 311-314, 1993.
- Kim, Y. P., J. H. Seinfeld and P. Saxena, Atmospheric gas/aerosol equilibrium I. Thermodynamic model, *Aerosol Sci. Technol.*, *19*, 157-181, 1993a.
- Kim, Y. P., J. H. Seinfeld and P. Saxena, Atmospheric gas/aerosol equilibrium II. Analysis of common approximations and activity coefficient calculation methods, *Aerosol Sci. Technol.*, *19*, 182-198, 1993b.
- Kim, Y. P., and J. H. Seinfeld, Atmospheric gas/aerosol equilibrium III. Thermodynamics of crustal elements Ca<sup>2+</sup>, K<sup>+</sup>, and Mg<sup>2+</sup>, *Aerosol Sci. Technol.*, *22*, 93-110, 1995.
- Koch, D., D. Jacob, I. Tegen, D. Rind, and M. Chin, Tropospheric sulfur simulation and sulfate direct radiative forcing in the Goddard Institute for Space Studies GCM., *J. Geophys. Res.*, *104*, 23,799-23,822, 1999.
- Köpke, P., M. Hess, I. Schult, and E. P. Shettle, Global aerosol data set, *J. Theor. App. Climatol.*, 1997.
- Köhler, H., The nucleus in and the growth of hygroscopic droplets, *Trans Faraday Soc.*, *32*, 1152-1162, 1936.
- Krol, M., and M. van Weele, Implication of variation of photodissociation rates for global atmospheric chemistry, *Atmosph. Environ.*, *31*, 1257-1273, 1997.
- Kulmala, M., H. Vehkamäki, T. Vesala, J. C. Barret, and C. F. Clement, Aerosol formation in diffuse boundary layer: binary homogenous nucleation of ammonia and water vapors, *J. Aerosol Sci.*, *26*, 547-558, 1995.
- Kulmala, M., A. Laaksonen, and L. Pirjola, Parameterizations for sulfuric acid/water nucleation rates, *J. Geophys. Res.*, *103*, 8301-8307, 1998.
- Kusik, C. L., and H. P. Meissner, Electrolytic activity coefficients in inorganic processing, *A.I.Ch.E. Symp. Ser.*, *173*, 14-20, 1978.
- Langner, J., and H. Rodhe, A global three-dimensional model of the tropospheric sulfur cycle, *J. Atmos. Chem.*, *13*, 225-263, 1991.
- Lelieveld, J., and P. J. Crutzen, The role of clouds in tropospheric photochemistry, *J. Atmos. Chem.*, *12*, 229-267, 1991.
- Lelieveld, J., and F. Dentener, What's controlling tropospheric ozone, *J. Geophys. Res.*, *105*, 3531, 2000.
- Liousse, C., J. E. Pennner, C. Chuang, J. J. Walton, H. Eddleman, and H. Cachier, A global three-dimensional model study of carbonaceous aerosols, *J. Geophys. Res.*, *101*, 19,411-19,432, 1996.



- Liss, P., and L. Merlivat, Air-sea gas exchange rates: Introduction and synthesis, in *The Role of Sea-Air Exchange in Geochemical Cycling*, edited by P. Menard, Reidel, Dordrecht, 113-127, 1986.
- Lohmann, U., et al., Comparison of the vertical distribution of sulfur species from models participated in the COSAM exercise with observations, *J. Geophys. Res.*, submitted, 1999.
- Louis, J. F., M. Tiedtke, and J. F. Geleyn, A short history of PBL parameterization at ECMWF, in *Proceedings of the ECMWF workshop on boundary layer parameterization*, 59-79, 1982.
- Low, R. D. H. J. A generalized equation for the solution effect in droplet growth, *Atmos. Sci.*, 26, 608, 1969a.
- Low, R. D. H., A comprehensive Report on nineteen Condensation Nuclei, Part I - Equilibrium Growth and Physical Properties, *Research Rept. Ad 691700, ECOM - 5249, Atmos. Sci. Lab., White sands Missile Range, New Mexico*, 1969b.
- Mason, B. J., *The physics of clouds*, p. 671, Clarendon, Oxford, 1971.
- Meng, Z., J. H. Seinfeld, P. Saxena, and Y. P. Kim, Atmospheric gas/aerosol equilibrium. IV: Thermodynamics of carbonates, *Aerosol Sci. Technol.*, 131-154, 1995.
- Meng, Z., and J. H. Seinfeld, Time scales to achieve atmospheric gas/aerosol equilibrium for volatile species, *Atmos. Environ.*, 30, 2889-2900, 1996.
- Meng, Z., D. Dabdub, and J. H. Seinfeld, Size-resolved and chemically resolved model of atmospheric aerosol dynamics, *J. Geophys. Res.*, 103, 3419-3435, 1998.
- Metzger, S. M., F. J. Dentener, and J. Lelieveld, Aerosol multiphase chemistry - a parameterization for global modeling, *Internal Report No. 99-12, available from the Institute for Marine and Atmospheric Research Utrecht (IMAU), Princetonplein 5, NL-3584 CC Utrecht, The Netherlands*, 1999.
- Mozurkewich M. The dissociation constant of ammonium nitrate and its dependence on temperature, relative humidity and particle size. *Atmos. Environ.* 27A, 261- 270, 1993.
- Nenes A., C. Pilinis, and S. N. Pandis, Isorropia: A new thermodynamic model for multiphase multicomponent inorganic aerosols, *Aquatic Geochemistry*, 4, 123-152, 1998.
- Olivier, J., Description of EDGAR version 2.0, *Tech. Rep. 771060002, RIVM, Bilthoven, Netherlands*, 1996.
- Olson, J., J. A. Watts, and L. J. Allison, Carbon in live vegetation of major world ecosystems, *Tech. Rep. ORNL-5862, Oak Ridge National Laboratory, Oak Ridge, Tennessee*, 1983.
- Pham, M., J.-F. Müller, G. P. Brasseur, C. Granier, and G. M. egie, A three-dimensional study of the tropospheric sulfur cycle, *J. Geophys. Res.*, 100, 26,061-26,092, 1995.
- Pilinis, C., and J. H. Seinfeld, Continued development of a general equilibrium model for inorganic multicomponent atmospheric aerosols, *Atmos. Environ.*, 32, 2453-2466, 1987.
- Pilinis, C., J. H. Seinfeld, and D. Grosjean, Water content of atmospheric aerosols, *Atmos. Environ.*, 23, 1601-1606, 1989.
- Pilinis, C., S. N. Pandis, and J. H. Seinfeld, Sensitivity of direct climate forcing by atmospheric aerosols to aerosol size and composition, *J. Geophys. Res.*, 100, 18739-18754, 1995.
- Pilinis, C., K. P. Capaldo, A. Nenes, and S. N. Pandis, MADM-A New Multicomponent Aerosol Dynamics Model, *Aerosol Sci. Technol.*, 32, 5, 2000.
- Pitzer, K. S., and G. Mayorga, Thermodynamics of electrolytes - II. Activity and osmotic coefficients for strong electrolytes with one or both ions univalent, *J. Phys. Chem.*, 77, 2300-2308, 1973.
- Potukuchi S. and Wexler A. S. Identifying solid-aqueous phase transitions in atmospheric aerosols. I. Neutral acidity solutions. *Atmos. Environ.* 29, 1663-1676, 1995a.
- Potukuchi S. and Wexler A. S. Identifying solid-aqueous phase transitions in atmospheric aerosols. II. Acidic solutions. *Atmos. Environ.* 29, 3357-3364, 1995b.
- Potukuchi, S., and A. S. Wexler, Predicting vapor pressures using neural networks, *Atmos. Environ.*, 31, 741-753, 1997.
- Pruppacher, H. R., and J. D. Klett, *Microphysics of Clouds and Precipitation*, Dordrecht, Holland, D. Reidel Publ. Co., 950p, 1980.
- Pruppacher, H. R., and J. D. Klett, *Microphysics of Clouds and Precipitation*, Dordrecht, Holland, D. Reidel Publ. Co., 950p, 1997.
- Quinn, P. K., Asher, W. E. and Charlson, R. J. Equilibria of the marine multiphase ammonia system. *J. Atmos. Chem.*, 14, 11-30, 1992.
- Rasch, P. J., N. M. Mahowald, and B. E. Eaton, Representations of transport, convection, and the hydrological cycle in chemical transport models: Implications for the modeling of shortlived and soluble species, *J. Geophys. Res.*, 102, 28,127-28,138, 1997.

- Robinson, R. A. and Stokes, R. H., Electrolyte solutions. *Second Ed., Butterworths, London, 1965.*
- Roedel, W., Measurements of sulfuric acid saturation vapor pressure: implications of aerosol formation by heteromolecular nucleation, *J. Aerosol Sci. 10*, 375-386, 1979.
- Roedel, W., Physik unserer Umwelt: Die Atmosphäre, *Springer Verlag, p457, 1992.*
- Roelofs, G.-J., and J. Lelieveld, Distribution and budget of O<sub>3</sub> in the troposphere calculated with a chemistry general circulation model, *J. Geophys. Res.*, *100*, 20,983-20,998, 1995.
- Roelofs, G.-J., J. Lelieveld, and L. Ganzeveld, Simulation of global sulfate distribution and the influence on effective cloud drop radii with a coupled photochemistry- sulfur cycle model, *Tellus*, *50B*, 224-242, 1998.
- Roelofs, G.-J., et al., Analysis of regional budgets of sulfur species modeled for the COSAM exercise, *Tellus B*, submitted, 2000.
- Rood M.J., M.A. Shaw, T.V. Larson and D.S. Covert, Ubiquitous nature of ambient metastable aerosol. *Nature*, *Vol. 337*, pp. 537-539, 1989.
- Russell, and A. Lerner, A infinite difference scheme for the tracer transport equation, *J. Appl. Meteorol.*, *20*, 1483, 1981.
- Saxena, P., C. Seigneur, A. B. Hudischewskyj, and J.H. Seinfeld, A comparative study of equilibrium approaches to the chemical characterization of secondary aerosols, *Atmos. Environ.*, *20*, 1471-1484, 1986.
- Saxena, P. and Peterson, T. W., Thermodynamics of multicomponent electrolytic aerosols. *J. Coll. Interdis. Sci.* *79*, 496-510, 1981.
- Schwartz, S. E. and Andreae, M. O., Uncertainty in climate change caused by aerosols. *Science* *272*, 1121-1122 (1996).
- Seinfeld, J. H., Atmospheric chemistry and physics of air pollution, *John Wiley & Sons, Chichester, New York, 1986.*
- Seinfeld J. H. and S. N. Pandis, Atmospheric Chemistry and Physics: From Air Pollution to Climate Change, *John Wiley & Sons, Chichester, New York, 1998.*
- Skoog, A. D. and D. M. West, Fundamentals of Analytical Chemistry, *Holt-Saunders Internat. Ed.*, 1982.
- Spiro, P. A., D. J. Jacob, and J. A. Logan, Global inventory of sulfur emissions with 1°x1° resolution, *J. Geophys. Res.*, *97*, 6023-6036, 1992.
- Stelson A.W. and J.H. Seinfeld, Thermodynamic prediction of the water activity, NH<sub>4</sub>NO<sub>3</sub> dissociation constant, density and refractive index for the NH<sub>4</sub>NO<sub>3</sub>-(NH<sub>4</sub>)<sub>2</sub>SO<sub>4</sub>-H<sub>2</sub>O System at 25°C. *Atmos. Env.*, *16*, No. 10, 2507-2514, 1982.
- Stokes, R. H., and R. A. Robinson, Interactions in aqueous nonelectrolyte solutions. I. Solute solvent equilibria, *J. Phys. Chem.*, *70*, 2126-2130, 1966.
- Sun, Q., and Wexler, A. S., Modeling Urban and Regional Aerosols-Condensation and Evaporation Near Acid Neutrality, *Atmos. Environ.*, *32*, 3527-3531, 1998.
- Tang, I.N., Deliquescence properties and particle size change of hygroscopic aerosols, *In Generation of Aerosols and Facilities for Exposure Experiments*, Ann Arbor Science Publishers, 1980.
- Tang I. N. and Munkelwitz H. R. Composition and temperature dependence of the deliquescence properties of hygroscopic aerosols. *Atmos. Environ.* *27A*: 467-473, 1993.
- Tang I. N., and H. R. Munkelwitz, Aerosol phase transformation and growth in the atmosphere, *J. Appl. Meteorol.*, *33*, 791-796, 1994.
- Tanré, D., M. Herman, and Y. J. Kaufman, Information on aerosol size distribution contained in solar reflected radiances, *J. Geophys. Res.*, *101*, 19,043-19,060, 1996.
- Tegen, I., and I. Fung, Modeling of mineral dust in the atmosphere: Sources, transport and optical thickness, *J. Geophys. Res.*, *99*, 22,897-22,914, 1994.
- Ten Brink, H. M., J. P. Veefkind, A. Waijers-Ijpelaan, and J. C. van der Hage, Aerosol light-scattering in The Netherlands, *Atmos. Environ.*, *30*, 4251-4261, 1996.
- Tiedtke, M., A comprehensive massflux scheme for cumulus parametrization in large-scale models, *Mon. Wea. Rev.*, *117*, 1641, 1989.
- Tiedtke, M., Representation of clouds in large-scale models, *Mon. Wea. Rev.*, *121*, 3040-3061, 1993.
- Twomey, S., Influence of pollution on the short-wave albedo of clouds, *J. Atmos. Sci.*, *34*, 1149-1152, 1977a.
- Twomey, S., Atmospheric aerosols, *Elsevier Scientific Publ. Company*, 302 p., 1977b.
- Van Aardenne, J. A., F. J. Dentener, C. G. M. K. Goldewijk, J. Lelieveld, and J. G. J. Olivier, A high resolution data set of historical anthropogenic trace gas emissions for the period 1890-1990, *Global Biogeochem. Cycles*, submitted, 1999.

- Van Dorland R., F. J. Dentener, and J. Lelieveld, Radiative forcing due to tropospheric ozone and sulfate aerosol, *J. Geophys. Res.*, 102, 28079-28100, 1997.
- Van der Hurk, B., P. Viterbo, A. Beljaars, and A. Betts, Online validation of the ERA40 surface scheme, *Tech. Rep. Tech. memo 295, ECMWF*, 1999.
- Umweltatlas Hamburg, Umweltbehörde Hamburg, Billstraße 84, 20539 Hamburg, Germany. ISSN, 0946-3984, 1994.
- Wagman, D.D., W.H. Evans, V.B. Parker, R.H. Schumm, I. Harlow, S.M. Bailey, K.L. Churney, and R.L. Nutall, The NBS Tables of Chemical Thermodynamic Properties. *J. Phys. Chem. Ref. Data*, 11, Suppl. 2, 1982.
- Warneck, P., Chemistry of the Natural Atmosphere, *Internat. Geophys. Series*, 41, Academic Press, Inc., 1988.
- Wexler, A. S., and J. H. Seinfeld, The distribution of ammonium salts among a size and composition dispersed aerosol, *Atmos. Environ.*, 24A, 1231-1246, 1990.
- Wexler, A. S., and J. H. Seinfeld, Second-generation inorganic aerosol model, *Atmos. Environ.*, 25A, 2731-2748, 1991.
- Wexler A. S., and Potukuchi, Kinetics and Thermodynamics of Tropospheric Aerosols, *Atmospheric Particles*, John Wiley & Sons Ltd., 1998.
- Winkler, P., The growth of atmospheric aerosol particles as a function of the relative humidity - II. An Improved concept of mixed nuclei. *Aerosol Sci.* 4, 373-387, 1973.
- Winkler, P., The growth of aerosol particles with relative humidity, *Physica Scripta* 37, 223-230, 1988.
- Zadanovskii, A. B., New methods of calculating solubilities of electrolytes in multicomponent systems, *Zhu. Fiz. Khim.*, 22, 1475-1485, 1948.
- Zhang, Y., C. Seigneur, J. H. Seinfeld, M. Jacobson, S. L. Clegg, and F. S. Binkowski, A comparative review of inorganic aerosol thermodynamic equilibrium modules: similarities, differences, and their likely causes, *Atmospheric Environ.*, 34, 1, 117-137, 1999a.
- Zhang, Y., C. Seigneur; J. H. Seinfeld, M. Z. Jacobson, and F. S. Binkowski, Simulation of Aerosol Dynamics: A Comparative Review of Algorithms Used in Air Quality Models, *J. Aerosol Sci.*, 31, 6, 487-514, 1999b.

## Epilogue

My motivation to start this thesis was the opportunity to initialize my own project, funded by a grant from the “European Community”. To initialize this, I had support from Dr. J. Feichter at the “Max-Planck Institut für Meteorologie, Hamburg”. The subject should be the direct and indirect climate effect of nitrate aerosols. This was something new and challenging, since at that time only sulfate aerosols were under investigation in climate models.

I was particularly interested in this subject because I already had some insight into climate research due to the work performed during my M.Sc. thesis. On the other hand, at the same time while doing my community service in the air pollution protection section of the environmental office in Hamburg, I automatically was confronted with reality. It was apparent that for Hamburg and probably many other western industrial cities, the emission of air pollutants had clearly shifted from sulfur dioxide to nitrogen oxides. Therefore, I became particularly interested to investigate what this would mean in climate model calculations. However, what I did not realize at the beginning of this thesis was how complicated this “simple” scientific question really was.

First, I realized that nitrate aerosols are, in contrast to sulfate aerosols, volatile, since nitric acid is a weaker acid than sulfuric acid and thus their salts less stable. Consequently, nitrate aerosols partition between the gas and the aerosol phase, and maintain gas/aerosol equilibria, contrary to sulfate aerosols. Therefore, I had to dig out knowledge of a certain part of my physics studies, “The Thermodynamics”, which I liked very much during my studies in Heidelberg. Unfortunately, I had almost forgotten everything, since my diploma thesis in Hamburg focused on a rather different subject, namely the combination of ensemble climate forecasts of the El Niño / Southern Oscillation Phenomenon (ENSO). Thus, I had to study again the text book literature, and looked at old and new publications on aerosol thermodynamics.

While studying the literature of the thermodynamics, I realized that the numerical representation of the present knowledge of aerosol thermodynamics was by far too complex for application in climate models. Consequently, I had to think of a parameterization, which would allow representation of gas/aerosol partitioning sufficiently accurately and fast enough to be useful for climate modeling. Especially, since climate models are used to make simulations on long time scales, i.e. over decades and centuries at relatively high resolutions, the numerical representation had to be sufficiently fast and accurate.

Although I soon found an appropriate way to parameterize the calculation of activity coefficients which is essential for the gas/aerosol partitioning, I learned by bitter experience how difficult it can be to get as an outsider new and unusual results accepted in the science community. By comparing textbook knowledge with recent aerosol literature, I had found a method with which I have been obviously stepped into a minefield. Some of the international reviewers have described it as a new, useful and a novel method, while others completely rejected the proposed idea, regardless the promising results.

The entire process of proposing and trying to get the new method accepted for publication was very time consuming and demotivating. As it became apparent to me that the complex system of the gas/aerosol partitioning can be parameterized in an even simpler manner, I found new motivation for the development of a completely new gas/aerosol routine, which is suited for global modeling. This routine appeared to be sufficiently accurate and fast for climate modeling, which became evident by the results of the application of the new gas/aerosol routine to global modeling, and by the comparison with more complex thermodynamic gas/aerosol models. Especially the latter comparison showed that it is not necessary to use a too complex numerical representation of individual physical processes in a coupled atmosphere/chemistry transport model. The reason is that

on larger scales, the dynamics of the “entire system” are dominating the details of secondary processes as the aerosol thermodynamics. This means that meteorology, transport and deposition processes, as well as the temporal and spatial variability of emissions and the chemistry govern the main uncertainties of the gas/aerosol partitioning. Details of the aerosol thermodynamics are only a small part of the overall uncertainties.

The work presented in this thesis provides know-how for the investigation of the original idea of this thesis: “The investigation of the direct and indirect climate effect of aerosols beyond sulfate-only simulations, with special emphasis to the aerosol composition and the aerosol associated water content”. Both effects are important for estimating the climate effect of aerosols, but especially the aerosol-cloud interaction i.e. the indirect aerosol effect is not well understood yet. It therefore remains a challenging task with many more barriers to cross before the climate effect of aerosols is well understood and quantified.

This work was performed at the “Instituut voor Marine en Atmosferisch Onderzoek” (IMAU), at the “Universiteit Utrecht”, The Netherlands. The thesis was partly financed through a bursary from “The European Community”, according to Article 6 of the ‘Fixed Contribution Contract for Training through Research’, N° ENV4-CT96-5036 (DG 12-ASAL), and partly by the SINDICATE (Study of the INdirect and DIrect Climate influences of Anthropogenic Trace gas Emissions) program, which was also funded by “The European Community”.

At this point, I would like to thank my promoters, Prof. Jos Lelieveld, and Prof. Hartmut Grassl for their stimulating support and their help with the realization of this thesis. Special thanks to my co-promoter Dr. Frank Dentener for all the fruitful discussions. In particular, I am grateful to Jos and Frank who supported me under all circumstances.

I further want to thank Ad (now Dr. Jeuken) for the effective and close cooperation during our common aerosol modeling with TM3; without the excellent work of my colleagues Frank, Ad, Sander (now Dr. Houweling), and Maarten (Dr. Krol), aerosol modeling with TM3 would not be possible. Thanks to all other colleagues who stimulated me during my time at IMAU and who contributed to the very pleasant working atmosphere. “Een extra dank je” to Dr. Axel Timmermann and Dr. Jason Williams for cross-checking this thesis, and Jos, Frank and Maarten for proofreading. Ad, thanks for the help with the Dutch summary. I also wish to thank Prof. W. Roedel, who actually rose my attention to aerosols during my studies, for his interest and comments on theoretical aspects of this work.

I acknowledge Prof. G. Carmichael, Prof. S. Pandis, and Dr. Y.P. Kim for providing the thermodynamic models. Dr. Harry ten Brink (ECN), kindly provided the surface measurements of aerosol composition at Petten, and Dr. Hans Bergwerff (RIVM) provided data of the Dutch national air pollution monitoring network for the model validation.

Special thanks go out to Prof. S. Pandis for being part of the “Promotion Committee”.

I am deeply grateful to you Katharina for your support, power and patience.

Utrecht, July 2000

## **Curriculum Vitae**

I was born 1967 in Heidelberg, Germany. Nearby, in my hometown Eberbach, I went to school and became an electrician (graduation with the “Gesellenbrief” at the company ABB, formerly BBC). I extended my education at the Technische Oberschule in Mannheim with the German “Abitur”, and, thereafter, at the Ruprecht-Karls University in Heidelberg with the “Vordiplom” in Physics, Mathematics and Chemistry (Bachelor equivalent). With a bursary from the German government, I followed a Research Program (Honors) in Physical Oceanography and Marine Science at the James Cook University of North Queensland, Australia, staying in total 15 months abroad, which included traveling around the world with various stops in Asia, New Zealand, Fiji, Mexico, and the United States of America. I continued my studies in Heidelberg, Berlin, and Hamburg, and graduated in Physics (“Diplom” degree) at the University of Hamburg. At the Max-Planck-Institute for Meteorology in Hamburg (MPIM), I wrote my diploma thesis on the subject “Combination of ensemble climate forecasts of the El Niño / Southern Oscillation (ENSO)” under the supervision of Prof. Dr. H. Grassl, and Dr. M. Latif. Thereafter, I absolved my community service at the Environmental Office (Umweltbehörde) in the section “Environment Protection and Air Pollution”, while I continued scientific research at MPIM with data analysis from climate model studies for Dr. J. Feichter, and the preparation of data for a model intercomparison of the WCRP-workshop in Cambridge. This work motivated me to start an own research project in atmospheric chemistry in close cooperation with Prof. Dr. J. Lelieveld, IMAU, and with support from Prof. Dr. H. Grassl, MPIM. This project finally led to this Ph.D. thesis “Gas/Aerosol Partitioning: A simplified Method for Global Modeling”.

